

2002

PARTICLE FORMATION BY RAPID EXPANSION OF SUPERCRITICAL SOLUTIONS

Chandra S. Vemavarapu
University of Rhode Island

Follow this and additional works at: https://digitalcommons.uri.edu/oa_diss

Terms of Use

All rights reserved under copyright.

Recommended Citation

Vemavarapu, Chandra S., "PARTICLE FORMATION BY RAPID EXPANSION OF SUPERCRITICAL SOLUTIONS" (2002). *Open Access Dissertations*. Paper 195.
https://digitalcommons.uri.edu/oa_diss/195

This Dissertation is brought to you by the University of Rhode Island. It has been accepted for inclusion in Open Access Dissertations by an authorized administrator of DigitalCommons@URI. For more information, please contact digitalcommons-group@uri.edu. For permission to reuse copyrighted content, contact the author directly.

DOCTOR OF PHILOSOPHY DISSERTATION
OF
CHANDRA S. VEMAVARAPU

APPROVED:

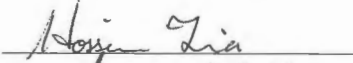
Dissertation Committee:

Major Professor











DEAN OF THE GRADUATE SCHOOL

UNIVERSITY OF RHODE ISLAND

2002

PARTICLE FORMATION BY
RAPID EXPANSION OF SUPERCRITICAL SOLUTIONS

BY
CHANDRA S. VEMAVARAPU

A THESIS SUBMITTED IN PARTIAL FULFILLMENT OF THE
REQUIREMENTS FOR THE DEGREE OF
DOCTOR OF PHILOSOPHY
IN
PHARMACEUTICS

UNIVERSITY OF RHODE ISLAND

2002

ABSTRACT

Background. This body of work is intended to serve as a proof of concept for the application of supramolecular chemistry in drug development. More specifically, this work is designed to evaluate crystal doping by recrystallization from supercritical media. The rapid nucleation and growth implicit to supercritical fluid based crystallizations were tested in doping drug crystals with structurally related impurities. The ultimate motive was to tailor the physicochemical properties of active pharmaceutical ingredients (API) through crystal doping. This, in turn provides the ability to tie functionality to API's at early stages of drug discovery and synthesis. **Methods.** The rapid expansion of supercritical solution (RESS) process was evaluated for these purposes. Pure and co-solvent modified supercritical fluid CO₂ was used as the recrystallizing solvent. The supercritical region investigated for these studies included pressures from 1071-9000psi and temperatures ranging from 31-100°C. The pharmaceutical solids studied included α -naphthalene acetic acid, aspirin, benzoic acid, caffeine, chlorpropamide, indomethacin, naproxen, phenytoin, piroxicam, salicylic acid, theobromine, theophylline, tolbutamide and urea. For comparison purposes, model chlorpropamide+urea system was also recrystallized from three liquid organic solvents using evaporative crystallization. The composition, morphology and the energetics of the crystals thus produced are characterized utilizing techniques such as microscopy (polarizing optical, SEM), thermal analysis (DSC, mDSC, TGA and thermomicroscopy) and HPLC. **Results.** Selective extraction and a reduction in crystallinity were consistently seen in all of the drug-impurity mixtures co-

crystallized by RESS process. In addition, a number of interesting phenomena were revealed. These include habit modification, solubility enhancement, particle size reduction, eutectic formation, amorphous conversion, hydrate formation and polymorph conversion. In viewing each of these phenomena from an application standpoint, this work serves as proof of concept for enhancing the physicochemical and mechanical attributes of API's using supercritical fluid crystal doping. Comparative evaluation studies indicated RESS to be superior to organic solvent-based recrystallizations in crystal doping. In summary, RESS offers great promise as a hybrid technique to control both the crystalline and the particle morphologies of API's in a single stage. **Conclusions.** The presence of an impurity in the crystallization medium exhibits varied effects depending on the phase in which it is present prior to nucleation and its affinity to the host relative to the crystallizing solvent. This in turns dictates the rate at which it nucleates and grows in relation to that of the host. The domain of effects that these kinetics dictate on one extreme includes the formation of a solid solution or a solid dispersion of the impurity in the host lattice. On the other hand, selective extraction of each of the components with respect to time can also occur, the extent of which primarily depends on the resolution factor of the recrystallizing solvent. While the former mechanism is largely aided by the rapid nucleation and growth implicit to supercritical fluid recrystallizations, the latter forms the scope of supercritical fluid chromatography. An optimal compromise between these extremes can be reached by utilizing the adjustable solvent power of supercritical fluids.

ACKNOWLEDGEMENTS

Many have helped and influenced me during the course of my study whose names are impossible to list here and by no means limited to the following. To them all I am ever grateful. To begin, I would like to thank my major professor, Dr. Thomas Needham for his guidance and support throughout this seemingly never ending process. His style of writing is one quality that I have always admired and attempted to pick up. I would also like to thank my co-advisor Dr. Matthew Mollan who made himself available throughout this work notwithstanding his Pfizer activities. He is a man of alternatives, if not solutions and never can arise a complex situation to bog one down under his direction. Thanks are also due to Dr. Hossein Zia and Dr. Arijit Bose for their time and effort spent serving on my dissertation committee.

I am also grateful to Pfizer Inc. that provided me the facility to perform dissertation work in an industrial setting. In particular, I would like to thank Dr. KS Murthy, Dr. David Pope and Dr. Isaac Ghebre-Sellassie who instituted this joint research program and for being instrumental in monitoring the progress. Thanks are due to the members of Technology Development group who have been very supportive and encouraging throughout. I feel fortunate in having had the support and project-related cynicism of Jeremy Salter. His meticulous lab conduct had the greatest impact on my cGLP skills. I wish to thank Dr. Meb Fessehaie and Dr. Zeri Teweldemedhin for their useful discussions. I am perhaps the greatest benefactor of the ad hoc electrical and machining services of Alex Mircea and Ben Azzaro. I am

truly grateful for their anytime-help and also for parental advises on the day to day routine. The administrative assistance of Kathy Hayes (URI) and Kathy Gandy (Pfizer) is greatly acknowledged. Thanks to Kathy Gandy for taking time to read the dissertation and provide helpful suggestions.

A special thanks is due to Tooba Murshedkar for her generous, non-complaining and reliable help with my eleventh hour situations at URI. I feel fortunate in having had her support throughout my externship at Pfizer. As for sources of distraction, the list includes Niraj Amin, Maurice Lobo, Soms Manepalli, Vishnu Sharma, Atul Sharma, Vikas Srivastav, Peter Bernardt and Radi Hejazi. Thanks are due to all my friends who made my graduate pauperhood pleasurable and worthwhile.

Finally, I would like to thank my parents, brother, Drs. VS Laxmi, KNM Rao and Padma Surpaneni, whose understanding and constant support helped me accomplish this goal. I shall be ever grateful to all of them.

PREFACE

This dissertation is written in the 'Standard Format' as described in the Guide to Dissertations Manual of the University of Rhode Island. The entire body of this dissertation is organized into five chapters. The dissertation work reported here serves as a proof of concept for using supercritical fluid aided crystal doping to alter the physicochemical properties of pharmaceutical actives. Chapter one reviews the current status of supercritical fluid particle formation in pharmaceuticals. The design and process aspects of laboratory scale SCF equipment are covered in chapter two. The main body of this dissertation can be found in chapters three to five. Investigative supercritical fluid co-crystallization studies involving twelve drug-impurity mixtures are excerpted from the appendix and reported in chapter three. A more rigorous evaluation of crystal doping was performed on chlorpropamide+urea system, which forms chapter four. In a parallel study, qualitative phase behavioral and solubility studies that aid in the supercritical recrystallizations were performed. Such studies are reported in chapter five. At the end of the dissertation, a bibliography, which cites all the sources used in this dissertation is included.

TABLE OF CONTENTS

ABSTRACT	i
ACKNOWLEDGEMENTS	iii
PREFACE	v
TABLE OF CONTENTS	vi
LIST OF TABLES	ix
LIST OF FIGURES	xi

CHAPTER ONE

Supercritical Fluid Technologies in Pharmaceutical Material Processing

0. Abstract.....	1
1. Introduction.....	2
2. Background.....	4
3. Static Supercritical Fluid Process.....	14
4. Rapid Expansion of Supercritical Solutions (RESS)	18
5. Particles from Gas Saturated Solution (PGSS)	30
6. Supercritical Antisolvent Processes.....	36
7. Solution Enhanced Dispersion by Supercritical Fluids (SEDS)	49
8. Summary.....	58
9. List of References.....	60

CHAPTER TWO

Design and Process Engineering of Laboratory Scale Supercritical Fluid Equipment

0. Abstract.....	71
1. Introduction.....	72
2. Supercritical Fluid Delivery.....	76
3. Reaction.....	79
4. Pre-Expansion.....	82

5. Spray Configurations.....	83
6. Particle Collection.....	84
7. Summary.....	86
8. List of References.....	88

CHAPTER THREE

Co-Crystallization of Pharmaceutical Actives and Their Structurally Related Impurities

0. Abstract.....	91
1. Introduction.....	92
2. Background	
A. Theory of Crystal Doping.....	93
B. Pharmaceutical Applications.....	97
C. Characterization of Crystal Doping.....	100
3. Materials and Methods.....	108
4. Results and Discussion	
A. Habit modification and Solubility enhancement.....	120
B. Eutectic Formation.....	125
C. Reduction in Crystallinity/Amorphous Conversion.....	128
D. Hydrate Formation.....	148
E. Polymorph Conversion.....	153
F. Selective Extraction.....	161
5. Conclusions.....	175
6. List of References.....	179

CHAPTER FOUR

Crystal Doping Aided by Rapid Expansion of Supercritical Solutions

0. Abstract.....	185
1. Introduction.....	186

2. Materials and Methods.....	190
3. Results and Discussion	
A. Polymorphism in Chlorpropamide.....	203
B. RESS Of Pure Chlorpropamide.....	212
C. RESS Of Chlorpropamide + Urea.....	222
4. Conclusions.....	234
5. List of References.....	239

CHAPTER FIVE

Solubility and Phase Behavior of Pharmaceutical Solids in Supercritical CO₂

0. Abstract.....	242
1. Introduction.....	244
2. Design of Phase Monitor.....	245
3. Experimental.....	247
4. Results and Discussion.....	248
5. Recommendations	
A. Design of Equipment.....	255
B. Operation of the Equipment.....	258
6. Conclusions.....	259
7. List of References.....	260

APPENDIX.....	261
---------------	-----

BIBLIOGRAPHY.....	344
-------------------	-----

LIST OF TABLES

<u>No.</u>	<u>TITLE</u>	<u>Page</u>
1.	Potential Applications of SCF Processes in Solid Drug Processing.....	3
2.	Properties of CO ₂	5
3.	Distinguishing Various Supercritical Fluid Processes.....	7
4.	Applications of the Static Supercritical Fluid Process.....	17
5.	Summary of RESS Studies.....	26
6.	Summary of PGSS Studies.....	33
7.	Pharmaceutical Studies using Supercritical CO ₂ as an Antisolvent.....	44
8.	Summary of SEDS studies.....	55
9.	Vendor Information of Supercritical Fluid Equipment & Accessories...	75
10.	Drug-Impurity Mixtures Evaluated in RESS Recrystallization Studies..	114
11.	HPLC Method of Assay for Theophylline & Caffeine.....	117
12.	HPLC Method of Assay for Theophylline & Theobromine.....	118
13.	Validation Results of HPLC Method of Analysis of Theophylline and Caffeine.....	117
14.	Validation Results of HPLC Method of Analysis of Theophylline & Theobromine.....	118
15.	Thermal Analysis of RESS Recrystallized Salicylic acid.....	124
16.	Formation of Low Melting Mixtures of Drugs + Impurities upon RESS Recrystallization.....	130
17.	Summary of RESS Co-crystallization Studies of Various Drug-Impurity Mixtures.....	131
18.	Representative XRD Peaks Showing Peak Shifts and Peak Broadening Upon Doping Crystals with Impurities.....	137
19.	Composition of Co-Crystals Produced from 80/20 Mixture of Theophylline +Caffeine.....	163

20. Composition of Co-Crystals Produced from 20/80 Mixture of Theophylline +Caffeine.....	163
21. HPLC Method of assay for Chlorpropamide and Urea.....	200
22. Melting data and Heat of Solutions of Different Polymorphs of Chlorpropamide.....	214
23. Nomenclature/Properties of Reported Chlorpropamide Polymorphs.....	216
24. Summary of RESS Recrystallization Of Chlorpropamide.....	217
25. Polymorph Conversion of Chlorpropamide by RESS Recrystallization..	219
26. Summary Of RESS Recrystallization Of Chlorpropamide+ Urea.....	224
27. Selectivity of Extraction as a function of T/P of SC CO ₂	227
28. Results of Doping Chlorpropamide with Urea.....	227
29. Peak Shifts and Peak Broadening in Doped Chlorpropamide Crystals...	228
30. Peak Broadening as a function of impurity levels in the doped crystals..	229
31. Thermal Analysis of Chlorpropamide+Urea mixtures Recrystallized from Liquid Organic Solvents.....	236
32. Supercritical Fluid Conditions for Enhanced Solubilization.....	252

LIST OF FIGURES

<u>No.</u>	<u>TITLE</u>	<u>Page</u>
1.	Schematic of Static Supercritical Fluid Process.....	8
2.	Schematic of Rapid Expansion of Supercritical Solution Process.....	8
3.	Schematic of Particles From Gas Saturated Solution Process.....	10
4.	Schematic of Gas AntiSolvent Process.....	10
5.	Schematic of Batch PCA/ASES/SAS Processes.....	12
6.	Schematic of Continuous PCA/ASES/SAS Processes.....	12
7.	Schematic of Solution Enhanced Dispersion by Supercritical fluid Process.....	13
8.	Schematic of RESS Process for Crystal Doping.....	110
9.	RESS Equipment used in Crystal Doping.....	110
10.	Typical HPLC Chromatogram Showing the Resolution of Theophylline and Caffeine in a Mixture.....	119
11.	Typical HPLC Chromatogram Showing the Resolution of Theophylline and Theobromine in a Mixture.....	119
12.	Change in the Crystal Morphology of Salicylic acid upon Doping with Aspirin.....	121
13.	Effect of Precipitation Conditions On the Morphology of Salicylic Acid + Aspirin Co-Crystals.....	122
14.	DSC Thermograms of RESS Recrystallized Salicylic Acid.....	124
15.	Effect of Precipitation Conditions On the Morphology of Salicylic Acid Crystals.....	126
16.	Effect of Co-solvents On Amounts of Theophylline+Caffeine Collected By RESS Process.....	127
17.	DSC Thermograms of Salicylic acid + Aspirin Mixtures.....	127
18.	DSC Thermograms of Salicylic acid + Benzoic Acid Mixtures.....	127
19.	DSC Thermograms of Aspirin + Benzoic Acid Mixtures.....	129

20. DSC Thermograms of Tolbutamide + Chlorpropamide Mixtures.....	129
21. Reduction in the Crystallinity of Salicylic Acid Co-crystallized with Aspirin.....	133
22. Reduction in the Crystallinity of Salicylic acid Co-crystallized with Benzoic Acid.....	134
23. Effect of Doping with Aspirin on the Crystallinity Of Salicylic Acid....	135
24. Peak Broadening Upon Doping Crystals with Impurities : Aspirin + Benzoic Acid.....	138
25. Peak Broadening Upon Doping Crystals with Impurities : Tolbutamide + Urea.....	139
26. Peak Broadening Upon Doping Crystals with Impurities Naproxen + α -Naphthalene acetic acid.....	140
27. Reduction in the Crystallinity in RESS Produced Co-Crystals of Naproxen + α -Naphthalene Acetic Acid.....	142
28. Reduction in the Crystallinity Upon doping Piroxicam with Theophylline.....	143
29. Amorphous Conversion in RESS Produced Piroxicam + Benzoic Acid Mixtures.....	144
30. DSC Analyses of Piroxicam + Benzoic Acid Mixtures.....	145
31. Reduction in Crystallinity and Amorphous Conversion of RESS Produced Indomethacin + Salicylic acid.....	146
32. Amorphous Conversion and Selective Extraction in RESS Produced Phenytoin+Caffeine.....	147
33. Hydrate formation during RESS Expansion of Theophylline+Caffeine .	149
34. Recrystallization of Theophylline+Caffeine From SCCO_2 +MeOH.....	151
35. Recrystallization of Theophylline+Caffeine From SCCO_2 +Acetone.....	152
36. Recrystallization of Theophylline+Caffeine with Micrometering Valve Setting at 150°C.....	154
37. DSC Thermograms of Tolbutamide Polymorphs I and II.....	155

38. XRPD Patterns Tolbutamide Polymorphs I and II.....	155
39. XRPD Patterns of Tolbutamide Crystals Doped with Urea.....	157
40. DSC Thermograms of Tolbutamide Crystals Doped with Urea.....	158
41. Polymorph Conversions in Tolbutamide+Chlorpropamide: DSC Results.....	160
42. Polymorph Conversions in Tolbutamide+Chlorpropamide: XRPD Results.....	160
43. Selective Extraction from a 80/20 Mixture of Theophylline And Caffeine.....	164
44. Selective Extraction from a 20/80 Mixture of Theophylline And Caffeine.....	164
45. Effect of Process Conditions on the Compositions of RESS Produced Co-Crystals of Theophylline + Caffeine.....	165
46. Effect of Process conditions on the Compositions of RESS Produced Co-Crystals of Theophylline + Theobromine.....	167
47. Selectivity of Extraction in Salicylic Acid+Benzoic Acid Mixtures as a Function of Extraction Conditions.....	168
48. Selectivity of Extraction in Aspirin+Benzoic Acid Mixtures as a Function of Extraction Conditions.....	171
49. Selective Extraction in Indomethacin+Salicylic acid Mixtures.....	173
50. Selective Extraction in Phenytoin+Caffeine Mixtures.....	189
51. Chemical Structures of Chlorpropamide and Urea.....	182
52. Typical Chromatogram of Chlorpropamide + Urea in a Mixture.....	201
53. Calibration Curves at different levels of Chlorpropamide.....	202
54. DSC of Polymorph-A at Different Heating Rates.....	205
55. TGA Thermograms of Chlorpropamide-A.....	206
56. Results of mDSC Analysis performed At a Heating Rate of 5°C/min....	209
57. Results of mDSC Analysis Performed At a Heating Rate of 1°C/min....	209
58. Thermograms of Different Polymorphs of Chlorpropamide.....	210

59. Heat Capacity Values Different Polymorphs of CPD as function of Temperature: 25°C-60°C.....	211
60. Heat Capacity Values Different Polymorphs of CPD as function of Temperature: 60°C-100°C.....	211
61. Photomicrographs of Various Polymorphs of Chlorpropamide.....	213
62. XRPD Patterns of Various Polymorphs of Chlorpropamide.....	215
63. Yields from RESS Recrystallization of CPD as a function of Temperature and Pressure.....	217
64. Dissolution Profiles of Various Polymorphs of Chlorpropamide.....	220
65. XRPD Patterns of RESS Produced Chlorpropamide.....	221
66. XRPD Patterns of RESS Produced Co-Crystals of Chlorpropamide + Urea.....	221
67. SEMs of RESS Recrystallized Chlorpropamide.....	223
68. Binary Phase Behavior of Chlorpropamide and Urea.....	226
69. Illustration of the Proposed Mechanisms of Crystal Disruption.....	230
70. Scanning Electron Micrographs of RESS Produced Chlorpropamide + Urea Co-Crystals.....	233
71. XRPD Patterns of Chlorpropamide+Urea Co-Crystals Recrystallized from Ethanol.....	235
72. XRPD Patterns of Chlorpropamide+Urea Co-Crystals Recrystallized from Ethyl Acetate.....	235
73. XRPD Patterns of Chlorpropamide+Urea Co-Crystals Recrystallized from Hexane.....	235
74. Schematic of SFT Phase Monitor.....	246
75. Phase Behavior of Salicylic acid + SCCO ₂	249
76. Phase Behavior of Chlorpropamide + SCCO ₂	250
77. Phase Behavior of Chloramphenicol + SCCO ₂	251
78. Phase Behavior of Salicylic acid + Aspirin + SCCO ₂	254
79. Phase Behavior of Salicylic acid + EtOH + SCCO ₂	254

CHAPTER ONE

Title: *Supercritical Fluid Technologies in Pharmaceutical Material Processing.*

Abstract: Material processing using supercritical fluids (SCF) has been a subject of recent interest in pharmaceutical drug development. The potential to integrate the synthesis and delivery stages of drug development brought about a wide recognition to the technology. Particle formation using supercritical fluid technology offers the possibility to reduce the number of unit operations, while imparting favorable particle characteristics for downstream processing. Further, SCF technology involves minimal usage of solvents, moderate operating conditions and provides the ability to continuously process materials under cGMP conditions. The technology is rapidly evolving as reflected by the number of modified processes reported since its inception in the pharmaceutical realm. These include Rapid Expansion of Supercritical Solutions (RESS), Gas Antisolvent process (GAS), Particles from Gas Saturated Solutions (PGSS), Precipitation from Compressed antisolvent (PCA), Aerosol Solvent Extraction System (ASES), Supercritical Antisolvent process (SAS) and Solution Enhanced Dispersion by Supercritical fluids (SEDS). The evolution of these technologies chronologically with advances in SCF science is addressed in this article. Applications of supercritical fluid technology in the processing of pharmaceutical solids are also emphasized in this review.

Key words: Supercritical fluids; Particle formation; Review; SCF Technology; Material processing.

1. INTRODUCTION

While organic solvents are extensively used in the processing of pharmaceuticals, there has been a growing concern of late in view of the potential health hazards caused by their emissions and residues in the product. Research aimed at eliminating or reducing their use is an area of particular interest both to the industry and the regulatory agencies. Towards this goal, environmentally safe supercritical fluids (SCF's) appear to be logical alternatives to traditional organic solvents.

While significant advances have been made in such fields as extraction, ceramics, separation science, polymer processing etc, it was not until the recent past [Krukonis 1984, McHugh 1994] that pharmaceutical SCF applications have been realized. Since then, the technology has rapidly progressed as reflected by the number of SCF related publications and patents in pharmaceutical literature. Supercritical fluids have not only established a place in the series of conventional GRAS solvents, but also possess other distinguishing features that make them attractive in a gamut of pharmaceutical applications. SCF technology accordingly holds an immense potential, although the progress to date is limited only to the research laboratories. Table 1 summarizes the various reported pharmaceutical applications of supercritical fluid technology. It is the purpose of this article to introduce the various SCF techniques evaluated to date primarily in pharmaceutical material processing. For purposes of clarity, each of these evolving techniques is dealt with in separate sections.

Table 1. Potential Applications of SCF Processes in Solid Drug Processing

<u>Application</u>	<u>References</u>
Extraction	Mulcahey LJ 1992, Yang 2002
Micronization	Donsi 1991, Rogers 2001
Nanoparticles	Mohamed 1989b, Chattopadhyay 2001
Microencapsulation	Kim 1996, Bleich 1996
Particle coating	York 1995, Subramaniam 1998
Crystal modification	Robertson 1996, Weber 1997
Solid dispersions	Mura 1995, Kerk 1999
Dissolution enhancement	Loth 1986, Van Hees 1999
Amorphous conversion	Ohgaki 1990, Jaarmo 1997
Infusion/Impregnation	Berens 1989, Carli 1999
Liposomes	Frederiksen 1997, Castor 1998
Granulation	Lindsay 1992, Mandel 1999
Polymorph separation	Kordikowski 1999, Beach 1999
Extrusion	Lee 1998, Daly 2001
Polymerization	Rajagopalan 1998, Muth 2000

A comprehensive review of origin, theory, practice and applications is included in each section.

2. BACKGROUND

Critical point for any pure substance is defined by the temperature and pressure coordinates above which no physical distinction exists between the liquid and gaseous states. Substances in this region of the phase diagram are referred to as 'supercritical fluids'. Many thermophysical properties change abruptly around the critical point. Due to the very high compressibilities of supercritical fluids, large changes in density and therefore solvent properties can be affected by fine adjustments of pressure. Supercritical fluids exhibit properties that are intermediate between liquids and gases [Tom 1991b]. These unique properties of SCF's are utilized in the material processing of pharmaceuticals. For example, liquid-like solvent strength can be continuously adjusted over a wide range from $\delta = 0$ to 9 (cal/cc)^{1/2} [Perry 1997] by changing the pressure and temperature while utilizing gas-like transport properties. Other properties of supercritical fluids as applicable to the various SCF techniques will be discussed in their respective sections. Supercritical carbon dioxide is the most commonly used SCF for pharmaceutical applications as it is considered non-toxic, nonflammable, inexpensive and has a moderately low critical point. Some of the physical properties of supercritical CO₂ are summarized in Table 2.

Table 2. Properties of CO₂

<u>Property</u>	<u>Value</u>	<u>Condition</u>
Molecular Weight	44.01	-
Boiling point	-78.4°C	Atmospheric pressure
Triple Point temperature	-56.5°C	-
Critical point	[31.1C, 1070.1psi]	-
Vapor pressure	838psi	At 21°C
Dipole moment	0	-
Quadupole moment		-
Acentric factor	0.224	-
Compressibility factor	0.277	At Critical Point
Thermal Conductivity	0.0166 W/m-K	At 25°C
Heat capacity	1.66×10^{-5} J/Kmol-K	At 25°C
Density	0.47 g/cc	At Critical Point
Solubility parameters	0 to 9 (cal/cc) ^{0.5}	[31-70°C, 14.7-14500psi]
Dielectric constant	1.6	-
Polarizability	26.5×10^{-25} cm ³	-
Diffusivity	10^{-3} to 10^{-4} cm ² /s	-
Viscosity	0.02-0.09 cps	[37-77°C, 580-5800psi]
Surface tension	~0	-

This section introduces the reader to the origin of SCF material processing and various modifications thereof. Various processes to be discussed hereunder (Table 3) can be best envisioned as the different permutations of contacting the solvent, solute(s), cosolvent, antisolvent and precipitating the solute thereafter. The state of solute prior to the precipitation and the mechanism of solute precipitation is what distinguishes one process from the other. In principle, the basic advantages of supercritical fluid particle formation such as rapid and uniform nucleation remain the same in all the various processes, although the mechanism of particle precipitation varies with the process. From a processing standpoint, the simplest of the processes (Figure 1) involves exposing the solute or a mixture of solutes to supercritical fluid for a fixed period of time. Rapid venting of the SCF leaves a solid product with enhanced attributes [Sand 1986]. In this process, SCF is used as a solvent or as a swelling agent, that may be rapidly removed via depressurization. An extension to this process that gives additional control over product morphology is called supercritical fluid nucleation [Krukoniš 1984] or rapid expansion of supercritical solutions (RESS, Figure 2) [Matson 1987]. Herein, the solute(s) of interest is dissolved in a SCF at fixed extraction conditions. The solution is then rapidly depressurized through a restrictive device that is designed to tailor the product morphology. Solute interaction with SCF leading to its dissolution/swelling is a primary requirement to process solids using the above methods. However, the solubility of most drugs and pharmaceutical polymers [Alessi 1997, Subramaniam 1998] in SC CO₂ is prohibitively low,

Table 3. Distinguishing Various Supercritical Fluid Processes

	PROCESS	ACRONYM	Solute(x1)	Solvent(x2)	Antisolvent(AS)
1	Rapid Expansion of Supercritical Solutions	RESS	Drug or Drug mixture	Pure or modified SCF	Absent
2	Particles from Gas Saturated Solutions	PGSS	Compressed gas/SCF	Melt of Drug/ Drug mix	Absent
3	Gas Antisolvent System	GAS	Drug or Drug mixture	Liquid Organic solvent	SCF/Compressed gas
4	Precipitation using Compressed Antisolvent	PCA	Drug or Drug mixture	Liquid Organic solvent	SCF/Compressed gas
4.a	-Acrosol Solvent Extraction System	ASES	Drug or Drug mixture	Liquid Organic solvent	SCF
4.b	-Supercritical Antisolvent System	SAS	Drug or Drug mixture	Liquid Organic solvent	SCF
5	Solution Enhanced Dispersion by Supercritical fluids	SEDS	Drug or Drug mixture	Liquid Organic solvent with/without water	SCF, also acts as dispersing fluid

	Method	Mechanism of particle precipitation
RESS	Solution of x1 in x2 rapidly expanded	Loss of SCF solvent power after rapid evaporation
PGSS	Solution/Dispersion of x1 in x2 rapidly expanded	Phase change in x1+Joule Thompson Cooling
GAS	AS bubbled through solution of x1+x2	Volumetric expansion of solvent by gas
PCA	x1+x2 sprayed into AS (or)	x2 evaporation into AS
ASES	Same as above	Same as above
SAS	Same as above	Same as above
SEDS	x1+x2 and AS flowed through coaxial nozzle	Dispersion of x1 by AS+x2 evaporation into AS

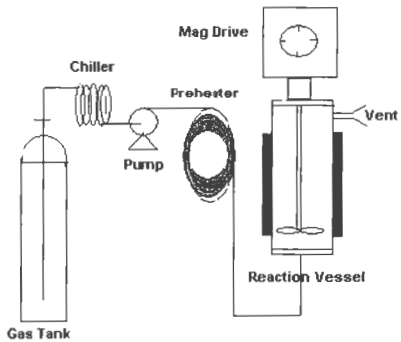


Figure 1. Schematic of Static Supercritical Fluid Process

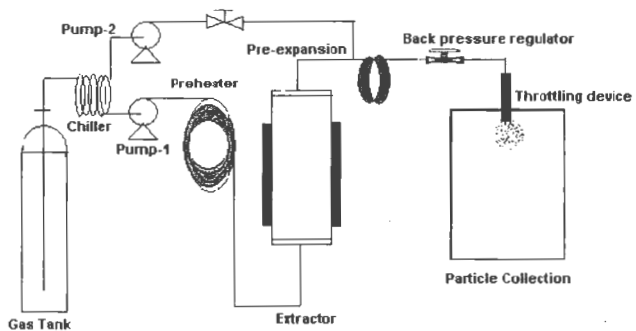


Figure 2. Schematic of Rapid Expansion of Supercritical Solution Process

resulting in poor yields. A further development involved the use of cosolvents that modify solubility behavior in supercritical fluids [Dobbs 1986]. The solubility enhancement factors although high (up to 500%) with certain cosolvents, still do not provide a realistic means to produce mass powders and mixtures on pilot scales. Further, the advantages of pure SCF crystallization may be compromised with the use of cosolvents. This stems from the fact that solute recrystallization occurs from the condensed cosolvent and not from the supercritical phase as observed by Larson & King [Larson 1986].

Another method of particle formation by recrystallization from pure SCF is particles from gas saturated solutions (PGSS, Figure 3) [Weidner 1995]. Unlike dissolving the solid in SCF (see RESS), PGSS involves dissolution of SCF in a solid melt and subsequent expansion through a restriction device. The process is based on the fact that gases have higher solubility and diffusivities in liquids than in solids. Thermal stability of drug compounds and significant solubility of SCF in the melt are the primary requirements for PGSS.

However, the poor solubilities of many drug compounds in SC CO₂ propelled research efforts towards the use of SCF's as antisolvents. This approach formed the basis for gas antisolvent precipitation [Gallagher 1989] (GAS, Figure 4), wherein a gas is bubbled through an organic drug solution. Large volumetric expansion of the organic solution as a result of dissolved gas coupled with solvent extraction by SCF leads to high supersaturation and hence solute precipitation. Solubility requirements in this case include (i) miscibility of

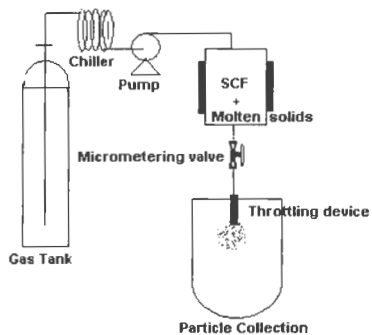


Figure 3. Schematic of Particles From Gas Saturated Solution Process

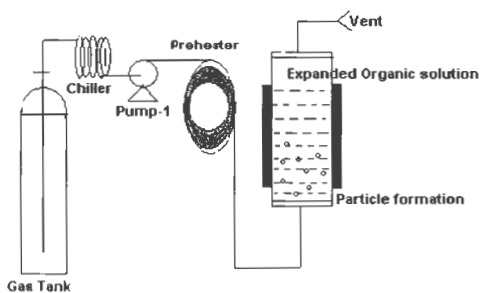


Figure 4. Schematic of Gas AntiSolvent Process

organic solvent with the SCF, (ii) negligible interaction between drug & SCF and (iii) partial solubility of drug in the organic solvent. Realizing the fact that solvent-SCF mass transfer rates are higher from a fine spray than from the bulk solvent, modifications have been made that constitute processes like precipitation using compressed antisolvent (PCA) [Bodmeier 1995], supercritical antisolvent process (SAS) [Bertucco 1996] and aerosol solvent extraction system (ASES) [Bleich 1993]. These processes are schematically shown in Figure 5. Herein, an organic drug solution is sprayed into a compressed gas (PCA) or a supercritical fluid (SAS or ASES) that selectively extracts the solvent and thereby causes precipitation of solute.

With the objective of improving extraction conditions, simultaneous introduction of the drug solution and SCF has also been evaluated. This formed the basis for continuous PCA/ASES/SAS processes [Figure 6] as well as solution enhanced dispersion by supercritical fluids process [York 1995] (SEDS, Figure 7). In SEDS, the mechanical energy of rapidly expanding gases is streamlined into dispersing a drug solution by passing through a coaxial nozzle. This enhances the extractive capability of the SCF's, thereby precipitating microparticles with desired attributes.

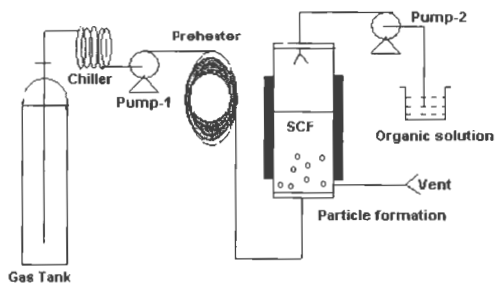


Figure 5. Schematic of Batch PCA/ASES/SAS Processes

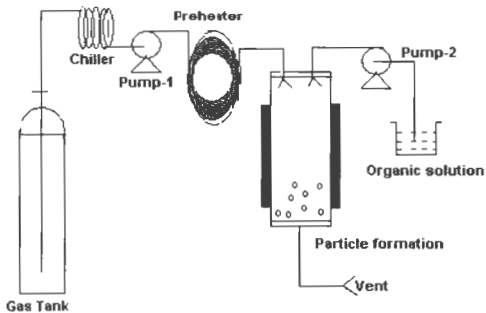


Figure 6. Schematic of Continuous PCA/ASES/SAS Processes

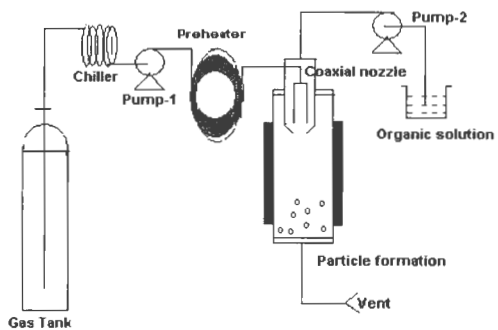


Figure 7. Schematic of Solution Enhanced Dispersion by Supercritical fluid Process

3. STATIC SUPERCRITICAL FLUID PROCESS

3.1 Mechanism:

Placing a solute or a mixture of solutes in contact with SCF or a near critical fluid for a fixed period of time is shown to affect the solute properties in different ways. If the solute(s) has some solubility in the SCF, the process is analogous to conventional solvent-based recrystallization with a compressed fluid or SCF replacing the organic solvent. Supercritical fluids exhibit a combination of the features of liquids and gases. Like liquid solvents, SCF's allow intimate mixing of solutes at a molecular level during solubilization. At the same time, the supercritical fluid turns into a rarified gas when depressurized. Owing to the high diffusivities, low viscosities and zero surface tension of gases, easy solvent removal is implicit with SCF recrystallization. Thus, the process offers a means of producing solvent free drugs and drug mixtures. The solvating and swelling properties of SCF coupled with their high diffusivities form the basis for this process.

Studies have shown that supercritical CO₂ has the ability to swell a number of glassy polymers [Wissinger 1987, Wissinger 1991, Shieh 1996b, Kazarian 1996]. Sorption of CO₂ into an amorphous polymer matrix weakens the intermolecular forces that bind the polymer chains together, leading to an increase in the molecular motion. As a result, a depression in T_g and plasticization of the polymer are observed upon CO₂ sorption. Theoretical and practical considerations of the sorption of supercritical fluids and gases in polymers have been extensively

dealt with by a number of authors. [McHugh 1994, Sefcik 1986a, Sefcik 1986b, Hirose 1986, Wissinger 1991; Wissinger 1987, Condo 1992, Shieh 1996a; Shieh 1996b, Kazarian 1997, Kazarian 1996] Pharmaceutical polymers that are relevant in this context include PLGA, Cross-linked PVP, Cross-linked PMMA, Cross-linked sodium starch glycolate, Ammonium glycyrrhizinate, Polyacrylic acid, Gelucire 50/02, Compritol 888ATO, Lubrifiant W13284, Carbopol 974P etc.

3. 2 Process:

The solution of drug in SCF is brought into contact with the polymer for a time sufficient to permit sorption into the polymer. Rapid decompression of the system results in the loss of SCF's solvent power leading to solute deposition within the polymer matrix. Also, SCF becomes gaseous and rapidly diffuses out of the polymer, leaving a solute laden polymer. System requirements to carryout this process include a high pressured vessel capable of withstanding the operating pressure and temperature (Figure 1, p8). Mixing of the contents in the vessel while under pressure is shown to be important for homogenous infusion [Juvekar 1994, Muth 2000]. Stirring of the contents in the pressurized vessels has an inherent difficulty arising from the moving parts that cause the leaks. This can be circumvented by the use of magnetic mixers. Typical operating conditions are T= -55 to 60°C, P=600-4300psi, t=15-300min, v=0.01-5 ft/sec [Lindsay 1992].

3.3 Applications:

Typical applications utilizing this process employ the impregnation/infusion of solutes in porous supports, forming intimate mixtures of actives & excipients, solid dispersions, polymerization and micronization. Reported applications of this technique are summarized in Table 4. As can be seen from the table, a number of small drug molecules have been impregnated into porous supports and polymers using the above technique. A preferred drug molecule is one that shows some degree of solubility (at least 0.1 wt%) in the SCF. Also, some degree of interaction between the SCF and the polymer is necessary for polymer dilation (at least 2 vol%) [Berens 1989]. Partitioning of the solute in a swollen polymer is controlled by adjusting the concentration of solute in SCF and the rate of venting. The degree of loading and the form of the resulting mixture therefore depend on the temperature (T), pressure (P), mixing conditions, time of exposure(t), and venting rate(v) as well as the properties of drug, SCF and polymer discussed above.

The degree of success achieved using this technique is limited, considering the poor interaction of many pharmaceutical compounds and excipients with SC CO₂. While a compound's solubility in SC CO₂ limits the level of loading that may be achieved, it is not the only factor in determining the efficacy of the process.

Table 4. Applications of the Static Supercritical Fluid Process

Agent	Substrate(s)	Conditions		Contact	Application	Reference
		T	P	Time		
Catalase	PLGA	45 C	2940psi	30 min	Solid dispersion of catalase in PLGA, Drug loading 1-50%	Howdle 1998
Dimenhydrinate	Oxyethylate lincolal + MCC + Calcium Stearate	20 C	1500psi	30min	Granulation for tableting	Lindsay 1992
Dimenhydrinate	Ethylene Glycol-Copolymer of Ethylene and Propylene Oxides	20 C	760psi	5 hr	Transdermal application	Lindsay 1992
Nimesulide	Cross-linked PVP	60 C	2350psi	8 hr	Impregnation, Loading 25%	Carli 1999
Acyclovir	Cross-linked PMMA	50 C	3230psi	24 hr	Impregnation, Loading 21%	Carli 1999
Ketoprofen	Cross-linked PVP	60 C	2350psi	9.25hr	Impregnation, Loading 25%	Carli 1999
Piroxicam	Cross-linked sodium-starch glycolate	60 C	2350psi	1hr	Impregnation, Loading 15%	Carli 1999
Cimetidine	Acrylic acid cross-linked-with allylic esters of sucrose	60 C	2350psi	2hr	Impregnation, Loading 20%	Carli 1999
Progesterone	Polyurethane; Polycarbonate	45 C	1031psi	4.5hr	Controlled Release, 8%, Loading	Bereus 1989
alpha-tocopherol acetate	Aerosil 972	40 C	4410psi	1.5hr	Impregnation upto 25%	Magnan 1996
Piroxicam	beta-cyclodextrin	150 C	2175psi	6hr	1:2.5mol:mol inclusion of Piroxicam in Cyclodextrin	Van Hees 1999
Scopolamine	NS	NS	NS	NS	Impregnation	Sand 1987
PLGA	-	22 C	800psi	72hr	Porous sponges	Mosney 1996
PVC	PMMA	40-80 C	5600psi	4 hr	Heterogenous Polymerization	Muth 2000

*C₀ is the SCF used in all the above reported studies

Recent reports have shown that the technique is amenable to hydrophilic drug and polymer processing [Zia 1997, Lindsay 1992, Howdle 1998]. Specific intermolecular interactions that come into play need to be addressed for the system under study in evaluating this process.

4. RAPID EXPANSION OF SUPERCRITICAL SOLUTIONS (RESS)

4.1 Introduction:

Supercritical fluids exhibit remarkable solvent properties compared to gases. In the vicinity of a fluid's critical point, solvent strength was found to be a very sensitive function of pressure and temperature. Increased solvent strengths of SCF's compared to gases are attributed to the liquid-like densities of the fluids [Kumar 1988]. CO₂ for example, has a density of 0.47 g/cc at its critical point, close to the density of Hexane (0.66g/cc at 25°C) [Dixon 1997]. On the other hand, SCF's also exhibit gas-like behavior (eg. high diffusivity, low viscosity and zero surface tension) [McHugh 1994]. These intermediate features of SCF's have been utilized in a variety of applications including RESS.

4.2 Mechanism:

In RESS, the solute of interest is dissolved in a supercritical fluid. The high solvent power of the SCF allows formation of a homogenous solution. Nucleation of solute is then induced by rapidly reducing the solution density through expansion to atmospheric conditions. A rapid decrease in solvent strength results

in high supersaturation that leads to very high nucleation rates [Mohamed 1989b]. The time for crystal formation and growth is very limited (typically 10^{-5} to 10^{-6} seconds) resulting in very small particles [Debenedetti 1993b, Turk 1999]. In addition, the rapid decompression of SCF generates mechanical perturbation within the solution that travels at the speed of sound. Consequently, very uniform conditions are reached within the nucleating media. Narrow size distributions typical of RESS processed materials is attributed to the above mentioned behavior [Tom 1991b]. Thus, RESS provides a means of forming microparticles with a unimodal particle size distribution.

The morphology of the particles formed essentially depends on the phase of solution from which the solute is precipitated. The thermodynamic factors that control the phase behavior of solutions are pre-expansion temperature and pressure (T,P), solution composition(x) and post-expansion temperature and pressure. While solute vapor pressure behavior and chemical interaction dictate solid solubility in the SCF, solvent physicochemical/transport properties need to be considered for precipitation. Preliminary solid solubility studies in the SCF not only help to choose the extraction conditions, but also identify the conditions ideal for solid precipitation. Researchers have attempted to correlate product morphology with the T,P,x conditions of the system and form a theoretical basis for particle growth [Mohamed 1989a, Helfgen 2000, Tom JW 1991b]. Most of such attempts to date have only resulted in qualitative models. To this end, density of the solution from which precipitation occurs, the time scale allowed for

precipitation and growth, as well as agglomeration were shown to have a major effect on particle morphology. A comprehensive model should take into account the combined effects of T, P, x at each stage of RESS process on the above factors.

Among the process variables that play an important role in particle tailoring, the geometry of the restriction device through which expansion occurs merits a special mention. A restriction device is designed to support the large pressure drop that occurs across it, while maintaining suitable conditions for precipitation. Various configurations have been evaluated to date, for example capillaries, nozzles, laser drilled discs and valves. The Joule-Thompson cooling effect, observed as a result of large volumetric expansion in turn produces a drop in the temperature of the nozzle. This leads to supersaturation and premature precipitation of the solute. Plugging of nozzles that is commonly observed in a continuous RESS process results from premature precipitation of solutes in the expansion line. The restriction devices are therefore heated to prevent clogging. Typical aspect ratios of the restriction devices evaluated to date are in the range of 6 to 20, with orifices from 20 to 1600 μ in diameter. The effects of different geometrical configurations of the restriction devices on the morphology of particles have also been investigated [Matson 1987, Mohamed 1989b, Kim 1996]. As a result of these studies, theoretical models addressing the fluid dynamics during expansion and particle growth therein are developed [Matson 1987, Lele 1992, Debenedetti 1993a].

Poor yields owing to the low solubility of many pharmaceuticals in SCF's is a major limitation of the RESS process. Use of co-solutes and co-solvents to improve the solubility of solutes in SCF's have been investigated. Tavana and Randolph [Tavana 1990] have shown that the solubility of salicylic acid in SC CO₂ can be enhanced by an order of magnitude in the presence of a more volatile co-solute like benzoic acid. Similar observations were reported by Kurnik [Kurnik 1982] and Pennisi [Pennisi 1986]. The enhancement of solubility has been attributed in all these cases to the vapor pressure effects of the more volatile co-solute. For further details about solubility of mixtures in supercritical fluids, the reader is advised to refer to a recent review by Lucien and Foster [Lucien 2000]. Various research groups have evaluated the design and synthesis of CO₂-philic polymers and surfactants that aid in the solubility enhancement of solutes in SC CO₂ [McClain 1996, Ghenciu EG 1997, Ghenciu 1998, Yazdi AV 1997, Super 1997]. To date, the success with such enhancement aids has been marginal, although the potential for such research using pharmaceutical polymers and surfactants is tremendous.

The practical and theoretical aspects of using co-solvents to enhance solid solubility in SCF's (for the most part SC CO₂) have been extensively evaluated by a number of researchers [Dandge 1985, Wong 1986, Dobbs 1986, Larson 1986, Ting 1993]. Various mechanisms of solubility enhancement by co-solvents have been postulated [Ekart 1993]. A co-solvent may enhance solute solubility through specific chemical interactions like hydrogen bonding, complexation and charge

transfer. Physical interactions with the solute like dipole-dipole, dipole-induced dipole and induced dipole- induced dipole may also lead to solubility enhancement. Further, a co-solvent can modify the physical properties of the solvent such as dielectric strength, polarizability, density, etc and thereby cause solubility enhancement. Tavana et al have demonstrated a systematic approach for screening co-solvents with two model compounds griseofulvin and digoxin [Tavana 1989]. The co-solvents are ranked based on the GC retention time with SCF+co-solvent being the mobile phase and solute as the stationary phase. Given the restrictions on the choice of organic solvents in pharmaceutical processing, co-solvent use in RESS processing has been very limited. In addition, the presence of a co-solvent can sometimes adversely effect the product characteristics by condensing in the precipitation vessel [Larson 1986]. In such instances, recrystallization occurs from the condensed co-solvent and not from the supercritical phase, thereby losing the very attributes of RESS [Larson 1986, Mohamed 1989b]. It is therefore important to select pre-expansion conditions that allow precipitation from a single fluid phase. Also, pre-expansion temperature and conditions in the precipitation vessel should be chosen such that the co-solvent stays in vapor phase after expansion. With proper choice of conditions, the removal of SCF and co-solvent should leave solid dry particles within the precipitation vessel. This however, is not an easy task considering the complex phase behavior exhibited by a three component SCF-solute-cosolvent system.

RESS has been evaluated in many of the processing areas where organic solvents can be replaced by a SCF. The pivotal role of solvents in crystallization, forming intimate mixtures of different substances that requires mixing at a molecular level, coating, etc requires no special mention. SCF solvents not only aid in serving these objectives, but also possess other distinguishing features that make the RESS process unique. One of the major advantages in RESS is the ease of solvent removal, in contrast to solvent evaporation. While the former is triggered by the thermal perturbations, the latter occurs due to mechanical decompression at supersonic velocities [Debenedetti 1993b]. The primary requirement for a solute to be processed by RESS is a significant solubility in SCF (>0.5 wt%) [Alessi 1996]. Among the pharmaceutical class of compounds, steroids with a basic perhydrocyclopentanophenanthrene ring have shown significant solubility in SC CO₂ and are particularly suitable for RESS processing.

4.3 Process:

The basic components of a RESS apparatus consist of a pump to deliver the SCF, preheater, extraction vessel, preexpansion chamber, throttling device and a precipitation vessel (Figure 2). Liquid CO₂ from a tank is fed to the preheater at a controlled flow rate using the pump. Typically, an air driven pump is used to pressurize the CO₂ prior to delivery to the preheater. The function of the preheater is to bring the temperature of the pressurized liquid to the supercritical region. The preheater is typically a lengthy stainless steel tube immersed in a temperature

controlled bath. Pressure and temperature in the preheater are read using pressure transducers and resistive temperature devices (RTD) that have a sensitivity of 0.05-0.1%. SCF from the preheater then flows into the extraction vessel that contains the material to be processed. Packing the extractor with alternate layers of glass wool and solute has been shown to improve extraction efficiency by providing better fluid contact with solute. Alternatively, a mixing device may be used that agitates or stirs the contents of the vessel. The pressure and temperature in the extractor are recorded using a pressure transducer and RTD respectively. The saturated solution from the extractor flows into the pre-expansion chamber that has independent temperature control and a line connecting it to the preheater. The saturated supercritical fluid solution can be diluted with fresh solvent from the preheater, allowing control over the composition of the solution prior to expansion. Interfacing a HPLC system at this point helps determine the exact composition of solution prior to expansion. The fluid from the pre-expansion chamber is rapidly expanded through a heated restriction device into the precipitation vessel. For the most part, the effects of post expansion pressure and temperature on product morphology are inconclusive or relatively insignificant. Excepting situations where post expansion conditions have been shown significant [Mohamed 1989a], or where fluid recompression costs are a factor, the precipitation vessel in most instances is maintained at atmospheric conditions. Typical extraction conditions are $T=40-80^{\circ}\text{C}$, $P=2000-5000\text{psi}$. The pre-expansion temperature is generally maintained at about 50°C higher than the

extraction temperature to prevent premature precipitation, which in turn leads to plugging of lines. Solute throughput in a RESS process depends on its solubility in the supercritical fluid and is typically up to 1 g/hr with solvent flow rates ranging between 20-80 standard liters per hour [Tom 1991b].

4.4 Applications:

One of the potential applications of rapid expansion of supercritical solution process is in the area of particle size reduction. The RESS process, in principle, offers the advantage of growing the crystals to a desired size unlike most other high energy comminution techniques like wet milling, spray drying etc. Most of these processes commonly involve energizing the particles to bring about size reduction. The implications of imparting energy into the system are pronounced when dealing with proteins, peptides, and other unstable compounds. Accordingly, particles generated using RESS process frequently retain their crystallinity and do not carry static charge. Particles with various morphologies like microspheres, needles, fibres, dendrites, etc. were produced by changing the process conditions. Production of micron and submicron particles with a narrow size distribution has been demonstrated with a range of compounds (Table 5). A universal model relating process conditions to product morphology is yet to be developed, but definitive trends have been observed in each of these compound specific studies. Agglomeration of particles was prominent, as observed with cyclosporine [Henriksen 1997] and lovastatin [Mohamed 1989b], when the

Table 5. Summary of RESS Studies

Agent	SCF	Extraction		Pre-expansion		Application	Average Diameter	Additional Comments	Reference
		T(°C)	P(psi)	T(°C)	P(psi)				
beta-carotene	CO ₂	70	4500	NS	NS	Micronization	0.3u	CO ₂ reacted with drug & formed an epoxide	Chang 1989
beta-carotene	C ₂ H ₆ + Toluene	70	4500	NS	NS	Micronization	0.5u	Agglomeration reduced by precipitation into gelatin Tween 80	Chang 1989
beta-estradiol	CO ₂	55	5070	NS	NS	Micronization	1.1u	-	McHugh 1994
Grisofulvin	CHF ₃	60	2600-3200	60-150	2600-3200	Micronization	1.1u	Long needles to quasispherical particles	Reverchon 1995
Medroxyprogesterone acetate	CO ₂	50-60	2200	40-60	NS	Micronization	1.5u	-	Alessi 1996
Lovastatin	CO ₂ + MeOH	40	5500	NS	NS	Micronization	10-50u	Recrystallized from cosolvent	Larson 1986
Nifedipine	CO ₂	70	8700	NS	NS	Micronization	1-3u	-	Stahl 1987
Progesterone	CO ₂	50-60	1800-3600	40-60	NS	Micronization	4-8u	Large dendrites to micron particles	Alessi 1996
Salicylic acid	CO ₂	40-60	2940-3800	60-140	3800	Micronization	1-10u	Needles,Spheres,Network	Reverchon 1995
Testosterone	CO ₂	60	5150	NS	NS	Micronization	2-3u	-	McHugh 1994
HYAFF-11	CO ₂	60-80	2940			Micronization	1-10u	Microspheres to aggregates	Henedetts 1997
L-PLA	CO ₂	55	3675	70	NS	Micronization	4-10u	Needles to Microspheres	Tom 1991a
L-PLA	CO ₂ + acetone	55	2900-3400	75-120	NS	Micronization	10-25u	Microparticles to dendrites	Tom 1991a

Table 5. Summary of RESS Studies (Cont'd)

Agent	SCF	Extraction		Pre-expansion		Application	Average Diameter	Additional Comments	Reference
		T(°C)	P(psi)	T(°C)	P(psi)				
L-PLA	CCl ₄	55	1700	70-83	NS	Micronization	2-20 μ	Needles to microspheres	Tom 1991a
PGA	CO ₂	55	2650-3000	82	NS	Micronization	10-20 μ	Ovals&Rectangles and Needles	Tom 1991a
Poly(methyl methacrylate)	ClCH ₂	70-100	2000-3000	110-130	NS	Micronization	NS	Powder to Fibre precipitates	Lele 1992
Polycaprolactone	ClCH ₂	100	2000-3000	90-145	NS	Micronization	1-5 μ	Spherical particles to fibres	Lele 1992
Polystyrene Poly(methyl methacrylate) copolymer	ClCH ₂	75-100	1500-4000	110-130	NS	Micronization	NS	Powder to Fibre precipitates	Lele 1992
Lovastatin-DL-PLA	CO ₂	55	2900-3700	75-85	NS	Microencapsulation	10-100 μ	Loading 27%	Tom 1993
Naproxen-L-PLA	CO ₂	60	2750-3100	90-140	NS	Microencapsulation	1-15 μ	Agglomerates, Microparticles, Microspheres	Kim 1996
Carbamazepine	CO ₂	35-100	2000-5000	NS	NS	Polymorph conversion	<3 μ	alpha to gamma form	Gosselin 2000
Phenacetin	CO ₂	60	8820	NS	NS	Dissln enhancement	8 μ	20-30 fold improvement	Loth H 1986
Phenacetin	ClF ₃	80	7350	NS	NS	Dissln enhancement	10 μ	Same as above	Loth 1986
Stigmasterol	CO ₂	35	1450-2030	100-150	1450-2030	Amorphous Conversion	0.05-0.2 μ	Amorphous globes to Whiskers	Ohgaki 1990
Benzoic acid	CO ₂	45-70	1470-3700	NS	NS	Crystal modification	10-20 μ	Change in crystal habit	Robertson 1996
Cyclosporine	CO ₂	35	3000	40	NS	Nanoparticles	80nm	Precipitated into Tween80-Phospholipid	Henriksen 1997
Lovastatin	CO ₂	75	5500	105-135	NS	Nanoparticles	200nm	Deggregated by sonication in Heptane	Mohamed 1998b

particle size was in the nanometer range. Deaggregation of nanoparticles by precipitating into a surfactant is a solution, although it involves further downstream processing in an otherwise single-step RESS process.

The potential of RESS micronization in dissolution rate enhancement has been verified by Loth and Hemgesberg [Loth 1986]. Twenty to thirty-fold enhancement in aqueous dissolution rate of RESS processed phenacetin is observed after it is blended with aerosol R972 or mannitol. The majority of the compounds produced by RESS have crystallinity unaltered as a result of processing. Exceptions are few where the process has resulted in a change of crystallinity of the solute. Ohgaki et al produced stigmasterol particles with varied morphology from amorphous globes to whisker-like crystals [Ohgaki 1990]. While a change in the crystal habit of benzoic acid is claimed in the study by Robertson J et al, further characterization remains to be done before any definitive conclusions can be made [Robertson 1996]. In a more recent study, Gosselin PM et al have demonstrated the controlled polymorphic conversion of carbamazepine by RESS process [Gosselin 2000]. RESS as such can be potentially used in cleaning up polymorphs by utilizing the selective extraction capabilities of SCFs. Efforts to understand the mode of particle growth from supercritical fluid solutions are still ongoing and involve an interplay of the complex SCF phase behavior and the SCF fluid dynamics during expansion.

Another area of potential RESS application is in the microencapsulation of drugs within polymeric matrices for controlled release applications. Polymers

studied in RESS include poly ([L+]-lactic acid) (L-PLA), poly(D,L-lactic acid) (DL-PLA), poly(glycolic acid) (PGA), polycaprolactone, poly(methyl methacrylate), styrene/methyl methacrylate and polystyrene/poly(methyl methacrylate) block copolymer. Polymers are selectively extracted by SCF's with the lower molecular weight fractions solubilizing faster than the higher end. It is therefore important that the polydispersity of the polymers is kept to a minimum to produce identical microspheres throughout the process. Initially, the polymer and the drug are screened independently to select appropriate conditions for microsphere formation [Tom 1993, Kim 1996]. Coprecipitation of drug and polymer is then carried out with an optimal balance of process conditions to form microparticles or microspheres. A complete understanding of the 3-component phase behavior is necessary to prevent independent precipitation of solutes. Microcapsules (10-100 μ) of lovastatin needles embedded in DL-PLA have been produced [Tom JW 1993]. The authors proposed that the readily soluble lovastatin was extracted first and then acted as a nucleating site for the later precipitating polymer. Similar results with a better dispersion of drug within polymer were reported for pyrene and naproxen in L-PLA [Tom 1994, Kim 1996].

In comparison with the conventional solvent evaporation and coacervation techniques of solid formation, RESS offers an effective means of producing micron and submicron particles with unimodal size distribution. However, the limited solubility of many pharmaceuticals in the most widely used SCF viz. CO₂

restricts its application to a few low molecular weight lipophilic compounds. Also, theoretical understanding of the process is limited and further complicated by the introduction of a third component such as a co-solvent or a polymer. Future research should aim at identifying potential approaches to improve solute solubility in SCF and generalize the effect of process conditions on RESS product morphology.

5. PARTICLES FROM GAS SATURATED SOLUTIONS (PGSS)

5.1 Introduction:

The solubility of solid solutes in SCFs and vice versa have been explored in RESS and the basic supercritical fluid processes discussed above. Considering the scarcity of interaction observed leading to low solubilities and poor yields, a logical alternative is to exploit the solubility of SCFs in solid melts (liquids). This approach forms the basis for yet another particle formation process called PGSS.

The solubility of SCFs in liquids is about three to four orders of magnitude higher than the typical solid solubilities in SCF [Weidner 1996]. Accordingly, the product yield of PGSS process is significantly high in comparison to poor RESS throughputs. Also, the fluid consumption in PGSS is considerably reduced compared to RESS. A distinguishing feature of PGSS, in contrast to the other SCF techniques of particle formation is the complete absence of co-solvent use.

5.2 Mechanism:

The schematic of a typical PGSS process is shown in Figure 3. In PGSS, the solid(s) to be processed is melted to form a single liquid phase prior to saturation with a compressed gas or a supercritical fluid. The pressure and temperature conditions of the SCF are chosen such that solid melt is highly saturated with SCF. The highly saturated solution of SCF-solid melt is then rapidly expanded through a restriction device, similar to the one described in RESS section. Rapid expansion causes precipitation of a dry powder via two different mechanisms. Due to the temperature drop of the solid melt and the high supersaturation caused as a result of rapid expansion, solid micron particles precipitate in the collection chamber. Compounds with negligible solubility in SCF, a low melting point, thermal stability and sufficient solvent strength for the SCF are reported to be most suitable for PGSS processing.

The solubility of a compressed gas in a liquid (or a solid melt) depends on the pressure, temperature and physicochemical interactions between the gas and the liquid [Martin 1993]. With proper choice of pressure and temperature conditions for the system under study, up to 50% by weight of compressed gas can be dissolved in the solid melt [Weidner 1996]. Preliminary solubility and phase behavior studies of the compressed gas in drug or drug-excipient mixtures are critical to the selection of proper conditions. A general rule of thumb is to start at the liquefaction conditions of the drug/ drug mixture that result in the formation of solid drug particles, devoid of gas after expansion. The pressure of

the compressed gas has varied effects on the liquefaction temperature of the compound(s). While static pressure overhead causes melting point elevation, dissolved gas in the solid leads to a drop in its melting point. The combined effects of these competing factors on the liquefaction temperature should be evaluated as a function of pressure, prior to choosing the saturation conditions.

To date, studies on the solubility of compressed gases/SCFs in pharmaceutical solids are very limited. Also, understanding of the relation between the physicochemical properties of compounds and their solvation power for compressed gases is rather primitive. Within the same chemical class of polyethylene glycol polymers, Weidner et al have shown that the solubility of compressed CO₂ is practically independent of the polymer molecular weight [Weidner 1996]. Reported studies using a divergent class of chemical compounds (Table 6) support the theory that the properties of a compound have a weak influence on the SCF solubility, often outweighed by the P,T effects of the process. The PGSS process involving dispersion of a compressed gas in a solid melt is also shown to form powder particles [Mura G 1995]. A clear understanding of the solubility influence on product morphology remains to be established.

5.3 Process:

The basic components used in producing particles from gas saturated solutions are a pump to pressurize carbon dioxide, a saturation vessel capable of withstanding

Table 6. Summary of PGSS Studies

Agent	SCF	Conditions Measured		Application	Mean particle size	Remarks
		T(°C)	P, psi			
Felodipine	CO ₂	150	2940	Dissolution Enhancement	42u	Improved after mixing with lactose
Felodipine+PEG4000	CO ₂	60-150	2575-2800	Solid dispersion	NS	Dissolution rate improved 13.5 times
Fenofibrate	CO ₂	65-80	2800	Dissolution Enhancement	7-32u	Agglomeration
Fenofibrate+PEG4000	CO ₂	65-80	2800	Solid dispersion	NS	Agglomeration
Nifedipine	CO ₂	175-185	1470-2940	Dissolution Enhancement	15u	Porous particles, Dissln rate increased
Nifedipine+PEG4000	CO ₂	50-70	1750-2800	Solid dispersion	<100u	Dissolution rate improved 9 times
PEG's 1500,35000	CO ₂	45-70	1470-3700	Micronization	170-370u	Fibres,Spheres,Sponges
Phenacetm	CH ₂ F ₂	141	600	Micronization	5u	Homogenous powder

high pressures and temperatures, a restriction device and a collection vessel that is temperature controlled. Pure drugs and drug mixtures are melted by maintaining the saturation vessel at the liquefaction conditions of the solids. Addition of a low melting component may reduce the melting temperature of the other components(s), which allows use of milder PGSS conditions. Sencar-Bozic et al demonstrated this phenomena using PEG 4000 to reduce the melting temperature of nifedipine [Sencar-Bozic 1997]. The saturation vessel is maintained at the liquefaction conditions of the solids, corrected for the effects of compressed gas and other components on melting temperature. Compressed CO₂ is pumped into the saturation vessel, which dissolves or disperses in the solid melt. The gas saturated solution in the saturation vessel is rapidly expanded through a restriction device into the collection vessel. The drop in temperature and the supersaturation caused as a result of rapid expansion allows the formation of solid drug particles. The morphology of the particles formed depends on the location and time scale over which particle congealing occurs. Particle growth and agglomeration occurs if the decrease in temperature across the restriction device is insufficient to congeal the particles at the tip of restriction device. In such instances, the pre-expansion conditions may be modified by the introduction of fresh SCF to the gas saturated solution.

Typical operating conditions of the PGSS process are: Saturation temperature= 40-200°C, Saturation pressure=1500-4000 psi, CO₂ consumption =0.1-0.8Kg gas/ Kg of solids processed. Powder processing using PGSS has been

demonstrated both in a lab scale setup processing 200-400g of solids [Weidner 1996] to pilot scale designs producing 1000 Kg solids/hr [Mura 1995].

5.4 Applications:

Reported applications of PGSS process are in the grinding of difficult-to-comminute PEG polymers, micronization of drugs, formation of solid dispersions aimed at improving aqueous dissolution rate of hydrophobic drugs, etc. (Table 6). Weidner et al have processed polyethylene glycols with molecular weights ranging between 1500 to 35,000 and formed unimodal microparticles with different morphologies, such as fibers, spheres and sponges by varying the process conditions [Weidner 1996]. Micronization of phenacetin to produce homogenous 5 μ particles has been demonstrated by Mura and Pozzoli using a pilot scale PGSS process with product yields up to 1000 kg/hr [Mura 1995]. PGSS, as a means of forming solid dispersions has been evaluated using a number of hydrophobic drugs. Improving the aqueous dissolution rate of a series of drugs has been evaluated in view of the micronization and solid dispersion capabilities of particles from gas saturated solution process. Up to a 15 fold enhancement in dissolution rate is achieved with felodipine and nifedipine when the agglomeration of produced particles is kept to minimum [Kerc 1999]. Another feature of PGSS that aids in aqueous dissolution enhancement is the morphology of particles produced, which in most instances are porous microparticles with rough surfaces [Sencar-Bozic 1997, Mura 1995]. Of the various process

conditions evaluated, the pre-expansion temperature and geometry of the restriction device have been found to have a significant influence on the morphology of the particles.

Compressed gases have zero surface tension, high diffusivity and significant solubility in liquids and solid melts. They can be dissolved or dispersed in the molten solids easily under pressure. The ease of processing such gas saturated solutions owing to their reduced viscosity, makes PGSS unique in comparison to other methods like fusion, melt granulation, melt extrusion etc. Further, the milling step associated with all the latter methods of solid processing is avoided in the single-step PGSS process. In comparison to other SCF techniques of powder processing, PGSS operates at much higher energy conditions. The feasibility of the PGSS process for the compounds under consideration should be critically evaluated along the lines described above, prior to selecting the process.

6. SUPERCRITICAL ANTISOLVENT PROCESSES

6.1 Introduction:

Poor solubilities of many pharmaceutical compounds and polymers in SC CO₂, coupled with the high-energy requirements associated with RESS and PGSS processes prompted the use of SC CO₂ as an antisolvent. Initial experiments using supercritical antisolvents were performed on thermo-sensitive materials like explosives [Gallagher 1989], proteins & peptides [Yeo 1993] and other

biologicals [Tom 1993]. Since then, the technique has been extended to the processing of a variety of pharmaceutical actives & polymers. Also, several modifications of the technique have been made with the objective of achieving better particle morphology with low residual organic content. These constitute **Gas AntiSolvent process (GAS)**, **Precipitation using Compressed Antisolvent (PCA)**, **Aerosol Solvent Extraction System (ASES)** and **Supercritical Antisolvent System (SAS)**.

Review of literature reveals that some of these terms are loosely and interchangeably used, with no rigid definitions distinguishing one from the other. A general conception of the terminology is stated unambiguously by Subramaniam et al and is followed here [Subramaniam 1997]. GAS is generally used for a batch process (Figure 4) wherein a gas/subcritical or supercritical fluid is bubbled through a stationary bulk of solute laden organic solvent. Decrease in solvent density as a result of large volumetric expansion leads to a rapid loss of solvent power and therefore the solute precipitates out instantly. Particle formation occurs in the liquid phase and a secondary solvent removal process is required to produce dry particles. A modification of this process with the objective of enhancing mass transfer by spraying organic solution into compressed fluid is broadly called PCA. Due to the improved transfer rates of organic solvent into the compressed fluid and vice versa, rapid evaporation of organic solvent and droplet expansion take place respectively, leading to the precipitation of fine particles. The process is termed ASES or SAS when the state

of compressed fluid used as the antisolvent is supercritical. The PCA process has been investigated both under batch and continuous modes. The former involves spraying organic solution into a vessel containing compressed fluid (Figure 5) [Bodmeier 1995], while concurrent administration of compressed fluid and organic solution at predetermined flow rates in a continuous manner constitutes the latter process (Figure 6) [Yeo 1993].

6.2 Mechanism of particle formation:

The mechanism of particle formation is by solvent-antisolvent precipitation. The solute(s) to be processed is dissolved or dispersed in an organic solvent that has preferential affinity to the compressed fluid rather than the solute. When brought in contact with the compressed fluid, the organic solvent instantly throws out the solute owing to the loss of its solvent power. Particle precipitation is postulated to occur through two different mechanisms [Tom 1993]. The influx of compressed fluid into the bulk of organic solution or the spray droplets brings about a large volumetric expansion of the solvent. This is followed by a loss of solvent power and very high supersaturation within the organic solution. The degree of supersaturation in the organic solution and particle growth are controlled by the rate and extent of antisolvent addition. Preliminary studies to determine the nature of solvent expansion caused by a compressed gas, as a function of pressure and temperature allows selection of appropriate process conditions [Gallagher 1989, Yeo 1993].

On the other hand, solvent flux into the compressed fluid causes rapid evaporation of the solvent, thereby supersaturating the solution. This is influenced by the relative affinity of solvent to the compressed fluid versus the solute. Also, other conditions such as the solute concentration in the organic solvent, relative rates of flow of organic solution and compressed fluid, pressure and temperature conditions of the compressed fluid etc. affect solvent evaporation. The rate of solvent evaporation and the degree of antisolvent penetration in the droplets have been shown to have a major effect on the porosity of the particles formed [Dixon 1993, Werling 1999].

While solvent expansion by the gas is shown to potentially influence particle morphology in the GAS process, solvent evaporation and other spraying conditions mostly affect particle formation and growth in spray processes. Mass transport rates and the dynamics of jet breakup dictate particle morphology in spray processes. The former is found to have greater influence on particle morphology compared to the latter. Werling and DeBenedetti have developed an integrated model of the effects of these mechanisms on particle morphology [Werling 1999]. The choice of process conditions should take into account the effects of these two different mechanisms on optimal particle formation. In addition, the phase of the medium where particle formation occurs is another factor affecting particle morphology. Particle formation in the GAS process occurs in the liquid organic phase and involves secondary solvent removal and drying steps. On the other hand, spray processes offer particle formation in the

supercritical phase in which the solvent is instantly extracted, leaving dry microparticles. In a recent development, spraying organic solution into a two phase vapor over a liquid antisolvent has also been evaluated [Young 1999]. It is postulated that particles formed in the vapor phase are later solidified in the liquid antisolvent beneath it. Preliminary phase behavior studies of the ternary system will form a basis for understanding the site of particle formation and thereby allow control of particle morphology.

Compounds most suitable for antisolvent processing should have negligible interaction with the SCF and sparing solubility in the solvent used. In the presence of interactions between the compounds and the antisolvent, the solute is extracted along with the solvent. These interactions not only effect the ease of solvent removal, but also result in low overall yields. While visual inspection of compound behavior in SCF is one way of determining compound suitability for antisolvent processing [Bodmeier 1995], Steckel et al. have attempted to rationalize it based on partition coefficients of compounds [Steckel 1997]. The authors have shown for glucocorticoids that a log P (octanol/water) value of less than four eliminates the possibility of compound extraction by SC CO₂. Ideal solvents for use in supercritical antisolvent processes should have a significant affinity for SCF and a high vapor pressure. Most common solvents used to date with CO₂ as the antisolvent include methylene chloride, dimethyl sulfoxide, methanol and ethanol. Minimal solvent residues that are an order of

magnitude below the permitted levels have been achieved through proper choice of operating conditions.

6.3 Process:

The basic components of a GAS system (Figure 4) are a precipitator with ends fitted with filters, pumps to precisely deliver compressed gas and organic solution into the precipitator and optionally, a post expansion vessel to separate the compressed gas from organic solvent for reuse. The solute(s) to be processed is dissolved in the organic solvent, typically in the concentration range of 0.1-5 mg/ml and is introduced into the precipitator using a pump. In the particle formation step, a predetermined amount of compressed gas flows through the organic solution at a regulated rate. Owing to the volumetric expansion of the solvent, particle precipitation occurs. The morphology of particles formed depends on expansion path followed, regulated by the rate of addition of compressed gas and the solute concentration in the organic solution. Particle precipitation is followed by an extended drying step where generous amounts of compressed gas are bubbled through the precipitator. During this process, particles are restored in the precipitator using filters at both ends. The pressure and temperature conditions within the precipitator are controlled and recorded using a pressure transducer and a RTD. Typical operating conditions are 30-40°C and 1000-1500psi and antisolvent flow rates of 17-18 SLPM. In comparison to RESS, the gas antisolvent process operates at milder conditions and produces

higher yields. On the other hand, particle agglomeration and the additional drying step in the GAS process owing to low rates of mass transfer prompted spraying organic solution into the compressed fluid.

Spray processes require an atomizing device in addition to the components described above. Various spray devices that range from simple capillaries and nozzles to vibrating, energized nozzles have been evaluated. The influence of nozzle configuration on the final particle morphology has been found to be rather insignificant compared to other operating conditions like relative rates of flow of organic solution and antisolvent, pressure, temperature, etc. This is explained by the fact that mass transport rates between the solvent and SCF have greater influence on particle size relative to the dynamics of jet break up and initial droplet size [Werling 1999].

In a batch spray process (Figure 5), organic solution is sprayed into the precipitator containing a compressed fluid where the particles are formed. Additional compressed antisolvent is then swept through the precipitator to remove the organic solvent completely. Typical flow rates of organic solution are between 0.1-1ml/min. In the continuous mode (Figure 6), organic solution and the compressed fluid are simultaneously administered at predetermined flow rates into the precipitator. Typical flow rates of organic solvent and compressed fluid during particle precipitation are 0.1-3ml/min and 6-20 SLPM respectively. At the end of particle precipitation, spraying of organic solution is stopped while additional amounts of compressed fluid is passed through the precipitator to

remove the organic solvent. With proper choice of operating conditions, dry particles containing very low levels of residual volatile organic content can be produced.

6.4 Applications:

The advantages of using supercritical antisolvent crystallization in the micronization of drugs and pharmaceutical excipients are numerous. Energy requirements for the process are low and the technique offers the ability to process compounds under mild conditions. As summarized in Table 7, a number of pharmaceutical actives and excipients have been processed and various particle morphologies have been achieved. While the process has mostly been evaluated in the production of dry particles for nasal administration, it can also be extended to tailor particle morphology for any desired situation. Schmitt patented the micronization of a number of API's including alprazolam, triazolam, ibuprofen, erythromycin, penicillin, ampicillin, glyburide, dexamethasone, hydrocortisone etc. [Schmitt 1990]. The technique offers the ability to form discrete microparticles with a tight size distribution using mild process conditions while preserving the activity of sensitive molecules [Yeo 1993, Young 1999]. Other aerodynamic attributes for the particles such as flowability, surface roughness, charge, density, porosity can also be tailored specific to the end use. With the proper choice of process conditions, low residual solvent content that are an order

Table 7. Pharmaceutical Studies using Supercritical CO₂ as an Antisolvent

Agent	Process	Solvent	Percent Solute	Conditions		Application	Particle characteristics	Reference
				T(°C)	P(psi)			
Ascorbic acid	PCA	EtOH	NS	NS	650-2200	Micronization	1-10 μ	Weber 1997
Ascorbic acid + Aspirin	PCA	EtOH	NS	NS	650-2200	Amorphous Conversion	-	Weber 1997
Betamethasone-17-valerate	ASES	MeCl ₂ + MeOH	1wt%	40	1230	Micronization	-	Steckel 1997
β -poly-D,L-lactide-co-D,L-lactide-co-Glycolide + F-streol	ASES	MeOH + MeCl ₂ + TFE	3%	34	1450	Microencapsulation	Microparticles with drug primarily on surface	Engwicht 1999
Budesonide	ASES	MeCl ₂ + MeOH	1wt%	40	1230	Micronization	Spherical, nonporous particles	Muller 1997
Budesonide + Lecithin + HP-beta-cyclodextrin	ASES	NS	NS	NS	NS	Micronization	Spherical microparticles, Improved aerodynamic behavior	Muller 1997
Camptothecin	SAS	DMSO	0.50%	55	1850	Micronization	0.5 μ	Subramaniam 1998
Catalase	GAS	EtOH/H ₂ O	0.01%	35	1320	Micronization	1 μ , Spherical or Rectangular	Tom 1992
Chloramphenicol-Urea	PCA	DMSO	NS	40	1450-1740	Solid solution	-	Weber 1997
Clonidine HCl-L-PLA	PCA	MeCl ₂	0.02% & 20%	60	1470	Microencapsulation	100 μ , Spherical particles, Controlled release	Fischer 1991
CPM-L-PLA	PCA	MeCl ₂	0.4&4%	23	1015	Microencapsulation	1-5 μ Microspheres, Drug loading = 3.73%	Bodmeier 1995
Dexamethasone-21-acetate	ASES	MeCl ₂ + MeOH	1wt%	40	1230	Micronization	-	Steckel 1997
Flunisolide	ASES	MeCl ₂ + MeOH	1wt%	40	1230	Crystal modification	Reduced crystallinity	Steckel 1997
Fluticasone-17-propionate	ASES	MeCl ₂ + MeOH	1wt%	40	1230	Crystal modification	Reduced crystallinity	Steckel 1997
Gentamicin sulfate-L-PLA	PCA	MeCl ₂	0.1% & 0.9%	35	1250	Microencapsulation	Impaired Microparticles	Steckel 1997
HYAFF-11	SAS	DMSO	0.5-1.5wt%	35-50	1470	Micronization	0.1-0.7 μ	Bettucco 1996

Table 7 . Pharmaceutical Studies using Supercritical CO₂ as an Antisolvent (Cont'd)

Agent	Process	Solvent	Percent Solute	Conditions		Application	Particle characteristics	Reference
				T(°C)	P(psi)			
HYAFF-11	SAS	DMSO	0.05-1%	35-60	1250-1470	Nanoparticles	Nanospheres(400nm) to Aggregates(5-30u)	Benedetti 1997
HYAFF-11 + Model Drugs	SAS	DMSO	1wt%	40	1470	Microencapsulation	Nanospheres(320-400nm) ,Drug Loading :20-86%	Bertucco 1996
Hydrocortisone	SAS	DMSO	0.5-3%	35	1500	Micronization	Agglomerated, Spherical, 0.5-1u particles to whiskers	Subramaniam 1998
Hydrocortisone	SAS	DMSO	0.5-3%	55	1850	Nanoparticles	Discrete spherical particles - 500nm	Subramaniam 1998
Bioscane Butyl Bromide +L-PLA	ASES	MeCl ₂	2 wt%	40	1320-2940	Microencapsulation	Spherical microparticles(8-80u) , Loading :97.5%	Bleich 1996
Ibuprofen	SAS	DMSO	3%	35	1500	Nanoparticles	Discrete micron size particles - 0.6u	Subramaniam 1998
Indomethacin	PCA	Acetone	9.9wt%	25	Upto4000	Nanoparticles	143nm, precipitated into phospholipid	Henriksen 1997
Indomethacin +L-PLA	PCA	MeCl ₂	0.4% &4%	23	1015	Microencapsulation	1-5u Microspheres, drug loading :0.73%	Bodmeier 1995
Indomethacin +L-PLA	ASES	MeCl ₂	2 wt%	40	1320-2940	Microencapsulation	Spherical microparticles(2-40u), Loading :25%	Bleich 1996
Insulin	GAS	EtOH:H ₂ O		35	1320	Micronization	Microspheres: 1u) & Thick needles :5uL	Tom 1993
Insulin	GAS	DMSO	0.5-1.5%	25-35	1275	Micronization	1-4u powders	Yeo 1993
Insulin	GAS	DMF/A	0.50%	35	1275	Micronization	2.5u	Yeo 1993
L-PLA	PCA	MeCl ₂	0.3-1 wt%	31	800-1400	Micronization	0.3-2u	Bodmeier 1995
L-PLA	PCA	MeCl ₂	1-6%wt	0-32	1200		Spherical,free flowing,Non-agglomerated&: 5u	Bodmeier 1995
L-PLA	PCA	MeCl ₂	1wt%	20	1515	Micronization	1-4u	Young 1999
L-PLA	ASES	MeCl ₂	1.5-3%	40	1230-2940	Micronization	Spherical microparticles(6-50u)	Thies 1998

Table 7. Pharmaceutical Studies using Supercritical CO₂ as an Antisolvent (Cont'd)

Agent	Process	Solvent	Percent Solute	Conditions		Application	Particle characteristics	Reference
				T(°C)	P(psi)			
Lysozyme-L-PLA	PCA	MeCl ₂	0.5%&5%	24	1515	Microencapsulation	250-500µ microencapsuled Particles	Young 1999
Lysozyme-PGLA	PCA	MeCl ₂	0.5%&5%	-20	1515	Microencapsulation	10-60µ microencapsuled particles	Young 1999
PDLA	ASES	MeCl ₂	1.50%	40	1320-2940	Micronization	.	Bleich 1993
PGLA	PCA	MeCl ₂	1-10wt%	24 to -20	1515	Micronization	0.5-50µ	Young 1999
PGLA	ASES	MeCl ₂	1.50%	40	1320-2940	Micronization	Polymer film	Bleich 1993
PIIB	ASES	MeCl ₂	1.50%	40	1320-2940	Micronization	Porous microparticles	Bleich 1993
Proxicam-L-PLA	ASES	MeCl ₂	2 wt%	40	1320-2940	Microencapsulation	Spherical microparticles(1-14µ), loading 2.5%	Bleich 1996
Prednisolone	ASES	MeCl ₂ +MeOH	1wt%	40	1230	Amorphous Conversion	Nearly amorphous particles.residual solvent 51ppm	Steckel 1997
Prednisolone acetate	PCA	Acetone	0.5-0.6% w/v	40-80	1470-2940	Micronization	0.5-3µ particles,polydispersity < 4	Kulshreshtha 1998
Tetracaine HCl	PCA	Acetone	0.97%	25-45	Upto 4500psi	Nanoparticles	10-170nm, Precipitated into tween 80	Henriksen 1997
Thymopentim-L-PLA	ASES	MeCl ₂ +MeOH	2 wt%	40	1320-2940	Microencapsulation	Spherical microparticles(1-30µ), loading 96%	Bleich 1996
Tramadolone acetamide	GAS	THF	4.50%	49	1620	Micronization	5-10µ	Schmitt 1990
Tramadolone acetamide	ASES	MeCl ₂ +MeOH	1wt%	40	1230	Crystal modification	Microspheres with reduced crystallinity	Steckel 1997
Urea	PCA	EtOH	2.5-4.2%	35-40	1015-1450	Micronization	Caked aggregates(<50µ)	Weber 1997
Urea	PCA	DMSO	5-30%	35-75	1015-1450	Micronization	Micron particles, 2-8µ	Weber 1997

of magnitude lower than FDA regulated limits have been achieved [Ruchatz 1997, Steckel 1997]. Compared to solvent based crystallization, the levels of solvent waste can be significantly reduced by reusing the solvent. Removal of CO₂ from the solvent after particle formation can be affected by simple depressurization and both the solvent and antisolvent can be recirculated for reuse.

Another potential pharmaceutical application in the area of controlled release by microencapsulation of drugs is reflected in a number of reported publications. The efficiency of encapsulation can be improved by mixing at the molecular level, which is only possible with solvent based microencapsulation techniques. Supercritical microencapsulation, in principle, combines the advantages of solvent based techniques while providing a number of other advantages. These include the ability of controlling particle morphology and the ease of solvent removal. As can be seen in the Table 7, a number of pharmaceutical actives have been microencapsulated in various polymers using supercritical microencapsulation. The effect of the lipophilicity of drugs on the efficiency of loading into L-PLA has been investigated by Bleich et al. [Bleich 1996]. The least hydrophilic among the compounds studied showed maximum loading in L-PLA, while lipophilic piroxicam was found to be extracted by the antisolvent. Preliminary studies of the ternary phase behavior for the selected system should help in choosing appropriate solvent and process conditions to form the desired microcapsules.

Typical polymers evaluated to date include L-PLA, HYAFF-11, PGLA, etc. The thermal and crystal attributes of these polymers that make them particularly suitable for particle formation using the antisolvent process was reported recently by Engwicht et al. [Engwicht 1999]. Due to the fact that the thermodynamic and phase behavior of only a few polymers in supercritical CO₂ are well documented, a majority of the supercritical microencapsulation studies are restricted to a selective few polymers. It remains to be seen how other pharmaceutical polymers will perform in supercritical microencapsulation.

Rapid dissolution and absorption of actives of thermodynamically unstable forms of drugs has been a subject of interest in the recent past. In this direction, a nearly amorphous form of prednisolone has been produced by Steckel et al. [Steckel 1997]. The processing of drug mixtures to alter crystallinity has been reported by Weber et al. [Weber A 1997]. Varying degrees of crystallinity of aspirin and chloramphenicol were achieved by coprecipitation with ascorbic acid and urea using supercritical conditions. Although the technique in principle seems to offer the ability to alter crystallinity, more investigation needs to be performed before definitive conclusions can be made.

Utilizing this technique, Subramaniam et al patented the process of coating actives with excipients and forming free flowing microparticles in a single step [Subramaniam 1998]. Possible applications are in the taste masking, controlled release and enhancing dissolution rates of pharmaceutical actives. With the objective of improving wetting and thereby dissolution, Steckel et al. [Steckel

1997] have coprecipitated a series of steroids with phosphatidyl choline and observed a significant decrease in contact angle with water. If this study could be extended to other poorly soluble pharmaceutical actives, this approach may provide a convenient way to form free flowing discrete microparticles with enhanced solubility attributes in a single stage processing.

The supercritical antisolvent technique has the potential for use in a multitude of applications for particle formation. However, the current level of understanding of a ternary phased supercritical mixture is rather primitive, restricting its application to a few excipients and actives. Pharmaceutical applications utilizing this technique have mostly been restricted to processing drugs with a few excipients. Extension of the technique to new molecules requires better understanding of the physicochemical properties of compounds that make them amenable to antisolvent processing as well as the phase behavior of ternary system under consideration.

7. SOLUTION ENHANCED DISPERSION BY SUPERCRITICAL FLUIDS

7.1. Introduction:

With an ever-increasing need to tailor the particle morphology of pharmaceutical powders and to overcome the limitations of above described particle formation methods, alternate combinations of particle precipitation techniques have been explored. A more recent development among these supercritical fluid processes is what is known as 'Solution enhanced dispersion by supercritical fluids' (SEDS)

[York 1995]. In SEDS, the solute(s) of interest is dissolved or suspended in an organic and/or aqueous solvent that is brought into contact with pure or modified SCF (antisolvent) using a coaxial nozzle. Mixing of the two fluids takes place in the nozzle just prior to the expansion through a restriction. The efficiency of particle precipitation by SCF is enhanced in SEDS by utilizing the energy of the rapidly expanding gas in dispersing the solvent. This feature of SCF's coupled with their solvent-extraction capability is believed to enhance the mass transport between fluids. Improved mass transfer between the solvent and the SCF assists in complete removal of solvent, which in turn aids in the formation of non-agglomerated powders [York 1999]. Among the several SCF particle formation methods evaluated to date, SEDS offers a convenient means of forming non-agglomerated powders under mild processing conditions while placing fewer restrictions on the solubility properties of the compounds.

7.2 Mechanism of Particle Formation:

Similar to the supercritical antisolvent processes, antisolvent-induced precipitation of solute from a solution or a suspension forms the basis for particle formation in SEDS. Refer to Section 4.2 for details about precipitation by supercritical antisolvents. A major limitation to the processes discussed in Section 4 arises from poor mass transfer between the fluids, leading to incomplete solvent removal and hence agglomerated particles. While the morphology of newly formed primary particles depends on such factors as pressure, temperature,

density of SCF, initial droplet size, nucleation rates, spray velocities etc, incomplete solvent removal leads to growth and agglomeration of primary particles. To retain the characteristics of the primary particles, it is therefore important to remove the solvent immediately upon particle formation. From a theoretical standpoint, solvent flux from the droplet into the SCF is higher from a finely dispersed mist of solution. Dispersing the solution in SEDS is brought about by the use of a coaxial nozzle. In principle, SEDS is an extension of the supercritical antisolvent spray process and operates similar to the continuous PCA process. The major difference from the PCA process lies in the use of a coaxial nozzle with multiple passages for different fluids. The nozzle not only helps in reproducibly contacting the fluids at a specific site of interest, but also helps in streamlining the mechanical energy of the rapidly expanding SCF to disperse the solvent.

The solute of interest is dissolved or suspended in a solvent, which can be organic or aqueous. Precipitation of solute from its solution is caused by contact with pure or modified supercritical fluid. A multi-channeled nozzle with a mixing chamber allows convenient contact between the fluids at the site of interest, prior to dispersion and extraction of solvent and particle formation. Complete understanding of the mode of particle growth and the effects of process variables on particle morphology requires knowledge of the phase behavior of the system under study. The importance of fluid phase behavior is addressed in a recent review by Palakodaty and York, in which the authors addressed the fundamentals

of binary and ternary phase behavior involving SCFs [Palakodaty 1999]. The literature on the phase behavior of solvents and solutes that are routinely used in pharmaceuticals, however is scarce and therefore are limited to predictive calculations to date. One such study, characterizing the crystallization mechanisms of paracetamol by SEDS was recently published by Shekunov et al. [Shekunov 1999]. With rapidly increasing SCF applications in the field of pharmaceuticals, it remains to be seen how new developments would aid in understanding the process better.

7.3 Process:

A general schematic of the SEDS process is shown in Figure 7. The basic components of SEDS process include pumps to deliver the fluids at desired rates, a co-axial nozzle, and a particle formation vessel. Solute(s) to be processed is dissolved or suspended in the solvent, typically in the concentration range of 0.5-3% w/v and is fed to the coaxial nozzle using a liquid pump. Typical flow rates of the solute laden solution or suspension are in the range of 0.2-3 ml/min. Pulse-dampened supercritical fluid is delivered to the coaxial nozzle at flow rates of 9-45ml/min. Preferably, the ratio of flow rates of the solution and SCF are maintained between 0.01 and 0.07 [York 1995]. The T,P conditions of the supercritical fluid are fairly mild, generally ranging between 40-80°C and 1150-2940psi respectively. The fluids are brought into contact within the mixing chamber of the nozzle. A coaxial nozzle has multiple passages for different fluids.

Specific designs of various coaxial nozzles can be found in York's patent [York 1995]. In the particle formation step, the fluids are expanded through the nozzle where solvent dispersion and extraction take place instantly. Particles are retained by frits placed at the outlet end of particle formation vessel. Temperature and pressure of the particle formation vessel are controlled using an oven and a back pressure regulator respectively. At the end of the run, pure SCF is flowed through the system for 10-15 min to remove any remaining solvent.

The solvent of choice should have a preferential affinity for the SCF compared to the solute. It can be a pure organic solvent that is miscible with the SCF of choice or it can be an aqueous solvent which can be extracted by a modified SCF. A modified SCF is one that is doped with traces of a polar co-solvent like methanol or ethanol and offers the ability to extract aqueous components of the solution. SEDS thus offers the ability to process a wide variety of pharmaceutical compounds while placing fewer restrictions on their solubility attributes. Much of the development in SEDS process has been brought about by Bradford Particle Design Ltd., UK and it is proposed that the process has the capability to be scaled up to the tune of producing 1 ton/year [Bonner 2000].

7.4 Applications:

One of the potential areas of SEDS application is in the crystallization of pure drugs. Compared to conventional crystallization, SEDS has been shown to generate particles that have better attributes such as crystallographic purity,

uniformity in size and size distribution, lower solvent residues, etc. For delivery purposes, conventional crystallization methods often require secondary processing of the material that may effect the activity of the molecules, besides adding to the economics of production. SEDS, on the other hand offers the ability to combine the processes such as crystallization, purification, micronization, etc. into one unit operation, while providing better control over particle morphology [York P 1999]. As can be seen from Table 8, the technique is particularly attractive in producing dry particles (pure, 1-5 μ , static free, non-cohesive, free flowing, freely dispersible) intended for insufflation. Pulmonary delivery of such compounds places demanding requirements on the particle size, size distribution and other aerodynamic properties of the powders. Studies involving comparative evaluation of various processes in producing such powders have revealed that SEDS generated particles have better attributes [York 1996, Palakodaty 1997].

Utilizing the selective nature of supercritical fluids and the rapidity of extraction in the SEDS process, it is possible to separate polymorphs [Beach 1999] and enantiomers [Koordikowski 1999]. This provides a convenient way of cleaning up active pharmaceutical ingredients (APIs) and thereby producing pure drug substances. To the same objective, the amorphous and metastable domains in APIs that would otherwise compromise their stability can be removed by selective SEDS based crystallization. Highly crystalline forms of salmeterol xinafoate, lactose and fluticasone propionate have been produced using SEDS process. Conversely, crystal to amorphous conversion of pharmaceutical actives can be

Table 8 . Summary of SEDS studies

Agent	Solvent	Antisolvent/ Dispersing Agent	Percent Solite(s) [w/w]	Conditions		Application	Particle Characteristics	Reference
				T [°C]	P [psi]			
Lysozyme	DMSO	CO ₂	0.5-1	40-50	1150-2940	Micronization	Spherical microparticles(1-8u)	Moshshaeze 2000
Lysozyme	Water+EtOH	CO ₂	3	40-50	1470-2940	Micronization	Spherical microparticles(1-12u)	Moshshaeze 2000
Salmeterol Xinafoate	Ethanol	CO ₂	0.5	60	4410	Micronization	1-10u. Improved aerodynamic properties	York 1995
Salmeterol Xinafoate	Acetone	CO ₂	0.5	50	2940	API Clean up.	1-10u, Separated polymorphs I and II	Hanna 1998
alpha-Lactose monohydrate	Water+MeOH	CO ₂	0.25	90	2200	Micronization	3u water-like crystals	Palakodaty 1997
alpha-lactose monohydrate	Water	CO ₂ +MeOH	10	80-90	2200-4410	Micronization	1-20u with 2-5% water content	Palakodaty 1998
alpha-lactose monohydrate	Water	CO ₂ +EtOH	10	50	2200	Micronization	11-15u crystals water content 2.5-5%	Palakodaty 1998
DI-PI G	EtAc+Acetone+ Isopropanol	CO ₂	2.3	33-38	1900-2700	Micronization	Discrete spherical particles(20-200u)	Ghadery 1999
DI-PI G	MeCl ₂ +MeOH	CO ₂	2.3	33-38	1900-2700	Micronization	Spherical beads connected by solid bridges	Ghadery 1999
I-PI A	MeCl ₂ +Acetone+ Isopropanol	CO ₂	2.3	35-40	1900-2700	Micronization	0.1-50u Microparticles	Ghadery 1999
DI-PI A	Acetone+EtAc+ Hexane	CO ₂	2.3	35-40	1900-2700	Micronization	Discrete particles + aggregates (30-200u)	Ghadery 1999
Polycaprolactone	Acetone+MeCl ₂ + Isopropanol	CO ₂	2.3	35-40	1900-2700	Micronization	Large irregular shaped particles(5-1000u)	Ghadery 1999

Table 8 . Summary of SEDS studies (Cont'd)

Agent	Solvent	Antisolvent/ Dispersing Agent	Percent Solute(s) [w/w]	Conditions		Application	Particle Characteristics	Reference
				T [°C]	P [psi]			
Budesonide	Acetone	CO ₂	1-2.5	60-80	1470	Micronization	Smooth crystalline powder- 5u	Bisrat 1998
Salmeterol Xinafoate + Fumed Silica	MeOH	CO ₂	NS	45	4410	Crystal modification	Free flowing particles, altered crystallinity	York 1995
Salmeterol Xinafoate + HPC	Acetone	CO ₂	0.45&0.05	60	1750	Coprecipitation	Fluffy white intimate mixture	York 1995
Nicotinic acid	Ethanol	CO ₂	0.625	70-90	1320	Micronization	Non-charged, free flowing 5.75u	York 1997
Paracetamol	Ethanol	CO ₂	0.01	40-60	1320-3625	Micronization	Non-charged, free flowing 5.75u	York 1997
Albuterol sulfate	Water + Acetone + MeOH	CO ₂		50	2200		Smooth surfaced, free flowing crystals	York 1997
Salbutamol Sulfate								
Ibuprofen	DBMSO	CO ₂	0.05	35	1500	Micronization	0.6u particles	
Sodium Cromoglycate	MeOH	CO ₂	0.25-0.75	40-73	1470-2940	Amorphous Conversion	0.1-20u spherical particles, Amorphous to moderately crystalline	Jaarmo 1997

achieved by SEDS as demonstrated by Jarmao et al [Jarmao 1997]. The study reports a controlled crystal to amorphous conversion of sodium cromoglycate by antisolvent recrystallization using methanol and SC CO₂. A stable amorphous form of sodium cromoglycate was produced that did not exhibit crystallinity for five months. The authors attributed the conversion and the stability of the product to the residual levels of methyl alcohol. However, a major limitation of this approach stems from the fact that the drug may revert back to the thermodynamically favored crystalline form, compromising drug stability. The likelihood of such conversion is less when dealing with the pure drug, as seen in Jarmao et al's study. A theoretical basis for this phenomenon, if consolidated, may have implications in improving the biopharmaceutical properties of crystallographic origin. It would also enable to extend these observations for any compound in general.

Processing mixtures of drugs and excipients by SEDS has also been shown to be effective in a variety of situations. Coprecipitation and surface adsorption of salmeterol xinafoate on to different excipients was reported by York and Hanna [York 1995] to control the release and enhance the fluidization efficiency of the drug. Polymer processing using SEDS technology has recently been reported by Ghaderi et al. Various morphologies of polymers like L-PLA, DL-PLA, polycaprolactone have been produced using the SEDS process.

Processing of pharmaceutical solids frequently involves optimizing particle size, purity, crystallinity, flow, static charge, cohesiveness, solvent-

content, stability besides other features specific to the delivery system. A particle formation process that effectively combines all these steps into one unit operation is of particular interest in the context of integrating chemical synthesis and formulation development. With increasing emphasis on reducing the time scales of different phases of drug development, there is a growing attention to such techniques with feasibility for scale up. Understanding the basic mechanism of particle nucleation and growth is essential in reproducibly producing the powders and in scale-up. Such understanding to date is limited and future work in this field should aim at forming a general basis for processing a wider variety of compounds. It is noteworthy that SEDS and PGSS are the only two processes, among several SCF particle formation methods that approached commercialization on a pilot scale.

8. SUMMARY:

In the reality of growing competition and emphasis on reducing the drug development time, search for new technologies continues to be a part of pharmaceutical research. Supercritical fluid technology, among other contemporary technologies has been gaining increased focus owing to its potential to integrate the synthesis and delivery stages of drug development. Other advantages include minimizing the usage of solvents, reducing the number of unit operations while offering the ability to continuously process materials under cGMP conditions. The technology is rapidly evolving while continuing research

efforts aimed at maximizing the benefits of supercritical fluids are in progress in order to process a wider variety of compounds on a pilot scale. Consequently, a number of supercritical fluid techniques have been reported to date. Each of these techniques discussed in this review utilize the remarkable properties of supercritical fluids in producing pure drugs and drug composites of various particle and crystallographic morphologies. In providing a comprehensive summary of various supercritical fluid techniques, this review presents the scope for supercritical fluid technology in pharmaceutical material processing. A large domain of supercritical fluid research still remains unexplored, considering the number of supercritical fluids and pharmaceuticals investigated to date, the extent of supercritical region evaluated, current process throughputs and the present level of understanding of the SC CO₂ based material processing. While exploring the other potential applications of the technology in pharmaceutical material processing, future research should also aim at theoretical understanding of the different processes. Such an understanding will then form a basis for processing a wider variety of pharmaceuticals and achieving better efficiency for process scaleup.

9. LIST OF REFERENCES

1. Alessi P et al. Determination and correlation of solubility of pharmaceutical products in supercritical carbon dioxide. *Chemical and Biochemical Engineering Quarterly* 1997, 11(1) :p19-23.
2. Alessi P et al. Particle production of steroid drugs using supercritical fluid processing. *Industrial and Engineering Chemistry Research* 1996, 35 : p4718-4726.
3. Beach S et al. Control of the physical form of Salmeterol Xinafoate. *Organic process Research and Development* 1999, 3:p370-376.
4. Benedetti L et al. Production of micronic particles of biocompatible polymer using supercritical carbon dioxide. *Biotechnology and Bioengineering* 1997, 53(2) : p232-237.
5. Berens AR et al. Process for incorporating an additive into a polymer and product produced thereby. *United States Patent* 1989, Number:4820752.
6. Bertucco A et al. Formation of biocompatible polymer microspheres for controlled drug delivery by a supercritical antisolvent technique. *Process Technology Proceedings: High Pressure Chemical Engineering* 1996, 12: p:217-222.
7. Bisrat M, Moshashae S. Composition comprising finely divided, crystalline particles of budesonide. *International Patent Publication* 1998, Number : WO 98/52544.
8. Bleich J et al. Aerosol solvent extraction system- a new microparticle production technique. *International Journal of Pharmaceutics* 1993, 97 : p111-117.
9. Bleich J, Muller BW. Production of drug loaded microspheres by the use of supercritical gases with the aerosol solvent extraction system (ASES) process. *Journal of Microencapsulation* 1996, 13(2) : p131-139.
10. Bodmeier R et al. Polymeric microspheres prepared by spraying into compressed carbon dioxide. *Pharmaceutical Research* 1995, 12980 : p 1211-1217.
11. Bonner J. A particularly fine way of making drugs. *Chemistry & Industry*, June 2000.

12. Carli F et al. Pharmaceutical compositions having the shape of powders of cross-linked polymers loaded with drugs and related preparation process by supercritical fluids. *International Patent Publication* 1999, Number: WO 99/25322.
13. Castor TP, Chu L. Methods and apparatus for making liposomes containing hydrophobic drugs. *United States Patent* 1998, Number: 5776486.
14. Chang CJ, Randolph AD. Precipitation of microsize organic particles from supercritical fluids. *AIChE Journal* 1989, 35(11) : p1876-1882.
15. Chattopadhyay P, Gupta RB. Production of griseofulvin nanoparticles using supercritical CO(2) antisolvent with enhanced mass transfer. *International Journal of Pharmaceutics* 2001, 228(1-2):19-31.
16. Coffey MP and Krukonis VJ. Supercritical fluid nucleation: An improved ultrafine particle formation process. PhaseX Corporation Final report to National Science Foundation, Contract ISI 8660823, 1989. Cited in *Supercritical Fluid Extraction*. McHugh MA, Krukonis VJ Eds.; 2nd Edition; Butterworth-Heinemann:Newton, MA, 1994, p:340-343
17. Condo PD et al. Glass transition behavior including retrograde vitification of polymers with compressed fluid diluents. *Macromolecules* 1992, 25 :p6119-6127
18. Daly, AT et al. Continuous processing of powder coating compositions. *United States Patent* 2001, Number: 6228897.
19. Dandge DK et al. Structure solubility correlations : Organic compounds and dense carbon dioxide binary systems. *Industrial and Engineering Chemistry Product Research and Development* 1985, 24 : p162-166.
20. Debenedetti PG et al. Application of supercritical fluids for the production of sustained release delivery devices. *Journal of Controlled Release* 1993b, 24 : p27-44.
21. Debenedetti PG et al. Rapid expansion of supercritical solutions (RESS): Fundamentals and applications. *Fluid Phase Equilibria* 1993a, 82 : p311-321.
22. Dixon DJ et al. Polymeric materials formed by precipitation with a compressed fluid antisolvent. *AIChE Journal* 1993, 39(1) : p127-139.
23. Dixon DJ, Johnston KP. On Supercritical fluids in *Kirk-Othmer Encyclopedia of Chemical Technolog* 1997, Vol.23, Ed.4; p 453-477.

24. Dobbs JM et al. Modification of supercritical fluid phase behavior using polar cosolvents. *Industrial and Engineering Chemistry Research* 1987, 26 : p56-65.
25. Dobbs JM et al. Nonpolar co-solvents for solubility enhancement in supercritical fluid carbon dioxide. *Journal of Chemical and Engineering Data* 1986, 31 : p303-308.
26. Donsi G, Reverchon E. Micronization by means of supercritical fluids: possibility of application to pharmaceutical field. *Pharmaceutica Acta Helvetica* 1991;66(5-6):p170-3.
27. Ekart MP et al. Cosolvent interactions in supercritical fluid solutions. *AIChE Journal* 1993, 39(2) : p235-248.
28. Engwicht A et al. Critical properties of lactide-co-glycolide polymers for the use in microparticle preparation by the aerosol solvent extraction system. *International Journal of Pharmaceutics* 1999 185 p:61-72.
29. Fischer et al. Method and apparatus for the manufacture of a product having a substance embedded in a carrier. *United States Patent* 1991, Number: 5043280.
30. Frederiksen L et al. Preparation of liposomes encapsulating water-soluble compounds using supercritical carbon dioxide. *Journal of Pharmaceutical Sciences* 1997, 86(8) : p921-928.
31. Gallagher PM et al. Gas antisolvent recrystallization : New process to recrystallize compounds insoluble in supercritical fluids. *Supercritical fluid science and technology*, ACS Symposium Series-406; Johnston KP, Penninger JML Eds., American Chemical Society, Washington DC, 1989, Chapter 22 : p334-354.
32. Ghaderi R et al. Preparation of biodegradable microparticles using solution enhanced dispersion by supercritical fluids. *Pharmaceutical Research* 1999; 16(5) p:676
33. Ghenciu EG, Beckman EJ. Affinity extraction into carbondioxide I. Extraction of Avidin into CO₂ using a Biotin-Functional fluoroether surfactant. *Industrial and Engineering Chemistry* 1997, 36:p5366
34. Ghenciu EG, Beckman EJ. Extraction of subtilisin into carbon dioxide via fluoroaether surfactants. *Biotechnology and Bioengineering* 1998, 58:p572

35. Gosselin PM et al. Comparison of microparticles prepared from the rapid expansion of supercritical solutions and by spray drying. Paper Presentation #3599, *AAPS Annual meeting*, Indianapolis 2000.
36. Greiner RW. Treating skin lesions. *United States Patent* 1993, Number:5183663.
37. Hanna M et al. Control of the polymorphic forms of a drug substance by SEDS. Poster presentation-*5th Meeting of Supercritical Fluids*, Nice, France; March 1998.
38. Helfgen B et al. Theoretical and experimental investigations of the micronization of organic solids by rapid expansion of supercritical solutions. *Powder Technology* 2000, 110:p22-28
39. Henriksen IB et al. Insoluble drug delivery. *International Patent Publication* 1997, Number :WO 97/14407.
40. Hirose Y et al. Dilution of polyethylene by sorption of carbon dioxide. *Journal of Polymer Science: Part B : Polymer physics* 1986, 24 : p2107-2115.
41. Howdle S. Biofunctional polymers prepared in supercritical fluid. *International Patent Publication* 1998, Number: WO 98/51347.
42. Jaarmo S et al. Particle tailoring with supercritical fluids:Production of amorphous pharmaceutical particles. *Proceedings: 4th International Symposium on Supercritical Fluids*, May 11-14, 1997, Sendai p:263-266.
43. Juvekar A. Study of a novel polymer loading process using near-critical carbon dioxide and a model drug. *M.S. Thesis, University of Rhode Island*, 1994.
44. Kazarian SG et al. In situ spectroscopy of polymers subjected to supercritical CO₂: Plasticization and dye impregnation. *Applied Spectroscopy* 1997, 51(4) : p491-494.
45. Kazarian SG et al. Specific intermolecular interaction of carbon dioxide with polymers. *Journal of American Chemical Society* 1996, 118 : p1729-1736.
46. Kerc J et al. Micronization of drugs using supercritical carbon dioxide. *Farm Vestn (Ljubljana)* 48(Post Stev) 1997 p:282-283.

47. Kerc J et al. Micronization of drugs using supercritical carbon dioxide. *International Journal of Pharmaceutics* 1999, 182 : p33-39.
48. Kim JH et al. Microencapsulation of naproxen using rapid expansion of supercritical solutions. *Biotechnology Progress* 1996, 12(5) : p650-661.
49. Kordikowski et al. Resolution of ephedrine in supercritical CO₂ : A novel technique for separation of chiral drugs. *Journal of Pharmaceutical Sciences* 1999, 88(8):p786-791.
50. Krukonis VJ. Supercritical fluid nucleation of difficult-to-comminute solids. Paper presented at the *AICHE Annual Meeting*, San Francisco, CA, November 1984.
51. Kulshreshtha AK et al. Process for sizing prednisolone acetate using a supercritical fluid anti-solvent. *United States Patent* 1998, Number: 5803966.
52. Kumar SK. Modelling the solubility of solids in supercritical fluids with density as the independent variable. *Journal of Supercritical Fluids* 1988, 1 : p15-22.
53. Kurnik RT, Reid RC. Solubility of solid mixtures in supercritical fluids. *Fluid Phase Equilibria* 1982, 8:p93
54. Larson KA, King ML. Evaluation of supercritical fluid extraction in the pharmaceutical industry. *Biotechnology Progress* 1986, 2(2) : p73-82.
55. Lee M et al. Extrusion of PE/PS blends with supercritical carbon dioxide. *Polymer Engineering and Science* 1998, 38(7):p1112-1120.
56. Lele AK, Shine AD. Morphology of polymers precipitated from a supercritical solvent. *AICHE Journal* 1992, 38(5) : p742-752.
57. Lindsay AD, Omilinsky BA. Method of preparing mixtures of active ingredients and excipients using liquid carbon dioxide. *United States Patent* 1992, Number:5169433.
58. Loth H, Hemgesberg. Properties and dissolution of drugs micronized by crystallization from supercritical gases. *International Journal of Pharmaceutics* 1986, 32 : p265-267.
59. Lucien FP, Foster NR. Solubilities of solid mixtures in supercritical carbon dioxide : a review. *Journal of Supercritical Fluids* 2000, 17:p111-134.

60. Magnan C et al. Impregnation of porous supports with active substances by means of supercritical fluids. *High Pressure Chemical Engineering*, Rudolph von Rohr, Trepp C Eds., Elsevier Science 1996, p509-514.
61. Mandel FS. Mixing system for processes using supercritical fluids. *United States Patent* 1999, Number: 5993747.
62. Martin A, Swarbrick J, Cammarata A, Chun AH (Eds). *Physical Pharmacy* 1993, 4th Edition; Lea & Febiger, Philadelphia.
63. Matson DW et al. Rapid expansion of supercritical fluid solutions : Solute formation of powders, thin films and fibres. *Industrial and Engineering Chemistry Research* 1987, 26 : p2298-2306.
64. McClain JB et al. Design of nonionic surfactants for supercritical carbon dioxide. *Science* 1996, 274:p2049-2052.
65. McHugh MA, Krukoni VJ. *Supercritical Fluid Extraction*. 2nd Edition; Butterworth-Heinemann:Newton, MA, 1994.
66. Mohamed RS et al. Effects of process conditions on crystals obtained from supercritical mixtures. *AIChE Journal*, 1989a, 35(2), p:325-328
67. Mohamed RS et al. Solids formation after the expansion of supercritical mixtures. Supercritical fluid science and technology, *ACS Symposium Series-406*; Johnston KP, Penninger JML Eds., American Chemical Society, Washington DC, 1989b, Chapter 23 : p355-378.
68. Mooney DJ et al. Novel approach to fabricate porous sponges of poly(D,L-lactic-co-glycolic acid) without the use of organic solvents. *Biomaterials* 1996, 17(14):p1417-1422.
69. Moshashae S et al. Supercritical fluid processing of proteins. I: lysozyme precipitation from organic solution. *European Journal of Pharmaceutical Sciences* 2000 Sep;11(3):239-45.
70. Mulcahey LJ, Taylor LT. Supercritical fluid extraction of active components in a drug formulation. *Analytical Chemistry* 1992, 64(9):p981-984.
71. Muller BW, Steckel H. Budesonide microparticles for pulmonary delivery produced by supercritical carbon dioxide. *Proceedings-International symposium on Controlled Release of Bioactive Materials* 1997, 24 : p69-70.

72. Mura G, Pozzoli S. Process for the production of powders with controlled particle sizes and powdery product so obtained. *European Patent Application* 1995, Publication Number 0661091A1.
73. Muth O et al. Polymer modification by supercritical impregnation. *Journal of Supercritical Fluids* 2000, 17 :p65-72.
74. Ohgaki K et al. Whisker formation from jet of supercritical fluid solution. *Journal of Supercritical Fluids*, 1990, 3, p:103-107.
75. Palakodaty S et al. Particle formation using supercritical fluids- A novel approach.. In Proc. 1997 *IChemE Event*, UK 1997, p501-504.
76. Palakodaty S et al. Supercritical fluid processing of materials from aqueous solutions: The application of SEDS to lactose as a model substance. *Pharmaceutical Research* 1998, 15(12) : p1835 -1843.
77. Palakodaty S, York P. *Phase behavioral effects on particle formation processes using supercritical fluids. Pharmaceutical Research* 1999, 16(7):p976-985.
78. Pennisi KJ, Chimowitz EH. Solubilities of solid 1,10-Decanediol and a solid mixture of 1,10-Decanediol and benzoic acid in supercritical carbon dioxide. *Journal of Chemical and Engineering Data* 1986, 31:p285.
79. *Perry's Chemical Engineers' Handbook*, Mc Graw-Hill, New York, 7th Ed. 1997.
80. Rajagopalan P, McCarthy TJ. Two-Step Surface Modification of Chemically Resistant Polymers: Blend Formation and Subsequent Chemistry. *Macromolecules*. 1998, 31(15):p4791.
81. Reverchon E et al. Solubility and micronization of griseofulvin supercritical CHF₃. *Industrial and Engineering Chemistry Research* 1995, 34(11) : p4087-4091.
82. Reverchon E, Donsi G. Salicylic acid solubilization in supercritical CO₂ and its micronization by RESS. *Journal of Supercritical Fluids* 1993, 6(4) : p241-248.
83. Robertson J et al. Novel techniques for particle production from supercritical solutions. *IChemE Research. Event. Conf. Young Res. Che. Eng.*, Publisher: Institute of Chemical Engineers, Rugby UK. 1996, 2:p988-990.

84. Rogers TL, Johnston KP, Williams RO 3rd. Solution-based particle formation of pharmaceutical powders by supercritical or compressed fluid CO₂ and cryogenic spray-freezing technologies. *Drug Development and Industrial Pharmacy* 2001.27(10):p1003.
85. Ruchatz F et al. Residual solvents in biodegradable microparticles. Influence of process parameters on the residual solvent in microparticles produced by the aerosol solvent extraction system (ASES) process. *Journal of Pharmaceutical Sciences* 1997, 86(1) : p 101-105.
86. Sand ML. Method of impregnating a thermoplastic polymer. *United States Patent* 1986, Number : 4,598,006.
87. Sand ML. Method of impregnating a thermoplastic polymer. *United States Patent* 1987, Number : 4,678,684.
88. Schmitt WJ. Finely divided solid crystalline powders via precipitation into an anti-solvent. *International Patent Publication* 1990, Number: WO 90/03782.
89. Sefcik MD. Dilation and plasticization of polystyrene by carbon dioxide. *Journal of Polymer Science: Part B : Polymer Physics* 1986, 24 : p957-971.
90. Sefcik MD. Dilation of polycarbonate by carbon dioxide. *Journal of Polymer Science: Part B : Polymer Physics* 1986, 24 : p935-956.
91. Sencar-Bozic P et al. Improvement of nifedipine dissolution characteristics using supercritical CO₂. *International Journal of Pharmaceutics* 1997, 148 : p123-130.
92. Shekunov BY et al. Crystallization in turbulent supercritical flows. *Journal of Crystal Growth* 1999, 198/199 p:1345-1351.
93. Shieh YT et al. Interaction of supercritical carbon dioxide with polymers. I. Crystalline polymers. *Journal of Applied Polymer Science* 1996a, 59 : p695-705.
94. Shieh YT et al. Interaction of supercritical carbon dioxide with polymers. II. Amorphous polymers. *Journal of Applied Polymer Science* 1996b, 59 : p707-717.
95. Steckel H et al. Micronizing of steroids for pulmonary delivery by supercritical carbon dioxide. *International Journal of Pharmaceutics* 1997, 152 : p99-110.

96. Subramaniam B et al. Methods for a particle precipitation and coating using near- critical and supercritical antisolvents. *United States Patent* 1998, Number: 5833891.
97. Subramaniam B et al. Pharmaceutical processing with supercritical carbon dioxide. *Journal of Pharmaceutical Sciences* 1997, 86(8) : p885-890.
98. Super, Beckman EJ. Copolymerizations employing CO₂ as comonomer. *Trends in Polymer science* 1997, 5:p236.
99. Tavana A et al. Scanning cosolvents for supercritical fluids solubilization of organics. *AIChE Journal* 1989, 35 : p645-648.
100. Tavana A, Randolph AD. Isobaric-isothermal fractional crystallization of organic solids from supercritical fluid mixtures : Particle design via crystallization, *AIChE Symposium Series* 1990, 87(284):p5-15.
101. Ting SST et al. Solubility of Naproxen in supercritical carbon dioxide with and without cosolvents. *Industrial and Engineering Chemistry Research* 1993, 32 : p1471-1481.
102. Tom JW et al. Applications of supercritical fluids in the controlled release of drugs. *Supercritical fluid engineering science, ACS Symposium Series-514*; Brennecke JF, Kiran E Eds., American Chemical Society, Washington DC, 1993, Chapter 19 : p238-257.
103. Tom JW, Debenedetti PG. Formation of bioerodible polymeric microspheres and microparticles by rapid expansion of supercritical solutions. *Biotechnology Progress* 1991a, 7(5) : p403-411.
104. Tom JW, Debenedetti PG. Particle formation with supercritical fluids-A review. *Journal of Aerosol Science* 1991b, 22(5) : p555-584.
105. Tom JW, Debenedetti PG. Precipitation of Poly (L-Lactic acid) and composite Poly(L-Lactic acid)-Pyrene particles by rapid expansion of supercritical solutions. *Journal of Supercritical Fluids* 1994, 7 : 9-29.
106. Turk M Formation of small organic particles by RESS: Experimental and theoretical investigations. *Journal of Supercritical Fluids* 1999, 15:p79-89.
107. Turk M et al. Micronization of pharmaceutical substances by the Rapid Expansion of Supercritical Solutions: A promising method to improve bioavailability of poorly soluble pharmaceutical agents. *Journal of Supercritical Fluids* 2002, 22:p75-84.

108. Van Hees T et al. Application of supercritical carbon dioxide for the preparation of a Piroxicam- β -Cyclodextrin inclusion compound. *Pharmaceutical Research* 1999; 16(12) :p1864-1870.
109. Weber A et al. Compressed fluid antisolvent crystallization for controlled particle design. *Crystal Growth in Organic Matter*. 4, Int. Workshop. Issue 4 1997 p:214-221
110. Weidner E et al. Powder generation from polyethyleneglycols with compressible fluids. *Process Technology Proceedings-12, High Pressure Chemical Engineering*; Rudolf von Rohr P, Trepp C Eds., Elsevier Science B. V, 1996, p223-228.
111. Weidner E et al. Process for preparing particles or powders. *International Patent Publication* 1995, Number: WO 95/21688.
112. Werling JO, Debenedetti PG Numerical modeling of mass transfer in the supercritical antisolvent process. *Journal of Supercritical Fluids* 1999, 16:p167-181.
113. Wissinger RG, Paulaitis ME. Glass transitions in polymer/CO₂ mixtures at elevated pressures. *Journal of Polymer Science: Part B : Polymer Physics* 1991, 29 : p631-633.
114. Wissinger RG, Paulaitis ME. Swelling and sorption in polymer-CO₂ mixtures at elevated pressures. *Journal of Polymer Science: Part B : Polymer Physics* 1987, 25 : 2497-2510.
115. Wong JM, Johnston KP. Solubilization of biomolecules in carbon dioxide based supercritical fluids. *Biotechnology Progress* 1986, 2(1) : p29-39.
116. Yang C, Xu YR, Yao WX. Extraction of pharmaceutical components from Ginkgo biloba leaves using supercritical carbon dioxide. *Journal of Agricultural and Food Chemistry* 2002, 50(4):p846.
117. Yazdi AV, Beckman EJ. Design of highly CO₂-soluble chelating agents II. Effect of chelate structure and process parameters on extraction efficiency. *Industrial and Engineering Chemistry* 1997, 36:p2368
118. Yeo SD et al. Formation of microparticulate protein powders using a supercritical fluid antisolvent. *Biotechnology and Bioengineering* 1993, 41(3) : p341-346.

119. York P et al. Controlled particle formation using the solution enhanced dispersion by supercritical fluids (SEDS) process. Presented at *16th Pharmaceutical Technology Conference*, Athens, Greece, April 1997.
120. York P et al. *Proceedings, Respiratory Drug Delivery*, South Carolina May 1998.
121. York P, Hanna M. Salmeterol Xinafoate with controlled particle size. *International Patent Publication* 1995, Number: WO 95/01324.
122. York P, Hanna M. Particle engineering by supercritical fluid technologies for powder inhalation drug delivery. *Respiratory Drug Delivery V* 1996, p231-239.
123. York P. Strategies for particle design using supercritical fluid technologies. *Pharmaceutical Science & Technology Today* 1999, 2(11).
124. Young TJ et al. Encapsulation of lysozyme in a biodegradable polymer by precipitation with a vapor-over-liquid antisolvent. *Journal of Pharmaceutical Sciences* 1999. 88(6) p:640-650.
125. Zia H et al. Comparison of nasal insulin powders prepared by supercritical fluid and freeze-drying techniques. *Particulate Science and Technology* 1997, 15:p273-301.

CHAPTER TWO

Title: *Design and Process Engineering of Laboratory Scale Supercritical Fluid Equipment.*

Abstract: Consistent production of solid drug materials of desired particle and crystallographic morphologies under cGMP conditions is a challenge often faced by pharmaceutical researchers. Supercritical fluid (SCF) technology gained significant attention in the pharmaceutical arena by not only showing a promise in this regard, but also accommodating the principles of green chemistry. Given that this technology attained commercialization in food industry, a majority of the off-the-shelf SCF instrumentation is designed for extraction purposes. Only a selective few vendors are in the early stages of manufacturing equipment designed for particle formation. The scarcity of information on the design and process engineering of laboratory scale equipment is recognized as a significant shortcoming to the technological progress. It is therefore the purpose of this article to provide the information and resources necessary for startup research involving particle formation using supercritical fluids. The various stages of supercritical particle formation can be broadly classified into Delivery, Reaction, Pre-expansion, Expansion and Collection. The importance of each of these processes from the standpoint of tailoring the particle morphology is discussed in this article, while also providing various alternatives to perform these operations.

Key words: Supercritical fluid Equipment; Particle formation; Design; Vendors

1. INTRODUCTION

The central role of solvents in the processing of pharmaceutical materials is widely accepted since the origin of modern pharmaceutical processing. It is only in the recent past that the adverse effects of the residual solvents from both processing and environmental standpoints have been recognized. Strict regulations on the use of organic solvents and their content in the end products forms a major limitation to the traditional techniques. In an effort to eliminate or reduce the use of volatile organics, search for alternative techniques of material processing developed as a new facet to pharmaceutical research. Supercritical fluid (SCF) technology is a recent outcome of such research with particular emphasis in the green synthesis and particle formation. Particle formation using supercritical fluids involves negligible or no use of organic solvents, while the processing conditions are relatively mild. In contrast to the conventional particle formation methods where a larger particle is originally formed and then comminuted to the desired size, SCF technology involves growing the particles in a controlled fashion to attain the desired morphology. The adverse effects originating from the energy imparted to the system to bring about size reduction can thus be circumvented. This feature makes supercritical fluid technology amenable to processing biomolecules and other sensitive compounds.

Particle engineering using supercritical fluids is a relatively recent development in the pharmaceutical arena. Growing demands on the particle and crystalline morphologies of pharmaceutical actives and excipients, coupled with

the limitations of current methods, brought wide attention to this technology [York 1999]. The technology is rapidly evolving, as reflected by the number of modified processes reported since its inception. These include Static Supercritical Fluid process [Lindsay 1992], Rapid Expansion of Supercritical Solutions (RESS) [Matson 1987], Particles from Gas Saturated Solutions (PGSS) [Weidner 1995], Gas Antisolvent process (GAS) [Gallagher 1989], Precipitation from Compressed antisolvent (PCA) [Bodmeier 1995], Aerosol Solvent Extraction System (ASES) [Bleich 1993], Supercritical Antisolvent process (SAS) [Bertucco 1996] and Solution Enhanced Dispersion by Supercritical fluids (SEDS) [York 1995]. Refer Table 3 and Figures 1 through 7 (Chapter-1) to distinguish the various processes from a mechanistic standpoint and to identify the critical attributes controlling the particle morphology. Solubilization, plasticization and diffusion properties of supercritical fluids are utilized in Static supercritical fluid process, RESS and PGSS processes. On the other hand, mass transport, dispersion and antisolvent properties of SCF's are of interest while dealing with the other processes. In principle, the supercritical fluids are used as recrystallizing aids in pharmaceutical particle formation. The basic advantages like rapid and uniform nucleation of solute(s) remain the same in all the processes, although the mechanism of particle precipitation varies with the process.

Carbon dioxide is regarded as an ideal processing medium [Subramaniam 1997] for a number of reasons. It is generally regarded as safe (GRAS), non-flammable, inexpensive; has a low critical temperature and pressure and exhibits

solubilization and plasticization effects that can be varied continuously by moderate changes in pressure and temperature. The solvent properties of supercritical carbon dioxide are reported to resemble those of hexane, toluene, isopentane and methylene chloride depending on the pressure and temperature conditions of the fluid [Hyatt 1984, Dandge 1985, Dobbs 1987, Ting 1993]. From a feasibility standpoint, compounds exhibiting significant solubility behavior in the SCF of interest (for example- lipophilic compounds with low molecular weight and high vapor pressure for SC CO₂) are most suitable for RESS process. PGSS is ideal for processing low melting compounds that exhibit negligible interaction with the SCF and more importantly, significant thermal stability. Antisolvent processes, on the other hand provide more flexibility in choosing the precipitation conditions through the use of solvents and solvent mixtures and by manipulating the solvent extraction conditions of SCF. Excepting PGSS [Mura 1995] and SEDS [Bonner 2000] processes which have been scaled up to the tune of producing 1 ton per year, the progress with other techniques is by far only limited to the research laboratories. The potential for SCF technology however is immense, as reflected by the wide gamut of pharmaceutical applications reported to date. Table 1 (Chapter-1) summarizes the various applications of supercritical fluid technologies in pharmaceutical material processing.

The majority of the off-the-shelf SCF instrumentation currently available is designed for extraction purposes. Only a selective few vendors are in the early stages of manufacturing equipment specific to particle formation (Table 9).

Table 9. Vendor Information of Supercritical Fluid Equipment And

Accessories

<u>ITEM</u>	<u>REPRESENTATIVE VENDORS</u>
Gas suppliers	Air Products, PA ; BOC Gases, NJ; Matheson, PA
Gas Pumps	Haskel, CA; Isco, NE; Jasco, MD
Liquid metering Pumps	Eldex, CA; Ivek, CA
Heat Exchanger/Chiller	Lytron, MA; Polyscience, IL
Tubing/Fittings	Vici Valco, TX; High Pressure Equipment Company, PA
Reaction Vessels	Thar Designs, PA; Pressure Products Industries, PA
Valves	High Pressure Equipment Company, PA; Vici Valco, TX
Back Pressure Regulators	Tescom, MN; Thar Designs, PA; Jasco, MD
Mixing loops	Thar Designs, PA; Autoclave Engineers, PA
Whole units	Supercritical Fluid Technologies, DE; Thar Designs, PA
Phase monitors	Supercritical Fluid Technologies, DE; Thar Designs, PA
Pressure Transducers	Texas Instruments, TX; Omega, CT
RTD/Thermocouples	Omega Engineering, CT
Flow meters	Dwyer, IN; Porter Instruments, CA; Coriolis Liquid Controls, IL
Nozzles	Thar Designs, PA; Applied Surface Technologies, NJ; BPD, UK
Sapphire windows	Thermo Oriel, CT; Mindrum Precision, CA; Insaco, PA
Toll processing	Thar Designs, PA; Lavipharm, NJ; Bradford Particle Design, UK
Technical Consultants	Phasex, MA; Supercritical fluid technology Consultants, PA

A general practice however, as reflected from the reported publications and patents, is to reconfigure a commercially available system specific to the end use. It is the purpose of this article to provide the information and resources necessary for startup research involving particle formation using supercritical fluids. The various stages of supercritical particle formation can be broadly classified into Delivery, Reaction, Pre-expansion, Expansion and Collection. The importance of each of these processes from the standpoint of tailoring the particle morphology is discussed in the following sections while also providing various alternatives to perform these operations.

2. SUPERCRITICAL FLUID DELIVERY

The critical point for any pure substance is defined by the temperature and pressure coordinates above which no physical distinction exists between the liquid and gaseous states. Substances above the critical point are referred to as 'supercritical fluids'. In contrast to the other transitions of state, the phase change from the liquid or gaseous state to the supercritical fluid state is not a first order phenomenon, although most physical and transport properties change abruptly around the fluid's critical point. Accurate determination of the solvent critical point is therefore not a straight forward task and often relies on a number of complimentary techniques involving the study of critical opalescence, mixture phase behavior and theoretical equations of state [McHugh 1994]. The binary critical phase behavior, however for a number of frequently used supercritical

fluids and fluid mixtures can be readily obtained from scientific literature [Walas 1985, Mc Hugh 1994, Perry 1997].

Among the various possible pathways, the most common and economic route of reaching the supercritical region is from a gas through the liquid state into the SCF phase. Compressed gases are readily available in large quantities and purity and are reasonably inexpensive. These gases are liquefied by passing through cooling lines prior to charging the pump (Figures 1 to 7). Delivering the fluid to the pump in a liquid state ensures effective pressurization without any cavitation problems. Frictional forces from the pump and the heat of compression can raise the temperature of the fluid, thereby inducing phase change and needs to be compensated using a heat exchanger. While circulating a coolant in an external chill-can surrounding the pump head can be an option, more sophisticated pumps rely on improving efficiency by internal circulation. Refer to Table 9 for details of major gas suppliers and pump vendors. Given that CO₂ is the SCF of choice in a number of reported pharmaceutical applications, pumps that efficiently perform up to 10,000psi are most commonly used. For applications that do not require high pressures or situations where the difference between the properties of fluids at sub and supercritical states is not distinctive, liquid tanks with a dip tube can be readily obtained from a number of gas suppliers that can be directly connected to a preheater.

Pressurized liquid from the pump is then brought to the supercritical state by it passing through a heat exchanger (preheater). Given the high thermal

conductivities of these fluids [Perry 1997], supercritical temperatures are easily reached although the residence time of fluids in the preheater is not long. A lengthy piece of coiled tubing up to 5 meters in length is typically used as a heat exchanger. The temperature of the coil is controlled using either a temperature bath/oven or a heating tape, and is chosen such that equilibrium supercritical temperatures are attained by the time the fluids reach the end of the coil. The flow of the SCF at this point is pulsed depending on the efficiency of the pump and exacerbated by the high kinetic energies of the fluids. Steady flow rates of SCFs assist in creating uniform conditions for nucleation in a number of supercritical fluid processes and is therefore of interest in the context of particle formation. Wherever uniformity in flow rates is considered important, pulse dampeners or snubbers can be used to buffer these pulsations. Alternatively, an additional vessel can be placed upstream of the reaction vessel that delays the frequency of pulsation and thereby stabilizes the flow rates. Flow measurement of the fluid in supercritical state is relatively difficult considering the high pressures and temperatures that the flow meters need to handle. Gas flow meters are typically used to monitor the supercritical fluid flow rates and are placed down stream of the particle collection vessel where the fluid is in gaseous state. Allowing the gas to flow through a lengthy tubing would not only assist in dropping any residual solutes or solvents well before the gas enters the flow meter, but also helps in the equilibration of temperature. Various flow meters are currently available and the choice of the meter should take into account such factors as the operating range,

sensitivity, type of fluid, moisture levels of the gas, inlet temperature and pressure, etc. While applications requiring accurate measurement such as the measurement of solute solubility in supercritical fluids require sensitive meters (eg. Thermo mass flow meter) with the totalizing function, other applications can function as well with inexpensive rotameters.

In operations involving the use of co-solvents, the phase behavior of the resulting supercritical mixture needs to be developed. A liquid metering pump is additionally required to deliver the co-solvent and can be purchased off the shelf from vendors dealing with the liquid chromatographic systems. It is noteworthy that such a metering pump should be capable of pumping the cosolvent against the head pressure of the compressed fluid. Mixing of the fluids can then be affected at the junction where they meet in T-configuration or more effectively, through the use of a sampling loop. The fluid mixture can then be delivered to the preheater that raises the temperature of the resulting mixture to the supercritical state.

3. REACTION

A reaction vessel is where the supercritical fluid is brought in contact with the material(s) to be processed. Essential requirements for a reaction vessel are chemical inertness, ability to withstand the operating temperature and pressure conditions and ASME specified design. Several designs of the pressure vessels are currently available and in general are distinguished by the type of closures.

Different closures vary in the nature and site of formation of the seal to contain the supercritical pressures. Finger tight closures with a 'c'cup seal formed of a graphite reinforced teflon ring containing an energized spring (Thar Designs, PA) can withstand pressures up to 10,000psi and are most suitable for pharmaceutical applications. Refer to Table 9 for particulars of some of the vendors of pressure vessels and reactors.

Reaction vessels made for pharmaceutical applications are typically made of stainless steel (316 SS) due to the sturdiness and chemical inertness of the material. The temperature of the vessel can be controlled either by using a heating mantle or a temperature controlled bath or oven. Controlled conditions of temperature and pressure in the reaction vessel are important to attain reproducible results and can be achieved through the use of sensitive pressure transducers and temperature measuring devices. Through a proper choice of the heaters and temperature controller and by an appropriate placement of the thermocouple(s), the temperature of the contents in the vessel can be accurately controlled.

Intimate mixing of the supercritical fluid with the material to be processed is critical in SCF material processing [Juvekar 1994, Muth 2000]. The effects are particularly pronounced in rapid expansion of supercritical solution (RESS) and particles from gas saturated solutions (PGSS) processes. Channeling of the supercritical fluid in continuous operations of RESS and PGSS processes limits the contact of the fluid with the material(s) of interest. Packing of solute(s) in the

reaction vessel is therefore critical in these processes and should maximize the interaction while limiting the entrainment of solute. Mixing the material with glass beads and glass wool prior to loading it to the reaction vessel is frequently used to improve the degree of interaction. The glass beads not only help in improving the contact of materials with SCF's, but also assist in buffering the flow pulsations by reducing the free volume in the reaction vessel. Alternatively, stirring or agitation in the reaction vessel can be provided using an impeller and a motor. Extrusion of the commonly used seals in mixing devices due to the sorption of gases into the polymers at relatively high temperatures forms a major limitation to using ordinary devices. Moreover, the wear and tear of the moving parts of the mixing device is exacerbated by the high pressures of the SCF process. To compensate for these limitations, magnetic mixing devices have been designed that effectively provide a leak proof agitation in a pressure vessel without the use of polymeric seals and other moving parts. Patented devices for mixing in pressure vessels such as PPI Dyna Magnetic Mixers and Ferro Micron Mixers are available as off-the-shelf items (Table 9).

For investigative studies requiring the physical observation of events occurring in the reaction vessel, view cells can be fitted in the vessel caps. Commonly used view cells are made of such materials as quartz, sapphire, polycarbonate etc. The compatibility of the cells and the seals with supercritical fluids needs to be verified prior to their use. Sorption of SCF's into the o-rings combined with the leaching capability of the fluids is a frequent cause of leakages

inherent in supercritical systems. Preventive maintenance of the system should therefore include replacing the seals at frequent intervals of time. For studies involving milder operating conditions, a Jerguson gauge (Clark-Reliance Corporation, OH) can be used as a reaction vessel and also to qualitatively view the events of the reaction. Solubility and phase behavioral events of the pharmaceutical materials in supercritical fluids can be developed using the above mentioned designs, although special devices called phase monitors are specifically designed and frequently used for such studies.

4. PRE-EXPANSION

The composition and phase of the supercritical solution from which particles are precipitated is found to have a major effect on the morphology of particles in RESS and PGSS processes and is controlled during the pre-expansion stage [Helfgen 2000, Weidner 1996]. Independent control of the temperature and pressure during the pre-expansion stage is therefore critical in these processes. Additionally, the phase changes in the supercritical solutions, which often lead to plugging of the lines, can be eliminated through the use of a controlled pre-expansion line. While one end of the pre-expansion line is connected to the reaction vessel, the other end feeds the supercritical solution through a back pressure regulator to the expansion device (Figures 2,3). The composition of the solution in this line may not only be controlled by changes in temperature, but also by adding fresh SCF solvent to the line. Typically, the pre-expansion line is a

lengthy coiled tubing having the same dimensions as the other lines with a port for the addition of fresh solvent. It is usually maintained at approximately 50°C higher than the temperature of the reaction vessel using a heating tape or a temperature bath/oven. Premature precipitation of solutes in the lines can thus be avoided unless the solute exhibits retrograde behavior in the operating temperature regime. In such instances, plugging can be prevented by the addition of fresh supercritical solvent to dilute the supersaturated solution. The fluids can be effectively mixed through the use of mixing loops that are most commonly used in pre-column reactions of HPLC analysis.

5. SPRAY CONFIGURATIONS

In supercritical fluid particle formation, the fluids are expanded through a restriction device in a controlled fashion. A restriction device is designed to support the large pressure drop that occurs across it, while maintaining suitable conditions for precipitation. The geometry of the restriction device has been shown to influence the morphology of the particles to varying degrees and by different mechanisms [Matson 1987, Debenedetti 1993a, Subrahmaniam 1998]. In RESS and PGSS processes, the device controls the growth of particle after the nucleation process by affecting the dynamics of jet expansion. On the other hand, the restriction device in antisolvent processes affects particle morphology by controlling the initial droplet size and also the rate of solvent extraction by the SCF. Various configurations have been used to date, namely capillaries, nozzles,

laser-drilled discs and valves. For investigative purposes, capillaries are preferred to other specialized designs owing to their availability, cost and the ease of changing the geometry of the device in house [Kim 1996]. Typical aspect ratios of the restriction devices evaluated to date are in the range of 6 to 20, with orifices from 20 to 1600 μ in diameter. Joule-Thompson cooling, resulting from the large volumetric expansion across the restriction device, causes a drop in temperature, thereby affecting a phase change and subsequently leads to plugging of the device. The restriction devices are therefore heated to compensate for such effects. While stainless steel nozzles are most frequently used owing to their strength to withstand the large pressure differential, they are limited by their poor thermal conductivities. Wherever necessary, they can be replaced with sapphire nozzles that provide better heat transfer to the fluid while also maintaining the material strength. The devices for the most part are custom designed according to the specific needs of the researcher. Off the shelf devices with standard configurations can also be obtained from selective supercritical fluid vendors (Table 9). Other coaxial nozzles that are specific to the SEDS process are regulated by the stringent patent protection and can be purchased for purposes notwithstanding the claims of the patent [Hanna 1999].

6. PARTICLE COLLECTION

Retaining the original characteristics of the particles produced by supercritical fluid process is as critical as forming the particles and constitutes the particle

collection step. This step is critical in that the distinct characteristics of the particles can be completely lost owing to a poor collection technique [Turk 1999]. In rapid expansion of supercritical solution and particles from gas saturated solution processes, the rapidly expanding supercritical fluids impart high kinetic energies to the particles produced. Insufficient path for expansion can therefore result in the agglomeration of particles. The agglomeration is even worse in the presence of residual amounts of co-solvent in RESS process or uncongealed portions in PGSS process. Design of particle collection vessel in these processes should be such that agglomeration is kept to a minimum by providing a sufficient path of expansion for the supercritical fluids. While a logical solution is to make the collection vessel very large, the collection of small amounts of material from a relatively larger vessel can be difficult, resulting in low yields. This problem can be circumvented in part by inserting detachable baskets inside the vessel. The baskets can be taken apart at the end of the process to collect the particles. While precipitating the solutes into a non-solvent containing a surfactant is another solution to agglomeration, it adds one more step to an otherwise continuous unit operation. An optimum balance between the ease of collection and the expansion path of the SCFs should be reached in designing the particle collection vessel. Other design factors that merit consideration include: surface finish of the inside of the baskets/vessel, shape of the vessel, alignment etc. [Matson 1987, Debenedetti 1993b, Turk 1999]. The role of post expansion conditions on the morphology of particles has been found to be inconclusive or relatively

insignificant. Excepting situations where post expansion conditions have been shown significant [Mohamed 1989a], or where fluid recompression costs are a factor, the collection vessel in RESS and PGSS processes is for the most part, maintained at atmospheric conditions.

The collection of particles in the antisolvent processes occurs in the same vessel where solvent extraction takes place. The particles are retained in the vessel by placing frits at either ends of the vessel while the solvents are extracted out with the flowing supercritical fluid. Particle agglomeration and solvent removal from the vessel in these processes are less dependent on the design of the vessel and are outweighed by other thermodynamic effects. The design of collection vessels used for antisolvent applications should however take into account the interaction between the materials and the supercritical fluids without plugging the lines [Hanna 1999].

7. SUMMARY

Current advances in pharmaceutical research have not only contributed to the discovery of various new technologies, but also identified the potential limitations of the conventional techniques of material processing [York 1999]. Among the different nascent technologies currently under investigation, supercritical fluid aided particle formation is reported to operate under relatively mild conditions making the process amenable to sensitive molecules, enzymes, proteins and other macromolecules [Yeo 1993, Moshashae 2000]. Volatile organic solvents can be

reused making their usage minimal. Different SCF processes have been demonstrated to produce particles with residual organic content of an order below the permitted levels [Steckel 1997]. Further, control over the morphology and crystallographic purity of the particles is shown to be better than several other conventionally used processes [Beach 1999]. The potential for SCF technology in the pharmaceutical realm manifests from all the above-mentioned features combined with the feasibility of producing particles under cGMP conditions in a unit operation. The information provided in this article is intended to assist investigative researchers in evaluating such potential either through setting up a particle formation system in house or by contracting the work to established supercritical fluid consultants.

8. LIST OF REFERENCES

1. Beach S et al. Control of the physical form of Salmeterol Xinafoate. *Organic Process Research and Development* 1999, 3:p370-376.
2. Bertucco A et al. Formation of biocompatible polymer microspheres for controlled drug delivery by a supercritical antisolvent technique. *Process Technology Proceedings: High Pressure Chemical Engineering* 1996, 12: p:217-222.
3. Bleich J et al. Aerosol solvent extraction system- a new microparticle production technique. *International Journal of Pharmaceutics* 1993, 97 : p111-117.
4. Bodmeier R et al. Polymeric microspheres prepared by spraying into compressed carbon dioxide. *Pharmaceutical Research* 1995, 12:980 : p 1211-1217.
5. Bonner J. A particularly fine way of making drugs. *Chemistry & Industry*, June 2000.
6. Dandge DK et al. Structure solubility correlations : Organic compounds and dense carbon dioxide binary systems. *Industrial and Engineering Chemistry Product Research and Development* 1985, 24 : p162-166.
7. Debenedetti PG et al. Rapid expansion of supercritical solutions (RESS): Fundamentals and applications. *Fluid Phase Equilibria* 1993a, 82 : p311-321.
8. Dobbs JM et al. Modification of supercritical fluid phase behavior using polar cosolvents. *Industrial and Engineering Chemistry Research* 1987, 26 : p56-65.
9. Gallagher PM et al. Gas antisolvent recrystallization : New process to recrystallize compounds insoluble in supercritical fluids. *Supercritical fluid science and technology*, ACS Symposium Series-406; Johnston KP, Penninger JML Eds., American Chemical Society, Washington DC, 1989, Chapter 22 : p334-354.
10. Hanna M et al. Method of particle formation. *International Patent Publication* 1999, Number: WO99/44733.
11. Helfgen B et al. Theoretical and experimental investigations of the micronization of organic solids by rapid expansion of supercritical solutions. *Powder Technology* 2000, 110:p22-28

12. Hyatt, JA. Liquid and supercritical carbon dioxide as organic solvents. *Journal of Organic Chemistry* 1984, 49 : p5097-5101.
13. Juvekar A. Study of a novel polymer loading process using near-critical carbon dioxide and a model drug. *M.S. Thesis, University of Rhode Island*, 1994.
14. Kim JH et al. Microencapsulation of naproxen using rapid expansion of supercritical solutions. *Biotechnology Progress* 1996, 12(5) : p650-661.
15. Lindsay AD, Omilinsky BA. Method of preparing mixtures of active ingredients and excipients using liquid carbon dioxide. *United States Patent* 1992, Number:5169433.
16. Matson DW et al. Rapid expansion of supercritical fluid solutions : Solute formation of powders, thin films and fibres. *Industrial and Engineering Chemistry Research* 1987, 26 : p2298-2306.
17. McHugh MA, Krukonis VJ. *Supercritical Fluid Extraction*. 2nd Edition; Butterworth-Heinemann:Newton, MA, 1994.
18. Mohamed RS et al. Effects of process conditions on crystals obtained from supercritical mixtures. *AIChE Journal*, 1989a, 35(2), p:325-328.
19. Moshashae S et al. Supercritical fluid processing of proteins. I: lysozyme precipitation from organic solution. *European Journal of Pharmaceutical Sciences* 2000 Sep;11(3):239-45.
20. Mura G, Pozzoli S. Process for the production of powders with controlled particle sizes and powdery product so obtained. *European Patent Application* 1995, Publication Number 0661091.
21. Muth O et al. Polymer modification by supercritical impregnation. *Journal of Supercritical Fluids* 2000, 17 :p65-72.
22. *Perry's Chemical Engineers' Handbook*, Mc Graw-Hill, New York, 7th Ed. 1997.
23. Steckel H et al. Micronizing of steroids for pulmonary delivery by supercritical carbon dioxide. *International Journal of Pharmaceutics* 1997, 152 : p99-110.
24. Subramaniam B et al. Pharmaceutical processing with supercritical carbon dioxide. *Journal of Pharmaceutical Sciences* 1997, 86(8) : p885-890.

25. Ting SST et al. Solubility of Naproxen in supercritical carbon dioxide with and without cosolvents. *Industrial and Engineering Chemistry Research* 1993, 32 : p1471-1481.
26. Turk M Formation of small organic particles by RESS: Experimental and theoretical investigations. *Journal of Supercritical Fluids* 1999, 15:p79-89.
27. Walas SM. *Phase Equilibria in Chemical Engineering* 1985, Butterworth Publishers, Stoneham, MA.
28. Weidner E et al. Powder generation from polyethyleneglycols with compressible fluids. *Process Technology Proceedings-12, High Pressure Chemical Engineering*; Rudolf von Rohr P, Trepp C Eds., Elsevier Science B. V, 1996, p223-228.
29. Weidner E et al. Process for preparing particles or powders. *International Patent Publication* 1995, Number: WO 95/21688.
30. Yeo SD et al. Formation of microparticulate protein powders using a supercritical fluid antisolvent. *Biotechnology and Bioengineering* 1993, 41(3) : p341-346.
31. York P, Hanna M. Salmeterol Xinafoate with controlled particle size. *International Patent Publication* 1995, Number: WO 95/01324.
32. York P. Strategies for particle design using supercritical fluid technologies. *Pharmaceutical Science & Technology Today* 1999, 2(11).

CHAPTER THREE

Title: *Co-Crystallization of Pharmaceutical Actives and Their Structurally Related Impurities By RESS Process.*

Abstract: Pharmaceutical research in the area of crystal doping to date has mostly been focussed towards understanding the impurity-induced effects on the host molecules. From an application standpoint, doping crystalline active pharmaceutical ingredients (API) can provide the ability to tie functionality to API's at early stages of drug discovery and synthesis. It is with this objective that a number of drugs were recrystallized in the presence of impurities from supercritical media. The rapid expansion of supercritical solution (RESS) process was evaluated for these purposes. Results of RESS aided crystal doping studies involving twelve drug-impurity mixtures are reported in this manuscript. It was concluded from these studies that RESS offers great promise as a hybrid technique to control both the crystalline and the particle morphologies of API's in a single stage. In addition, a number of interesting phenomena were revealed. These include habit modification, solubility enhancement, particle size reduction, eutectic formation, reduction in crystallinity, amorphous conversion, hydrate formation, polymorph conversion and selective extraction. In viewing each of these phenomena from an application standpoint, this manuscript serves as proof of concept for enhancing the physicochemical and mechanical attributes of API's using supercritical fluid crystal doping.

Key words: Co-Crystallization; Crystal Doping; RESS; Rapid Expansion.

1. INTRODUCTION

Imperfections prevail in virtually all solids to varying degrees, resulting in a wide range of materials from almost-perfect crystals to amorphous substances. While the nature of these imperfections can be studied in crystalline substances, the effects on an already disordered amorphous state are rather difficult to isolate [Suga 1997, Suga 1999]. The extent and nature of imperfections largely depend on the structural properties of solids, kinetics of crystallization and impurity levels, as well as other crystallization conditions [Weissbuch 2001]. The defects in crystals impart higher localized energies as a result of the elastic strain arising from the reduction in symmetry [Burt 1981, Weisinger 1989]. The higher energy of the system contributed by such pockets, although slightly compensated by increased entropy, is what renders higher free energy to imperfect crystals. Increased chemical potential and thermodynamic instability of such crystals can have profound implications in a wide variety of pharmaceutical applications.

The utility of impurities in causing crystal disruption is evaluated in this work by controlled co-crystallization of API and impurity from supercritical media. Besides modifying the energy of crystals, impurities are also reported to elicit a broad range of effects on the polymorphism, habit, size, true density and surface area of host crystals [Zhang 1999]. The combined effects on the morphology and energetics of the host crystals can be advantageously used in tailoring crystals to pharmaceutical needs and forms the scope of this research. Such research is of both fundamental and practical relevance. From a theoretical

standpoint, the role of impurities on crystal disruption can be studied and can be extended to tailoring additives for specific purposes. From an application perspective, the bulk properties of crystalline pharmaceutical actives can be modified according to their functional utility at early stages of chemical synthesis.

2.BACKGROUND

2.A. THEORY OF CRYSTAL DOPING:

Doping is defined as the deliberate addition of an impurity (guest) into the crystallizing medium of the host drug substance. Depending on molecular size and shape, stereochemistry, solubility and chemical affinity towards the host, impurities can profoundly alter the kinetics of nucleation and growth of the host crystals [Rauls 2000, Weissbuch 2001]. To date, various mechanisms have been proposed that typify the impurity-induced effects on the host crystals at both molecular and bulk levels. Firstly, the impurity can function as a co-solute in either enhancing or reducing the solubility of host crystals in the crystallization media. As a consequence of altered supersaturation, the induction time for nucleation and the metastable zone width are modified leading to changes in crystal size, size distribution and habit as observed with acetaminophen doped with p-acetoxyacetanilide [Prasad 2001].

Other means of crystal modification by impurities involves stereoselective adsorption of impurity onto specific faces of a crystal, causing differential inhibition of growth [Addadi 1982]. Inhibition of growth in a specific direction

manifests in increased surface area of the face perpendicular to that direction. Such selective inhibition might lead to modified aspect ratios, a change in habit and in some instances, crystallization of selective isomers and polymorphs. This phenomenon has been illustrated in several host-guest systems such as racemic glutamic acid mixtures, adipic acid+n-alkanoic acids, Benzamide+Benzoic acid, Sucrose+Raffinose, [Weissbuch 2001] Triglycine sulfate + L-alanine [Aravazhi 1997], Phenytoin + 3-acetoxymethyl-5,5-diphenyl hydantoin [Chow 1991], and Phenytoin+ 3-butanoyloxymethyl-5,5-diphenyl hydantoin [Chow 1995a]. Thirdly, the impurities can selectively displace host atoms, molecules or ions from their lattice points and thereby change the unit cell dimensions. While such substitutions are common among inorganic crystals, the substitutional point defects are seldom seen in pharmaceutically relevant crystals as reflected in the published literature. Instead, other zero and first order defects are frequent in organic crystals, perhaps through interstition of small molecules both within and outside the lattice. The basic criterion, however in either case is that the topology of networks should be complementary [Biradha 1999]. The interstition of impurities is reported to most frequently lead to lower dimensional defects such as point defects or edge and screw dislocations, resulting in an overall reduction in symmetry [Duddu 1995]. Finally, non-specific inclusion as observed in channeled impurities is another means by which impurities can induce crystal defects in the hosts. In a recent publication, Zhang and Grant evaluated eight guest-host systems

to report that the guest molecules most commonly exist in a solid solution rather than in liquid inclusions [Zhang 1999].

Depending on the differential rates at which the host and guest are precipitated out of a supersaturated solution and the specificity of interactions between them, the guest molecules either form a homogenous dispersion within the host matrix or are limited to surface sites as adsorbates. Several analytical techniques such as adsorption measurements, surface washing, progressive dissolution etc are currently in place to distinguish surface adsorption from solid solutions [Zhang 1999]. A solid solution can be viewed as the homogenous dispersion of the guest molecules at specific sites of the host during the early nucleation step, which subsequently get occluded as the growth of crystals continues. The presence of guest molecules therefore leads to the formation of defective crystals composed of mosaic blocks with totally different local symmetries and energies compared to pure crystals [Weisinger-Lewin 1989]. The implications of altered surface and bulk energies are profound in crystal dissolution [Burt1981], wetting [Chow 1995b] and reactivity [Duddu 1995] among other biopharmaceutical properties. Given the complexity of the crystallization process and the inadequacy of current analytical techniques to specify the exact location of impurity within lattices, the selection of doping agents has mostly been by trial and error. A direct correlation between the nature of the impurity and its role on the crystallization process is yet to be established, although significant inroads have been made towards this goal [Weissbuch 2001].

The defects in the crystals can spread, change their nature and at times may vanish depending on the molecular mobility and diffusivity of the impurities in the host crystals and other external stress factors. Given that such properties are orders of magnitude lower when dealing with solid substances, the thermodynamic instability of the defective crystals can be sustained throughout the typical shelf life of pharmaceutical actives. In theory, the stabilization of defective crystals requires similarity in the morphological, chemical and thermodynamic properties of the guest and host molecules. This theoretical intuition is substantiated in several model host/guest systems where similarity in molecular size, shape, melting point and solubility are found to be important [York 1985, Pikal 1987]. Also, large supersaturation aiding in fast nucleation and growth is demonstrated to be critical in locking the guest molecules into the lattices of the host [Burt 1981]. In this context, the RESS process (**R**apid **E**xpansion from **S**upercritical **S**olutions) appears particularly attractive, owing to the uniform and large supersaturation implicit in RESS aided crystallizations. Other factors such as vapor sorption, residual solvents and external stress can adversely mediate conversion of doped crystals to their thermodynamically stable forms. The RESS process proves viable even in this respect, as it involves neither the use of liquid solvents nor any large mechanical stresses in producing uniform sized crystals.

2.B. EFFECTS OF DOPING ON THE PROPERTIES OF CRYSTALS AND THEIR PHARMACEUTICAL APPLICATIONS:

A number of properties of the crystals are affected as a result of doping host molecules with impurities. The various properties are broadly classified based on their specific influence on the morphology and energy of the crystals. They are further subclassified into surface and bulk effects. This section covers the various modifications in the properties induced by doping of crystals with illustrated examples excerpted from the published literature. Possible applications of each of these modifications are also addressed wherever applicable.

Habit modification in the host crystals as a result of the incorporation of an impurity translates into changes in such properties as particle size, aspect ratio, density, specific surface area and surface roughness. The effects on particle size are based on the impurity effects on supersaturation and hence the crystallization kinetics, besides being habit related. A decrease in the particle size of phenytoin crystals is reported when doped with 3-propanoyloxymethyl-5,5-diphenyl hydantoin, which the authors attributed to habit thinning [Gordon 1992]. Changes in the aspect ratio of host crystals are frequently observed owing to the differential inhibition of growth in specific directions by the impurity. Chow and Grant investigated the influence of p-acetoxyacetanilide on the aspect ratios of acetaminophen [Chow 1989a] and further correlated such influence to the aqueous dissolution rates of acetaminophen [Chow 1989b]. True density of the crystals was found to be sensitive to the presence of impurities and is claimed to

be a sensitive indicator in quantifying the extent of crystal disruption. The influence of impurities on crystal densities has been experimentally verified using adipic acid/oleic acid and acetaminophen/p-acetoxyacetanilide as host/guest systems. [Duncan-Hewitt 1986] Another habit related property that was shown to be largely influenced by the doping process is specific surface area. Significant increases in the surface areas of acetaminophen [Chow 1985] and phenytoin [Gordon 1992, Chow 1995a] were observed when doped with impurities. Part of this enhancement has been attributed to the surface irregularities arising from the dislocation sites during measurements by gas adsorption techniques [Chow 1985]. As a result of crystal doping, surface irregularities have also been reported in few instances that significantly contribute to enhanced dissolution rates [Chow 1991]. A majority of the above mentioned properties are habit dependent. Inducing changes in habit, for example from acicular prisms to long thin plates as observed in phenytoin [Chow 1991] and from columnar to plate-like in acetaminophen [Prasad 2001] can have potential implications in processes such as wetting, dissolution, compaction etc. Another means of altering the properties of pharmaceutical actives is through the conversion of polymorphs & isomers [Kopp 1989, Laihanen 1996, Bosela 1997, Badawi 1997]. In theory, polymorphism arising from differences in conformation and packing can both be controlled using tailor made impurities. Reported proof of concept studies substantiating this fact include impurity induced crystallization of the polar polymorph of N(2-acetamido-4-nitrophenyl)pyrrolidene (PAN) [Staab 1990] and α -form of L-

glutamic acid [Sano 1997]. Resolution of equi-energetic conglomerates was also made possible utilizing tailor made impurities [Addadi 1982].

Doped crystals in general have lower crystallinity, melting point, enthalpy of fusion and higher entropy, free energy and disruption index compared to perfect crystals. The energy related effects of crystal doping originate from the lattice defects and other secondary manifestations in the host crystals. The defects in the crystals are stated to be associated with higher localized energies compared to the regions of normal configuration [Burt 1981]. These high-energy pockets are composed of the excess energy resulting from lattice strain and the core potential energy stored in the dislocation sites [Burt 1981, Weisinger 1989]. The higher energy of the system contributed by such pockets is slightly compensated by increased entropy of the disordered solids. In effect, impurities thereby render higher free energy to the imperfect crystals. Consequently, an increase in chemical potential and thermodynamic instability results in such crystals. The combined effects of loss of symmetry and increased activity lead to increased wettability, intrinsic dissolution rates and crystal reactivity in general [Chow 1995b]. This has been unambiguously proven using model systems like phenytoin [Chow 1995b] and adipic acid [Chan 1989] as hosts and a number of structurally related impurities as guests. Dissolution enhancement utilizing such subtle crystal modifications appears particularly attractive in the wake of recent amorphization efforts of a number of active pharmaceuticals [Yu 2001].

2.C. CHARACTERIZATION OF CRYSTAL DOPING:

The various techniques for evaluating the nature and magnitude of crystal disruption can be broadly classified into ones that characterize modifications in crystal morphologies and others that quantify the crystal energetics. Among the spectroscopic and microscopic techniques that study the primary morphological changes following crystal doping include optical microscopy [Burt 1981, Chow 1985, Prasad 2001], SEM [Chow 1991, Gordon 1992, Chow 1995a, Prasad 2001], atomic force microscopy [Li 2000], single crystal x-ray diffraction, [Bettinetti 2000, Williams-Seton 2000, Prasad 2001, Lynch 2000, Atencio 2000, Foxman 2001] powder x-ray diffraction [Burt 1981, Chow 1985, Gordon 1992, Chow 1995a], neutron X-ray diffraction, [Weisinger-Lewin 1989], IR [Aravazhi 1997, Bondar 2000] and solid state NMR [Yatsenko 1997, Bauer 2001, Gustafsson 1998]. Secondary manifestations that are sensitive to morphology changes such as density [Duncan-Hewitt 1986, Chow 1991] and thermal expansivity [Duncan-Hewitt 1986] are also used as indicators in evaluating crystal disruption. As reported by Burt [Burt 1981], Chow [Chow 1985] and Prasad [Prasad 2001] in their studies involving doped potassium perchlorate and acetaminophen crystals, optical microscopy aids in characterizing the aspect ratios, habit and dislocation sites such as etch pits in the doped crystals. In addition, changes in birefringence of the doped crystals can also be studied using polarizing optical microscopy. While gross structural changes are easily detectable using this technique, subtle crystal modifications are rather difficult to study and require further sensitive

techniques such as x-ray topography, scanning electron microscopy and atomic force microscopy. By contributing to the sensitivity, these techniques can also aid in locating the impurity in the doped crystals. Differentiation of surface adsorption from lattice incorporation of impurities is clearly demonstrated utilizing these techniques [Chow 1991, Gordon 1992, Chow 1995a, Prasad 2001, Li 2000].

Whenever growth of sufficiently large crystals is attainable, single crystal X-ray diffraction is most frequently used in typifying the structure of doped crystals. Although not simple in nature, this technique provides the knowledge of even minute changes in the cell dimensions of the defective crystals. Twinning and disordering in adipic acid crystals doped with different monoalkanoic acids was studied utilizing this technique [Williams-Seton 2000]. In a recent study, Prasad et al. analyzed p-acetoxycetanilide doped acetaminophen crystals using single crystal x-ray diffraction [Prasad 2001]. The authors reported an increase in the mosaic spread as a result of the high lattice strain induced by the impurity. Similarly, neutron diffraction analysis of the asparagine/aspartic acid system afforded knowledge of a reduction in symmetry of host crystals as a result of doping [Weisinger-Lewin 1989]. Excepting situations involving gross structural changes, powder x-ray diffraction (XRPD) does not appear to be sensitive to subtle changes in the doped crystals. A review of the pharmaceutical literature on crystal doping substantiates this fact as no significant changes in the diffraction patterns or the d-spacings were observed in a majority of doped crystals. On the

other hand, peak broadening and a change in the peak intensities were seen in IR and solid state NMR spectra with increasing disorder in the crystals. Aravazhi et al found broadening of the peaks in the IR spectra of doped crystals of triglycine sulfate [Aravazhi 1997]. Similar observations were reported in Gustafsson et al's study where the crystalline disorder in lactose is quantified using solid state NMR and confirmed with solution microcalorimetry [Gustafsson 1998].

Given that the impurities in the crystals bring about a variety of changes and by different means, it is not always possible to characterize the doping process by any one particular method. The complexity of identifying subtle morphological changes prompted researchers into quantifying the manifestations of such changes. In this context, density and thermal expansivity were found to closely vary with the disruption of the crystals by impurities. Duncan-Hewitt and Grant developed and evaluated different experimental techniques for the determination of these properties in doped adipic acid crystals. A comparative evaluation of these properties in quantifying the crystal disruption revealed that thermal expansivity is a more reliable indicator of crystallinity than density at a fixed temperature [Duncan-Hewitt 1986].

Crystal dissolution rate is another indicator frequently used in evaluating the doping process. The mixed effects of habit and the energy modifications on the intrinsic dissolution rates of the doped crystals, however need to be individually addressed in such evaluations. For example, the impurities can act as poisons in inhibiting dissolution from specific surfaces and locations [Burt 1981]. Other

habit related effects like crystal anisotropy, shape and size could also adversely affect crystal dissolution. On the other hand, the increased thermodynamic activity of these high energy-metastable crystal forms lends the driving force for enhanced dissolution of these crystals. Other means of dissolution enhancement following crystal doping are based on the surface irregularity and the solid solution mediated effects. The isolation and quantification of each of these effects is therefore very critical in controlling the final dissolution rates. To this objective, Chan and Grant developed methods that distinguish habit-related effects from the energy effects and successfully demonstrated it in two host/guest systems [Chan 1989].

Calorimetric techniques are commonplace to pharmaceutical laboratories, applications of which are constantly evolving with the advancements in instrumentation. Also, crystal energies are more sensitive to doping as compared to the morphological changes and are relatively easier to quantify. Owing to these reasons, the characterization of crystal doping in the pharmaceutical field is frequently based on the energy changes in the crystals. Doped crystals in general have lower crystallinity, melting point, enthalpy of fusion, heats of solution and higher entropy and free energy compared to pure crystals. Calculation of crystallinity values based on a single parameter or a technique often was found to result in different values [Pikal 1987]. This prompted academicians to develop scales to measure disruption based on the thermodynamic analysis of crystalline

solids. Accordingly, two indices were defined namely disruption index (d.i) [York 1986] and excess entropy index (e.e.i). [Pikal 1987].

The dimensionless disruption index compares the disorder created in the solid with that created in the liquid host by incorporation of guest molecules. It is defined as rate of change of the difference between the entropy of the solid and that of the liquid, with respect to the ideal entropy of mixing. For impurity mole fractions (x_2) less than 0.05, a plot of the entropy change following solid to liquid transition of the doped crystals (ΔS) versus the ideal entropy of mixing (ΔS_{ideal}^m) was experimentally found to give a straight line according to the equation:

$$\Delta S = \Delta S_0 - (b-c) \cdot \Delta S_{ideal}^m .$$

where (b-c) is defined as the disruption index. This behavior has been experimentally verified in several host guest systems [York 1986] and used it to develop a thermodynamic basis for such behavior. A number of assumptions have been made in the theoretical development of disruption index such as : (i) Excess entropies of solid hosts as a result of the incorporation of guests are proportional to the ideal entropes of mixing and (ii) The concepts of ideal entropy of mixing, often used in gas and liquid mixtures are applicable to the compressed states also. Although the validity of these assumptions is arguable to a degree, the concept of disruption index is simple, of practical interest and experimentally substantiated by various host/guest systems at $x_2 < 0.05$ [Pikal 1987]. The values of disruption index in the experimental systems evaluated thus far were found to range from 5

to 800 [Duddu 1995]. A correlation between the d.i values and the dissimilarity in the properties of the host and the guest has also been established [York 1986].

The change in entropy (ΔS) as a result of the phase change can be obtained from either the entropy of fusion (S_f) or the entropy of solution (S_s). Following thermal analysis of the doped crystals, the entropy of fusion can be calculated from the values of the heat of fusion and the melting temperature according to the equation:

$$\Delta G = \Delta H_f - T_m \Delta S_f$$

Here, the Gibbs free energy term becomes zero at the equilibrium fusion temperature implying $\Delta S_f = \Delta H_f / T_m$.

At times, the thermal history of the doped crystals during DSC/DTA analysis can induce relaxation of lattice strain and/or changes in their crystallinity. Also, partial decomposition might be evident as a result of heating the samples. Large errors in the experimental determination of the entropy of fusion values can occur in these cases. In such instances, entropy of solution, $S_s = (\Delta H - \Delta G)/T$ can be used as an alternative approach. While the free energy of solution process (ΔG) can be obtained from the solubility/intrinsic dissolution experiments, solution calorimetry can be used to determine heat of solution values (ΔH) at a fixed temperature. [Simonelli 1976, Grant 1986, Aki 2001].

The ideal entropy of mixing quantifies the disorder induced in any host substance (irrespective of its state) by the simple mixing of guest molecules so as to form a solution of guest+host. It explicitly disregards any other interactions

between the guest and the host. It can be calculated from the knowledge of the composition of the doped crystals following the equation:

$$\Delta S_{\text{ideal}}^m = -R \sum x_j \ln x_j$$

where x_j is the mole fraction of component j in the solid mixture.

With the current state of the art analytical instrumentation and the advances in separation science, isolation & quantification of impurities in the host crystals is not outside the scope of the analytical chemist. Such analytical data can then be used in the calculation of the ideal entropy of mixing of doped crystals. Knowledge of the entropy change following fusion or dissolution of the doped crystals along with the ideal entropy of mixing thus allows calculation of the disruption index at low levels of impurities. The invalidity of thermodynamic assumptions at higher levels of impurities coupled with other developing interactions between the host and the guest (eg-Eutectic formation) at such levels limits the concept of disruption index to impurity mole fractions of less than 0.05.

In an attempt to theoretically strengthen the concept of disruption index while questioning the validity of its assumptions, Pikal and Grant developed an analogous index to quantify crystal disruption called the 'excess entropy index' (S_2^E/R) [Pikal 1987]. According to this development, the pure entropy change of doped crystal as a result of the solid to liquid phase change was redefined following a more rigorous thermodynamic treatment and the limitations of the earlier assumptions were identified and compensated. Also, the disruption index was expressed in terms of limiting partial molar excess entropy of the guest. The

changes in the entropies of the doped crystals during the fusion and solution processes are expressed as quadratic functions of the mole fraction of guests as,

$$\Delta S_f = \Delta S_o^f - (S_{2,o}^E) x_2 + K x_2^2$$

$$\Delta S_s = \Delta S_o^s - \Delta S_{ideal}^m - [(S_{2,o}^{\alpha,0} - S_{2,o}^*) + (S_{2,o}^E)] x_2 + K x_2^2$$

where $(S_{2,o}^E)$ = Partial molar excess entropy of the guest

x_2 is the mole fraction of the guest

ΔS_o^f is the entropy change during fusion of the pure crystalline host

ΔS_o^s is the entropy of solution of the pure crystalline host

$S_{2,o}^{\alpha,0}$ is the entropy of the guest in standard solution phase

$S_{2,o}^*$ is the entropy of the guest in pure liquid state

K is a positive constant

The partial molar excess entropy of the guest is converted into a dimensionless number after dividing by the universal gas constant and termed excess entropy index. While this is considered a more exact approach to quantify crystal disruption, it does not necessarily negate the concept of disruption index. Moreover, a correlation was established ($d.i.=0.35[(S_{2,o}^E)]^p$, $p=0.912$) between the two indices, within the limitations of the assumptions made in Pikal and Grant's analysis [Pikal 1987]. Disruption index is therefore most frequently used in view of the simplicity of the model and its ease of determination, notwithstanding the limitations in its assumptions.

3. MATERIALS AND METHODS

3.A. Materials:

Aspirin (Sigma, St.Louis,MO Lot# 88H0411), Benzoic acid (JT Baker, NJ, Lot# N10603), Caffeine (JT Baker, NJ, Lot# T06596), Chloramphenicol, (Sigma, St.Louis,MO, Lot# 48H0570), Chlorpropamide (Sigma, St.Louis,MO, Lot# 31H0722), Indomethacin (Sigma, St. Louis, MO, Lot# 60K0745), α -Naphthalene acetic acid (Sigma, St.Louis,MO, Lot# 99H3253), Naproxen (Sigma, St.Louis,MO, Lot# 79H3685), Phenytoin (Lot#, Pfizer, NJ) Piroxicam (Sigma, St.Louis,MO, Lot# 126H0820), Salicylic acid (Sigma, St.Louis,MO, Lot# 49H3435), Theobromine (Sigma, St.Louis,MO, Lot#50K2503), Theophylline (Sigma, St.Louis,MO, Lot# 30K0939, Lot# 68H0610), Tolbutamide (Sigma, St.Louis,MO, Lot# 47H1030), Urea (JT Baker, NJ, Lot# N37340).

All the solvents used were bought from JT Baker and are of HPLC grade.

3.B. Methods:

3.B. 1. Crystallization from supercritical solvent:

The Rapid Expansion of Supercritical Solution (RESS) process was used in the co-crystallization of solid active pharmaceuticals and their structurally related impurities. In the RESS process, the solutes of interest were dissolved in supercritical carbon dioxide (SC CO₂), forming a homogenous supercritical solution. Nucleation of solutes was then induced by rapidly reducing the solution density through expansion to atmospheric conditions. A rapid decrease in solvent

strength results in high supersaturation that leads to very high nucleation rates [Mohamed 1989]. The time for nucleation and growth is very limited (typically 10^{-5} to 10^{-6} seconds), resulting in very small particles [Debenedetti 1993, Turk 1999]. Also, the rapid nucleation and growth aids in locking the impurities into the crystal domains of the hosts by not providing sufficient time for the impurities to segregate. Absence of residual liquid solvents in the RESS produced crystals further reduces the possibility for segregation effects in the solid state.

In addition, the rapid decompression of SCF generates mechanical perturbation within the solution that travels at the speed of sound. Consequently, very uniform conditions are reached within the nucleating media. Uniform conditions in the nucleation media assist in homogenous dispersion of impurities in the crystal domains of the hosts. The crystal disruption following such uniform and rapid co-crystallization can be expected to be controlled and large. All the above factors contributed to the special interest in RESS aided crystal doping and formed the rationale for its choice. Further, the concept is fairly nascent as reflected by the number of SCF aided crystal doping studies reported in the published literature [Weber 1997, York 1995].

The commercially available supercritical fluid extraction equipment (SFT150, Supercritical Fluid Technologies Inc., Delaware) was reconfigured to produce co-crystals of drugs and impurities by the rapid expansion of supercritical solution process. The modified design for the RESS process is schematically represented in Figure 8 and shown in Figure 9.

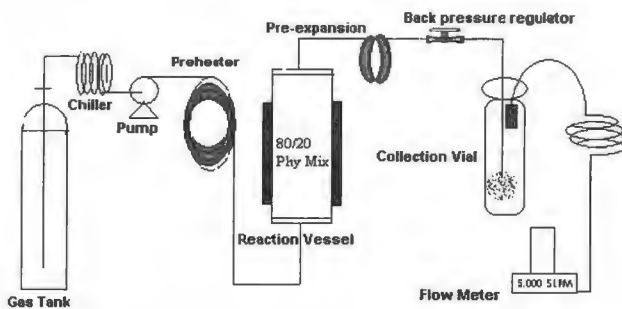


Figure 8. Schematic of RESS Process for Crystal Doping

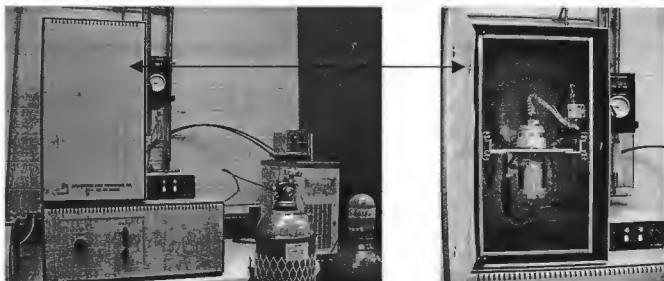


Figure 9. RESS Equipment used in Crystal Doping

Liquid CO₂ from a tank is pressurized using an air driven Haskel pump. The pump head is enclosed in a chiller-can through which a coolant at -10°C is continuously circulated. The coolant compensates for heat generation in the pump and prevents cavitation by maintaining CO₂ in the liquid state at all times. The pressurized liquid is then fed to the preheater at a controlled flow rate. The function of the preheater is to serve as a heat exchanger and raise the temperature of the pressurized liquid to the supercritical region. The preheater used was a five-metered stainless steel coil wrapped with Omegalux rope heaters (FGR, Omega Engineering Inc., Stamford, CT). The temperature of the preheater was controlled using a Glas-Col temperature controller (Glas-Col, Terre Haute, IN). The supercritical CO₂ from the preheater then flows into the 100 ml reaction vessel that contains the solutes to be recrystallized.

The reaction vessel was typically packed with 90 g of 3 mm glass beads and 10 g of solutes. The glass beads assist in improving the extraction efficiency of the SC CO₂ by providing better fluid contact with solutes while also serving to buffer the turbulent flow of the fluid through the vessel. The starting mixture in the reaction vessel consisted of a physical blend of 80% drug and 20% impurity. Placing glass wool at both ends of the reaction vessel supported the powder bed and also prevented the entrainment of solutes. Depending on the selectivity of extraction of the supercritical solvent, saturated solutions form in the reaction vessel with fixed compositions of the host and impurity. The saturated supercritical fluid solution from the reaction vessel flows through a 0.5 μ frit into

the pre-expansion chamber. It can be treated in the pre-expansion chamber to control the supersaturation prior to expansion. For the purposes of consistency in the crystal doping studies, the preexpansion chamber was maintained at 50°C above the extraction temperature. The presence of cold spots and abrupt temperature drop in the lines were found to cause premature precipitation of solutes, which in turn lead to plugging of lines. All the lines and connectors therefore were heated using Omega rope heaters controlled by a common Glas-Col temperature controller.

The saturated solution from the preexpansion chamber then passed through a heated restriction device maintained at 100-150°C prior to rapid expansion. The heated restriction valve compensates for the Joule-Thompson cooling that occurs as a result of rapid expansion. The expansion device used was a stainless steel capillary with an aspect ratio of 100 (5" L / 0.05" ID) that is securely inserted through the snap cap of a 40 ml glass vial (Daigger, Lincolnshire, IL). Given that the interest here is in the crystal morphology of the pharmaceutical actives rather than their particle size, a 40ml particle collection vial is best suited for these purposes. Use of a 40 ml glass vial also improved yields by preventing losses from the particle collection typically observed with larger vessels. CO₂ gas after deposition of the solids was exhausted through a custom filter and passed through lengthy tubing (5meters) prior to feeding to the thermo mass flow meter (Porter Instruments, Hatfield, PA). The gas flow rates were further measured (Infinity Rate Totalizer, Newport Electronics, Santa Ana, CA) over the course of the

experiment to get a more reliable estimate of the average CO₂ flow rates through the system. Typical flow rates of CO₂ through the system were between 5-10 SLPM. At the end of each run, yields of the recrystallized materials were recorded and the vials stored in low humidity plastic bags at ambient temperature until further use.

Following the above method, a number of drug-impurity mixtures (Table 10) were recrystallized and the efficiency of SCF aided crystal doping was evaluated. The supercritical region investigated in these studies included a temperature regime of 45-100°C and pressures between 2000-8000 psi.

3.B. 2. Differential Scanning Calorimetry:

DSC analysis was performed using a Perkin-Elmer DSC-7 equipped with an intercooler. Accurately weighed milligram samples were scanned in pin-holed aluminum pans (TA Instruments, Dupont) under a dry nitrogen purge. Various heating rates of 1,3,5 and 10°C/min were used to scan the different temperature regimes that were of interest to the samples under consideration. The instrument was calibrated for temperature and enthalpy using high purity Indium and USP Water.

3.B. 3. Thermogravimetric Analysis:

Thermal decomposition, moisture and residual solvent contents of the recrystallized materials were investigated using Perkin-Elmer TGA-7 at a heating

Table 10. Drug-Impurity Mixtures Evaluated in RESS Recrystallization

Studies

API	Dopant
Salicylic acid	Aspirin
Salicylic acid	Benzoic acid
Aspirin	Benzoic acid
Tolbutamide	Chlorpropamide
Tolbutamide	Urea
Piroxicam	Theophylline
Piroxicam	Benzoic acid
Theophylline	Caffeine
Theophylline	Theobromine
Phenytoin	Caffeine
Indomethacin	Salicylic acid
Naproxen	α -Naphthalene-acetic acid

rate of 5°C/min. Samples were heated in an open platinum pan with the nitrogen purge at 60 mL/min. The temperature scale was calibrated by measuring the Curie point (354°C) of standard PE ferromagnetic Nickel, while standard weights were used to calibrate the weight scale.

3.B. 4. Powder X-ray diffractometry:

XRPD was performed using a Rigaku-Geigerflex KD-2660-N X-ray diffractometer controlled by the D-Max B controller and Datascan MDI software. The diffractometer is equipped with a copper target, yielding X-rays of wavelength 1.54° Å. Diffractograms were obtained over the 2θ range 3° to 50° and analyzed using MDI Jade-5 software. Depending on amounts of the samples available for XRPD analysis, the powders are either packed into the 0.2 mm groove of a glass slide (Regular Method) or sprinkled onto a thin film of Apiezon grease applied onto the glass slide (Grease Method). The operating conditions included: scan speed 3°/minute, sampling interval 0.020° and X-ray power (tube input) of 40kV/40mA. The path of x-rays is controlled utilizing standard slits such as: ½ divergence, ½ scatter slits, 0.3mm receiving and 0.6mm receiving monochromator slits, in that order. The instrument is routinely calibrated under these operating conditions using Rigaku Quartz as standard.

3.B. 5. Polarizing Optical Microscopy:

The bulk particle morphology and the crystalline birefringence behavior of the

samples were investigated using a polarizing optical microscope (Leitz Lab 12 Pol S) with a tungsten lamp as the light source. The objects are viewed and photomicrographs developed utilizing such accessories as a Sony video camera, Boeckeler Via-70 Video marker and Sony 5600MD Video printer. A first order red compensator was used to enhance the clarity of the photomicrographs. Untreated powders or powders dispersed in suitable media were placed on a glass slide and covered with a cover slip, prior to staging them in the path of brightfield light. The objects were viewed in the magnification range 200-800X, calibrated using an Olympus calibration slide.

3.B. 6. HPLC Analysis:

The quantities of host and guest in theophylline+caffeine and theophylline+theobromine co-crystals were assayed by liquid chromatography (LC). Isocratic, reversed phase LC separation methods were developed and validated following modifications to the respective USP methods for the hosts and using external standards. Specific details of the methods are summarized in Tables 11 and 13, while the representative chromatograms of these mixtures are shown in Figures 10 and 11. The results of the validation experiments of theophylline+caffeine and theophylline+theobromine are respectively summarized in Tables 12 and 14. Calibrated HP1100 series LC system equipped with a diode array detector was used in these analyses.

Table 11. HPLC Method of Assay for Theophylline & Caffeine

Column	Supelco C-18 column, 4.6mm x 15cm
Mobile Phase	15% Acetonitrile + 85% Sodium acetate buffer (pH of mix = 3.97)
Flow rate	1.0 ml/min
Runtime	6 minutes
Injection Volume	20 µL
Detector	HP Diode array, 280nm
System	HP 1100 series
Retention times	2.5 min (Theophylline) and 3.5 min(Caffeine)

**Table 13. Validation Results of HPLC Method of Analysis of Theophylline
And Caffeine**

Parameter*	<u>Theophylline</u>	<u>Caffeine</u>
Range	40-240 µg/ml	2-60 µg/ml
Precision	0.22-0.37%	0.2-0.54%
Accuracy	98-100%	97-102%
Linearity	0.07%	0.05%
Reproducibility	-----Demonstrated over 1 week-----	
Theoretical Plates	>15000	>18000
Resolution	-	7

*Refer USP 24/NF 19, 2001 for the definitions of validation parameters and their significance.

Table 12. HPLC Method of Assay for Theophylline & Theobromine

Column	Supelco C-18 column, 4.6mm x 15cm
Mobile Phase	5% Tetrahydrofuran + 95% USP Water
Flow rate	1.0 ml/min
Runtime	10 minutes
Injection Volume	20 µL
Detector	HP Diode array, 280nm
System	HP 1100 series
Retention times	2.4 min (Theobromine) and 3.7 min(Theophylline)

Table 14. Validation Results of HPLC Method of Analysis of Theophylline & Theobromine

Parameter*	<u>Theophylline</u>	<u>Theobromine</u>
Range	10-300 µg/ml	2-160 µg/ml
Precision	0.08-0.40%	0.06-0.34%
Accuracy	98-101%	98.5-100%
Linearity	0.02%	0.07%
Reproducibility	----Demonstrated over 1 week----	
Theoretical Plates	>16000	>14000
Resolution	-	8.5

*Refer USP 24/NF 19, 2001 for the definitions of validation parameters and their significance.

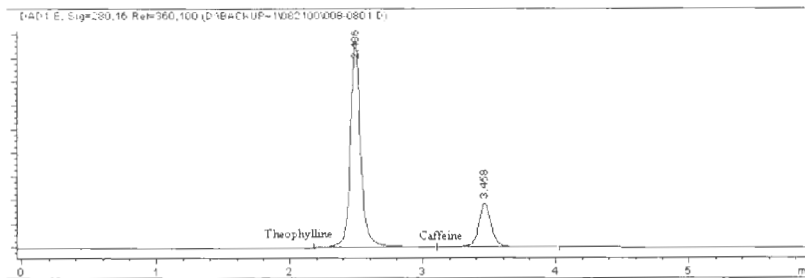


Figure 10. Typical HPLC Chromatogram Showing the Resolution of Theophylline and Caffeine in a Mixture

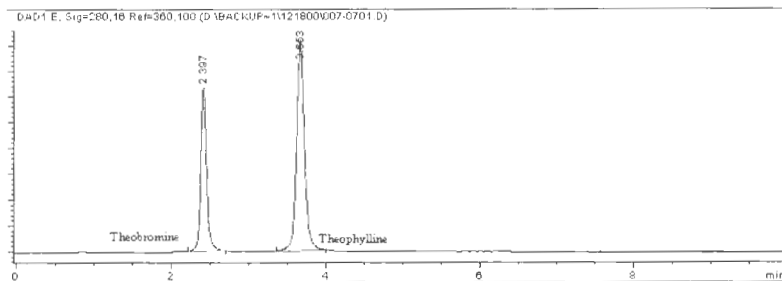
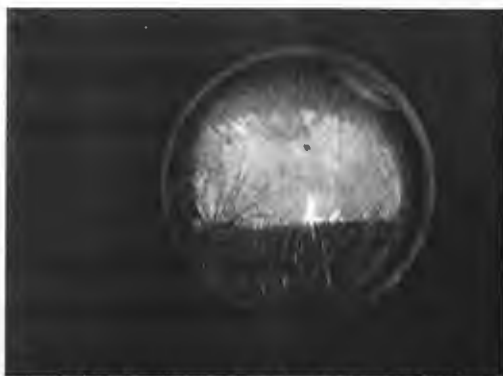


Figure 11. Typical HPLC Chromatogram Showing the Resolution of Theophylline and Theobromine in a Mixture

4. RESULTS AND DISCUSSION

4.A. Habit modification and Solubility enhancement:

Qualitative observations of the phase behavioral events of Salicylic acid +Aspirin in supercritical CO₂ revealed that the three component mixture exists in a single phase at 75°C, 4000 psi (Chapter 5). The solvent power of SC CO₂ (30 ml) at these P,T conditions is therefore sufficiently high to dissolve salicylic acid (4 mg) and aspirin (1 mg) and form a clear solution. Knowledge from the phase behavioral studies provided the ability to perform rapid co-crystallizations from the homogenous supercritical solutions of host + impurity in SC CO₂. The presence of aspirin as an impurity was found to affect the crystallization of salicylic acid in two different ways. Firstly, the bulk morphology of recrystallized salicylic acid changed from long needles to short dense network in the presence of aspirin. (Figures 12a and 12b) The effects of varying supersaturation on the crystallization kinetics and hence the particle size were observed by changing the pressure conditions prior to expansion. As can be seen from Figures 13a to 13e, the crystal size appears to be increasing as a combined effect of the lowered supersaturation and increased time for growth upon lowering the pressure from 4500 psi to 750 psi. The use of ethanol as a cosolvent with SC CO₂ promoted selective extraction of salicylic acid while reducing the impurity effects on the crystal morphology of salicylic acid (Figure 13f). Particle size reduction, however was still evident even in this case that is implicit in RESS processing.

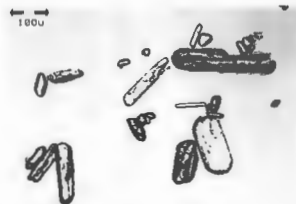


12a. Salicylic acid recrystallized from SC CO₂ at 75°C, 4000psi



12b. Salicylic acid recrystallized in the presence of Aspirin from SC CO₂ at 75°C, 4000psi

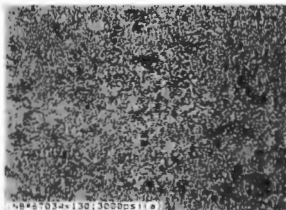
**Figure 12. Change in the Crvstal Morphology of Salicylic acid Upon Doping
with Aspirin**



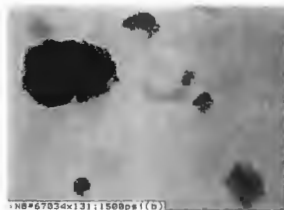
a. 80/20 Physical Mixture of SA + Aspirin



b. Recrystallized from SC CO₂ at 75°C, 4500psi



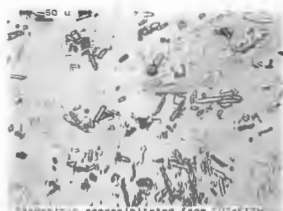
c. Recrystallized from SC CO₂ at 75°C, 3000psi



d. Recrystallized from SC CO₂ at 75°C, 1500psi



e. Recrystallized from SC CO₂ at 75°C, 750psi



f. Recrystallized from SC CO₂+EtOH at 45°C, 3000psi

Figure 13. Effect of Precipitation Conditions On the Morphology of Salicylic Acid + Aspirin Co-Crystals

The effects on the crystallinity of pure salicylic acid recrystallized by RESS were investigated using DSC and XRPD. The results of DSC analysis of SCF recrystallized salicylic acid are shown in Figure 14 and summarized in Table 15. As can be seen from Table 15, no significant differences in the melting temperature or the enthalpy of fusion values are observed in salicylic acid recrystallized from SC CO₂ compared to the original material. These results are consistent with the XRPD observations where no changes in the crystallinity of salicylic acid were seen as a result of supercritical recrystallization. However, as can be seen from Figure 15, the crystal habit was significantly altered from plates to acicular needles, depending on the expansion conditions. Supercritical fluid recrystallization herein provides the independent ability to change the crystal habit while not altering the polymorphic form of the API. In addition to the changes in the crystal habit, particle size reduction was also apparent in RESS produced salicylic acid the extent of which depended on the expansion conditions.

The secondary effects of the presence of a co-solute in the crystallization medium included enhancement of the yields. For example, a five-fold increase in the salicylic acid yield was observed in the presence of aspirin. While crystallization of pure salicylic acid at the same conditions of pressure and temperature yielded 390 mg of product, the presence of aspirin increased the yield up to 2050 mg per 100 L of recrystallizing solvent CO₂ used (at STP) (see Appendix A, sections 1B and 2B for further details). Co-solute mediated enhancement of salicylic acid solubility in SC CO₂ in the presence of aspirin is

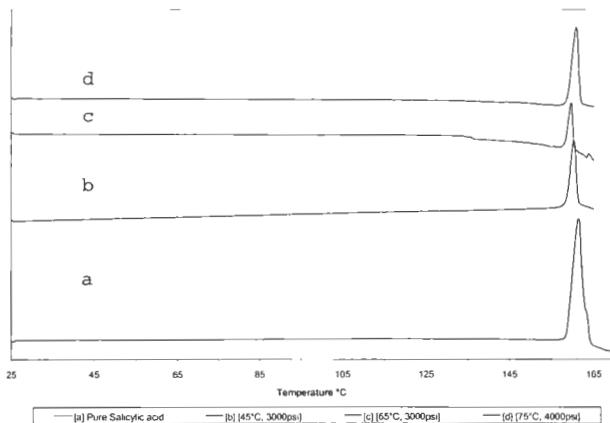


Figure 14. DSC Thermograms of RESS Recrystallized Salicylic Acid

Table 15. Thermal Analysis of RESS Recrystallized Salicylic acid

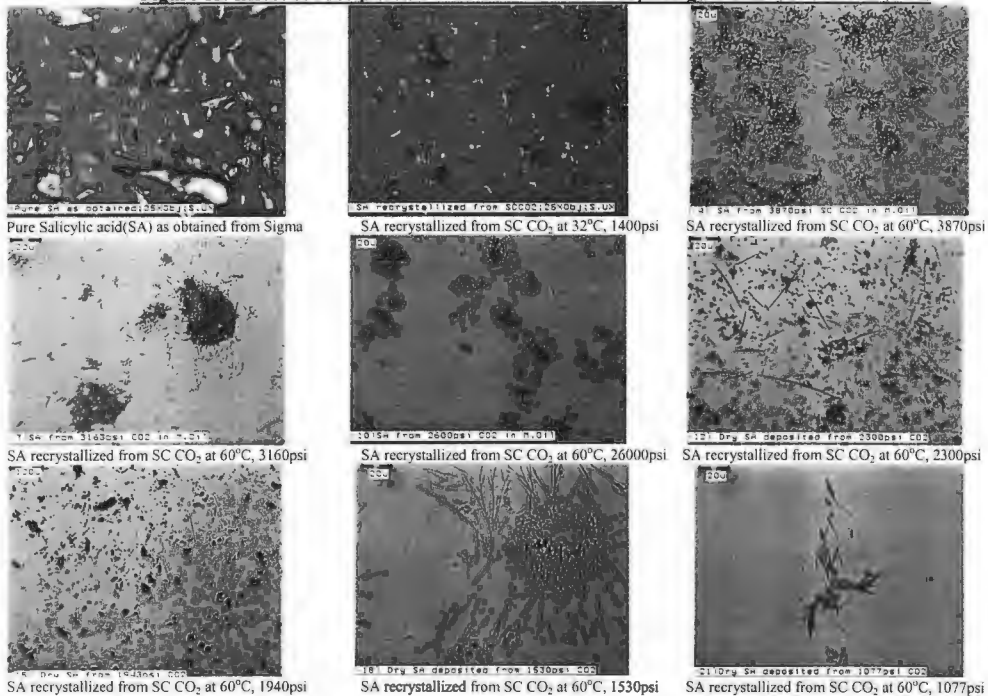
Material	Melting Point °C	Onset °C	End °C	Melting Range °C	Delta H J/g
Pure Salicylic acid as obtained from Sigma	161.3	158.7	163.1	4.5	188.3
Recrystallized from SC CO ₂ at [45°C, 3000psi]	160.3	158.6	161.4	2.7	175.6
Recrystallized from SC CO ₂ at [65°C, 3000psi]	159.8	158.3	160.4	2.1	175.4
Recrystallized from SC CO ₂ at [75°C, 4000psi]	160.8	157.5	161.9	4.4	169.9

expected be the cause for improved yields. In a similar study, the effect of trace amounts of methanol and acetone on the solubility of theophylline+caffeine was also investigated. The results of these studies are summarized in Figure 16. As can be seen from figure 16, acetone appears to significantly enhance the solute uptake by SC CO₂ at lower temperatures. Higher temperatures, on the other hand reduced the solute uptake, perhaps because of a reduction in the solvent density. The results of the effects of methanol were inconclusive owing to the difficulty in preventing MeOH from condensing in the collection vial during particle formation.

4.B. Eutectic Formation:

Addition of aspirin as an impurity to the crystallization media of salicylic acid resulted in the formation of a low melting mixture. As can be seen from Figure 17, recrystallization from pure SC CO₂ at 75°C and 4000 psi formed a low melting mixture that melted at 115°C. On the other hand, use of SC CO₂ + ethanol at 45°C and 3000 psi as the solvent system resulted in the formation of a similar low melting mixture as a minor component and pure salicylic acid as the major component. Selective salicylic acid crystallization is evident in the latter case. Although no eutectic formation between salicylic acid and aspirin has been reported to date, similar melting point depressions were observed in these mixtures by Mroso et al. [Mroso 1982]. Depression in the melting point depended on the amount of aspirin present as can be seen from Figure 17.

Figure 15. Effect of Precipitation Conditions On the Morphology of Salicylic Acid Crystals



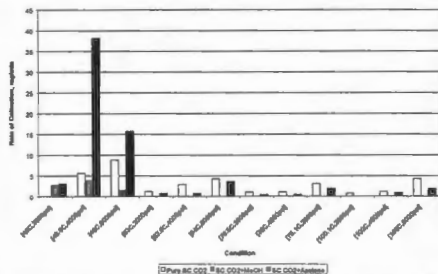


Figure 16. Effect of Co-solvents On Amounts of Theophylline+Caffeine Collected By RESS Process

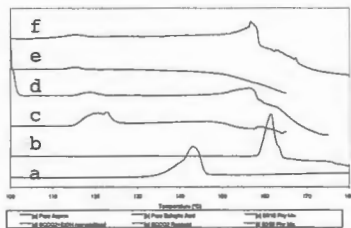


Figure 17. DSC of Salicylic acid +Aspirin Mixtures

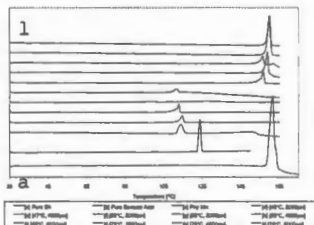


Figure 18. DSC of Salicylic acid+ Benzoic Acid Mixtures

Thermal analysis of RESS produced mixtures revealed that a constant composition mixture that melted at 115°C was formed at the various conditions studied. Similar melting depressions were seen in RESS recrystallized mixtures of salicylic acid+benzoic acid (Figure 18), aspirin+benzoic acid (Figure 19), tolbutamide+ chlorpropamide (Figure 20) as compiled in Table 16. Such reproducibly large shifts in the melting temperatures indicate the formation of low melting compositions of drugs and impurities and possibly eutectic formation.

4.C. Reduction in Crystallinity/Amorphous Conversion:

Depending on the affinity of the impurity to the host and the relative rates of nucleation and growth, solid solutions or solid dispersions of the impurity in the host matrix are formed. A reduction in the crystallinity and subsequent amorphous conversion of a number of host crystals was affected by this means following the RESS aided co-crystallization of host and the impurity (Table 17). Weber et al reported a similar study involving the co-precipitation of chloramphenicol+urea and ascorbic acid+aspirin systems by the PCA (precipitation from compressed antisolvent) process [Weber 1997]. Following the NMR analysis, the authors stated that a general reduction in crystallinity and an increase in the amorphous content was seen in these co-crystals. The authors further expressed the difficulty in detecting modest changes in the crystallinity of doped crystals, when NMR revealed no specific information in the ascorbic acid+aspirin co-crystals. In view of this fact, a number of complementary techniques discussed in section D were

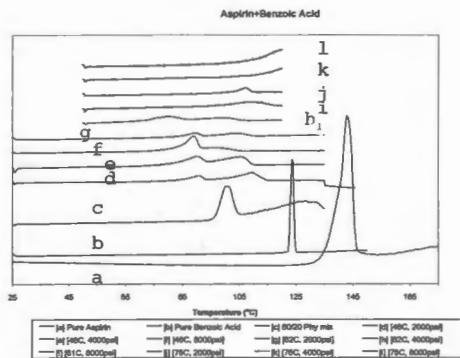


Figure 19. DSC Thermograms of Aspirin + Benzoic Acid Mixtures

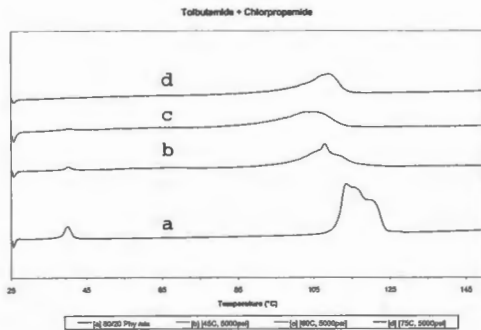


Figure 20. DSC Thermograms of Tolbutamide + Chlorpropamide Mixtures

**Table 16. Formation of Low Melting Mixtures of Drugs + Impurities Upon
RESS Recrystallization**

Drug(1)+Impurity(2)	T _{m1} (°C)	T _{m2} (°C)	T _{m1+2} RESS Co-Crystals (°C)
Salicylic acid+Aspirin	161.3	142.9	115
Salicylic acid+Benzoic acid	161.3	123.7	112
Aspirin+Benzoic acid	142.9	123.7	90, 105
Tolbutamide+Chlorpropamide	130.5	121.5	108

Table 17. Summary of RESS Co-crystallization Studies of Various Drug-Impurity Mixtures

API	Dopant	Observation [†]
Salicylic acid	Aspirin	Habit modification, Improved Yield, Low melting Mixture
Salicylic acid*	Benzoic acid*	Low melting Mixture, Selective extraction
Aspirin*	Benzoic acid*	Low melting Mixture, Selective extraction
Tolbutamide	Chlorpropamide	Polymorphic Conversion
Tolbutamide	Urea	Polymorphic Conversion
Piroxicam	Theophylline	Amorphous Conversion
Piroxicam	Benzoic acid	Amorphous Conversion
Theophylline	Caffeine*	Selective Extraction, Hydrate Formation
Theophylline*	Theobromine	Selective Extraction
Phenytoin	Caffeine*	Amorphous Conversion, Selective extraction
Indomethacin	Salicylic acid*	Amorphous Conversion, Selective extraction
Naproxen	α -Naphthalene-acetic acid	Amorphous Conversion

[†]Reduction in Crystallinity seen in all the doped crystals.
[‡]Component Preferentially Extracted.

utilized in this study. XRPD analysis served as a very powerful tool in monitoring the sensitive changes in the crystallinity of doped crystals. The initial examination of the diffraction patterns of the recrystallized materials and physical blends revealed no gross differences in a majority of the drug-impurity mixtures studied. Exhaustive analysis of the raw XRPD data was then undertaken following which the FWHM (full width at half maximum) values were calculated for individual peaks. Section C of Appendix A tabulates the analyzed XRPD data of all the drug-impurity mixtures reported in this chapter. Although no crystallinity scales were developed from these values, a comprehensive evaluation of the crystallinity was made based on such factors as the intensity of diffraction, peak shifts and FWHM values. Comparison of the intensity of reflections from doped crystals with those of the pure crystals and the physical mixtures indicated a general reduction in the crystallinity in all the drug-impurity mixtures studied (Section C, Appendix A). Figures 21 and 22 illustrate this fact where a drastic reduction in the intensity of salicylic acid was seen upon co-crystallizing with aspirin and benzoic acid respectively. Polarizing optical microscopy of salicylic acid doped with aspirin indicated a loss in the birefringence further validating the reduction in crystallinity (Figure 23). This reduction in crystallinity may be mediated through the eutectic formation between SA and aspirin reported in section-B.

Reduction in crystallinity, in theory, reduces the extent to which different planes diffract x-rays while also causing the broadening of peaks. On the other hand, an impurity can also influence the crystal geometry by not only altering the

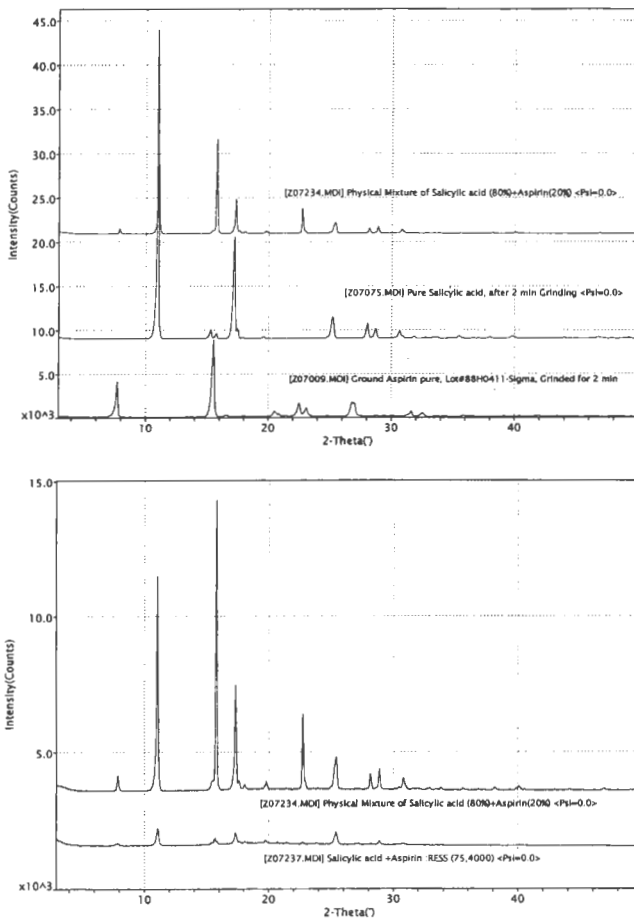


Figure 21. Reduction in the Crystallinity of Salicylic Acid Co-crystallized With Aspirin

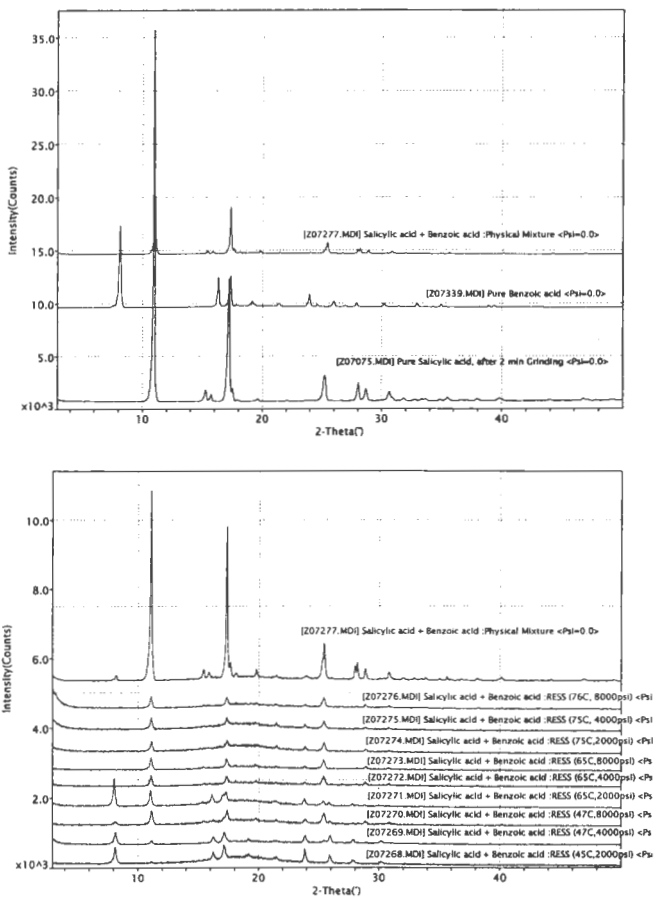
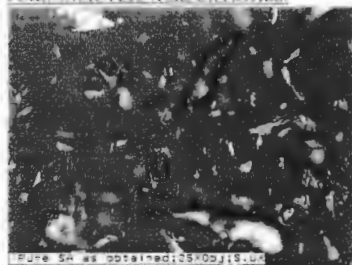


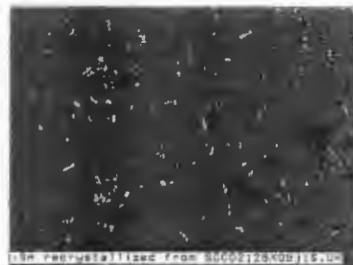
Figure 22. Reduction in the Crystallinity of Salicylic acid Co-crystallized With Benzoic Acid

Figure 23. Effect of Doping with Aspirin on the Crystallinity Of Salicylic Acid

PURE SALICYLIC ACID CRYSTALS:

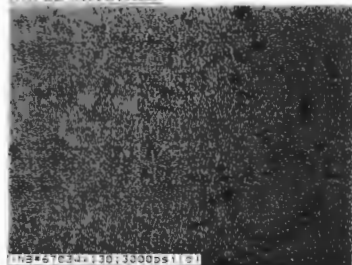


Pure SA as obtained from Sigma

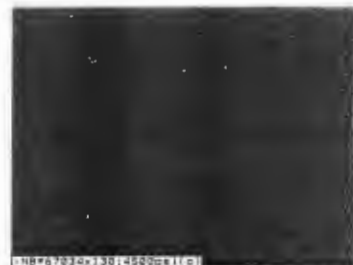


SA recrystallized from SC CO₂ at 32°C, 1400psi

DOPED CRYSTALS:



SA + Aspirin recrystallized from SC CO₂ at 75°C, 3000psi



SA + Aspirin recrystallized from SC CO₂ at 75°C, 4500psi

lattice parameters but also the order in which they pack. Such crystal disruption translates into a shift in the angle of diffraction and/or broadening and subsequent splitting of the peaks. Crystal disruption upon recrystallizing a number of drugs from SC CO₂ in the presence of structurally related impurities was also confirmed based on the broadening and shifts of the major x-ray diffraction peaks. A complete list of the altered major diffraction peaks from the XRPD analyses of several SCF recrystallized mixtures are tabulated in bold and italicized fonts (refer to sections C of Appendix for details).

Illustrative examples are excerpted from Appendix A to represent the broadening and shifts of XRPD peaks and are shown in Tables 18a to 18c and Figures 24 to 26. Tables 18a to 18c respectively list the major diffraction peaks and their FWHM values for aspirin+benzoic acid, tolbutamide+urea and naproxen+ α -naphthalene acetic acid co-crystals recrystallized at various conditions. As can be seen from Tables 18a to 18c, systematic shifts in the 2θ values are evident in various co-crystals. The possibility of preferred orientation to have caused the above reported peak shifts was excluded by establishing a single reproducible peak in each case. On the other hand, peak broadening indicated by the increased FWHM values can be seen in Figures 24 to 26. Of particular interest here is the broadening of consistently selective peaks that in part depended on the extraction conditions. From a crystallographer's standpoint, it is possible to identify the specific faces of the crystal that are likely to be attacked by the impurity utilizing the above data.

Table 18. Representative XRD Peaks Showing Peak Shifts and Peak Broadening Upon Doping Crystals with Impurities

Table 18a. Aspirin + Benzoic acid

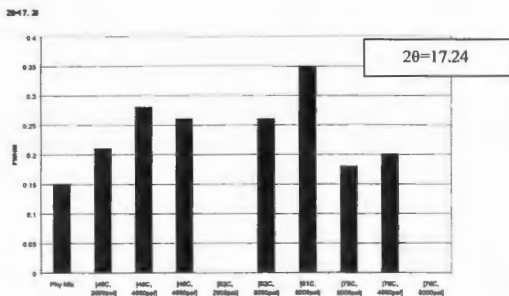
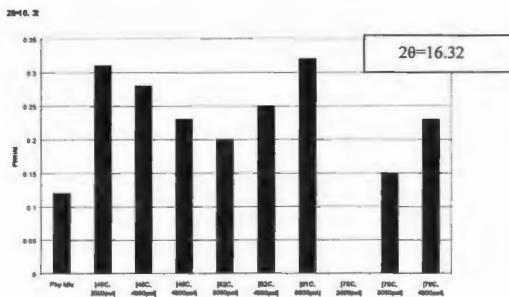
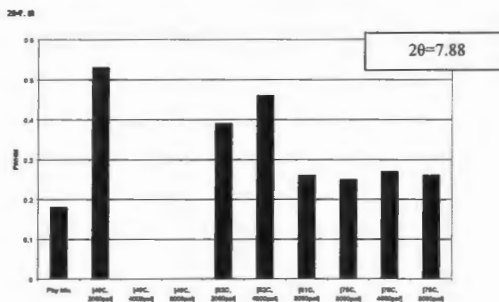
Condition	2θ(FWHM) Values					
[46C, 2000psi]	3.16(0.38)	7.88(0.53)	16.22(0.31)	17.14(0.21)	19.12(0.25)	23.78(0.21)
[46C, 4000psi]	8.16(0.35)	15.62(0.3)	16.3(0.28)	17.22(0.28)	19.18(0.3)	27.16(0.37)
[46C, 8000psi]	8.08(0.31)	15.64(0.27)	16.16(0.23)	17.12(0.26)	19.06(0.36)	27.18(0.41)
[62C, 2000psi]	7.42(0.13)	7.8(0.39)	8.08(0.28)	16.16(0.2)	19.03(0.28)	30.12(0.17)
[62C, 4000psi]	7.84(0.46)	8.1(0.44)	15.62(0.28)	19.06(0.32)	20.72(0.44)	21.16(0.54)
[61C, 8000psi]	3.22(0.34)	7.8(0.26)	16.74(0.32)	17.18(0.35)	22.66(0.25)	27.14(0.39)
[75C, 2000psi]	3.21(0.27)	15.64(0.28)	22.72(0.31)	25.23(0.38)	25.3(0.47)	27.2(0.25)
[76C, 4000psi]	15.62(0.24)	17.24(0.2)	23.26(0.36)	25(0.4)	27.16(0.37)	36.16(0.55)
[76C, 8000psi]	15.62(0.22)	16.78(0.23)	21(0.69)	22.7(0.26)	23.28(0.41)	27.16(0.38)
Phy Mix	7.86(0.18)	8.14(0.21)	15.66(0.19)	16.32(0.12)	17.24(0.15)	19.2(0.21)
	20.76(0.25)	21.06(0.28)	22.76(0.16)	27.04(0.3)	30.3(0.17)	36.02(0.13)

Table 18b. Tolbutamide + Urea

Condition	2θ(FWHM) Values						
[49C, 4000psi]	10.3(0.24)	10.65(0.18)	11.38(0.22)	15.02(0.51)	19.64(0.36)	21.38(0.31)	23.12(0.32)
[48C, 8000psi]	10.36(0.23)	10.61(0.18)	11.42(0.2)	15.62(0.32)	19.66(0.32)	21.4(0.4)	23.2(0.44)
[63C, 4000psi]	10.34(0.23)	10.62(0.23)	11.42(0.22)	15.62(0.3)	19.66(0.33)	21.44(0.27)	23.2(0.28)
[64C, 8000psi]	10.28(0.22)	11.34(0.15)	18.06(0.22)	19.62(0.26)	19.96(0.37)	26.38(0.26)	23.16(0.2)
[75C, 4000psi]	10.34(0.23)	10.34(0.23)	11.42(0.22)	19.64(0.35)	20.98(0.33)	21.3(0.44)	23.16(0.27)
[76C, 8000psi]	10.36(0.26)	10.36(0.26)	11.46(0.23)	19.62(0.36)	20.04(0.60)	20.94(0.42)	21.52(0.44)
Phy Mix	15.62(0.17)	19.6(0.21)	19.98(0.26)	20.94(0.18)	21.5(0.16)	23.18(0.18)	26.4(0.21)

Table 18c. Naproxen + α-Naphthalene acetic acid

Condition	2θ(FWHM) Values					
[50C, 4000psi]	6.69(0.57)	11.82(0.22)	13.96(0.24)	19.06(0.31)	22.3(0.37)	27.86(0.61)
[50C, 8000psi]	6.76(0.44)	11.86(0.23)	18.68(0.61)	19.12(0.36)	22.36(0.44)	27.9(0.44)
[63C, 2000psi]	6.7(0.42)	13.96(0.23)	18.64(0.71)	19.08(0.3)	22.35(0.33)	22.06(0.34)
[62C, 4000psi]	6.7(0.38)	6.94(0.48)	18.75(0.36)	19.1(0.31)	22.34(0.3)	27.42(0.38)
[63C, 8000psi]	6.73(0.28)	7.04(0.28)	18.69(0.67)	19.08(0.22)	22.38(0.35)	23.78(0.16)
[78C, 4000psi]	6.68(0.18)	11.8(0.04)	12.69(0.08)	19.1(0.23)	22.44(0.28)	22.64(0.4)
[76C, 8000psi]	3.4(0.44)	3.54(0.4)	6.64(0.31)	19.04(0.25)	22.66(0.39)	27.47(0.44)
Phy Mix	6.68(0.25)	11.84(0.09)	12.74(0.2)	13.94(0.15)	18.66(0.48)	19.1(0.2)
	22.4(0.37)	27.53(0.27)				



**Figure 24. Peak Broadening Upon Doping Crystals with Impurities :
Aspirin + Benzoic Acid**

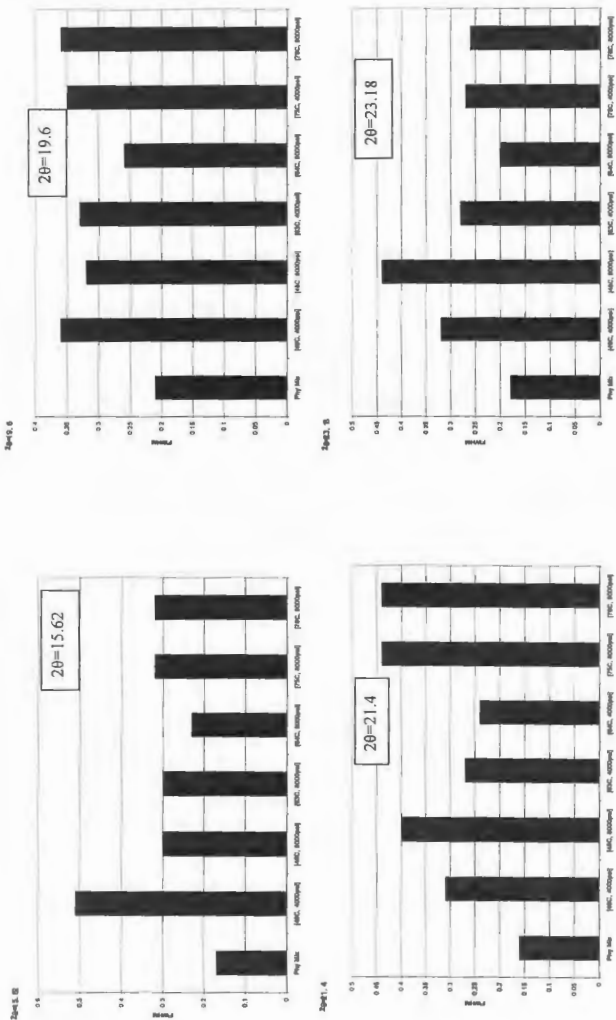


Figure 25. Peak Broadening Upon Doping Crystals with Impurities : Tolbutamide + Urea

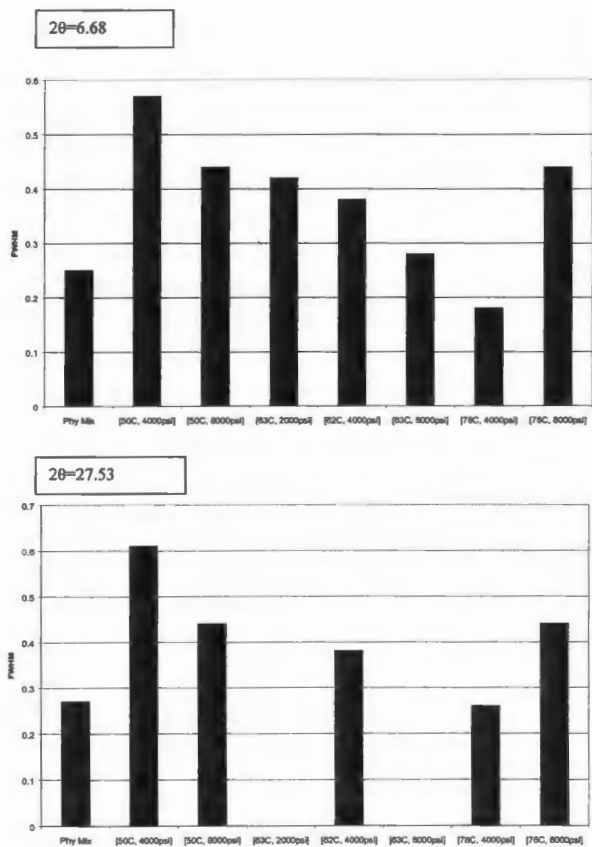


Figure 26. Peak Broadening Upon Doping Crystals with Impurities
Naproxen + α -Naphthalene acetic acid

While crystal doping for the most part resulted in a general reduction in the crystallinity, extreme situations were also identified where major loss of crystallinity and amorphous conversion ensued. For example, a drastic reduction in the crystallinity was seen upon SCF recrystallization of naproxen+ α -naphthalene acetic acid (Figure 27). As can be seen from the figure, both the increases in the pressure and temperature for extraction appeared to significantly reduce the crystallinity of the mixtures, perhaps by controlling the levels of the impurity in the host crystals. Piroxicam+theophylline co-crystals recrystallized from [65°C, 6000 psi] represent another example where drastic reduction in crystallinity occurred upon crystal doping (Figure 28). Similarly, reprecipitation of piroxicam+benzoic acid mixtures at low temperature conditions of [49°C, 2000 psi] and [50°C, 4000 psi] formed weakly crystalline, low melting mixtures (Figures 29 and 30). Further increases in the temperature and pressure during the extraction of these mixtures resulted in amorphous conversion. As indicated by Figures 29 and 30, complete amorphization is confirmed following the powder x-ray diffraction and DSC analyses of these mixtures. Analogous amorphous conversion was also evident in mixtures of indomethacin+salicylic acid extracted at higher temperature and pressure conditions as can be seen from Figure 31. Phenytoin+caffeine extracted from [76°C, 2000 psi] also formed an amorphous mixture while other extraction conditions selectively crystallized caffeine (Figure 32). All the above studies indicate that the composition of the mixtures prior to the rapid expansion in RESS process is the limiting factor in controlling the

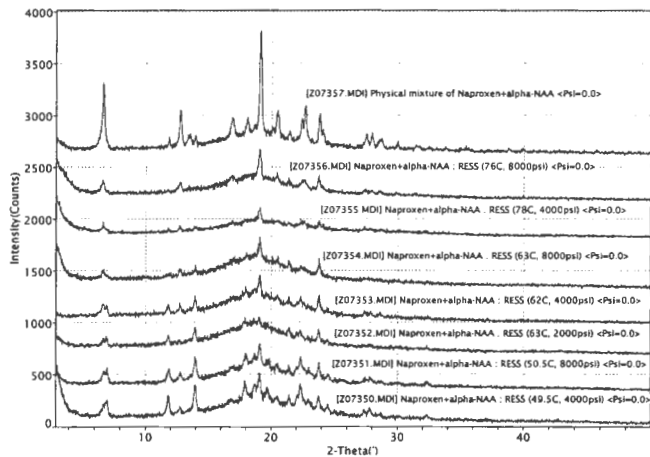
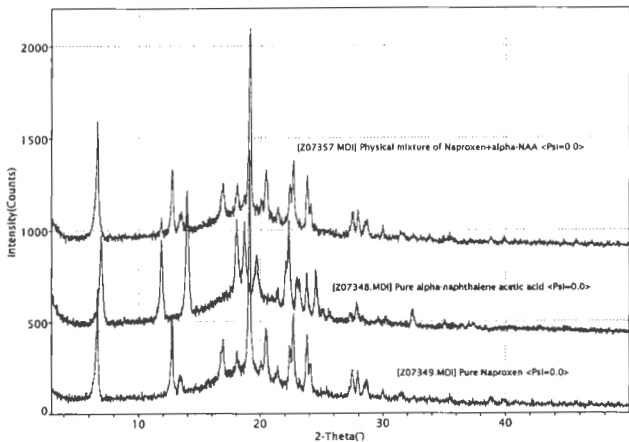


Figure 27. Reduction in the Crystallinity in RESS Produced Co-Crystals of Naproxen + α -Naphthalene Acetic Acid

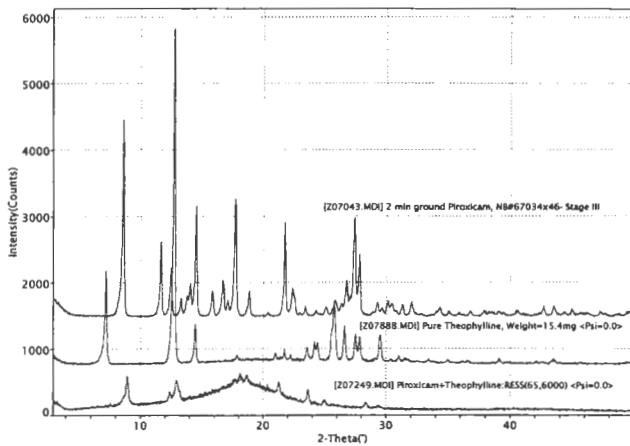


Figure 28. Reduction in the Crystallinity Upon doping Piroxicam with Theophylline

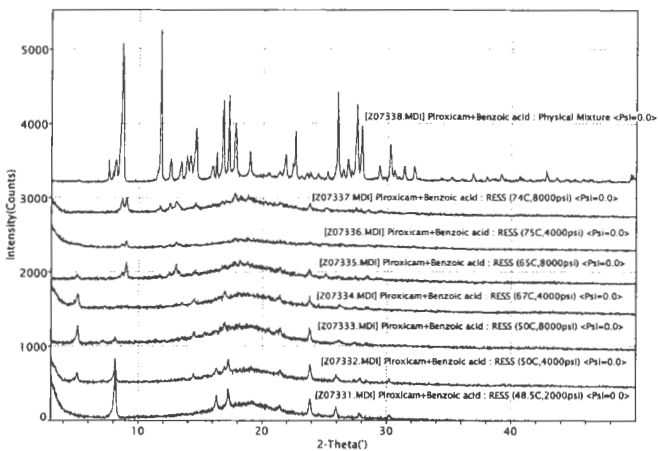
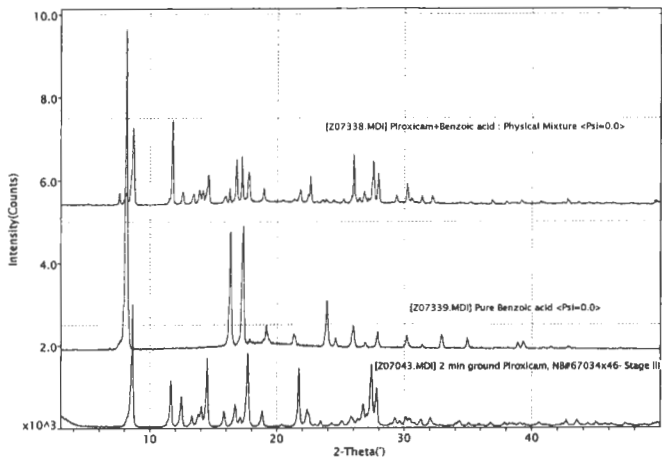


Figure 29. Amorphous Conversion in RESS Produced Piroxicam + Benzoic Acid Mixtures

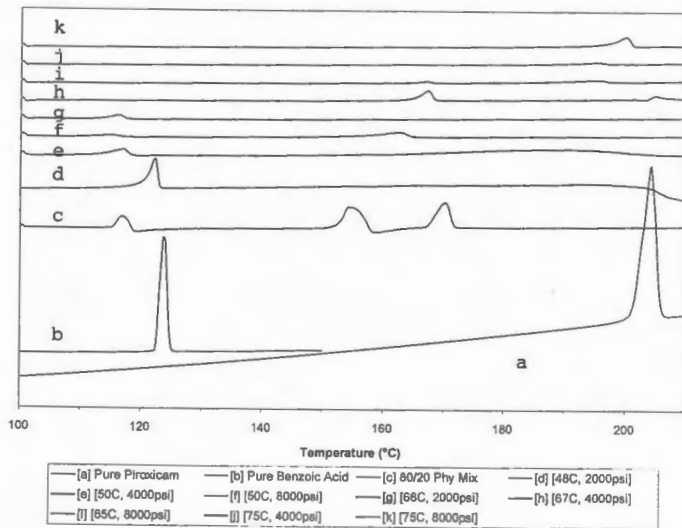
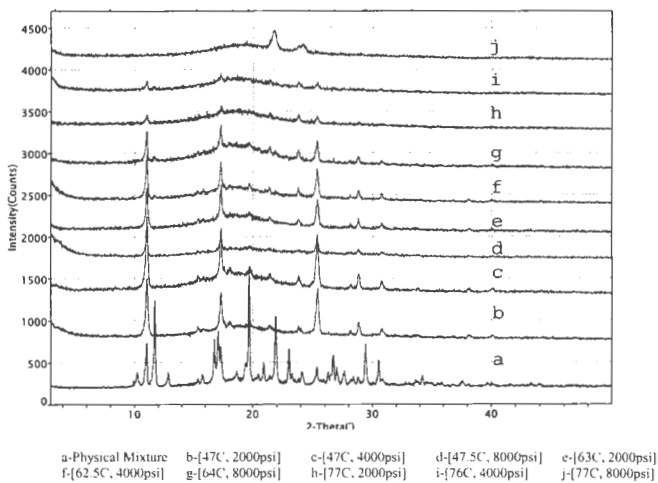
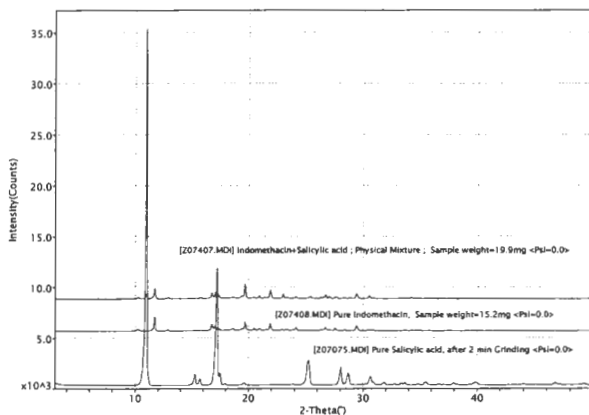
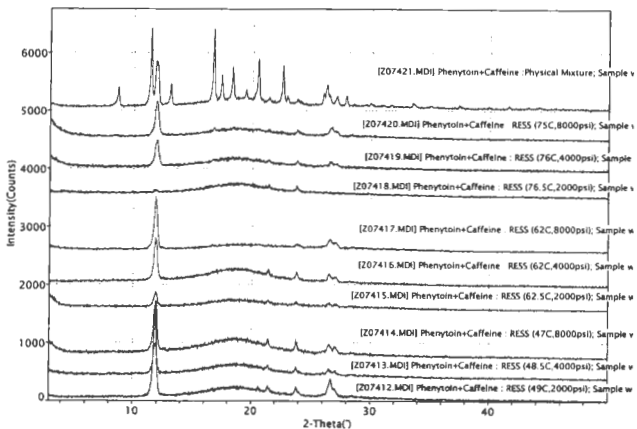
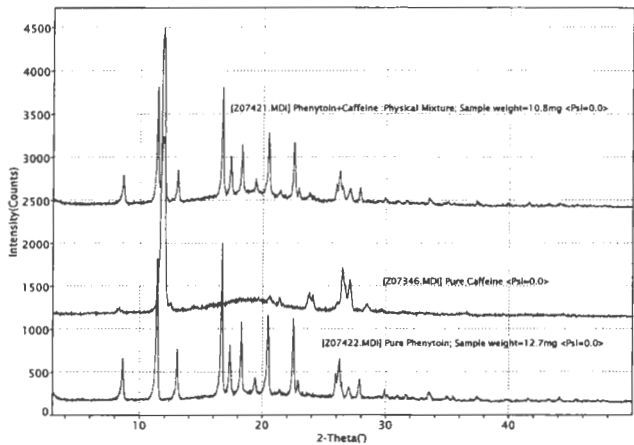


Figure 30. DSC Analyses of Piroxicam + Benzoic Acid Mixtures



**Figure 31. Reduction in Crystallinity and Amorphous Conversion of RESS
Produced Indomethacin + Salicylic acid**



**Figure 32. Amorphous Conversion and Selective Extraction in RESS
Produced Phenytoin+Caffeine**

crystallinity of the particles formed. Rapid recrystallization conditions of RESS process represent the far from equilibrium conditions during crystallization. In addition to the existing thermodynamic instability of the highly supersaturated SCF solution, the presence of impurity in the crystallizing medium of the host might have disfavored the formation of the most stable form of the host. Apparently, a reduction in the crystallinity was seen in all the drug-impurity mixtures recrystallized from SC CO₂. In instances where the impurity levels are adequate to cause severe crystal disruption, drastic reduction in crystallinity and subsequent amorphization conversion might have occurred.

4.D. Hydrate Formation:

In RESS, the saturated supercritical solution in the pre-expansion chamber at a significantly high pressure is rapidly expanded through a micrometering valve into a collection vial at atmospheric conditions. Owing to the large pressure drop across the micrometering valve, Joule-Thompson cooling occurs that has the potential to plug the valve and the lines downstream of it. The micrometering valve is therefore maintained at 100-150°C to compensate for the cooling effect. The effect of the temperature of the micrometering valve on the particles formed is often disregarded so long as the flow of supercritical solution through it is uniform. An extreme case where this norm does not hold was identified while dealing with the RESS of theophylline+caffeine mixtures. Figure 33 shows the XRPD patterns of theophylline +caffeine co-crystals produced by the RESS

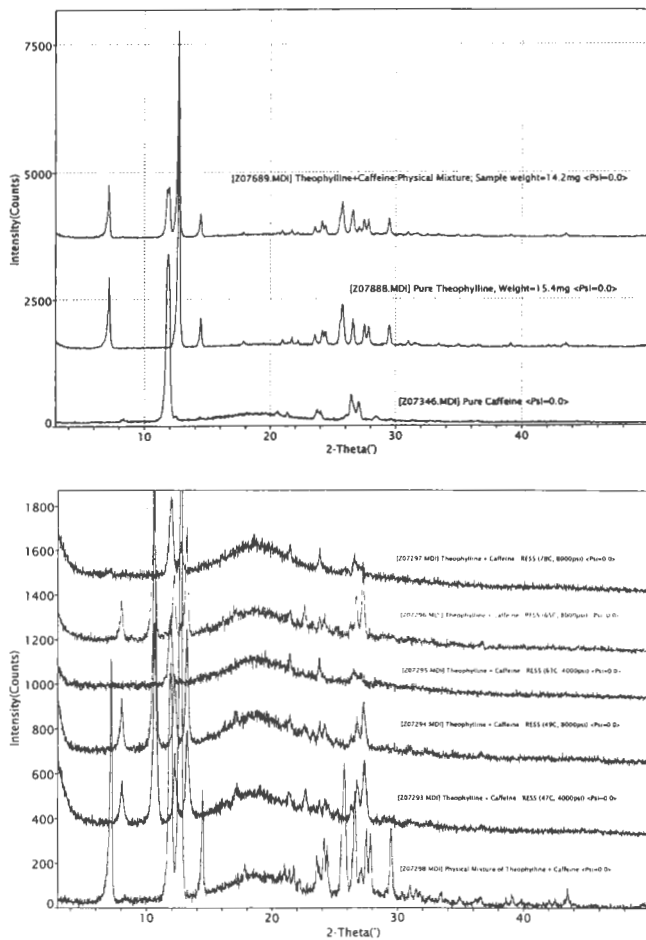


Figure 33. Hydrate Formation During RESS Expansion of Theophylline + Caffeine

process. The micrometering valve in this case was maintained at 100°C. As can be seen from the figure, the diffraction patterns of the RESS recrystallized mixtures extracted from lower temperatures were significantly altered. Comparison of these patterns to the various crystal forms of theophylline revealed that the end product was the monohydrate form. Although no significant temperature drop was evidenced during the expansion, RESS produced theophylline appeared to have picked up moisture from the atmosphere and instantly formed a hydrate. Similar conversion from anhydrous to hydrous form of theophylline has been reported during the wet granulation and pelletization of theophylline. [Herman 1989] Further, Rodriguez-Hornedo and Wu investigated the crystallization kinetics of the monohydrate form and reported that mechanism for the growth is defect mediated. This mechanism is of particular interest while dealing with doping of theophylline crystals. As can be seen from Figure 33, recrystallization of theophylline+caffeine from higher temperature conditions did not allow this conversion. Extending the mechanism proposed by Rodriguez-Hornedo and Wu, it is possible that higher levels of caffeine may have competed with water molecules during the crystallization step and disallowed the conversion. To further validate this hypothesis, Theophylline+Caffeine mixtures were recrystallized from $\text{SCCO}_2 + \text{MeOH}$ and $\text{SCCO}_2 + \text{Acetone}$ with the micrometering valve set at 100°C. As can be seen from Figures 34 and 35, altered proportions of drug and impurity as a result of modified solvent systems did not allow the water molecules to be doped into the crystals and form a hydrate.

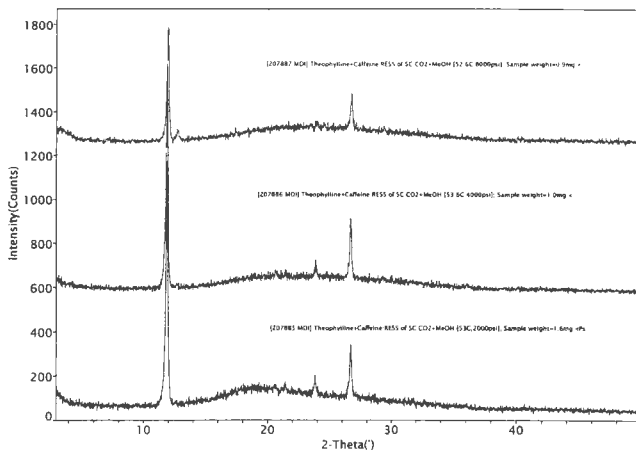
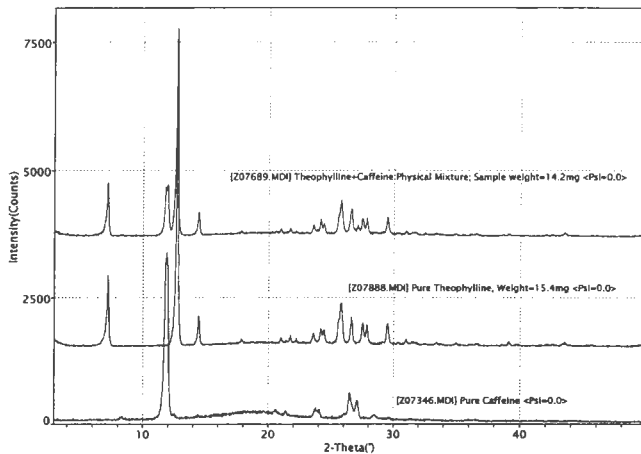


Figure 34. Recrystallization of Theophylline+Caffeine from SCCO₂+MeOH

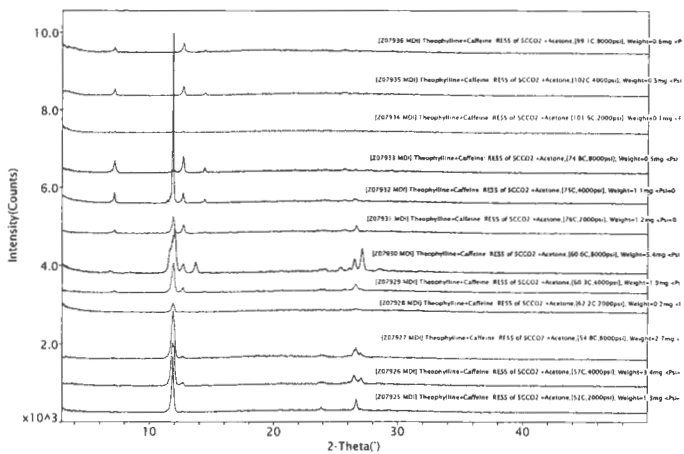
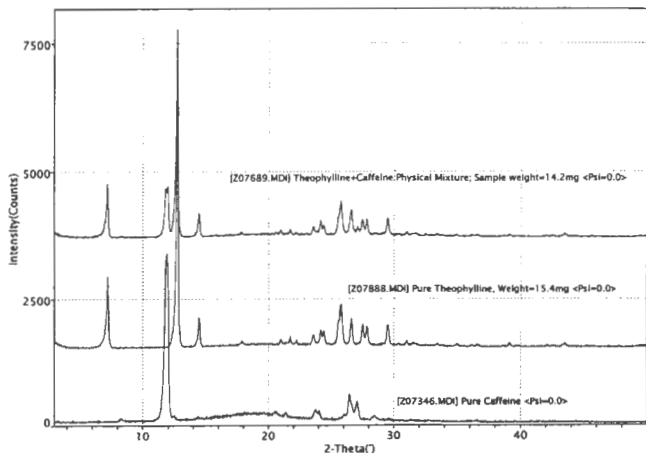
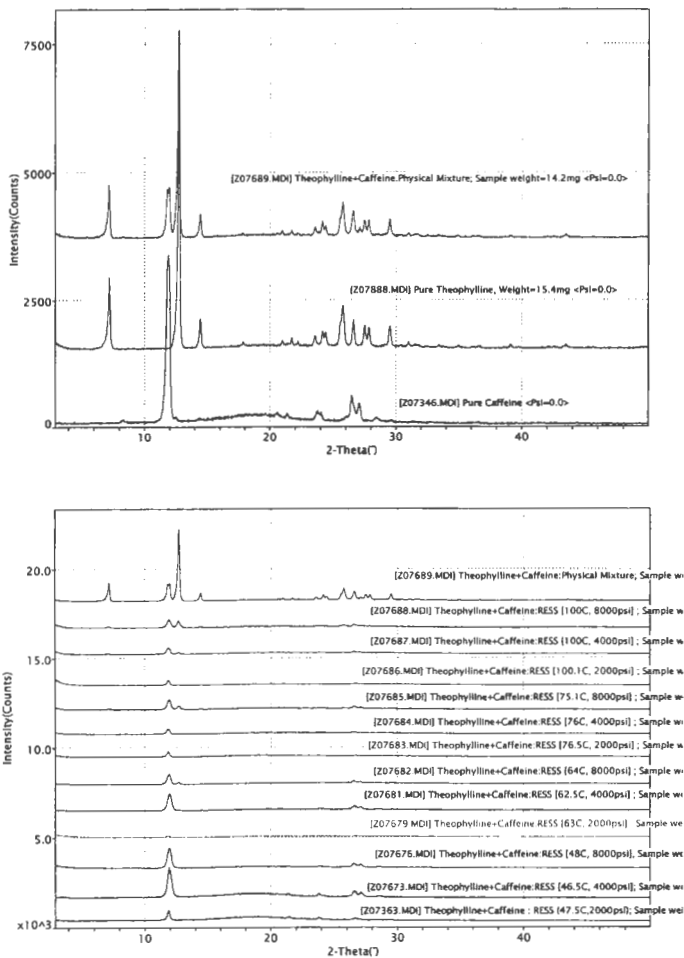


Figure 35. Recrystallization of Theophylline+Caffeine From SCCO₂+Acetone

Increase in the temperature of the micrometering valve to 150°C (Figure 36) also did not allow the conversion to a hydrate, perhaps by raising the temperature of the particles to the extent where no condensation from the atmosphere occurred.

4.E. Polymorph Conversion:

The commercially available polymorph of Tolbutamide is the orthorhombic form I that crystallizes as rectangular prisms [Leary 1981]. DSC thermogram and powder x-ray diffractogram of this form are distinctively different from form II as can be seen in Figures 37 and 38. Polymorph I was utilized for RESS recrystallization from three different supercritical fluid conditions viz. [45°C, 5000 psi], [60°C, 5000 psi] and [75°C, 5000 psi]. Recrystallization at all the three conditions resulted in the conversion of form I to form II as reflected by the shift in melting points (Figure 37). As can be seen from the figure, form I exhibits a melting endotherm at 130.5°C. The endotherm occurring at 40°C was reported to be due to the enthalpic relaxation from the rearrangement of hydrogen bonds in the molecule [Leary 1981]. On the other hand, the RESS recrystallized materials showed melting endotherms between 118°C and 123°C. The melting temperature of polymorph II could not be exactly determined due to the simultaneous conversion of form II to I during the heating step. In addition, this transformation was reported to occur in the solid state and not from the melt of form II, making the events rather difficult to distinguish [Kimura 1999]. A possible reason for this may be because of the spontaneous transformation from polymorph II to I,



**Figure 36. Recrystallization of Theophylline+Caffeine with Micrometering
Valve Setting at 150°C**

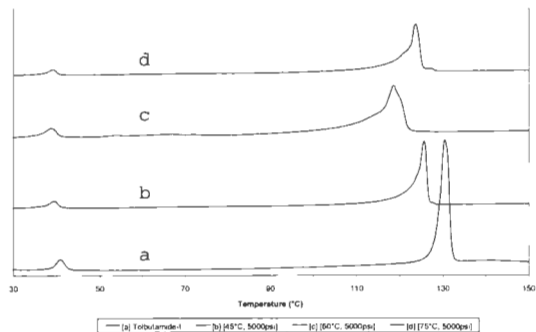


Figure 37. DSC Thermograms of Tolbutamide Polymorphs I and II

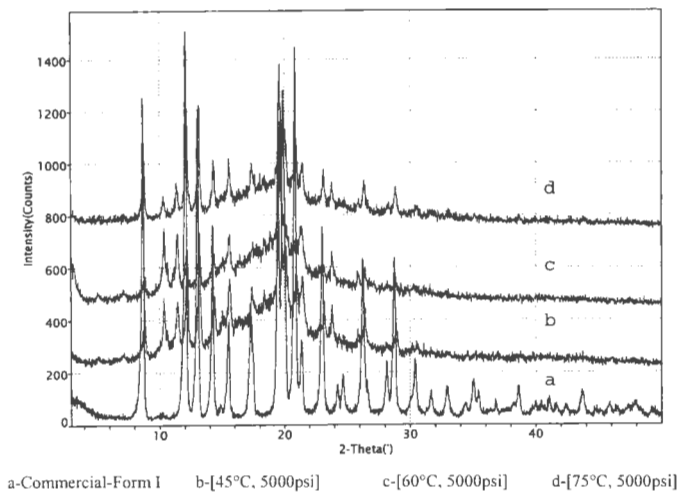


Figure 38. XRPD Patterns Tolbutamide Polymorphs I and II

dependent on the free energy difference between the two forms. Published literature however indicated that polymorph II is a low melting metastable form [Kimura 1999]. Reduction in the melting temperatures of RESS recrystallized materials is therefore ascribed to the conversion of form I to form II. The true identity of RESS recrystallized material is established from their x-ray diffraction behavior. XRPD results from Figure 38 confirm a polymorphic conversion from I to II, consistent with the results from thermal analysis. The conversion to a metastable form II upon RESS recrystallization can be attributed to the altered kinetics of nucleation and growth. These results are in agreement with Kimura et al's study [Kimura 1999] where polymorph II was produced from a spray dried intermediate (form IV).

It is noteworthy that polymorphs III and IV closely resemble forms I and II respectively, with negligible free energy differences within each pair [Rowe 1984]. It is therefore possible that reversible transformations between these forms may occur during the analytical characterization. The XRPD patterns of Tolbutamide+Urea mixtures recrystallized from SC CO₂ exemplifies this fact where a mixture of forms II and IV resulted at few extraction conditions (see Figure 38 and Section C, Appendix B). Conversion of form I to II following RESS recrystallization was evident even in the presence of urea as impurity. XRPD and DSC results of RESS mixtures summarized in Figures 39 and 40 validate the conversion to form II. In addition, a reduction in the crystallinity of tolbutamide was seen following doping with urea (refer to section C for details).

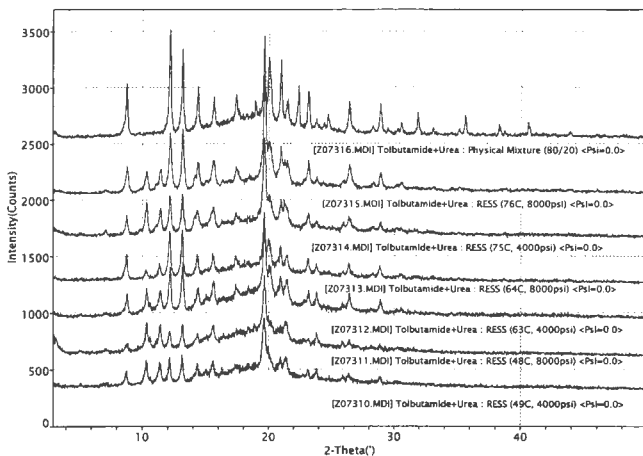
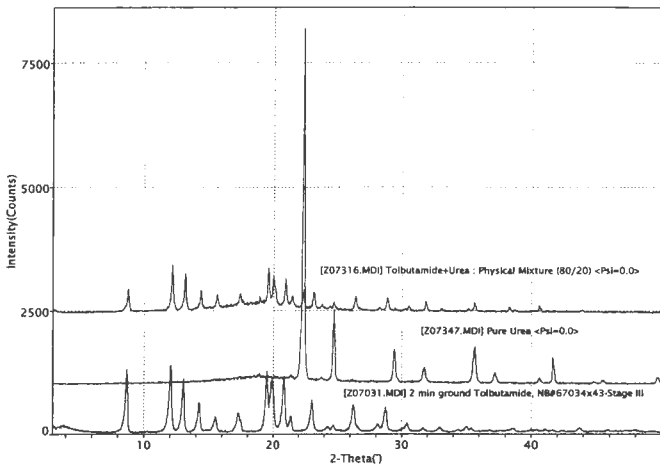


Figure 39. XRPD Patterns of Tolbutamide Crystals Doped with Urea

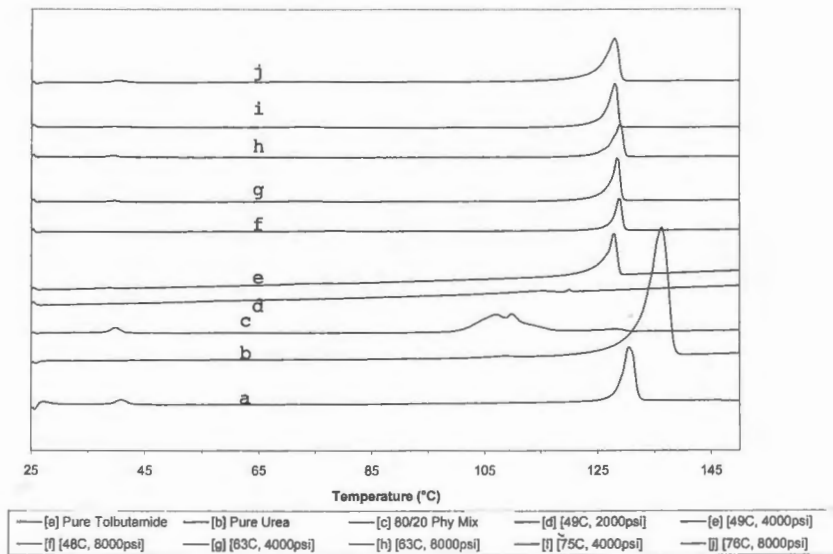


Figure 40. DSC Thermograms of Tolbutamide Crystals Doped with Urea

Reduction of the crystallinity in an already existing metastable form can be expected to enhance the dissolution rates, and thereby the bioavailability of the otherwise poorly soluble tolbutamide. Utilizing dog as the animal model, Kimura et al reported a two-fold enhancement in the bioavailability from polymorph II compared to form I. Dissolution is identified as the rate limiting step in achieving therapeutic bioavailability values for this compound. Producing a metastable form coupled with the impurity-induced crystal disruption is therefore particularly attractive from the standpoint of improving the dissolution rates. Results of tolbutamide studies in summary, served as the proof of concept for utilizing SCF aided crystal doping toward improving the bioavailability of poorly soluble compounds.

Among the other mixtures that also exhibited polymorphic conversions upon recrystallization from SC CO₂ included Tolbutamide+Chlorpropamide. The XRPD results of these mixtures are summarized in Figure 42. As can be seen, both the sulfonylurea compounds in this case were found to undergo polymorphic changes, making the study rather complex. Interestingly, DSC analyses of these mixtures revealed the formation of a low melting composition between these two hypoglycemic agents. (Figure 41). A rational extension to this study would be to test the bioavailability of the low melting composition of this metastable mixture and forms the scope for future research.

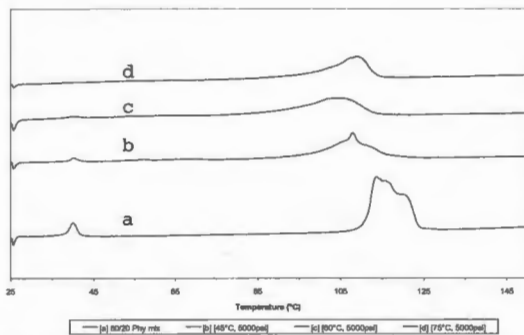


Figure 41. Polymorph Conversions in Tolbutamide+Chlorpropamide:

DSC Results

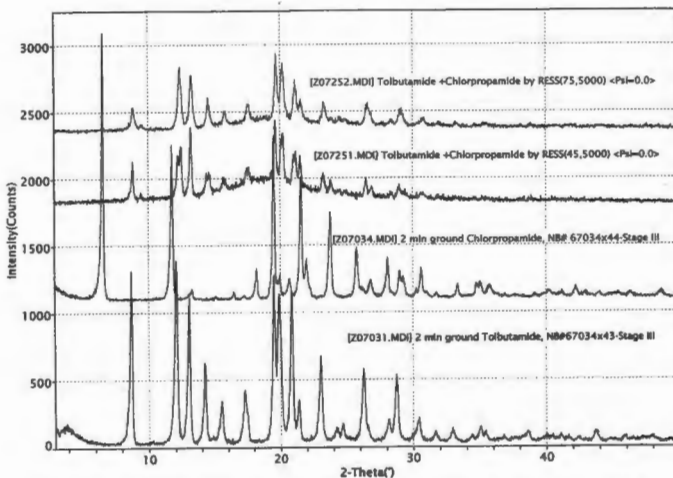


Figure 42. Polymorph Conversions in Tolbutamide+Chlorpropamide:

XRPD Results

4.F. Selective Extraction:

The potential for SCF based crystal doping was demonstrated in Sections A to E. Rapid nucleation and the growth implicit to RESS based crystallizations were taken advantage in doping the drug crystals with impurities. While supercritical fluid based crystal doping offers great promise in this regard, it has also been found to have a few shortcomings. This section addresses some of the limitations encountered in doping crystals by the RESS process. Firstly, the yields from crystallization are low due to the poor solubility of a majority of APIs in supercritical CO₂. The utility of co-solutes and co-solvents in improving the yields have been addressed in section A. Techniques to enhance the solubility of active pharmaceutical ingredients in SC CO₂ are of particular interest in this regard and are still at inception. Alternatively, supercritical antisolvent processes can be used to overcome this limitation of poor yields, although the advantages of liquid solvent-free RESS process maybe compromised to some extent.

Another shortcoming associated with RESS based crystal doping arises from the selective solvent nature of supercritical fluids. The high resolution capability of supercritical solvents is widely taken advantage in chiral separations and forms the basis for supercritical fluid chromatography [Wong 1993, Hoke 2000]. In an exact contrast to such applications, SCF aided crystal doping relies on extracting both the host and the impurity at equal rates and forming a homogenous mixture. The efficiency of SCF crystal doping therefore depends on the relative rates of solubilization and recrystallization. While an optimum between these two kinetic

processes was attempted by probing a wide domain of supercritical region, selective extraction of components appeared to have overtaken in a majority of the cases. Theophylline+Caffeine represents a classic example of the selective extraction by SC CO₂ and has been studied in detail.

The compositions of various co-crystals of theophylline and caffeine were determined by HPLC analysis and the results reported in Tables 19-20 and Figures 43-44. As can be seen from Figure 45, the relative amounts of theophylline and caffeine in the co-crystals formed are highly dependent on the supercritical extraction conditions. A general trend of increase in theophylline levels was found both with the increase in temperature and pressure. Within the constraints of the pressures and temperatures achievable with RESS equipment, it is therefore possible to control the levels of host and impurity in the co-crystals by changing the extraction conditions. For example, a 50/50 mixture of theophylline and caffeine was produced at 100°C, 8000psi. In a further study, the effect of impurity on the extraction efficiency of the host was evaluated by using two different starting mixtures viz. 80/20 and 20/80. Comparison of Figures 43 and 44 illustrates that the compositions of resultant co-crystals are dependent on that of the starting mixture. The presence of impurity therefore does play a role on the composition and the supersaturation of the supercritical solution prior to expansion. These results support the earlier findings that showed a reduction in crystallinity of the host induced by the impurity.

**Table 19. Composition of Co-Crystals Produced from 80/20 Mixture of
Theophylline +Caffeine**

Condition	% Theophylline*	%Caffeine*
[46.5°C, 4000psi]	1.80	98.20
[48°C, 8000psi]	4.58	95.42
[63°C, 2000psi]	1.51	98.49
[62.5°C, 4000psi]	6.92	93.08
[64°C, 8000psi]	17.61	82.39
[76.5°C, 2000psi]	4.46	95.54
[76°C, 4000psi]	12.05	87.95
[75.1°C, 8000psi]	32.99	67.01
[100.1°C, 2000psi]	12.40	87.60
[100°C, 4000psi]	25.11	74.89
[100°C, 8000psi]	45.98	54.02
Physical Mixture	81.49	18.51

**Table 20. Composition of Co-Crystals Produced from 20/80 Mixture of
Theophylline +Caffeine**

Condition	% Theophylline*	%Caffeine*
[47.7°C, 2000psi]	1.74	98.26
[48.2°C, 4000psi]	1.03	98.97
[47°C, 8000psi]	1.62	98.38
[63°C, 2000psi]	1.43	98.57
[63.2°C, 4000psi]	1.57	98.43
[62.2°C, 8000psi]	2.76	97.24
[75.8°C, 2000psi]	3.21	96.79
[74.5°C, 4000psi]	2.93	97.07
[76.4°C, 8000psi]	4.79	95.21
[100.9°C, 4000psi]	4.42	95.58
[98.7°C, 8000psi]	7.02	92.98
Physical Mixture	20.35	79.65

* Values reported are average of two runs with no significant differences between runs & within each HPLC analysis.

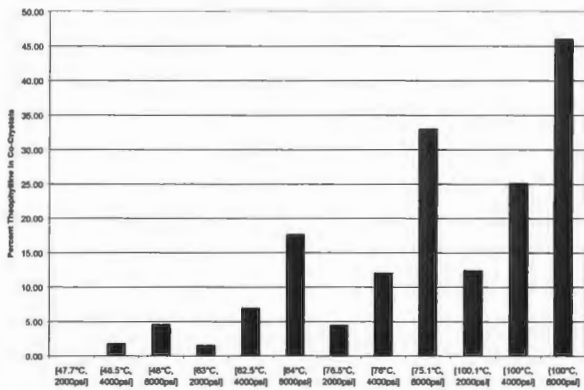


**Figure 43. Selective Extraction from a 80/20 Mixture of Theophylline
And Caffeine**

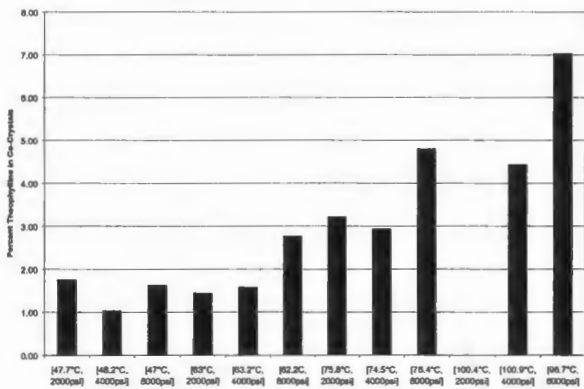


**Figure 44. Selective Extraction from a 20/80 Mixture of Theophylline
And Caffeine**

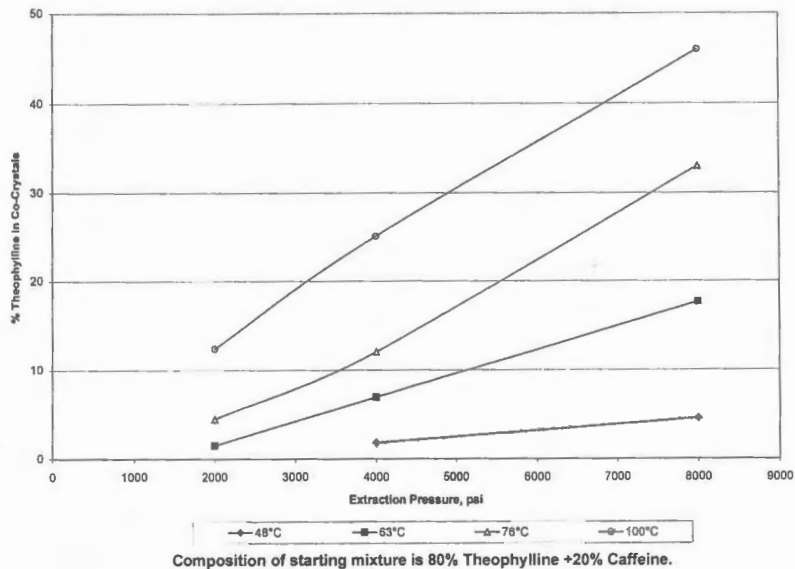
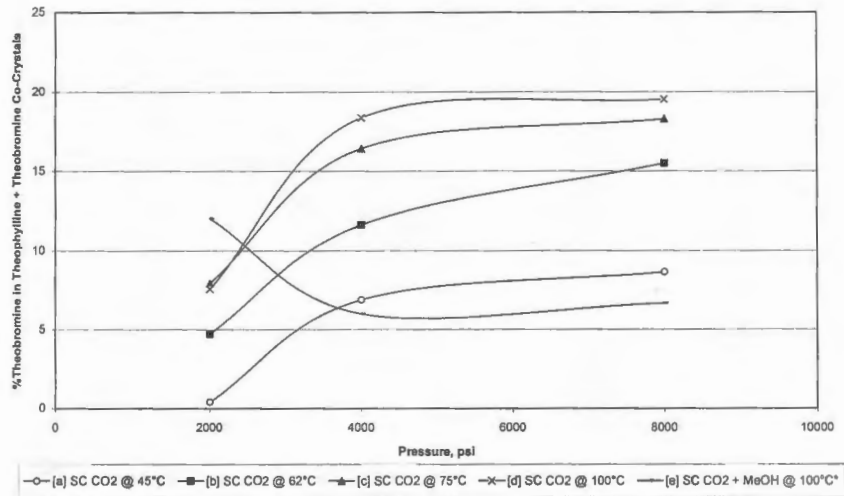


Figure 45. Effect of Process Conditions on the Compositions of RESS Produced Co-Crystals of Theophylline + Caffeine

In summary, the composition of the recrystallization media is not only dependent on the RESS extraction conditions, but also on the relative amounts of drug and impurity in the reaction vessel. Similar conclusions were reached in theophylline + theobromine co-crystals as summarized in Figure 46. As can be seen from the figure, theophylline appears to be more soluble in SC CO₂ than theobromine at all the conditions studied. A general trend of increased theobromine levels at higher temperatures and higher pressures of extraction can be seen. The use of methanol as a co-solvent in a further series of studies reversed this trend, exemplifying the tunable solvent power of supercritical solvents.

Other drug impurity mixtures that also exhibited selective extraction upon RESS processing include salicylic acid+benzoic acid, aspirin+benzoic, indomethacin+salicylic acid and phenytoin+caffeine. Selectivity of extraction in these systems was not quantified and is only derived on the basis of the qualitative observations of their XRPD patterns and DSC thermograms. For example, refer to Figures 47A and 47B that respectively show the XRPD patterns and DSC thermograms of salicylic acid+benzoic acid mixtures recrystallized from various extraction conditions. As can be seen from Figure 47A, the peaks occurring at 2θ values of 8.16° and 11.1° are distinct diffraction peaks of benzoic acid and salicylic acid respectively. Comparison of the patterns of recrystallized materials with particular attention to these 2θ values indicates that benzoic acid is selectively extracted at lower temperature conditions. As the temperatures increase above 65°C , selective extraction of salicylic acid is evident.



Composition of starting mixture is 80% Theophylline +20% Theobromine.

Figure 46. Effect of Process conditions on the Compositions of RESS Produced Co-Crystals of Theophylline + Theobromine

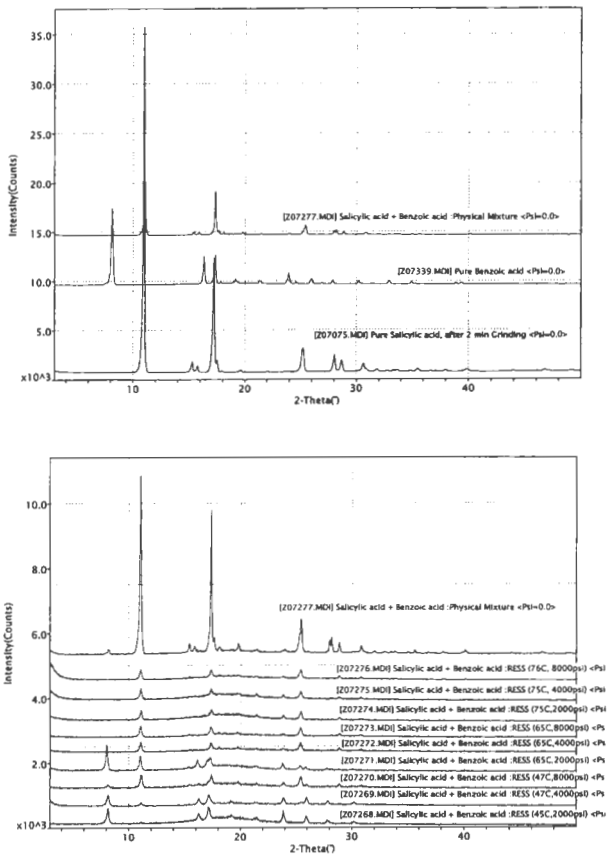


Figure 47A. Selectivity of Extraction in Salicylic Acid+Benzoic Acid Mixtures as a Function of Extraction Conditions

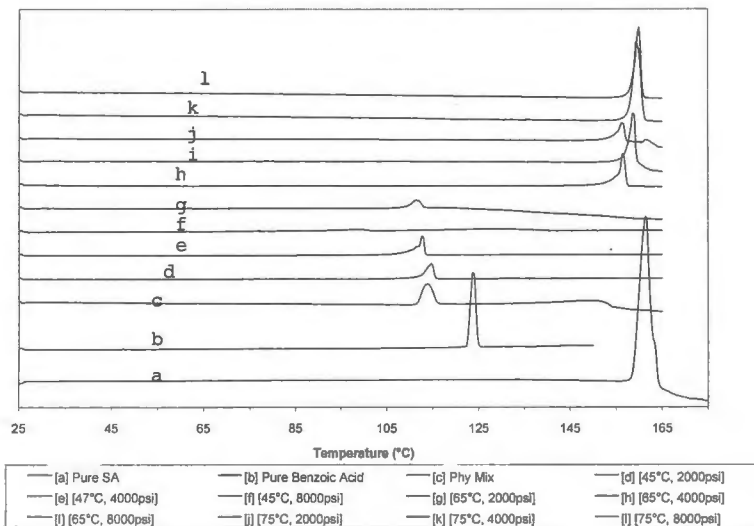


Figure 47B. Selectivity of Extraction in Salicylic Acid+Benzoic Acid Mixtures as a Function of Extraction Conditions

The above observations from XRPD analysis are consistent with the thermal behavior of the mixtures, as can be seen from Figure 47B. Interestingly, an intermediary condition was found at [45°C, 8000 psi] where significant amounts of both the components are extracted as can be seen from its diffraction pattern. This perhaps led to a significant reduction in crystallinity of the co-crystals (Figure 47A), which upon subjecting to DSC analysis did not exhibit any melting endotherms (Figure 47B). Aspirin+benzoic acid is another such system that exhibited selective extraction of benzoic acid at lower extraction temperatures, while aspirin was preferentially extracted at temperatures higher than 62°C (see figures 48A and 48B). Qualitative analysis of the XRPD and DSC data was performed analogous to salicylic acid+benzoic system discussed above. The DSC analysis in this case, however could not be performed above temperatures higher than 130°C as significant sublimation of the mixtures occurred.

Salicylic acid+indomethacin (Figure 49) and phenytoin+caffeine (Figure 50) are two other systems that exhibited selective extraction at most of the supercritical extraction conditions investigated. Preferential extraction of salicylic acid and caffeine occurred at a majority of the conditions from these two systems. Increases in the amounts of second component in these mixtures resulted in amorphous conversions as was discussed in section C. In summary, the composition of the recrystallization media is not only dependent on the RESS extraction conditions, but also on the relative amounts of drug and impurity in the reaction vessel.

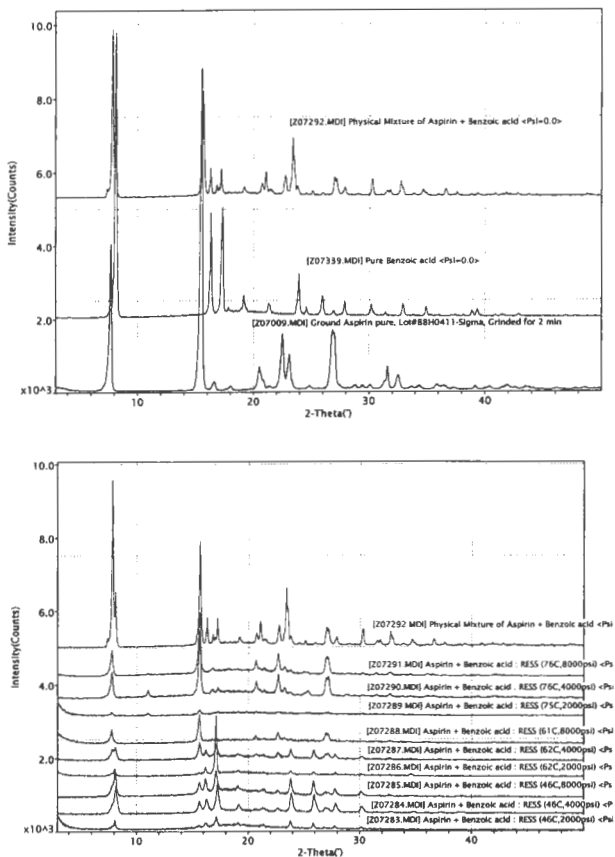


Figure 48A. Selectivity of Extraction in Aspirin+Benzoic Acid Mixtures as a Function of Extraction Conditions

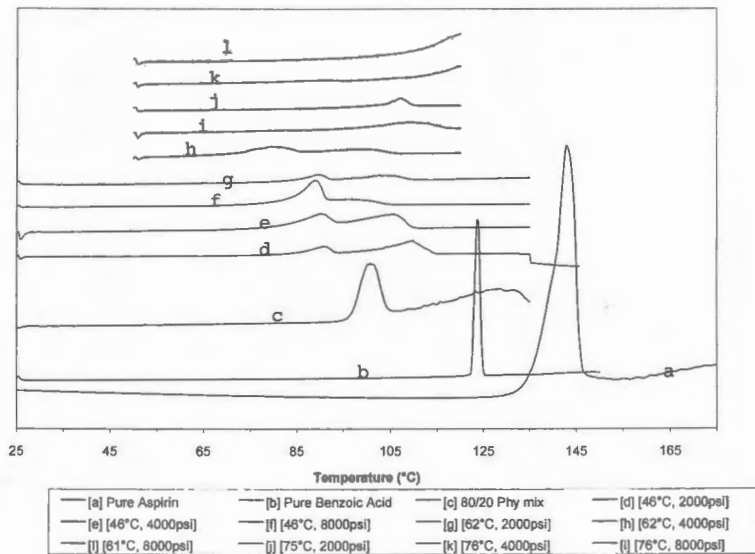
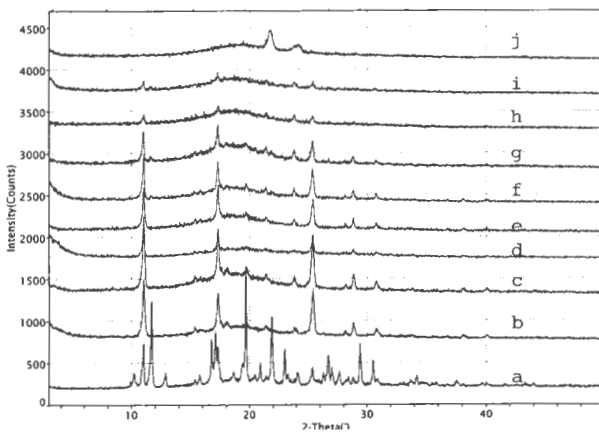
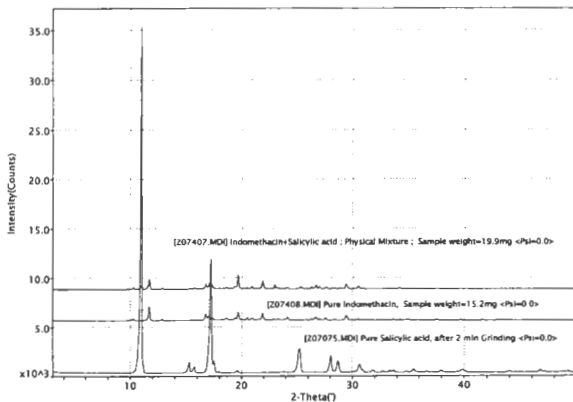
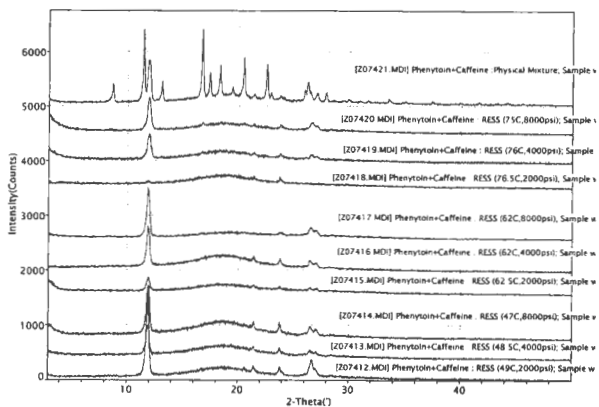
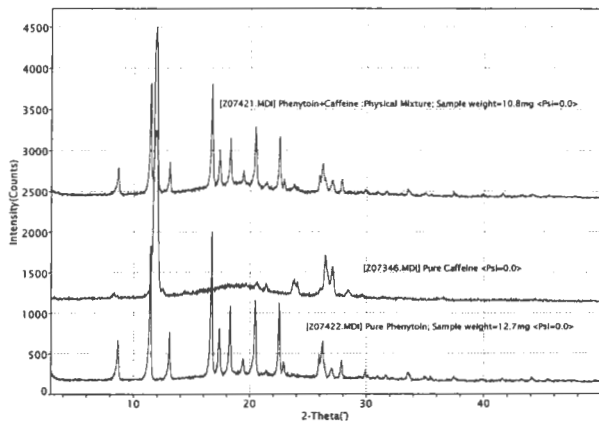


Figure 48B. Selectivity of Extraction in Aspirin+Benzoic Acid Mixtures as a Function of Extraction Conditions



a-Physical Mixture; b-[47°C, 2000psi]; c-[47°C, 4000psi]; d-[47.5°C, 8000psi]; e-[63°C, 2000psi]
 f-[62.5°C, 4000psi]; g-[64°C, 8000psi]; h-[77°C, 2000psi]; i-[76°C, 4000psi]; j-[77°C, 8000psi]

Figure 49. Selective Extraction in Indomethacin+Salicylic acid Mixtures



a-Physical Mixture; b-[47°C, 2000psi]; c-[47°C, 4000psi]; d-[47.5°C, 8000psi]; e-[63°C, 2000psi]
 f-[62.5°C, 4000psi]; g-[64°C, 8000psi]; h-[77°C, 2000psi]; i-[76°C, 4000psi]; j-[77°C, 8000psi]

Figure 50. Selective Extraction in Phenytol+Caffeine Mixtures

In summary, supercritical solvents are extremely selective in nature, which is a feature not favored in crystal doping. Notwithstanding this fact, SCF conditions were identified where significant amounts of impurity can still be doped into drug crystals. This was made possible by modifying the extraction conditions and through the use of co-solvents. Rapid nucleation and growth from such modified recrystallization media provide the ability to lock the impurities into the lattices of the drug hosts. Varying levels of crystallinities ranging from pure crystals to amorphous mixtures can thus be achieved by changing the relative amounts of drug and impurity in the co-crystals.

5. CONCLUSIONS

The presence of an impurity in the crystallization medium exhibits varied effects depending on the phase in which it is present prior to nucleation and its affinity to the host relative to the crystallizing solvent. This in turn dictates the rate at which it nucleates and grows in relation to that of the host. The domain of effects that these kinetics dictate on one extreme includes the formation of a solid solution or a solid dispersion of the impurity in the host lattice. On the other hand, selective extraction of each of the components with respect to time can also occur, the extent of which primarily depends on the resolution factor of the recrystallizing solvent. While the former mechanism is largely aided by the rapid nucleation and growth implicit to supercritical fluid recrystallizations, the latter forms the scope of supercritical fluid chromatography. An optimal compromise between these

extremes can be reached by utilizing the adjustable solvent power of supercritical fluids. This hypothesis was tested utilizing a number of host/guest systems and SC CO₂ as the recrystallizing medium. In this process, various interesting phenomena were identified (Table 17).

The presence of aspirin as an impurity was found to alter the habit of salicylic acid crystals from avicular to fibrous form. Supercritical fluid recrystallization herein provided the independent ability to change the crystal habit while not altering the polymorphic form of the API. On the other hand, the polymorphic conversion to a metastable form of tolbutamide was seen upon SCF recrystallization. Doping tolbutamide with urea not only promoted such conversion, but also induced a reduction in the overall crystallinity. Loss of crystallinity in an already existing metastable form can be expected to enhance the dissolution rates, and thereby the bioavailability of the otherwise poorly soluble tolbutamide.

Utilizing a co-solute and a co-solvent to alter the solvent power of SC CO₂, enhancement in the solid solubility in SC CO₂ was demonstrated in SA+aspirin and theophylline+caffeine systems respectively. In addition, a general reduction in crystallinity was seen in all the doped crystals. This manifested as a reduction in the heat of fusion values, melting point depressions and eutectic formation in salicylic acid+aspirin, salicylic acid+benzoic acid, aspirin+benzoic acid, tolbutamide+ chlorpropamide. In the drug-impurity systems that did not permit the use of thermal analysis, crystallinity was evaluated based on the XRPD

studies. Consistent broadening and shifts of XRPD peaks were seen in aspirin+benzoic acid, tolbutamide+urea and naproxen+ α -naphthalene acetic acid co-crystals, reiterating a loss in crystallinity. While crystal doping resulted in such reductions in crystallinity for the most part, extreme situations were also identified where major loss of crystallinity and amorphous conversion ensued. For example, a drastic reduction in the crystallinity and amorphous conversion were seen upon SCF recrystallization of piroxicam+theophylline, piroxicam+benzoic acid, indomethacin+salicylic acid phenytoin+caffeine mixtures. By adjusting the solvent power of SC CO₂ through changes in temperature and pressure, conditions were identified in the above systems that promoted incorporation of high levels of impurity in the drug. In addition to this, the rapid precipitation conditions of RESS may have led to the formation of a solid dispersion or a solid solution and consequently, the amorphous conversion. In a further series of investigations, the effect of the presence of caffeine as an impurity on the crystal form of theophylline was tested. It was found that higher levels of caffeine competed with water molecules during the crystallization step and disallowed the conversion from anhydrous to monohydrate form of theophylline.

Among the systems that exhibited pronounced selectivity of extraction of a particular component include theophylline+caffeine, theophylline+theobromine, salicylic acid+benzoic acid, aspirin+benzoic, indomethacin+salicylic acid and phenytoin+caffeine. The solvent power of supercritical CO₂ was modified in these systems either by changing the temperature and pressure of the SCF or through

the use of a co-solvent. By adjusting the solvent power of the recrystallizing solvent, conditions were found where higher levels of impurity could be extracted along with the active. The crystallinity and the morphology of such co-crystals can thus be altered by controlling the levels of impurity in the host matrix. In viewing each of these phenomena from the standpoint of pharmaceutical development, the studies reported here serve as a proof of concept for altering the physicochemical properties of API's by supercritical fluid crystal doping.

6. LIST OF REFERENCES

1. Addadi L Resolution of conglomerates with the assistance of tailor-made impurities : Generality and mechanistic aspects of the "Rule of reversal". A new method for assignment of absolute configuration. *Journal of American Chemical Society* 1982, 104:p4610-4617.
2. Aki H, Niiya T, Iwase Y, Yamamoto M. Multimodal inclusion complexes between barbiturates and 2-hydroxypropyl-beta-cyclodextrin in aqueous solution: Isothermal titration microcalorimetry, (13)C NMR spectrometry, and molecular dynamics simulation. *Journal of Pharmaceutical Sciences* 2001, 90(8):p1186-97.
3. Al-Saeiq SS, Riley GS. Polymorphism in sulfonyleurea hypoglycemic agents. I. Tolbutamide. *Pharmaceutica Acta Helvetica* 1981, 56(4-5):p125-129.
4. Aravazhi S et al. Growth and characterization of L-Alanine and L-Valine doped Triglycine sulfate crystals. *Materials Research Bulletin* 1997, 32(11):p1503-1513.
5. Atencio R et al. Synthesis and single crystal structure of the 1:1 binary complex between pyrene and ferrocene. *Crystal Engineering* 2000, 3:p63-69.
6. Badawi AA. High energy forms of Lorazepam. *Bulletin of the Faculty of Science of Cairo University* 1997, 35(3) : p207-211.
7. Bauer J et al. Ritonavir: an extraordinary example of conformational polymorphism, *Pharmaceutical Research* 2001, 18(6):p 859-866
8. Bettinetti G et al. Structure and solid state chemistry of anhydrous and hydrated crystal forms of the Trimethoprim-Sulfamethoxy pyridazine 1:1 molecular complex. *Journal of Pharmaceutical Sciences* 2000, 89(4):p478-489.
9. Biradha K et al. Interpenetrating covalent and non-covalent nets in the crystal structures of $[M(4,4'-Bipyridine)_2(NO_3)_2] \cdot 3C_{10}H_8$. *Crystal Engineering* 1999, 2(1):p37-45.
10. Bondar V. Photostimulated transformation of defects in cadmium iodide with copper and coactivators. *Materials Science and Engineering B* 2000, 71:p 258-262

11. Bosela AA. Improvement of dissolution and bioavailability of khellin by crystal modification technique. *Bulletin of the Faculty of Science of Cairo University* 1997, 35(2) : p163-169.
12. Burt HM, Mitchell AG. Crystal defects and dissolution. *International Journal of Pharmaceutics* 1981, 9 : p137-152.
13. Chan HK, Grant DJW. Influence of compaction on the intrinsic dissolution rate of modified acetaminophen and adipic acid crystals. *International Journal of Pharmaceutics* 1989, 57 ; p117-124.
14. Chow AHL et al. Assessment of wettability and its relationship to the intrinsic dissolution rate of doped phenytoin crystals. *International Journal of Pharmaceutics* 1995b, 126:p21-28.
15. Chow AHL et al. Modification of phenytoin crystals. III Influence of 3-butanoxyloxymethyl-5,5-diphenyl hydantoin on solution-phase crystallization and related crystal properties. *International Journal of Pharmaceutics* 1995a, 126:p11-19.
16. Chow AHL et al. Modification of phenytoin crystals. Modification of phenytoin crystals : Influence of 3-acetoxymethyl-5,5-diphenyl hydantoin on solution-phase crystallization and related crystal properties. *International Journal of Pharmaceutics* 1991, 75:p219-230.
17. Chow AHL, Grant DJW. Influence of crystallization conditions on the physical properties of acetaminophen crystals : Evaluation by multiple linear regression. *International Journal of Pharmaceutics* 1989a, 51 ; p115-127.
18. Chow AHL, Grant DJW. Physical factors influencing the aqueous dissolution rate of acetaminophen crystals doped with p-acetoxycetanilide : evaluation by multiple linear regression. *International Journal of Pharmaceutics* 1989b, 51 ; p129-135.
19. Chow AHL et al. Modification of phenytoin crystals : influence of growth in aqueous solutions containing p-acetoxycetanilide on crystal properties. *International Journal of Pharmaceutics* 1985, 24 ; p239-258.
20. Debenedetti PG et al. Rapid expansion of supercritical solutions (RESS): Fundamentals and applications. *Fluid phase equilibria* 1993, 82 : p311-321.
21. Duddu SP, Grant DJW. The use of thermal analysis in the assessment of crystal disruption. *Thermochimica Acta* 1995, 248:p131-145.

22. Duncan-Hewitt WC, Grant DJW. True density and thermal expansivity of pharmaceutical solids : comparison of methods and assessment of crystallinity. *International Journal of Pharmaceutics* 1986, 28 ; p75-84.
23. Foxman BM et al. Environmentally benign synthesis using crystal engineering:steric accommodation in non-covalent derivatives of hydroquinones. *Crystal Engineering* 1998, 1(1):p109-118.
24. Gordon JD, Chow AHL. Modification of phenytoin crystals. II. Influence of 3-propanoyloxymethyl-5,5-diphenylhydantoin on solution-phase crystallization and related crystal properties. *International Journal of Pharmaceutics* 1992, 79 : p171-181.
25. Grant DJW, York P. A disruption index for quantifying the solid state disorder induced by additives or impurities. II. Evaluation from heat of solution. *International Journal of Pharmaceutics* 1986, 28 : p103-112.
26. Gu CH, Grant DJ. Effects of crystallization in the presence of the diastereomer on the crystal properties of (SS)-(+)-pseudoephedrine hydrochloride. *Enantiomer* 2000, 5:p271-80.
27. Gustafsson C at al. Comparison of solid-state NMR and isothermal microcalorimetry in the assessment of the amorphous component of lactose. *International Journal of Pharmaceutics* 1998, 174: p243-252.
28. Herman J et al. Instability of drug release from anhydrous theophylline-microcrystalline cellulose formulations. *International Journal of Pharmaceutics* 1989, 55:p143-146.
29. Hoke SH et al. Comparison of packed-column supercritical fluid chromatography--tandem mass spectrometry with liquid chromatography--tandem mass spectrometry for bioanalytical determination of (R)- and (S)-ketoprofen in human plasma following automated 96-well solid-phase extraction. *Analytical Chemistry* 2000, 1;72(17):4235-4241.
30. Kimura K. Characterization of Tolbutamide polymorphs (Burger's forms II and IV) and polymorphic transition behavior. *Journal of Pharmaceutical Sciences* 1999, 88(4):p385-391.
31. Kopp S et al. Methodology for a better evaluation of the relation between mechanical strength of solids and polymorphic form. *Journal of Pharmacy and Pharmacology* 1989, 41 : p79-82.

32. Laihanen et al. Solubility and intrinsic dissolution rate of Alprazolam crystal modifications. *Pharmaceutical Development and Technology* 1996, 1(4) : p373-380.
33. Leary JR et al. On the characterization of the polymorphs of tolbutamide. *Pharmaceutisch Weekblad Scientific Edition* 1981, 3:p62-66.
34. Li T et al. Influence of solvent and crystalline supramolecular structure on the formation of etching patterns on acetaminophen single crystals: A study with atomic force microscopy and computer simulation. *Journal of Physical Chemistry B* 2000, 104:p2019-2032.
35. Lynch DE et al. Molecular cocrystals of 2-amino-5-chlorobenzooxazole. *Crystal Engineering* 2000, 3:p71-79.
36. Mohamed RS et al. Solids formation after the expansion of supercritical mixtures. *Supercritical fluid science and technology, ACS Symposium Series-406*; Johnston KP, Penninger JML Eds., American Chemical Society, Washington DC, 1989, Chapter 23 : p355-378.
37. Mroso PV et al. Solid-state stability of aspirin in the presence of excipients: Kinetic interpretation, modeling and prediction. *Journal of Pharmaceutical Sciences* 1982, 71(10): p1096-1101.
38. Pikal MJ, Grant DJW. A theoretical treatment of changes in entropy of solids caused by additives or impurities in solid solution. *International Journal of Pharmaceutics* 1987, 39 : p243-253.
39. Prasad KVR et al. Crystallization of paracetamol from solution in the presence and absence of impurity. *International Journal of Pharmaceutics* 2001, 215:p29-44.
40. Rauls M et al. The influence of impurities on crystallization kinetics-a case study on ammonium sulfate. *Journal of Crystal Growth* 2000, 213(1-2):p 116-128
41. Rodriguez-Hornedo N, Wu HJ. Crystal growth kinetics of theophylline monohydrate. *Pharmaceutical Research* 1991, 8(5):p643-648.
42. Rowe EL, Anderson BD. Thermodynamic studies of Tolbutamide polymorphs. *Journal of Pharmaceutical Sciences* 1984, 73(11):p1673-1675.
43. Sano C et al. Effects of additives on the growth of L-glutamic acid crystals (β -form). *Journal of Crystal Growth* 1997, 178(4):p568-574.

44. Simonelli AP, Mehta SC, Higuchi WI. Dissolution rates of high energy sulfathiazole-povidone coprecipitates II: characterization of form of drug controlling its dissolution rate via solubility studies. *Journal of Pharmaceutical Sciences* 1976, 65(3): p355-61.
45. Staab E et al. *Advanced Materials* 1990, 2:p40
46. Suga H. A facet of perspectives in materials science, 1999. <http://www.rist.kindai.ac.jp/no.12/suga.pdf>, Last accessed 4/3/02.
47. Suga H. A facet of recent ice sciences. *Thermochimica Acta* 1997, 300:p117-126.
48. Weber A et al. Compressed fluid antisolvent crystallization for controlled particle design. In 4th *International Workshop on Crystal Growth Organic Matter* 1997. Editors: Ulrich, Joachim. Publisher: Shaker Verlag, Aachen. Issue:4: p214-221.
49. Weisinger-Lewin Y et al. Reduction in crystal symmetry of a solid solution: A neutron diffraction study at 15K of the host/guest system asparagine/aspartic acid. *Journal of American Chemical Society* 1989, 111:p1035-1040.
50. Weissbuch I et al. Molecular recognition at crystal interfaces. *Science* 1991, 253:p637-645.
51. Weissbuch I et al.. Tailor made additives and impurities In : Mersmann A (Ed), *Crystallization Technology Handbook* 2001 , Second Edition, Marcel Dekker, New York.
52. Williams-Seton et al. Disorder and twinning in molecular crystals: Impurity-induced effects in adipic acid. *Journal of Pharmaceutical Sciences* 2000, 89(3): p346-354.
53. Wong SH. Advances in chromatography for clinical drug analysis: supercritical fluid chromatography, capillary electrophoresis, and selected high-performance liquid chromatography techniques. *Therapeutic Drug Monitoring* 1993, 15(6):p576-580.
54. Yatsenko AV et al. NMR study of intrinsic defects in congruent LiNbO₃. I. "Unoverlapping" defects. *Physica B. Condensed matter* 1997, 240(3):p254-262.

55. York P, Grant DJW. A disruption index for quantifying the solid state disorder induced by additives or impurities. I. Definition and evaluation from heat of fusion. *International Journal of Pharmaceutics* 1985, 25 : p57-72.
56. York P, Hanna M. Salmeterol Xinafoate with controlled particle size. *International Patent Publication* 1995, Number : W/O 95/01324.
57. Yu, L. Amorphous pharmaceutical solids: preparation, characterization and stabilization. *Advanced Drug Delivery Reviews* 2001, 48(1):p 27-42
58. Zhang GGZ, Grant DJW. Incorporation mechanism of guest molecules in crystals: solid solution or inclusion? *International Journal of Pharmaceutics* 1999, 181:p61-70.

CHAPTER FOUR

Title: *Crystal Doping aided by Rapid Expansion of Supercritical Solutions.*

Abstract: This body of work is intended to serve as a proof of concept for the application of supramolecular chemistry in drug development. More specifically, this work is designed to evaluate crystal doping by recrystallization from supercritical media. The rapid nucleation and growth implicit to supercritical fluid based crystallizations were advantageously used in doping drug crystals with structurally related impurities. Polymorph conversion and crystal disruption of a model API viz. chlorpropamide were accomplished in this work. Several metastable forms of the drug were formed by utilizing the tunable solvent nature of SC CO₂. Crystal disruption in chlorpropamide was induced by controlled co-crystallization in the presence of urea. Based on the results from these studies, two different mechanisms of crystal disruption are proposed. In a further series of investigations, comparative evaluation of RESS versus solvent based crystal doping was performed. Rapid crystallization kinetics proved vital in making RESS superior to conventional solvent based crystallizations. Finally, a particle size reduction of about an order magnitude was seen following RESS processing. In providing the ability to control both the particle and crystal morphology of APIs, RESS proved potentially advantageous to crystal engineering.

Key words: Rapid expansion of supercritical solutions; RESS; Crystal doping; Co-Crystallization; Chlorpropamide; Urea.

1. INTRODUCTION:

The role of residual impurities on the bulk physical properties of a crystalline substance has long been identified and is generally regarded to be adverse. The residual impurities often include unused reactants, catalysts, synthetic byproducts, chiral isomers, solvates, hydrates, surfactants, monomers, etc. that develop during the synthesis, extraction, recrystallization and storage. Although often challenging, the cleanup task is achieved by secondary recrystallization methods or by alternative methods of synthesis. In instances where purification beyond a certain level is far fetched, the effects of the presence of impurities on the efficacy, safety and stability profiles of the active pharmaceutical ingredient (API) have been established. Such studies have revealed a domain of effects that an impurity can have on the crystal morphology and crystal energetics of an API. While this awareness of the role of impurities manifested as an additional burden to the traditional synthetic chemist, it also opened up a realm of new science called 'Supramolecular chemistry'. Broadly defined as the science that deals with anything outside the scope of covalent chemistry, it involves selective incorporation of tailor made additives and impurities into the crystal lattice of a host substance. Incorporation of the additives is based on interactions such as H-bonding, ion pairing, van der Waals attractive forces, hydrophobic interactions, beta-stacking, non-specific inclusion, etc. [Cram 1988, Klamer 2001]. Design of composite materials with altered bulk properties is made possible through such crystal modification. Supramolecular chemistry combines the features of

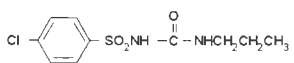
contemporary stereochemistry and biological enzyme-ligand systems in engineering crystal morphologies. Crystal engineering based on this science afforded among other applications a considerable promise in habit modification, racemate isolation, doping mediated induction of crystal defects & amorphous conversion, preferential crystallization of favored polymorph and synthesis of new molecular complexes.

A theoretical basis for the role of additives at molecular and bulk levels that will allow precise control over tailoring crystals still remains to be established. Efforts at such an understanding have mostly been limited to inorganics and other small molecules like (adipic acid, acetaminophen and alginate). The complexity of multiple conformations while dealing with pharmaceutically relevant molecules lends extension of such theories to pharmaceuticals rather difficult and may be the cause for limited progress in this area. While the advancement of supramolecular chemistry in disciplines such as ceramics, photography and semiconductor industries has therefore been significant to achieve commercialization, the concept is still at its inception in pharmaceuticals and only restricted to few research labs [Grant, Chow, Sherwood, Weissbuch 1991]. This body of work is intended to serve as a proof of concept for the application of supramolecular chemistry in drug development. More specifically, this work is designed to evaluate crystal doping by recrystallization from supercritical media. The rapid nucleation and growth implicit to supercritical fluid based crystallizations provided the motivation for choosing the **Rapid**

Expansion of Supercritical Solution (RESS) process. The ultimate motive in producing doped crystals is to add functionality to APIs at early stages of chemical synthesis. For example, producing low energy forms of the crystals can enhance the dissolution rates of poorly soluble drugs. Alternatively, crystallization of the most favored polymorph can be induced through doping. Such studies can prove particularly viable and timely in the context of the recent emphasis on the integration of the discovery and development research in pharmaceutical industry. For the purposes of this study, Chlorpropamide (CPD) was chosen as a model API and urea as the model dopant. The rationale for the selection of this API-dopant mixture was based on the structural similarity between the API and the dopant (Figure 51). In addition, doping is more controllable with a small molecule such as urea and in theory will reduce the propensity for segregation and associated stability problems.

Chlorpropamide belongs to the sulfonyl urea class of oral hypoglycemics. It is known to be practically insoluble in water and belongs to class II of biopharmaceutical classification (BCS). Five different polymorphs of CPD are identified to date, of which three are most commonly referred to in the published literature [Burger 1975, Aal-Saieq 1982, Simmons 1973, De Villiers 1999]. As is often the case with APIs exhibiting multiple conformations, the nomenclature of various forms of CPD is very confusing. For the purposes of consistency, the notation defined by Simmons [Simmons 1973] is used in this study. Even after the three decades since it was discovered, it is interesting to note that polymorphism

Chlorpropamide



Urea

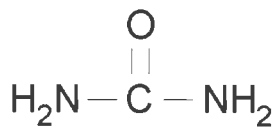


Figure 51. Chemical Structures of Chlorpropamide and Urea

in CPD has not been completely characterized. The specific objectives of this study are therefore to characterize the various polymorphs of Chlorpropamide prior to evaluating the efficacy of RESS process in doping CPD with urea.

2. MATERIALS AND METHODS:

2.A. Materials:

Chlorpropamide (Sigma, St.Louis,MO, Lot# 31H0722), Urea (JT Baker, NJ, Lot# N37340). All the solvents used were bought from JT Baker and are of HPLC grade.

2.B. Methods:

2.B. 1. Crystallization from supercritical solvent:

Rapid Expansion of Supercritical Solution (RESS) process was used in the co-crystallization of solid active pharmaceuticals and their structurally related impurities. In the process, the solutes of interest were dissolved in supercritical CO₂, forming a homogenous supercritical solution. Nucleation of solutes was then induced by rapidly reducing the solution density through expansion to atmospheric conditions. A rapid decrease in solvent strength results in high supersaturation that leads to very high nucleation rates [Mohamed 1989]. The time for nucleation and growth is very limited (typically 10⁻⁵ to 10⁻⁶ seconds), resulting in very small particles [Debenedetti 1993, Turk 1999]. Also, the rapid nucleation and growth aids in locking the impurities into the crystal domains of

the hosts by not providing sufficient time for the impurities to segregate. Absence of residual liquid solvents in the RESS produced crystals further reduces the possibility for segregation effects in the solid state.

In addition, the rapid decompression of SCF generates mechanical perturbation within the solution that travels at the speed of sound [Debenedetti 1993]. Consequently, very uniform conditions are reached within the nucleating media. Uniform conditions in the nucleation media assist in homogenous dispersion of impurities in the crystal domains of the hosts. The crystal disruption following such uniform and rapid co-crystallization can be expected to be controlled and large [Burt 1981]. All the above factors contributed to the special interest in RESS aided crystal doping and formed the rationale for its choice. Further, the concept is fairly nascent as reflected by the number of SCF aided crystal doping studies reported in the published literature [Weber 1997, York 1995].

The commercially available supercritical fluid extraction equipment (SFT150, Supercritical Fluid Technologies Inc., Delaware) was reconfigured to produce co-crystals of drugs and impurities by the rapid expansion of supercritical solution process. The modified design for the RESS process is schematically represented in Figure 8 and shown in Figure 9 (Chapter-3). Liquid CO₂ from a tank is pressurized using an air driven Haskel pump. The pump head is enclosed in a chiller-can through which a coolant at -10°C is continuously circulated. The coolant compensates for heat generation in the pump and prevents cavitation by

maintaining CO₂ in the liquid state at all times. Pressurized liquid was then fed to the preheater at a controlled flow rate. The function of the preheater is to serve as a heat exchanger and raise the temperature of the pressurized liquid to the supercritical region. The preheater used was a five metered stainless steel coil wrapped with Omegalux rope heaters (FGR, Omega Engineering Inc., Stamford, CT). The temperature of the preheater was controlled using Glas-Col temperature controller (Glas-Col, Terre Haute, IN). Supercritical CO₂ from the preheater then flows into the 100ml reaction vessel that contains the solutes to be recrystallized.

The reaction vessel was typically packed with 90 g of 3 mm glass beads and 10 g of solutes. The glass beads assist in improving the extraction efficiency of SC CO₂ by providing better fluid contact with solutes while also serving to buffer the turbulent flow of the fluid through the vessel. The starting mixture in the reaction vessel consisted of a physical blend of 80% drug and 20% impurity. Placing glass wool at either ends of the reaction vessel supported the powder bed and also prevented the entrainment of solutes. Depending on the selectivity of extraction of the supercritical solvent, saturated solutions form in the reaction vessel with fixed compositions of the host and impurity. The saturated supercritical fluid solution from the reaction vessel flows through a 0.5 μ frit into the pre-expansion chamber. It can be treated in the pre-expansion chamber to control the supersaturation prior to expansion. For the purposes of consistency in the crystal doping studies, the preexpansion chamber was maintained at 50°C above the extraction temperature. Presence of cold spots and abrupt temperature

drop in the lines were found to cause premature precipitation of solutes, which in turn lead to plugging of lines. All the lines and connectors therefore were heated using Omega rope heaters controlled by a common Glas-Col temperature controller.

The saturated solution from the preexpansion chamber then passes through a heated restriction device maintained at 100-150°C prior to rapid expansion. The heated restriction valve compensates the Joule-Thompson cooling that occurs as a result of rapid expansion. The expansion device used was a stainless steel capillary of aspect ratio 100 (5" L / 0.05" ID) that is securely inserted through the snap cap of a 40ml glass vial (Daigger, Lincolnshire, IL). Given that the interest here is in the crystal morphology of the pharmaceutical actives rather than their particle size, a 40 ml particle collection vial is best suited for these purposes. Use of 40 ml glass vial also improved yields by preventing losses from the particle collection typically observed with larger vessels. CO₂ gas after deposition of the solids was exhausted through a custom filter and passed through lengthy tubing (5 meters) prior to feeding to the thermo mass flow meter (Porter Instruments, Hatfield, PA). The gas flow rates were further totalized (Infinity Rate Totalizer, Newport Electronics, Santa Ana, CA) over the course of the experiment to get a more reliable estimate of the average CO₂ flow rates through the system. Typical flow rates of CO₂ through the system were between 5-10 SLPM. At the end of each run, yields of the recrystallized materials were recorded and the vials stored in low humidity plastic bags at ambient temperature until further use.

Following the above method, Chlorpropamide + Urea mixtures were recrystallized and the efficiency of SCF aided crystal doping was evaluated. The supercritical region investigated in these studies included a temperature regime of 45-100°C and pressures between 2000-8000 psi. The yields of co-crystals extracted at pressure less than 4000psi were very low to perform further characterization work and hence are not reported in this manuscript.

2.B. 2. Crystallization from Organic Solvents:

The role of the rapid crystallization kinetics in the supercritical fluid aided crystal doping can be best evaluated by comparing the doped crystals from RESS process to the ones crystallized at a much slower rate, for example by evaporative crystallization. Toward this objective, evaporative crystallization of chlorpropamide in the presence of varying amounts of urea as the impurity was undertaken. Other solvent related effects were in part normalized by choosing hexane ($\delta=7.24$ Hildebrand units) and ethyl acetate ($\delta=9.10$ Hildebrand units) as recrystallizing solvents, which are reported to closely correspond to supercritical CO₂ in their solubility behavior [Hyatt 1984, Dandge 1985, Dobbs 1987]. In addition, recrystallization from a relatively polar ethyl alcohol solvent was also performed in order to investigate the effect of the solvent polarity on the crystal doping of chlorpropamide+urea.

Evaporative crystallization experiments were carried out using a nitrogen analytical evaporator (The Myer N-Evap, Organomation Associates Inc., MA)

placed in a fume hood. One gram of chlorpropamide/urea mixtures in varying proportions (100/0, 80/20, 90/10, 99/1, 99.5/0.5 and 99.9/0.1, percent w/w basis) were accurately weighed into 40ml glass vials. 10ml of warm recrystallizing solvents at 45°C were added to these vials and the solutions thoroughly shaken. The open vials were securely fastened with clamps and immersed to fixed lengths into the 45°C temperature bath of the nitrogen evaporator. Needles connected to a common nitrogen source were inserted into the head space of the vials and fixed at standard heights such that uniform conditions prevailed in the different vials. The flow of nitrogen gas was controlled using a pressure regulator attached to the nitrogen tank. A 5psi pressure differential (20psi at the regulator to atmospheric pressure) was found to maintain suitable nitrogen flow rates into the vials. While solvent evaporation was complete in the case of hexane and ethyl acetate within 12 hours, recrystallization from ethyl alcohol took up to 24 hours owing to the lower vapor pressure of the hydralcoholic solution. At the end of the experiment, the recrystallized materials were spread in individual petri dishes, oven dried at 45°C overnight and sieved through a #60 (250 μ) screen. The screened materials were subsequently filled into vials, tightly capped and stored in low humidity plastic bags at ambient temperature until needed for further use.

2.B. 3. Differential Scanning Calorimetry:

DSC analysis was performed using a Perkin-Elmer DSC-7 equipped with an intercooler. Accurately weighed milligram samples were scanned in pin-holed

aluminum pans (TA Instruments, Dupont) under dry nitrogen purge. Various heating rates of 1,3,5 and 10°C/min were used to scan the different temperature regimes that are of interest to samples under consideration. The instrument was calibrated for temperature and enthalpy using high purity Indium and USP Water.

2.B. 4. Modulated DSC:

mDSC was used in an attempt to distinguish the kinetic events from the thermodynamic events in the thermal analyses of chlorpropamide+urea mixtures. About 10 mg of sample mixtures were accurately weighed (MT5, Mettler Toledo) and thermally scanned in the pin-holed, crimped aluminum pans (TA Instruments, Dupont) using TA Instruments Modulated DSC 2920. Samples were analyzed in the temperature range of 25°C-140°C. The scanning conditions included a heating ramp of 1°C/min with the modulation amplitude of 1°C in a 60sec period. Sapphire and Indium were used as calibration standards. The instrument was within the calibration period at all times when the reported analyses were performed.

2.B. 5. Hot Stage Microscopy:

Thermomicroscopy of these samples was performed using a Mettler FP82-HT Hot stage attached to the Mettler FP80-HT Controller and a Video System. Untreated samples were sprinkled onto a glass microscope slide, covered with a cover slip and placed on the hotstage. Changes in the particle and crystal morphologies,

among other thermal events that occur during the heating and cooling cycles were observed using Leitz Ortholux polarized optical microscope and recorded using a Sony 5600MD Video printer. The accuracy of the hot stage was routinely checked against USP melting standards.

2.B. 6. Thermogravimetric Analysis:

Thermal decomposition, moisture and residual solvent contents of the recrystallized materials were investigated using Perkin-Elmer TGA-7 at a heating rate of 5°C/min. Samples were heated in an open platinum pan with the nitrogen purge at 60 mL/min. The temperature scale was calibrated by measuring the Curie point (354°C) of standard PE ferromagnetic Nickel, while standard weights were used to calibrate the weight scale.

2.B. 7. Powder X-ray diffractometry:

XRPD was performed using a Rigaku-Geigerflex KD-2660-N X-ray diffractometer controlled by the D-Max B controller and Datascan MDI software. The diffractometer is equipped with a copper target, yielding X-rays of wavelength 1.54° Å. Diffractograms were obtained over the 2θ range 3° to 50° and analyzed using MDI Jade-5 software. Depending on amounts of the samples available for XRPD analysis, the powders were either packed into the 0.2mm groove of a glass slide (Regular Method) or sprinkled onto a thin film of Apiezon grease applied onto the glass slide (Grease Method). The operating conditions

included: scan speed 3°/minute, sampling interval 0.020° and X-ray power (tube input) of 40kV/40mA. The path of x-rays was controlled utilizing standard slits such as: ½ divergence, ½ scatter slits, 0.3mm receiving and 0.6mm receiving monochromator slits, in that order. The instrument was routinely calibrated under these operating conditions using Rigaku Quartz as standard.

2.B. 8. Polarizing Optical Microscopy:

Bulk particle morphology and the crystalline birefringence behavior of the samples were investigated using polarizing optical microscope (Leitz Lab 12 Pol S) with tungsten lamp as the light source. The objects are viewed and photomicrographs developed utilizing such accessories as Sony video camera, Boeckeler Via-70 Video marker and Sony 5600MD Video printer. A first order red compensator was used in enhancing the clarity of the photomicrographs. Untreated powders or powders dispersed in suitable media were placed on a glass slide and covered with a cover slip, prior to staging them in the path of brightfield light. The objects were viewed in the magnification range 200-800X, calibrated using an Olympus calibration slide.

2.B. 9. Scanning Electron Microscopy:

The morphology and surface characteristics of the samples were observed by scanning electron microscopy (SEM). Samples were mounted on an aluminum SEM stub and gold coated for 90 seconds at 45 mA with a Denton Vacuum Desk

II sputter coater (S/N 13156). SEM (Cambridge Stereoscan S360) examination was performed at 5-10 kV, 20 pA probe current, 100-4000x, and a working distance of 6-9 mm. Calibration is performed annually by LEO associates for morphological use only.

2.B.10. HPLC Analysis:

The amounts of host and guest in chlorpropamide+urea co-crystals were assayed by liquid chromatography (LC). Isocratic, reversed phase LC separation methods were developed and validated using external standards following modification in USP method for the hosts. Specific details of the method are summarized in Table 21, while the representative chromatogram of these mixtures is shown in Figure 52. A calibrated HP1100 series LC system equipped with a diode array detector was used in this analysis. Absence of chromophores in urea limited its detection by the diode array detector in both the UV and visible ranges. The separation however was accomplished by HPLC method and the interference from urea in the detection of CPD was established to be negligible. In the validation of this method of analysis, stock solutions of CPD and urea in the mobile phase were made at a concentration of 0.05% w/v each. Known aliquots of these solutions were then mixed to obtain varying proportions of CPD+Urea in the final mixture. These solutions were then subjected to HPLC analysis and the calibration curve was developed. Similar procedure was repeated at two other dilutions of stock

Table 21. HPLC Method of Assay for Chlorpropamide and Urea

Column	Supelco C-18 column, 4.6mm x 15cm
Mobile Phase	60% Dilute Acetic acid + 40% Acetonitrile
Flow rate	1.5 ml/min
Runtime	10 minutes
Injection Volume	10 μ L
Detector	HP Diode array, 240nm
System	HP 1100 series
Retention times	4.94 min (Chlorpropamide)

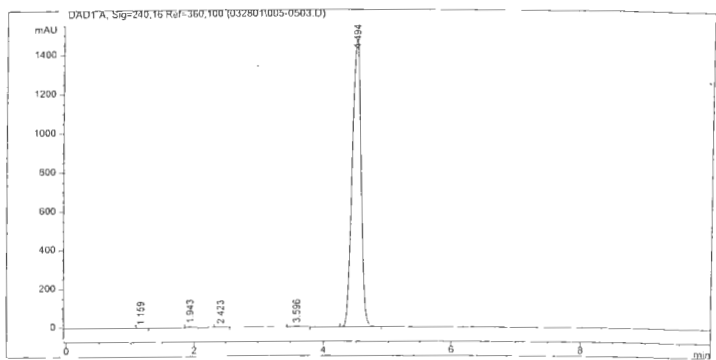
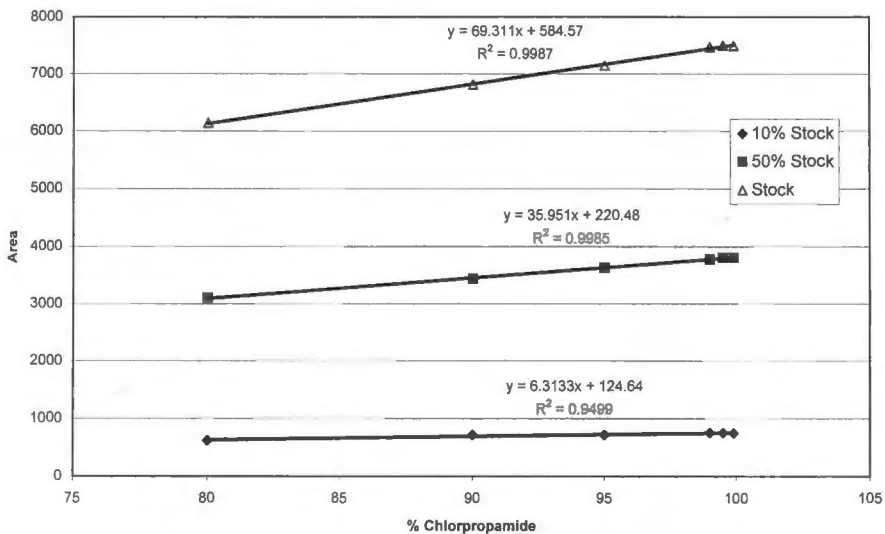


Figure 52. Typical Chromatogram of Chlorpropamide + Urea in a mixture

Figure 53. Calibration Curves at Different Levels of Chlorpropamide



solutions, viz. 0.025% and 0.005% w/v. The results of the above validation method are reported in Figure 53. As can be seen from the figure, urea in the mixture does not appear to interfere with the detection of CPD at any dilution. The amounts of urea in a mixture can thus be confidently calculated from the CPD levels in the mixture.

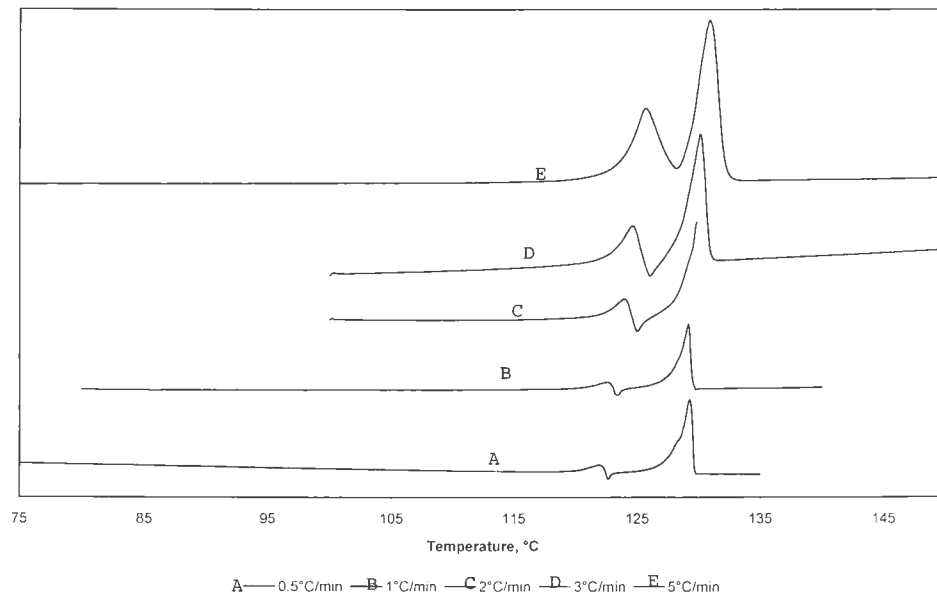
3. RESULTS AND DISCUSSION

3.A. POLYMORPHISM IN CHLORPROPAMIDE:

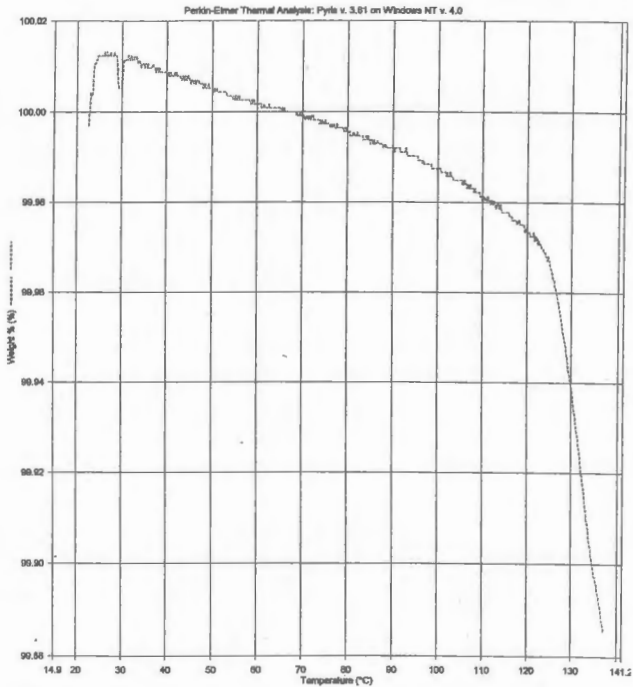
The commercially available form of CPD is obtained by crystallization from ethanol-water mixture and is called form-A. It is the most thermodynamically stable form at room temperature and has the lowest dissolution rate. Melt recrystallization of this form results in polymorph-B, which is monotropic with form-A [Yu 1995]. This form is unstable at all the temperatures and is stated to convert into form-A through multiple transformations [De Villiers 1999]. Polymorph C is obtained by heating form-A at 120°C for 4 hours. Taken as a pair, forms A and C are enantiotropically related, form C being the thermodynamically stable form at higher temperatures while form A is stable at lower temperatures. The transition temperature for this conversion, however is not reported to date. DeVilliers and Wurster determined the heats of solution of these forms in DMF at 25°C [De Villiers 1999]. The difference in the heats of solution between these forms was found significant (~4kJ/mol) in this study. This did not reflect in the DSC analysis, which did not show any endotherms corresponding to this heat of

transition even at heating rates as low as 0.5°C/min (Figure 54). Conversion for form-A to form-C was seen during the analysis, that did not permit calculation of individual melting data for these forms. The thermal behavior of polymorph A was therefore investigated in detail. As can be seen from Figure 54, subjecting form-A to DSC analysis at different heating rates revealed some interesting results. The endotherm at 121°C corresponds to the melting of form-A, while the one at 129°C to that of form-C. The transition from A to C was found to occur gradually with increase in temperature and was most rapid at temperatures nearing the melting point of A. Apparently, the melting endotherms overlap, making the heat of fusion values for these polymorphs indeterminable. Efforts at resolving these melting endotherms by reducing the heating rates revealed intermediate recrystallization that was hidden before at higher heating rates. Thermomicroscopy, simulating the heating ramps used in the above DSC analysis revealed that the transition from A to C is rapid around melting point of A, but does not necessarily occur from the melt. Apparent change in the particle morphology was seen upon gradually heating from 100°C to 120°C. TGA analysis of polymorph A (Figure 55a and 55b) did not indicate any weight loss around this temperature, excluding the possibility of solvent/water mediated transition. From the discussion above, it can be stated that the transition from A to C occurs in a solid state with no change in the composition of the solid. It is hoped that the intermediary recrystallization exotherm can be separated as a kinetic event, utilizing the modulations in heating by mDSC.

Figure 54. DSC of Polymorph-A at Different Heating Rates



Filename:	C:\PEP\pyn\data\TGA01387.d	Database No. 81038x	Chlorpropamide: TGA01387.d
Date Collected:	08/14/2001 1:30:55 PM		Unsubtracted Weight % (%): Step: 1
Baseline Filename:			
Operator ID:	Charndra Verna		
Sample ID:	Chlorpropamide		
Sample Weight:	17.079 mg		
Comment:	Run-3, HE7347997		

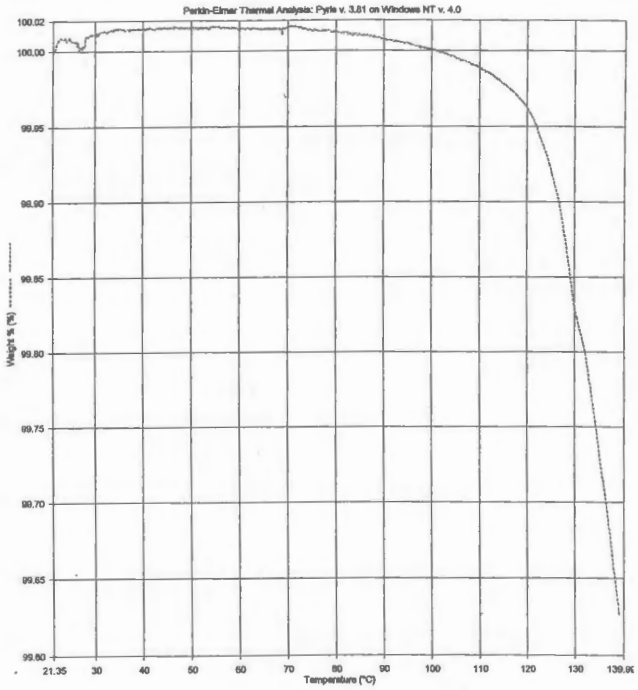


08/14/2001 2:52:38 PM

1) Heat from 25.00°C to 140.00°C at 5.00°C/min

Figure 55A. TGA Thermogram of Chlorpropamide-A at 5°C/min

Filename:	C:\E\Pyris\Data\TGA01388.tpd	Chlorpropamide; TGA01388.tpd
Date Collected:	08/14/2001 4:45:45 PM	Databook No. 81038x 10
Sample Name:		Unsubtracted Weight % (%) : Step: 1
Operator ID:	Chandra Varma	
Sample IC:	Chlorpropamide	
Sample Weight:	28.250 mg	
Comment:	Rust-4, NB734729-97	



08/14/2001 4:57:01 PM

1) Heat from 25.00°C to 140.00°C at 1.00°C/min

Figure 55B. TGA Thermogram of Chlorpropamide-A at 1°C/min

The results of mDSC performed at heating rates of 5°C/min and 1°C/min are shown in Figures 56 and 57. As can be seen from the reversing (enthalpy related) curves in the figures, even this method failed to isolate the two endotherms. This indicates that a reversible transformation between forms A and C occurs just before form-A melts. Calculation of the heat of fusion value of form-A, to be utilized in evaluating its crystallinity is therefore not possible by direct DSC analysis. For the purposes of this study, this value was calculated from the ΔH_f of form C in a manner analogous to Behme and Brooke's study [Behme 1991]. Unlike in the case of carbamazepine, the transition from one polymorph to other however did not occur during the DSC analysis of Chlp. For the purposes of this study, this heat of transition was estimated to be 4 kJ/mol (or 14.45 J/g), the difference in the heats of solution values reported by DeVilliers at 25°C. This estimation was made on the basis that a linear relationship exists between the heat of solution and the heat of fusion for the same polymorph with fixed chemical structure [Yoshihashi 2000]. Such an estimation is further supported by Hess Law that states that the energy associated with a transition depends on the final states and is independent of the path. Assuming that this difference is constant over the temperature range of 30-120°C, the heat of fusion of form-A can be estimated to be $85.77+14.45= 100.22$ J/g. This assumption was validated when the heat capacity values (C_p) of polymorphs A and C were found to vary similarly in this temperature range (notice the parallel baselines for various polymorphs in Figures 58-60). The ΔH_f values of polymorphs B and C are obtained from the

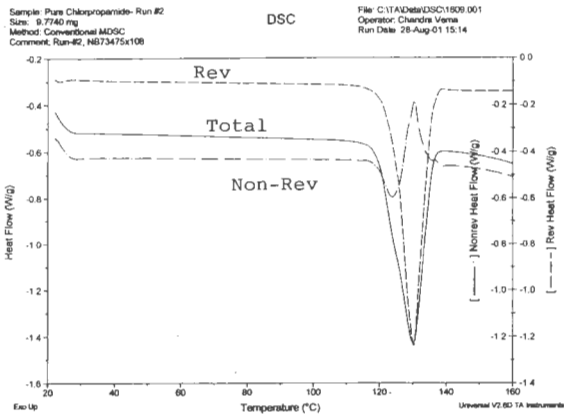


Figure 56. Results of mDSC Analysis Performed At a Heating Rate
 Of 5°C/min

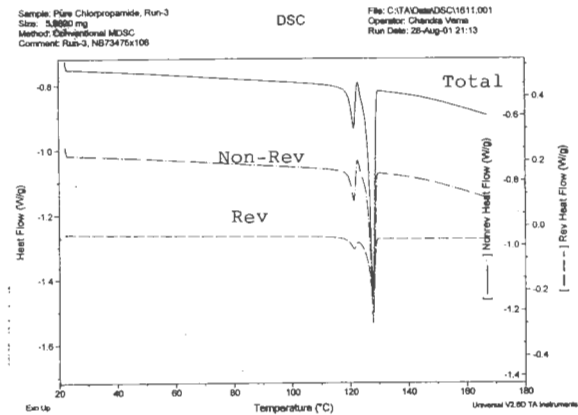


Figure 57. Results of mDSC Analysis Performed At a Heating Rate
 Of 1°C/min

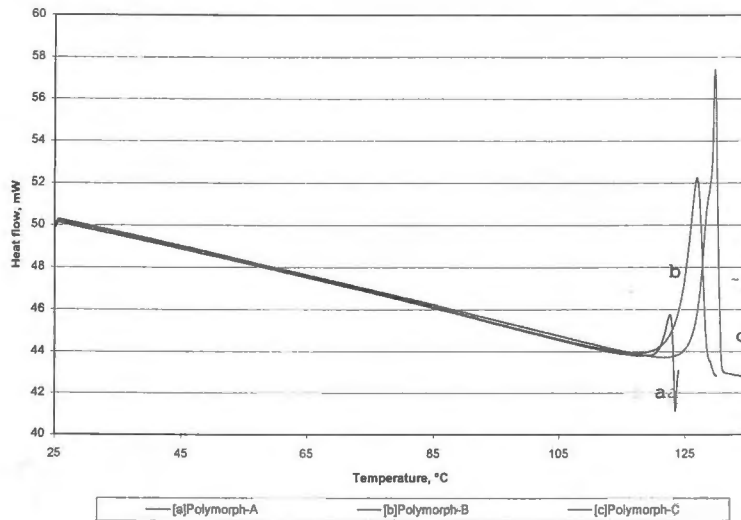


Figure 58. Thermograms of Different Polymorphs of Chlorpropamide

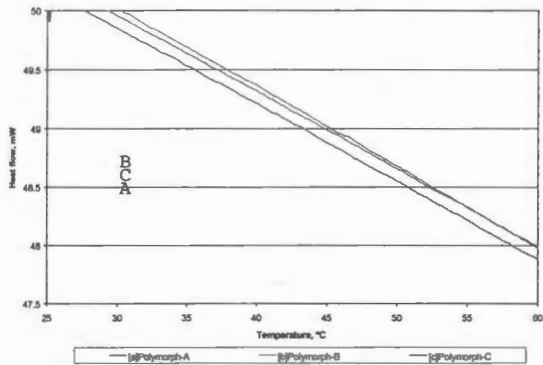


Figure 59. Heat Capacity Values Different Polymorphs of CPD As function of Temperature: 25°C-60°C

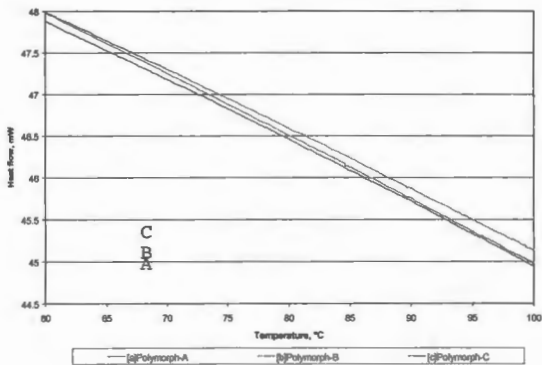


Figure 60. Heat Capacity Values Different Polymorphs of CPD As function of Temperature: 60°C-100°C

DSC analysis, given that these polymorphs can be produced in pure form and no concurrent phase changes occur during their thermal analysis. The melting data for polymorphs A, B and C, following the above discussion is summarized in Table 22.

Two other means of characterizing the various polymorphs of Chlp were also developed. The first used polarizing optical microscopy. As can be seen from Figures 61a to 61c, the crystal habit of the various polymorphs appear to be distinctly different. Polymorph A seemed to crystallize in tabular habit, while the metastable forms B and C appear as blades and plates respectively. In addition, XRPD serves as a very powerful tool in distinguishing these polymorphs. The diffraction patterns of the three forms are shown in Figure 62. The major diffraction peaks distinguishing the various polymorphs are shown in Table 23. In summary, polymorphs A, B and C are characterized by various analytical techniques and the results are tabulated in Table 23. Also, the thermodynamic data useful in evaluating the crystallinity of these polymorphs in the later doping studies is developed.

3.B. RESS OF PURE CHLORPROPAMIDE:

Pure Chlp was recrystallized from varying RESS conditions shown in Table 24. As can be seen from Figure 63, increased yields from crystallization are achieved both upon increasing the extraction pressure and also, the temperature of supercritical CO₂. Recrystallization of polymorph A from supercritical CO₂ at

Polymorph-A

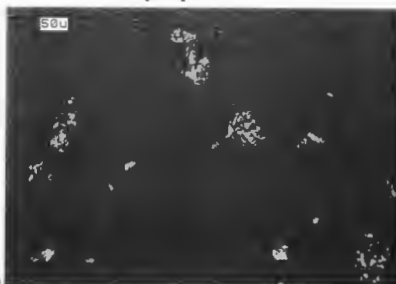


Fig. 61(a)

Polymorph-B



Fig. 61(b)

Polymorph-C

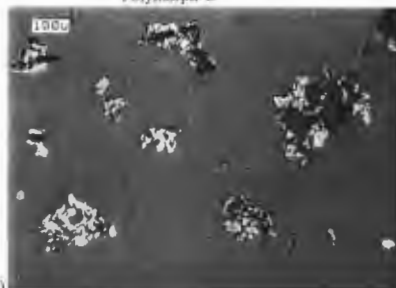


Fig. 61(c)

Figure 61. Photomicrographs of Various Polymorphs of Chlorpropamide

Table 22. Melting data and Heat of Solutions of Different Polymorphs of Chlorpropamide

Polymorph	$T_m(^{\circ}\text{C})$	$\Delta H_f, \text{J/g}$	$H_s \text{ at } 25^{\circ}\text{C J/g}$
A	121.5	100.22	21.25
B	125.35	77.03	15.22
C	128.85	85.77	36.07

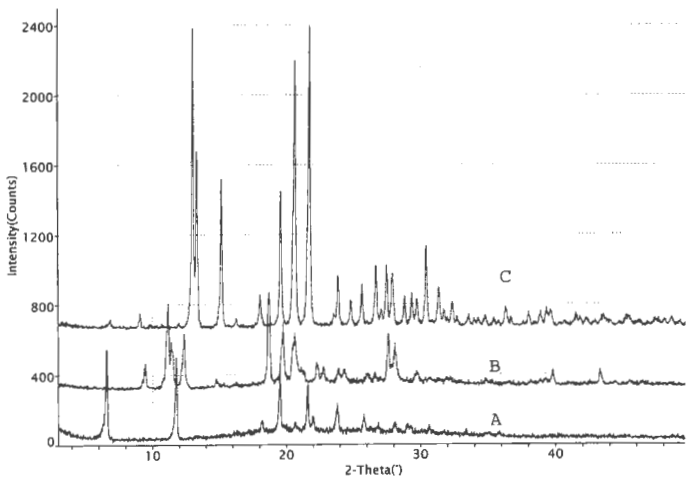


Figure 62. XRPD Patterns of Various Polymorphs of Chlorpropamide

Table 23. Nomenclature/Properties of Reported Chlorpropamide Polymorphs

Polymorph	Source	T _m (°C)	ΔH _f (J/g)	ΔH _s ¹ (KJ/mol)	Characteristic XRPD peak(2θ)	Habit
A / III / IV	Commercial	121-122	100.22	5.88	6.62, 11.78	Tabular
B / II / I'	Recrystallized from melt	124-127	77.03	4.21	12.36	Blades
C / I / I	Heat A @120°C for 3 hrs	128-130	85.77	9.98	15.18	Plates
IV	Crystallized from CCl ₄	122-123	-	-	-	-
V	Desolvation of Solvate of benzene < 118	-	-	-	-	-
II	Rapid evaporation from Chloroform	-	-	-	-	-
III	Rapid cooling from Hexanol	-	-	-	-	-

Simmons, Canadian Journal of Pharmaceutical Sciences, 8(4), 1973

Burger, Sci. Pharm 1975

Saiq, Pharm Acta Helvetica, 57(1), 1982

Table 24. Summary of RESS Recrystallization Of Chlorpropamide

Expt	[P,T conditions]	Weight Collected,mg	Collection Time, min	Collection Rate, mg/min
1	[46°C, 4000psi]	356.0	240	1.48
2	[48°C, 8000psi]	618.1	90	6.87
3	[60°C, 4000psi]	445.2	210	2.12
4	[61°C, 8000psi]	400.4	30	13.35
5	[75°C, 4000psi]	411.6	30	13.72
6	[75.5°C, 8000psi]	750.2	30	25.01
7	[101°C, 4000psi]	1266.4	60	21.11
8	[100°C, 8000psi]	1389.5	45	30.88

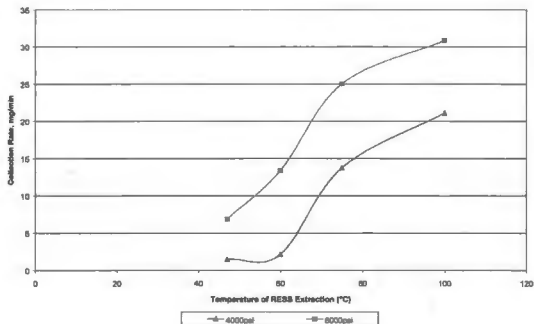


Figure 63. Yields from RESS Recrystallization of Chlorpropamide As a Function of Temperature and Pressure

different P,T conditions resulted in the formation of several metastable polymorphs (Table 25). Of interest here in view of enhancing the dissolution performance is the formation of polymorph C (Figure 64). While complete polymorph conversion from A to C was seen at certain conditions, the original form remained at other extraction temperatures and pressures (Table 25). The polymorphic identity of the RESS recrystallized materials was positively confirmed from their XRPD data (Figure 65). On the other hand, thermal behavior of RESS recrystallized materials as determined by DSC exhibited inconsistency with the XRPD results in certain cases. The melting temperatures, however exactly match Burgers polymorphs denoted by the Roman nomenclature (Table 25) [Burger 1975]. XRPD data for these polymorphs has not been reported in Burgers study and hence no definitive matches can be made.

The results of RESS recrystallizations of pure Chlp indicate the ability of the RESS process to form different polymorphs from the same solvent by mere changes in the temperature and pressure conditions. The polymorphic conversion from form A to C can be explained based on the individual effects of temperature and pressure on the Chlp crystallites during their nucleation and growth. The effect of temperature on this conversion was addressed in detail in section A. This conversion upon recrystallization from SC CO₂ is consistent with the reported effects of temperature and compression pressure during the tableting of Chlorpropamide [Matsumoto 1995]. It appears from these studies that these forms

Table 25. Polymorph Conversion of Chlorpropamide by RESS Recrystallization

Conditions of Rxn Vessel [T in °C, P in psi]	T _m °C (RSD)	Delta H _f (J/g) (RSD)	Polymorph Identity (XRPD)
[46, 4000]	112.43 (1.51)	23.67 (8.99)	C
[48, 8000]	122.05 (1.01)	49.97 (1.31)	C
[60, 4000]	111.58 (0.47)	32.99 (5.70)	A + C
[61, 8000]	117.50 (0.43)	54.14 (1.82)	A + C
[75, 4000]	126.58 (0.23)	68.63 (2.06)	A + C
[75, 8000]	127.08 (0.30)	70.72 (3.66)	C
[101, 4000]	124.56 (0.95)	60.43 (1.18)	A + C
[100, 8000]	125.58 (0.41)	62.62 (1.08)	C

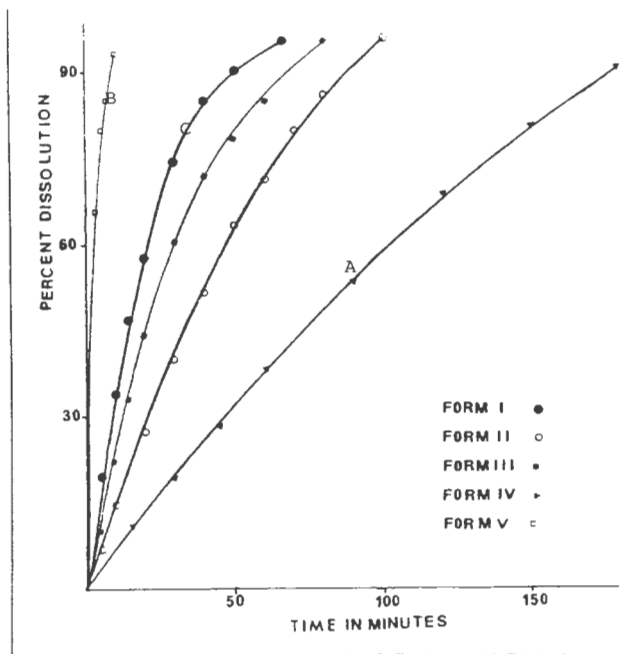


Figure 64. Dissolution Profiles of Various Polymorphs of Chlorpropamide

Reproduced from Saieq, Pharm Acta Helvetica, 1982

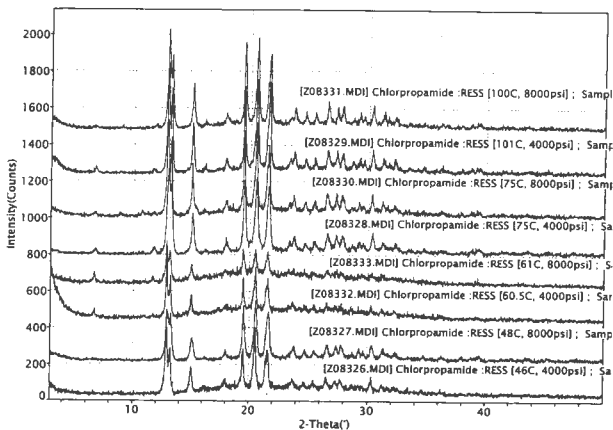


Figure 65. XRPD Patterns of RESS Produced Chlorpropamide

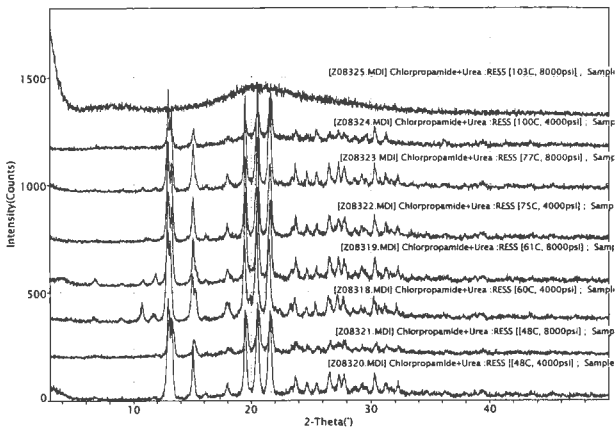


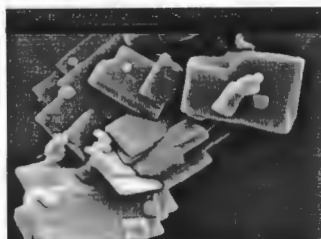
Figure 66. XRPD Patterns of RESS Produced Co-Crystals of Chlorpropamide + Urea

differ in the manner of their packing that is easily influenced by the temperature and pressure during SCF crystallization.

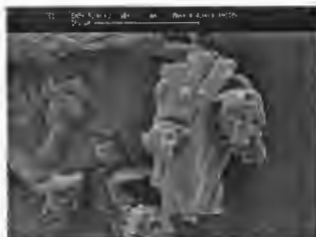
Scanning electron microscopy of recrystallized materials indicated a change in the habit and also, a general reduction in the particle size of the recrystallized materials (Figure 67). Agglomeration of the particles arising from bouncing with each other and with the walls of the smaller collection vial can be seen in relation to rather distinct crystals collected in a larger vessel (compare Figures 67.b-e vs. 67f). While a tabular habit can be seen in the commercially available material, all the RESS recrystallized samples attained the shape of blades that is typical of form-C. Consistent with the XRPD results, Chlp recrystallized from selective RESS conditions contained both the forms A and C reflected as a mix of tabular and plate like crystals. (Figure 67-b, c, d). Also, the particle size reduction was significant at the 75°C condition, perhaps due to higher supersaturations attained at this temperature versus the 60°C condition. As can be seen from Figures 67a to 67f, submicron to few micron sized particles were produced by RESS recrystallization.

3.C. RESS OF CHLORPROPAMIDE+ UREA:

The presence of urea in the crystallizing medium of Chlorpropamide reduced the yields as can be seen from Table 26. The solubility of Chlp appears to be significantly higher than urea in SC CO₂ at the various conditions studied. An apparent reduction in the overall yields can therefore be expected in the presence



[a] Pure Chlorpropamide-A, Commercial.



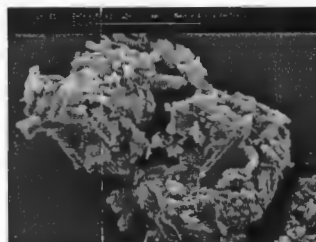
[b] Recrystallized from SCCO₂ at [60°C, 4000psi]



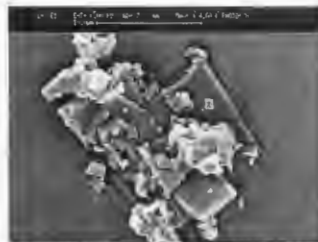
[c] Recrystallized from SCCO₂ at [61°C, 8000psi]



[d] Recrystallized from SCCO₂ at [75°C, 4000psi]



[e] Recrystallized from SCCO₂ at [75°C, 8000psi]



[f] Recrystallized from SCCO₂ at [75°C, 8000psi]

Figure 67. Scanning Electron Micrographs of RESS Recrystallized Chlorpropamide

Table 26. Summary Of RESS Recrystallization Of Chlorpropamide+ Urea

COMPOSITION OF STARTING MIXTURE: 80% Chlorpropamide + 20% Urea

CONTENTS OF REACTION VESSEL : 10g Chlorpropamide + 2.5g Urea (12.5g of blend)

Expt	[P,T conditions]	Weight collected mg	Collection time min	Collection Rate mg/min
1	[48°C, 4000psi]	292	180	1.62
2	[48°C, 8000psi]	325	180	1.81
3	[60°C, 4000psi]	507.6	120	4.23
4	[60.5°C, 8000psi]	361.7	30	12.06
5	[75°C, 4000psi]	465.9	60	7.77
6	[77°C, 8000psi]	1467.3	60	24.46
7	[100.5°C, 4000psi]	724.9	90	8.05
8	[103°C, 8000psi]	900.4	90	10.00

of a less soluble component like urea. The binary phase behavior of Chlp+ Urea mixtures was reported by Ford and Rubenstein (Ford 1977) and is shown in Figure 68. As can be seen, a mixture containing 89% Chlp+11%Urea forms a eutectic that melts at 89°C. Compositions containing >90% Chlorpropamide can be seen to form solid solutions. This region is of particular interest in the context of crystal doping. Co-crystallization of chlorpropamide in the presence of urea resulted in the formation of eutectic mixtures and solid solutions depending on the composition of the mixtures formed (Tables 27 and 28). A agreement between the thermal behavior of the co-crystals and their compositions can be seen from Tables 27 and 28.

Formation of the solid solutions of urea in chlorpropamide resulted in the crystal disruption of the host and eventually in amorphous conversion at urea levels higher than 40% w/w (Figure 66). Peak broadening and peak shifts in the x-ray diffraction patterns were seen in all the doped crystals (Tables 29 and 30). Two mechanisms are proposed that caused this consistent broadening and shifts in the XRPD peaks and illustrated in Figure 69. Firstly, as shown in mechanism-1, urea may have been adsorbed onto selective faces of the crystals of Chlp that apparently changed the way it packs. This leads to altered symmetry and increased mosaic spread mirroring in the manner in which different planes reflect x-rays. Apparently, peak broadening and a shift in the XRPD peaks is evident. Another fact that further validates this mechanism is the preferential crystallization of polymorph C in the presence of urea.

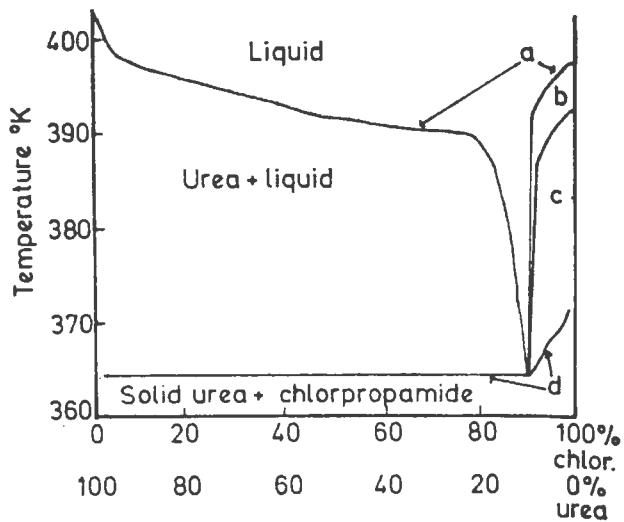


Figure 68. Binary Phase Behavior of Chlorpropamide and Urea

Reproduced from Ford JL, Journal of Pharmacy and Pharmacology 1977.

Table 27. Selectivity of Extraction as a function of T/P of SC CO₂

Extraction Conditions [T in °C, P in psi]	CO ₂ Density g/cc	Average Chlorpropamide%	RSD (n=3)	% Urea
[48, 4000]	0.8631	-	-	-
[48, 8000]	0.9852	85.87	1.07	14.13
[60, 4000]	0.8109	93.09	3.43	6.91
[61, 8000]	0.9509	93.55	3.12	6.45
[75, 4000]	0.7431	98.38	0.82	1.62
[77, 8000]	0.9055	85.61	5.48	14.39
[100, 4000]	0.6287	60.57	4.84	39.43
[103, 8000]	0.8355	42.08	0.95	57.92

Table 28. Results of Doping Chlorpropamide with Urea

Conditions of Rxn Vessel [T in °C, P in psi]	T _m °C (RSD)	ΔH _f (RSD) (J/g, n=3)	Polymorph Identity
[48, 4000]	123.42 (0.23)	47.40(7.03)	C
[48, 8000]*	No Drug Peak	-	C
[60, 4000]*	118.29 (0.66)	44.96 (5.17)	A+C
[61, 8000]*	121.08 (1.33)	54.80 (5.45)	C
[75, 4000]	121.57 (0.23)	40.01 (4.30)	C
[77, 8000]	119.58 (0.97)	26.39 (11.34)	C
[100,4000]	No Drug Peak	-	C/Amorphous
[103,8000]	No Drug Peak	-	Amorphous

* Eutectic Mixture Formed

Table 29. Peak Shifts and Peak Broadening in Doped Chlorpropamide Crystals

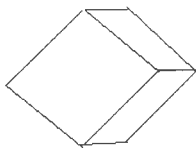
2 Theta	Pure	[48C, 4000psi]	[75C, 4000psi]	[60 5C, 8000psi]	[60C, 4000psi]	[48C, 8000psi]	[77C, 8000psi]	[100C, 4000psi]	[103C, 8000psi]
		% Urea=0	% Urea=1.62	% Urea=6.45	% Urea=6.91	% Urea=14.13	% Urea=14.39	% Urea=39.43	% Urea=57.92
-	-	-	-	<i>0.31</i>	-	-	-	-	-
6.89	0.22	-	-	0.31	0.24	-	-	-	-
9.08	0.12	-	-	<i>0.2</i>	<i>0.27</i>	-	-	-	-
-	-	-	-	<i>0.19</i>	<i>0.23</i>	-	-	-	-
-	-	-	-	-	0.29	-	-	-	-
13.04	0.18	0.43	0.51	0.38	0.41	0.48	0.41	0.41	-
15.18	0.15	<i>0.19</i>	<i>0.2</i>	0.25	0.46	0.27	<i>0.25</i>	<i>0.21</i>	-
16.27	0.15	<i>0.15</i>	-	-	-	-	-	-	-
18.04	0.19	<i>0.21</i>	<i>0.16</i>	0.29	0.33	<i>0.28</i>	0.32	-	-
19.6	0.15	-	<i>0.22</i>	-	<i>0.18</i>	-	<i>0.22</i>	-	-
20.68	0.18	0.25	<i>0.25</i>	<i>0.22</i>	<i>0.21</i>	0.29	-	<i>0.22</i>	-
21.76	0.17	0.27	<i>0.27</i>	<i>0.25</i>	<i>0.25</i>	0.29	<i>0.24</i>	<i>0.26</i>	-
23.84	0.19	-	<i>0.24</i>	<i>0.24</i>	<i>0.14</i>	-	-	-	-
24.78	0.14	-	0.35	-	<i>0.16</i>	-	-	-	-
25.64	0.15	<i>0.29</i>	0.41	-	<i>0.15</i>	-	<i>0.18</i>	0.34	-
26.66	0.18	<i>0.22</i>	<i>0.23</i>	0.24	0.31	-	<i>0.23</i>	<i>0.13</i>	-
27.46	0.17	-	<i>0.18</i>	-	<i>0.22</i>	-	<i>0.13</i>	<i>0.08</i>	-
27.9	0.19	-	<i>0.28</i>	0.17	-	-	<i>0.19</i>	<i>0.19</i>	-
29.7	0.18	0.48	0.4	0.35	-	0.34	-	<i>0.2</i>	-
30.42	0.15	0.21	<i>0.22</i>	-	-	0.29	0.33	<i>0.24</i>	-
31.34	0.18	0.64	-	-	-	0.48	0.37	0.3	-
32.36	0.17	0.3	-	0.38	-	<i>0.11</i>	0.41	-	-
-	-	-	-	-	-	<i>0.22</i>	-	-	-
38.02	0.17	<i>0.18</i>	-	-	-	-	-	-	-
39.62	0.39	<i>0.34</i>	-	-	-	-	0.25	-	-
43.5	0.41	-	-	<i>0.29</i>	-	-	-	-	-
-	-	-	-	<i>0.15</i>	-	-	-	-	-

Bold font **Broadened Peaks**
Italic font *Shifted Peaks*

Table 30. Peak Broadening as a function of impurity levels in the doped crystals

Condition	Percent Urea	FWHM Values									
		$2\theta=13.04$	$2\theta=15.18$	$2\theta=18.04$	$2\theta=20.68$	$2\theta=21.76$	$2\theta=26.66$	$2\theta=29.7$	$2\theta=30.42$	$2\theta=31.34$	$2\theta=32.36$
Pure Form-C	0	0.18	0.15	0.19	0.18	0.17	0.18	0.18	0.15	0.18	0.17
[48°C, 4000psi]	0.00	0.43	<i>0.19</i>	<i>0.27</i>	0.25	0.27	0.22	0.48	0.21	0.64	0.3
[75°C, 4000psi]	1.62	0.51	<i>0.2</i>	<i>0.16</i>	<i>0.25</i>	<i>0.27</i>	<i>0.23</i>	0.4	<i>0.22</i>		
[61°C, 8000psi]	6.45	0.38	0.25	0.29	<i>0.22</i>	<i>0.25</i>	0.24	0.35			0.38
[60°C, 4000psi]	6.91	0.41	0.46	0.33	<i>0.27</i>	<i>0.25</i>	0.31				
[48°C, 8000psi]	14.13	0.48	0.27	<i>0.28</i>	0.29	0.29		0.34	0.29	0.48	<i>0.11</i>
[77°C, 8000psi]	14.39	0.41	<i>0.25</i>	0.32		<i>0.24</i>	<i>0.23</i>		0.33	0.37	0.41
[100°C, 4000psi]	39.43	0.41	<i>0.27</i>		<i>0.27</i>	<i>0.26</i>	<i>0.13</i>	<i>0.2</i>	<i>0.24</i>	0.3	
[103°C, 8000psi]	57.92	AMORPHOUS CONVERSION									

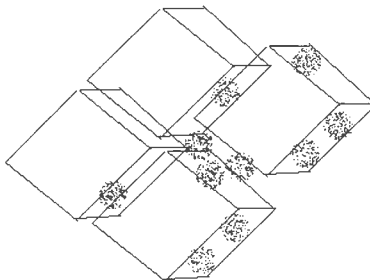
Chlp lattice (Orthorhombic eg- a rhombic prism)



Urea



Mechanism-1: Selective Adsorption of different faces



Mechanism-2:

Inclusion → Volumetric Expansion → Loss of Symmetry → Amorphous Conversion

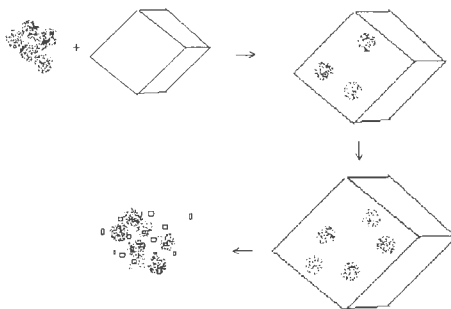


Figure 69. Illustration of the Proposed Mechanisms of Crystal Disruption

By adsorbing onto selective faces, urea may have mediated crystallization of polymorph C while stunting the growth of A. The second mechanism involves the inclusion of urea into the lattice of Chlp, increasing the volume of the crystal lattice, and thereby increasing the d-spacings. Increased volume as a result of the distortion induced by a foreign molecule thus also results in the shift of XRPD peaks. Interestingly, this is reflected in the majority of the peaks shifting toward lower 2θ 's. A combination of these two mechanisms is also possible where the levels of impurity are high, culminating in the eventual loss of symmetry and subsequent amorphous conversion. Although, single crystal data of the doped crystals will provide more insight into such mechanisms, single crystals are difficult to grow to tangible sizes using SCF recrystallization. On the other hand, the XRPD data generated in this study can be utilized in deducing the lattice parameters and other crystallographic data by iterative computer simulations. Published single crystal data however is only available for form A [Koo 1980] and such studies could not be performed for polymorph C, which is frequently formed in these studies. The evidence of crystal disruption was also confirmed by the lowering of the melting points and the heat of fusion values of the doped crystals compared to pure crystal of the same polymorph (Table 28). Melting point reductions up to 9°C were seen upon doping with urea. Also, significant reductions in the ΔH_f values of Chlp up to 50% were seen as a result of doping with urea. By imparting a strain in the lattices of chlorpropamide crystals that was observed in XRPD results, urea may have reduced the symmetry in the original

crystals and hence a reduction in the heat of fusion values were seen. Such reductions manifest in significant increases in the initial dissolution rates owing to the ease with which the solvent can destroy the crystal structure for subsequent dissolution. Following the log-linear relationship observed between these entities by Yoshihashi [Yoshihashi 2000], projected enhancement in the initial dissolution rates can be expected to be significant.

Scanning electron microscopy of the doped crystals indicated surface adsorption of urea onto Chlp crystals. Also, the particles appeared severely agglomerated owing to the use of a smaller collection vial. Given that the interest here is in the crystalline morphology of the RESS produced crystals of Chlp, no exhaustive attempts were made to restore the microcrystals formed by SCCO_2 from agglomeration. To prove the concept of agglomeration arising from the bouncing of particles coming at high velocities into the collection vessel (40 ml), a larger collection vessel was used (1 L). Owing to the altered dynamic of jet expansion in this case, agglomeration was significantly reduced (compare Figure 70f versus Figures 70b-e). The SEMs shown in figure 70f indicate that the particle size of the primary RESS produced particles is in the range of 1-2 μ while that of the starting material was around 10 μ . A particle size reduction of up to an order of magnitude was therefore produced upon RESS processing.

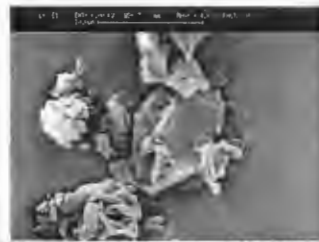
The efficiency of RESS process in doping was evaluated by direct comparison to the doped crystals produced from liquid organic solvents. Polymorphic conversion was not seen in Chlp recrystallized from ethanol, ethyl



[a] 80/20 Physical Mixture of Chlp+Urea



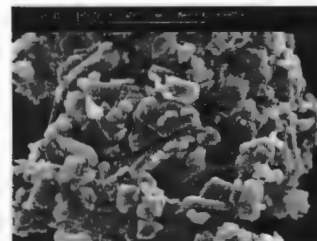
[b] Recrystallized from SCCO₂ at [60°C, 4000psi]



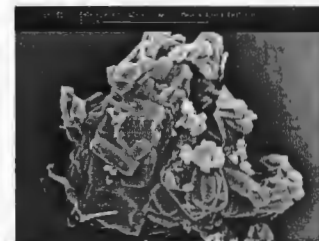
[c] Recrystallized from SCCO₂ at [60°C, 8000psi]



[d] Recrystallized from SCCO₂ at [75°C, 4000psi]



[e] Recrystallized from SCCO₂ at [77°C, 8000psi]



[f] Recrystallized from SCCO₂ at [77°C, 8000psi]*

Figure 70. Scanning Electron Micrographs of RESS Produced Chlorpropamide+Urea Co-Crystals

* 1L Collection Vessel Used

acetate or hexane. As can be seen from Figures 71 to 73, polymorph A was formed in all the solvent systems, irrespective of their polarities.

Although minor reductions in the melting temperatures and the heat of fusion values of Chlp were seen upon doping with urea (Tables 31A-C), no significant disruption in the crystallinity was evident from XRPD results. A possible cause for this may be due to the limited amounts of urea that actually got incorporated into the lattice of Chlp. On the other hand, the fast nucleation and growth from a supercritical solution may have locked rather high levels of urea into the crystal lattice of the host, causing large reductions in the crystallinity. The ability to adjust the level of impurity in this context provides the ability to control the levels of crystallinity of Chlp. This feature of RESS based crystal doping coupled with the polymorph conversion and particle size reduction ability may all be advantageously utilized towards enhancing the dissolution rates of poorly soluble drugs.

4. CONCLUSIONS

Towards the objective of enhancing the dissolution characteristics of poorly soluble drugs, amorphization of APIs is increasingly popular in the present day developmental research. A more subtle crystal modification approach toward the same goal if applied early on in the development process may ease subsequent development work. It is with this objective that the polymorph conversion and crystal disruption of a model API viz. Chlorpropamide were investigated in this

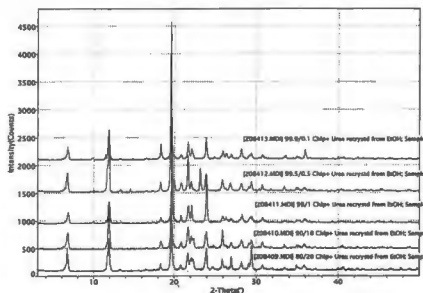


**Figure 71. XRPD Patterns of Chlorpropamide+Urea Co-Crystals
Recrystallized from Ethanol**

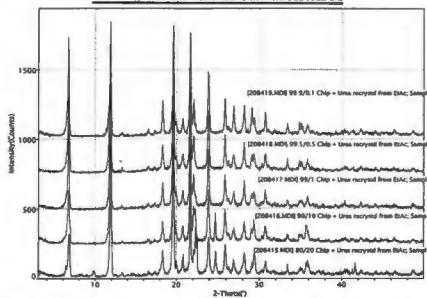


**Figure 72. XRPD Patterns of Chlorpropamide+Urea Co-Crystals
Recrystallized from EtAc**

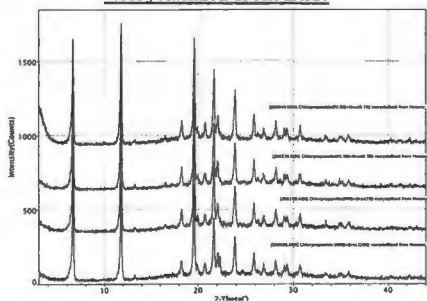


**Figure 73. XRPD Patterns of Chlorpropamide+Urea Co-Crystals
Recrystallized from Hexane**

Table 31. Thermal Analysis of Chlorpropamide+Urea mixtures Recrystallized from Liquid Organic Solvents

[A] Recrystallized from EtOH

Sample ID	Endotherm-1 (°C)	ΔH_{r-1} J/g	Endotherm-2 (°C)	ΔH_{r-2} J/g
80% Chlp+ 20% Urea (2)	98.63(0.33)	54.81(2.80)	122.67(0.92)	3.88(2.36)
90% Chlp+ 10% Urea (3)	96.07(0.51)	56.80(19.92)	-	-
99.5% Chlp+ 0.5% Urea (5)	117.20(0.85)	5.90(32.99)	126.33(0.54)	54.34(4.19)
99.9% Chlp+ 0.1% Urea	112.95(0.62)	60.73(12.95)	-	-

[B] Recrystallized from EtAc

Sample ID	Endotherm-1 (°C)	ΔH_{r-1} J/g	Endotherm-2 (°C)	ΔH_{r-2} J/g
Pure Chlorpropamide (7)	119.97(0.65)	8.41(4.63)	128.95(0.41)	76.97(2.20)
80% Chlp+ 20% Urea (8)	95.83(0.40)	68.11(19.14)	125.42(0.23)	3.97(25.03)
90% Chlp+ 10% Urea(9)	106.11(0.24)	87.55(2.30)	-	-
99% Chlp+ 1% Urea(10)	116.38(0.34)	21.19(58.34)	124.43(0.50)	53.35(9.68)
99.5% Chlp+ 0.5% Urea(11)	117.38(0.48)	22.13(73.28)	126.63(0.52)	70.39(2.43)
99.9% Chlp+ 0.1% Urea(12)	118.56(0.13)	17.59(8.21)	127.86(0.12)	72.44(1.20)

[C] Recrystallized from Hexane

Sample ID	Endotherm-1 (°C)	ΔH_{r-1} J/g	Endotherm-2 (°C)	ΔH_{r-2} J/g	Endotherm-3 (°C)	ΔH_{r-3} J/g
Pure Chlorpropamide, F	122.83(0.42)	16.25(11.72)	129.58(0.11)	82.596(1.83)	-	-
80% Chlp+ 20% Urea, G	99.00(0.25)	77.48(3.52)	115.50(0.75)	9.90(8.69)	-	-
99% Chlp+ 1% Urea, H	100.92(0.14)	7.92(100)	115.33(0.25)	31.10(8.36)	120.92(0.43)	32.57(5.31)
99.5% Chlp+ 0.5% Urea, I	121.08(0.66)	9.77(20.6)	129.25(0.51)	75.95(3.62)	-	-
99.9% Chlp+ 0.1% Urea, J	118.67(0.49)	9.81(12.13)	127.42(0.41)	66.95(2.22)	-	-

work. The utility of rapid co-crystallizations using the RESS process was tested for these purposes. Toward this objective, three different means of characterizing the various polymorphs of Chlp were developed in this study. Following polarizing optical microscopy, it was found that polymorph A crystallizes in tabular habit, while the metastable forms B and C appear as blades and plates respectively. The major XRPD diffraction peaks distinguishing the various polymorphs were also identified. Thirdly, the melting data useful in evaluating the crystallinity of these polymorphs was developed following thermal analysis by DSC.

RESS recrystallizations of pure Chlp indicate the ability of the RESS process to form different polymorphs from the same solvent by mere changes in the temperature and pressure conditions. Scanning electron microscopy of recrystallized materials showed a change in the habit and also, a general reduction in the particle size of the recrystallized materials.

The presence of urea in the crystallizing medium of chlorpropamide reduced the yields of crystallization. Co-crystallization studies also revealed the formation of eutectic mixtures and solid solutions depending on the composition of the mixtures formed. Formation of the solid solutions of urea in chlorpropamide resulted in the crystal disruption of Chlp and eventually in amorphous conversion at urea levels higher than 40% w/w. Consistent with these results were the reductions in melting point (up to 9°C) and in the ΔH_f values of Chlp (up to 50%). By imparting a strain in the lattices of chlorpropamide crystals,

urea may have reduced the symmetry in the original crystals and subsequently destroyed the crystal structure. Scanning electron microscopy of the doped crystals indicated surface adsorption of urea onto Chlp crystals. SEMS also revealed a particle size reduction of up to an order of magnitude upon RESS processing. Unlike RESS, recrystallizations from liquid organic solvents lacked the ability to affect polymorphic conversions. Also, incorporation of urea into the lattice of Chlp was found inadequate. The efficiency of RESS process in doping therefore was reported to be superior to organic solvent-based recrystallizations.

In summary, the results reported in this manuscript reflect the potential for RESS aided crystal doping in not only controlling the crystallinity levels in APIs, but also tailor the polymorphism and particle morphology.

5. LIST OF REFERENCES

1. Aal-Saeiq SS, Riley GS. Polymorphism in sulfonylurea hypoglycemic agents: II. Chlorpropamide. *Pharmaceutica Acta Helvetica* 1982, 57(1):p8-11.
2. Addadi L Resolution of conglomerates with the assistance of tailor-made impurities : Generality and mechanistic aspects of the "Rule of reversal". A new method for assignment of absolute configuration. *Journal of American chemical Society* 1982, 104:p4610-4617.
3. Behme RJ, Brooke D. Heat of fusion measurement of a low melting polymorph of carbamazepine that undergoes multiple phase changes during DSC. *Journal of Pharmaceutical Sciences* 1991, 80(10):p986-990.
4. Burger A. In German. *Sci. Pharm* 1975, 43:p152-161.
5. Burt HM, Mitchell AG. Crystal defects and dissolution. *International Journal of Pharmaceutics* 1981, 9 : p137-152.
6. Chow AHL et al. Assessment of wettability and its relationship to the intrinsic dissolution rate of doped phenytoin crystals. *International Journal of Pharmaceutics* 1995, 126:p21-28.
7. Dandge DK et al. Structure solubility correlations : Organic compounds and dense carbon dioxide binary systems. *Industrial and Engineering Chemistry Product Research and Development* 1985, 24 : p162-166.
8. De Villiers MM, Wurster DE. Isothermal interconversion of chlorpropamide polymorphs kinetically quantified by XRPD, diffuse reflectance FTIR and isoperibol solution calorimetry. *Acta Pharmaceutica* 1999, 49:p79-88
9. Debenedetti PG et al. Rapid expansion of supercritical solutions (RESS): Fundamentals and applications. *Fluid Phase Equilibria* 1993, 82 : p311-321.
10. Dobbs JM et al. Modification of supercritical fluid phase behavior using polar cosolvents. *Industrial and Engineering Chemistry Research* 1987, 26 : p56-65.
11. Ford JL et al. The assay and stability of chlorpropamide in solid dispersion with urea. *Journal of Pharmacy and Pharmacology* 1979, 31:p726-729.
12. Ford JL, Rubinstein MH. Phase equilibria and stability characteristics of chlorpropamide-urea solid dispersions. *Journal of Pharmacy and Pharmacology* 1977, 29:p209-211.

13. Hyatt, JA. Liquid and supercritical carbon dioxide as organic solvents. *Journal of Organic Chemistry* 1984, 49 : p5097-5101.
14. Koo et al. The crystal and molecular structure of chlorpropamide. *Archives of Pharmaceutical Research* 1980, 3(1):p37-49.
15. Matsumoto T et al. Effects of compression temperature on the consolidation mechanism of chlorpropamide polymorphs. *Journal of Pharmaceutical Sciences* 1995, 84(5):p614-618.
16. Mohamed RS et al. Solids formation after the expansion of supercritical mixtures. *Supercritical fluid science and technology, ACS Symposium Series-406*; Johnston KP, Penninger JML Eds., American Chemical Society, Washington DC, 1989, Chapter 23 : p355-378.
17. Prasad KVR et al. Crystallization of paracetamol from solution in the presence and absence of impurity. *International Journal of Pharmaceutics* 2001, 215:p29-44.
18. Simmons DL et al. Polymorphism in pharmaceuticals III. *Canadian Journal of Pharmaceutical Sciences* 1973, 8(4): p125-127.
19. Tudor AM. The qualitative and quantitative analysis of chlorpropamide polymorphic mixtures by near-infrared FTIR spectroscopy. *Pharmaceutical Research* 1993, 10(12):p1772-1776.
20. Turk M Formation of small organic particles by RESS: Experimental and theoretical investigations. *Journal of Supercritical Fluids* 1999, 15:p79-89.
21. Ueda H et al. Dissolution behavior of Chlorpropamide polymorphs. *Chemical and Pharmaceutical Bulletin* 1984, 32(1):p244-250.
22. Weber A et al. Compressed fluid antisolvent crystallization for controlled particle design. In *4th International Workshop on Crystal Growth Organic Matter* 1997. Editors: Ulrich, Joachim. Publisher: Shaker Verlag, Aachen. Issue:4: p214-221.
23. Weissbuch I et al. Molecular recognition at crystal interfaces. *Science* 1991, 253:p637-645.
24. York P, Hanna M. Salmeterol Xinafoate with controlled particle size. *International Patent Publication* 1995, Number: WO 95/01324.

25. Yoshihashi Y et al. Quantitative correlation between initial dissolution rate and heat of fusion of drug substances. *International Journal of Pharmaceutics* 2000, 204:p1-6.
26. Yu L. Inferring thermodynamic stability relationship of polymorphs from melting data. *Journal of Pharmaceutical Sciences* 1995, 84(8):p966-974.

CHAPTER FIVE

Title: *Solubility and Phase Behavior of Pharmaceutical Solids in Supercritical Carbon dioxide.*

Abstract:

Purpose. To study the phase behavior of selected pharmaceutical solids as a function of temperature, pressure and composition of the supercritical solvent.

Methods. A phase monitor was employed to characterize the phase behavior of 6 pharmaceutical solids in supercritical carbon dioxide. The basic design of the phase monitor includes a variable volume syringe pump fitted with a quartz view cell and a light source. The events occurring in the high pressure cell are observed by projecting the view onto a TV monitor through a variable focus camera attached to the view cell. The pharmaceutical solids studied included ketoprofen, piroxicam, tolbutamide, chlorpropamide, chloramphenicol and salicylic acid. The P,T region probed in this study included 0.1-55.2 MPa and 40-100°C. The effect of the presence of a second component (cosolute/cosolvent) on the behavior of solids in SC CO₂ was also studied. **Results.** By continuously tuning the solvent power of SC CO₂, regions were located that exhibited enhanced solubilization of the solids studied. Upon depressurization from these regions, a characteristic turbidity was seen that subsequently lead to recrystallization of the solids. In a further series of investigations involving low melting solids, reduction of melting temperatures was seen in the presence of SC CO₂. In some cases, the presence of a second component resulted in a shift in the conditions, while also affecting the

morphology of the reprecipitated crystals. **Conclusions.** Qualitative observations from such phase behavioral studies can assist in choosing the optimum extraction conditions for subsequent RESS processing. The melting point depression of solids in the presence of SC CO₂ may have potential implications in studies involving other supercritical fluid based processing techniques.

Key words: Supercritical CO₂, Phase Behavior, Solubility, Phase Monitor.

1. INTRODUCTION

Control over supercritical fluid (SCF) based crystallization processes depend on the knowledge of the mechanism of solute nucleation, supersaturation levels and the phase of the solution from which solutes nucleate and grow [Turk 1999, Palakodaty 1999, Bristow 2001, Diefenbacher 2002]. An understanding of the solubility and phase behavior of the solids in SCFs is therefore essential in optimizing the crystallization conditions. For example, the crystallization yields from Rapid Expansion of Supercritical Solution (RESS) process primarily depend on the solute solubilities in the supercritical solvent. The knowledge of the solubility behavior of the solute as a function of pressure and temperature of the SCF would allow to choose optimum extraction conditions. Similarly, establishing the phase behavior of a three component solid + cosolvent + SCF can assist in crystallizing the solute from the desired phase. Further, solvent removal can be eased by following appropriate path on the phase diagram. While the knowledge of such behavior is regarded to be vital in particle formation studies, very little has been accomplished to date in the pharmaceutical area [Mc Hugh 1994, Kordikowski 2002]. This stems from the inherently complex behavior of supercritical fluids, which is rather difficult to trace and model. Research efforts at such an understanding, even in a qualitative sense can serve as the basis for a yet larger goal that remains to be accomplished. It is with this objective that the solubility and phase behavior of different pharmaceutical solids were studied in supercritical CO₂.

2. DESIGN OF PHASE MONITOR

A Phase Monitor provides direct, visual observation of materials under SCF conditions, which may be controlled precisely. Depending on the supercritical fluid under consideration and the range of data desired, several designs of the phase monitors can be used, ranging from a simple Jerguson gauge to a complex diamond anvil cell [Zhen 1999]. For the purposes of this study, a simple phase monitor was purchased from Supercritical Fluid Technologies Inc, DE. The basic design of this apparatus (Figure 74) includes a 30ml capacity syringe pump, a high pressure vessel with quartz windows, a mixer, and a variable focus video camera. Pressures up to 10,000 psi are attainable with the sensor accuracy of ± 2 psi. The mantle heaters equipped with the temperature control system can heat the vessel up to 300°C. Temperature control is provided by a PID attached to a temperature sensing RTD that provides $\pm 0.5^\circ\text{C}$ temperature sensing accuracy and precise control. The solute is introduced through a port in the top of the horizontally oriented pump and carefully placed within the custom designed sample holder. Liquid CO_2 from a tank is delivered through the same port into the syringe pump. Upon pressurization and equilibration of the temperature, CO_2 changes to the supercritical fluid state. An additional module is also included using which a cosolvent can be co-introduced with CO_2 . The events in the high pressure vessel are viewed through a quartz window using a variable focus camera. The view is projected onto a TV/VCR monitor that provides the ability to record experiments for future review.

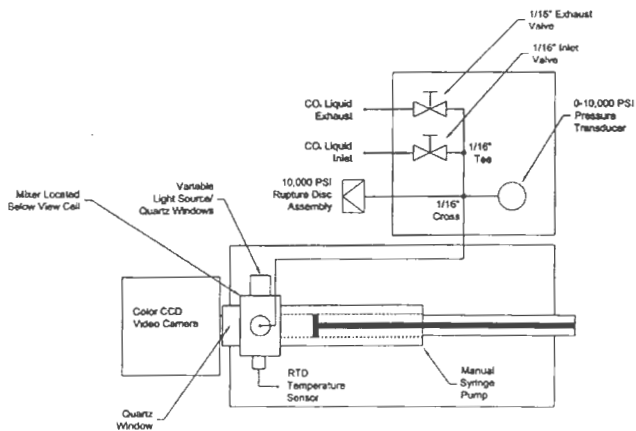


Figure 74. Schematic of SFT Phase Monitor

3. EXPERIMENTAL

3.1 Materials:

Aspirin (Sigma, Lot# 88H0411), Chloramphenicol, (Sigma, Lot# 48H0570), Chlorpropamide (Sigma, Lot# 31H0722), Ketoprofen (Sigma, Lot# 28H0344), Piroxicam (Sigma, Lot# 126H0820), Salicylic acid (Sigma, Lot# 49H3435), Tolbutamide (Sigma, Lot# 47H1030), Ethanol (190 Proof, Lot# 01D24QB, Aaper Alcohol Company).

3.2 Sample preparation:

About 50 mg of sample was introduced into the sample holder of the Phase Monitor. CO₂ from the tank was introduced and allowed to equilibrate at the set temperature for 5 minutes. Using the syringe pump, CO₂ was pressurized to the maximum value. Rapid depressurization of the supercritical solution from this stage allowed formation of crystals onto the quartz window and in the direct view of the camera.

3.3 Co-solvent addition:

Predetermined amount of a co-solvent was pumped using a liquid metering pump and co-introduced along with CO₂. Mixing of the two fluids was affected in a low dead volume-T as they are delivered into the syringe pump.

3.4 Qualitative Observations

The reproducibility of the solvent effects of SCCO₂ upon repeated pressurization and depressurization was initially confirmed. This was started with broad sweeps up and down in pressure hundreds of psi to characterize the significant events. Following this, the oscillations were attenuated with each pass until the degree of resolution was attained and the events were then recorded. In instances where the occurrence of an event is gradual, the onset and the endpoints are noted and the event was continuously recorded over a broad pressure range. A similar procedure was then repeated at a different temperature setting.

4. RESULTS AND DISCUSSION

The phase behavior of salicylic acid in SC CO₂ as a function of temperature and pressure is shown in Figure 75. Solid salicylic acid can be seen as needles at 75°C, 2300 psi condition. As can be seen from the figure, continuous pressurization of the supercritical solvent resulted in the dissolution of these crystals. Complete dissolution of the crystals at 75°C was evident when the pressure reached 4300 psi. Similar trend was seen at 100°C, although the pressure needed to completely dissolve the salicylic acid in this case was found to be 2700psi. Figures 76 and 77 represent the results from a similar study to identify the temperature and pressure conditions required for complete dissolution of chloramphenicol and chlorpropamide respectively. The optimum conditions for the maximum solubility of the various solids studied are summarized in Table 32.

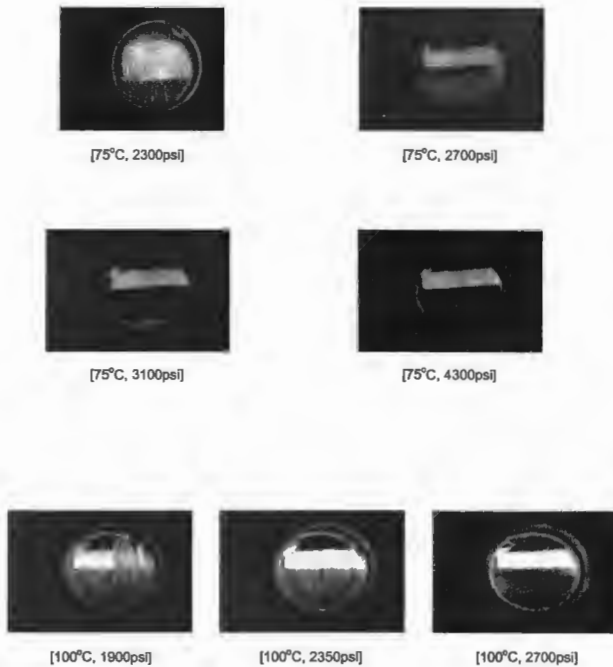
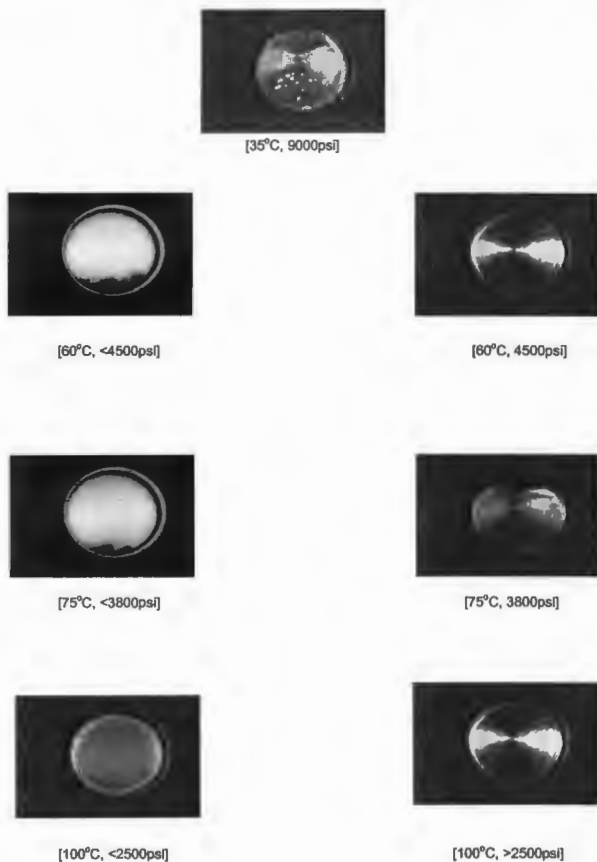


Figure 75. Phase Behavior of Salicylic acid + SCCO₂

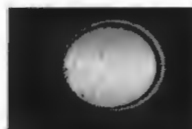


*Melting point of Chlorpropamide=121°C

Figure 76. Phase Behavior of Chlorpropamide + SCCO₂



[60°C, <math><3000\text{psi}</math>]



[60°C, >3500psi]



[75°C, <math><3000\text{psi}</math>]



[75°C, >3500psi]



[100°C, <math><3000\text{psi}</math>]



[100°C, >3500psi]

*Melting point of Chloramphenicol=154°C

Figure 77. Phase Behavior of Chloramphenicol + SCCO₂

Table 32. Supercritical Fluid Conditions for Enhanced Solubilization

Salicylic acid	[75°C, 4300psi]; [100°C, 2700psi]
Piroxicam	[40°C, 4500psi]; [60°C, 3500psi]
Chlorpropamide*	[60°C, 4500psi]; [75°C, 3800psi]; [100°C, 2500psi]
Tolbutamide*	[60°C, 3800psi]; [75°C, 6000psi]; [100°C, 2500psi]
Ketoprofen*	[55°C, 1400psi]
Chloramphenicol*	[75°C, 3500psi]; [100°C, 3500psi]

* Exhibited melting point depression

Depressurization of these supercritical solutions resulted in a characteristic turbidity that subsequently led to the formation of crystals. While this event is very responsive to small pressure changes in the case of chlorpropamide (Figure 76), other solids showed a gradually increasing turbidity with reduction in pressure. Identification of the significant events therefore should take into account both the pressurization and depressurization cycles for a more comprehensive understanding of the solid behavior in supercritical solvents.

The influence of a second component on the solubility behavior of salicylic acid in SC CO₂ was studied using aspirin as a cosolute and ethanol as a co-solvent. Results of these studies are respectively shown in Figures 78 and 79. The presence of aspirin changed the morphology of the recrystallized salicylic acid from needles to fibrous habitat (Figures 75, 78). Comparison of these figures also reveals that aspirin allowed complete dissolution of salicylic acid at a lower pressure condition by mediating in solubility enhancement. These results are consistent with the increased yields of RESS recrystallization for salicylic acid+ aspirin mixture, reported in chapter three.

The 75°C, 2400 psi condition in Figure 79 shows a 3-component, biphasic mixture of salicylic acid+ethanol (droplets) and SC CO₂ (continuous phase). Continuous pressurization from this stage resulted in a single phase when the pressure of SCF reached 3200psi. Again, a shift in the solubilization conditions was evident in the presence of ethanol as cosolvent (Figures 75, 79).

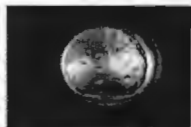


[75°C, 2400psi]

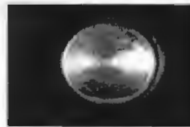


[75°C, 3200psi]

Figure 78. Phase Behavior of Salicylic acid + Aspirin + SCCO₂



[75°C, 2400psi]



[75°C, 3200psi]

Figure 79. Phase Behavior of Salicylic acid + EtOH + SCCO₂

In a different series of investigations involving low melting solids such as chlorpropamide (Figure 76) and chloramphenicol (Figure 77), a reduction in the liquefaction temperature of these solids was seen. The appearance of melt droplets of chlorpropamide and chloramphenicol can be seen in these figures at 100°C and 75°C respectively. Contrary to the effect of static pressure on the melting temperatures of solids, the presence of SCF in fact caused a reduction in the melting points. This behavior is attributed to the diffusion of supercritical fluid into the drug crystals in a manner analogous to the plasticization effects in amorphous polymers. While the former manifests as a reduction in melting point, the latter results in softening & lowered glass transition temperatures. The implications of such effects can be expected to be profound while dealing with processes such as PGSS and supercritical fluid extrusion.

5. RECOMMENDATIONS TO IMPROVE THE UTILITY OF PHASE MONITOR

5.A. Design of Equipment:

- 1) The view of the camera is too narrow and appears to represent only about 1 percent of the total volume in the view cell.
- 2) Areas where solids would tend to settle, dissolve and recrystallize/ reprecipitate typically are outside the scope of the camera. The design of the view cell needs to be corrected so that the camera is directed towards a larger area where solids would tend to be deposited.

- 3) The extension from the piston pump needs to be redesigned so that no portions are hidden from the view of the camera. A possible solution is to remove the circular extension at the end and instead have the same dimensions as the cylindrical piston pump, fitted with a larger diameter quartz window.
- 4) The magnetic stir bar under current design often is displaced from its position into the piston. The magnetic stir bar should be designed so that it stays in its only circular extension and does not get knocked out by the currents of liquid entering and exiting the cell.
- 5) Even when the magnetic stir bar stays in place, the mixer is not powerful enough for good mixing within the cell. Therefore, the motor needs to be more powerful and the magnet in the stir bar stronger to have complete mixing in the phase equilibrium monitor.
- 6) Another solution to the mixing problem would be to introduce a stir bar without a magnet and the view cell made capable of tilting about 45 degrees. The stir bar in this case can be made to slide from one end to the other end of the view cell, causing additional stirring.
- 7) There appears to be a design flaw in the standard configuration of the light source being 90 degrees from the view of the camera. The depth of the camera appears to be good and the resolution is reasonable for up to 1 foot, which is the length of the piston pump. The amount of light entering the view cell, however is limited by the position of the light source,

leaving the cell only dimly lit. On the other hand, increasing the wattage of the light source blurs the overall view due to excessive brightness. The light needs to be directed from the same direction as the camera or at 180 degrees from the camera to light up the whole cell. This would be beneficial for observing the critical opalescence since the refraction of light through the cell is required to observe this phenomenon. The present design only partially lights the cell that makes it difficult for the human eye to pick up the critical opalescence phenomenon. By positioning the light source in the same plane as the camera (by reflecting light off the fluid versus transmitting light in the current design), the visual effects can be enhanced. The intensity of the light being reflected back into the camera would also be much greater and would allow for a much more accentuated transition from a bright red color to a dark color when entering the critical fluid region. This might assist in a more precise determination of the critical points of fluid mixtures. It would also make for a much more powerful visual display when demonstrating the unit.

- 8) For polymer applications, the capability to determine the extent of polymer swelling in supercritical fluids is essential. To do this, the standard phase equilibrium system must be modified so that a) a polymer can be held in position in front of the camera at a fixed position and b) and a micrometer for optical measurements be placed next to the polymer to determine the degree of swelling. A correlation needs to be made between

the size of the particle on the TV screen and the size of the particle in the view cell.

- 9) For applications where the refractive index of the supercritical fluid and the solute are very close, use of a different colored light source may be advantageous. The contrast between the supercritical fluid and the solute can be accentuated by eliminating one wavelength (analogous to using a compensator in optical microscopy). An easier and cheaper solution, however is to use a different light source like a neon or sodium lamp.
- 10) In place of the camera in the back, a photo multiplier tube or a detector can be placed to quantitatively determine the solubility of solids in supercritical fluids.

5.B. Operation of the Equipment

- 1) Start off with broad sweeps up and down in pressure 100s of psi to get an approximate idea of where the solute is precipitating out of solution. Then attenuate the oscillations with each pass until the degree of resolution is attained.
- 2) Introduce the solute into the view cell. The current setup does not allow for accurate placement of quantitative amounts of solute, which is required to get quantitative data out of this instrument. If the system can be redesigned so that an exact weight of solute can be placed in the view of

the camera, semi quantitative investigations of solute solubilities as functions of pressure and temperature of SCF solvent can be made.

6. CONCLUSIONS

By continuously tuning the solvent power of SC CO₂, regions were located that exhibited enhanced solubilization of the solids tested. Upon depressurization from these regions, a characteristic turbidity was seen that subsequently lead to the recrystallization of solids. A general trend of increased solubilization with increasing pressures was seen in all the cases. Qualitative observations from such phase behavioral studies can assist in choosing the optimum extraction conditions for subsequent RESS processing. The melting point depression of solids in the presence of SC CO₂ may have potential implications in studies involving other supercritical fluid based processing techniques. Finally, the limitations of the commercially available design are identified and recommendations made in the design and operation for better performance of the phase monitor.

7. LIST OF REFERENCES

1. Bristow S et al. Analysis of the supersaturation and precipitation process with supercritical CO₂. *Journal of Supercritical Fluids* 2001, 21:p257-271.
2. Diefenbacher A, Turk M. Phase equilibria of organic solid solutes and supercritical fluids with respect to the RESS process. *Journal of Supercritical Fluids* 2002, 22:p175-184.
3. Kordikowski A et al. Phase equilibria for the CO₂ + methanol + sulfathiazole system at high pressure. *Fluid Phase Equilibria* 2002, 194-197:p905-917.
4. McHugh MA, Krukonis VJ. *Supercritical Fluid Extraction*. 2nd Edition; Butterworth-Heinemann:Newton, MA, 1994.
5. Palakodaty S, York P. Phase behavioral effects on particle formation processes using supercritical fluids. *Pharmaceutical Research* 1999, 16(7):p976-985.
6. Turk M Formation of small organic particles by RESS: Experimental and theoretical investigations. *Journal of Supercritical Fluids* 1999, 15:p79-89.
7. Zhen FR et al. Phase behavior and reaction of polyethylene terephthalate-water systems at pressures upto 173 MPa and temperatures up to 490°C. *Journal of Supercritical Fluids* 1999, 15:p229-243.

APPENDIX

INTRODUCTION :

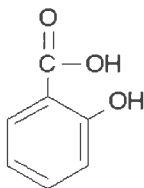
This appendix compiles the data generated in the recrystallization of pure drugs and drug-impurity mixtures by RESS process. Excerpts from this appendix are utilized in Chapter-3 to comprehensively report the various phenomena observed during the supercritical fluid recrystallizations. For clarity purposes, the data associated with each RESS study is divided into several individual sections. Section A in each study gives the chemical structures of the API and the dopant. The RESS conditions used in the recrystallization experiments are summarized in Section B. Section C compiles the thermal analysis data by differential scanning calorimetry. The data from XRPD analyses is divided into two subsections, D1 and D2. While the XRPD patterns in each analysis are shown in D1, the analyzed data demonstrating peak shifts and peak broadening is tabulated under D2. Broadened peaks in this subsection are shown in bold font and peak shifts in italicized font. Optical microscopy and HPLC analysis was performed only for a selective set of compounds. Wherever available, results from these studies are documented in sections E and F respectively.

Index for Appendix

Drug/ Drug-Impurity Mixture	Page Numbers
Pure Salicylic acid	263-264
Salicylic acid + Aspirin	265-270
Salicylic acid + Benzoic acid	271-278
Aspirin + Benzoic acid	279-287
Pure Tolbutamide	288-289
Tolbutamide + Chlorpropamide	290-294
Tolbutamide + Urea	295-303
Piroxicam + Theophylline	303
Piroxicam + Benzoic acid	304-306
Theophylline + Caffeine	307-318
Theophylline + Theobromine	319-321
Phenytoin + Caffeine	322-327
Indomethacin + Salicylic acid	328-336
Naproxen + α -Naphthalene-acetic acid	337-343

1. PURE SALICYLIC ACID:

1A. CHEMICAL STRUCTURE:



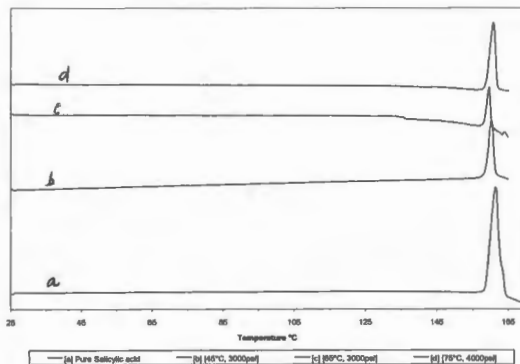
Salicylic Acid

1B. SUMMARY OF RESS RECRYSTALLIATION:

CONTENTS OF REACTION VESSEL : 5g of Salicylic acid

Experiment	[P,T conditions]	Weight collected mg	Collection time min	CO ₂ Used L at STP	Solubility mg/100L CO ₂ at STP
1	[45°C, 900psi]	25	10	24.58	101.71
2	[45°C, 3000psi]	158	10	36.28	435.50
3	[60°C, 4000psi]	481	20	99.92	481.39
4	[65°C, 3000psi]	152	10	44.02	345.30
5	[75°C, 4000psi]	436	20	112.271	388.35
6	[60°C, 750-4000psi]		Collected on glass slides using phase monitor.		

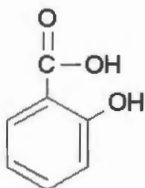
1C. DSC ANALYSIS:



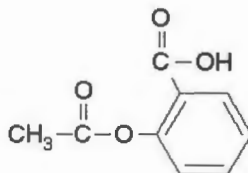
Material	Melting Point °C	Onset °C	End °C	Melting range °C	Delta H J/g
Pure Salicylic acid as obtained from Sigma	161.3	158.7	163.1	4.5	188.3
Recrystallized from SC CO ₂ at [45°C, 3000psi]	160.3	158.6	161.4	2.7	175.6
Recrystallized from SC CO ₂ at [65°C, 3000psi]	159.8	158.3	160.4	2.1	175.4
Recrystallized from SC CO ₂ at [75°C, 4000psi]	160.8	157.5	161.9	4.4	169.9

2. SALICYLIC ACID + ASPIRIN:

2A. CHEMICAL STRUCTURE:



Salicylic Acid



Aspirin

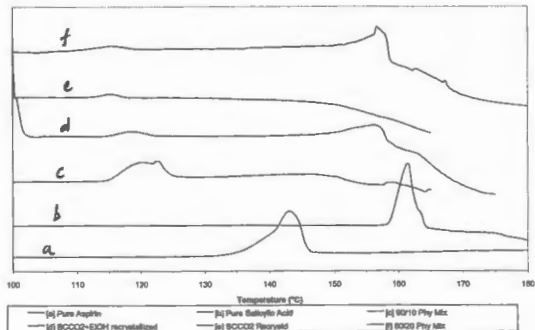
2B. SUMMARY OF RESS RECRYSTALLATION:

COMPOSITION OF STARTING MIXTURE: 80% Salicylic acid + 20% Aspirin

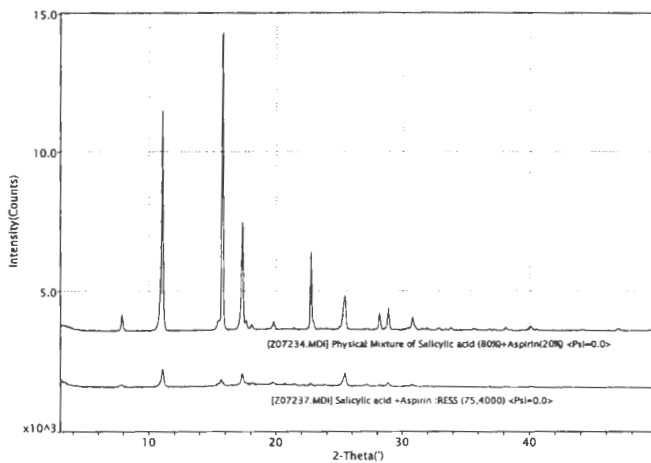
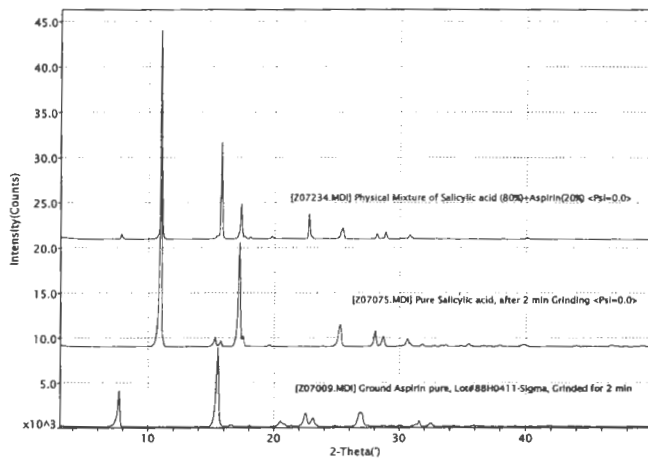
CONTENTS OF REACTION VESSEL : 4g Salicylic acid + 1g Aspirin (5g of blend)

Experiment	[P,T conditions]	Weight collected,mg	Collection time, min	Recrystallizing Solvent
1	[75C, 4000psi]	2511	20	SC CO ₂
2	[45C, 3000psi]	-	-	SC CO ₂ +EtOH

2C. DSC ANALYSIS:



2D.1. XRPD ANALYSIS:



2D.2. XRPD ANALYSIS:

Peak Search Report (21 Peaks, Max P/N = 46.7)

[Z07009.MDI] Ground Aspirin pure, Lot#88H0411-Sigma, Grinded for 2 min

PEAK: 23-pts/Parabolic Filter, Threshold=3.0, Cutoff=0.1%, BG=3/1.0, Peak-Top=Summit

2-Theta	d(A)	BG	Height	I%	Area	I%	FWHM	
7.72	11.443		43	4049	45.8	49590	41.9	0.21
15.52	5.705		60	8845	100	118408	100	0.23
16.66	5.318		54	280	3.2	3442	2.9	0.26
18.08	4.903		41	169	1.9	2192	1.9	0.29
20.54	4.321		54	677	7.7	13761	11.6	0.38
21.42	4.145		102	153	1.7	480	0.4	0.16
22.56	3.938		98	1567	17.7	28701	24.2	0.33
23.14	3.841		64	1015	11.5	20475	17.3	0.37
24.84	3.581		69	160	1.8	1431	1.2	0.27
26.88	3.314		80	1655	18.7	40381	34.1	0.44
28.8	3.097		83	171	1.9	1423	1.2	0.27
29.46	3.029		74	176	2	1759	1.5	0.29
30.08	2.968		75	186	2.1	1416	1.2	0.22
31.6	2.829		75	685	7.7	8727	7.4	0.24
32.5	2.753		69	437	4.9	6309	5.3	0.29
33.76	2.653		61	140	1.6	1316	1.1	0.28
34.38	2.606		55	165	1.9	1999	1.7	0.31
35.86	2.502		60	184	2.1	3980	3.4	0.55
39.14	2.3		43	144	1.6	1287	1.1	0.22
40.44	2.229		48	122	1.4	1566	1.3	0.36
41.96	2.151		51	165	1.9	3679	3.1	0.55

Peak Search Report (21 Peaks, Max P/N = 93.6)

[Z07075.MDI] Pure Salicylic acid, after 2 min Grinding <Psi=0.0>

PEAK: 19-pts/Parabolic Filter, Threshold=3.0, Cutoff=0.1%, BG=3/1.0, Peak-Top=Summit

2-Theta	d(A)	BG	Height	I%	Area	I%	FWHM	
10.98	8.051		41	35122	100	296650	100	0.14
15.28	5.793		41	1085	3.1	13023	4.4	0.21
15.74	5.625		46	667	1.9	6681	2.3	0.18
17.22	5.145		44	11620	33.1	142907	48.2	0.21
17.5	5.063		44	1237	3.5	30708	10.4	0.44
17.96	4.935		37	159	0.5	1286	0.4	0.18
19.62	4.52		36	259	0.7	2584	0.9	0.2
25.26	3.523		49	2452	7	39357	13.3	0.28
28.04	3.179		59	1790	5.1	21209	7.1	0.21
28.7	3.108		74	1172	3.3	14462	4.9	0.22
30.68	2.912		59	886	2.5	14469	4.9	0.3
31.82	2.81		53	294	0.8	2853	1	0.2
32.76	2.731		61	168	0.5	1013	0.3	0.16
33.34	2.685		48	244	0.7	3240	1.1	0.28

33.7	2.657	53	245	0.7	2968	1	0.26
34.86	2.571	52	161	0.5	1069	0.4	0.17
35.52	2.525	46	366	1	4493	1.5	0.24
38	2.366	48	226	0.6	2645	0.9	0.25
39.92	2.256	46	289	0.8	5969	2	0.42
44	2.056	46	149	0.4	1481	0.5	0.24
46.78	1.94	45	251	0.7	3900	1.3	0.32

Peak Search Report (22 Peaks, Max P/N = 51.5)

[Z07234.MDI] Physical Mixture of Salicylic acid (80%)+Aspirin(20%) <Psi=0.0>

PEAK: 17-pts/Parabolic Filter, Threshold=3.0, Cutoff=0.1%, BG=3/1.0, Peak-Top=Summit

2-Theta	d(A)	BG	Height	I%	Area	I%	FWHM
7.88	11.211	43	603	5.6	4912	6.3	0.15
11.04	8.007	48	7968	73.9	67631	86.9	0.15
15.48	5.719	73	407	3.8	6268	8.1	0.32
15.78	5.612	78	10780	100	77791	100	0.12
17.34	5.11	94	3921	36.4	38173	49.1	0.17
17.62	5.029	97	409	3.8	7536	9.7	0.41
18.06	4.907	118	263	2.4	1096	1.4	0.13
19.8	4.48	102	389	3.6	2568	3.3	0.15
22.72	3.91	92	2848	26.4	22318	28.7	0.14
25.44	3.499	87	1271	11.8	17393	22.4	0.25
28.16	3.166	83	647	6	5274	6.8	0.16
28.88	3.089	82	829	7.7	6794	8.7	0.15
30.46	2.932	72	164	1.5	1667	2.1	0.31
30.82	2.899	73	509	4.7	6424	8.3	0.25
31.58	2.831	71	121	1.1	598	0.8	0.2
32.9	2.72	65	145	1.3	775	1	0.16
33.82	2.648	59	150	1.4	1024	1.3	0.19
35.6	2.52	52	114	1.1	1010	1.3	0.28
38.16	2.356	44	156	1.4	1526	2	0.23
40.08	2.248	47	199	1.8	2586	3.3	0.29
40.52	2.224	45	93	0.9	772	1	0.27
46.88	1.936	37	107	1	1201	1.5	0.29

Peak Search Report (23 Peaks, Max P/N = 11.8)

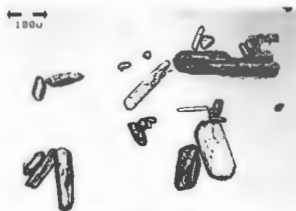
[Z07237.MDI] Salicylic acid +Aspirin :RESS (75,4000) <Psi=0.0>

PEAK: 19-pts/Parabolic Filter, Threshold=3.0, Cutoff=0.1%, BG=3/1.0, Peak-Top=Summit

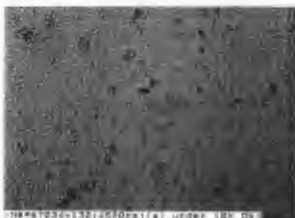
2-Theta	d(A)	BG	Height	I%	Area	I%	FWHM
3.16	27.968	114	287	40.9	4289	53.1	0.42
3.3	26.763	107	265	37.8	3201	39.6	0.34
5.75	15.362	71	106	15.1	392	4.9	0.19
7.89	11.19	69	161	23	1346	16.7	0.25
11.06	7.993	75	701	100	8082	100	0.22
15.42	5.74	106	197	28.1	1103	13.6	0.21
15.7	5.641	110	337	48.1	3420	42.3	0.26
17.32	5.115	146	526	75	5203	64.4	0.23

17.7	5.008	148	207	29.5	2580	31.9	0.74
18.1	4.896	163	211	30.1	433	5.4	0.15
19.73	4.497	148	243	34.7	1311	16.2	0.23
20.71	4.284	138	201	28.7	765	9.5	0.21
21.45	4.14	130	187	26.7	730	9	0.22
22.72	3.911	117	181	25.8	576	7.1	0.15
23.87	3.725	114	162	23.1	432	5.3	0.15
25.44	3.499	97	552	78.7	7091	87.7	0.26
27.08	3.29	94	141	20.1	799	9.9	0.29
27.22	3.274	92	149	21.3	800	9.9	0.24
28.22	3.159	88	140	20	678	8.4	0.22
28.86	3.091	85	214	30.5	1649	20.4	0.22
30.8	2.901	75	140	20	1352	16.7	0.35
38.26	2.351	48	81	11.6	311	3.8	0.16
40.18	2.243	44	83	11.8	790	9.8	0.34

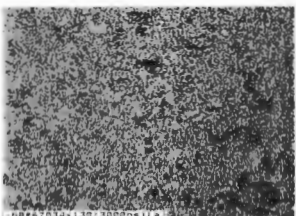
2E. OPTICAL MICROSCOPY:



80/20 Physical Mixture of SA + Aspirin



Recrystallized from SC CO₂ at 75°C, 4500psi



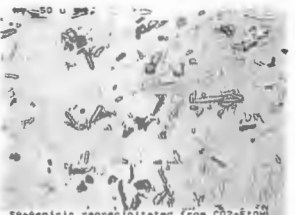
Recrystallized from SC CO₂ at 75°C, 3000psi



Recrystallized from SC CO₂ at 75°C, 1500psi



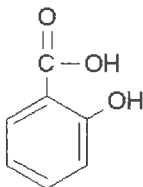
Recrystallized from SC CO₂ at 75°C, 750psi



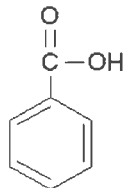
SA-Aspirin reprecipitated from CO₂-EtOH
Recrystallized from SC CO₂+EtOH at 45°C, 3000psi

3. SALICYLIC ACID + BENZOIC ACID:

3A. CHEMICAL STRUCTURE:



Salicylic Acid



Benzoic Acid

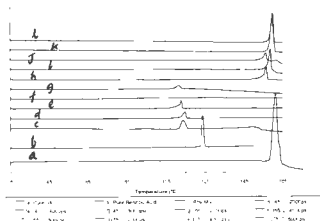
3B. SUMMARY OF RESS RECRYSTALLIATION:

COMPOSITION OF STARTING MIXTURE: 80% Salicylic acid + 20% Benzoic acid

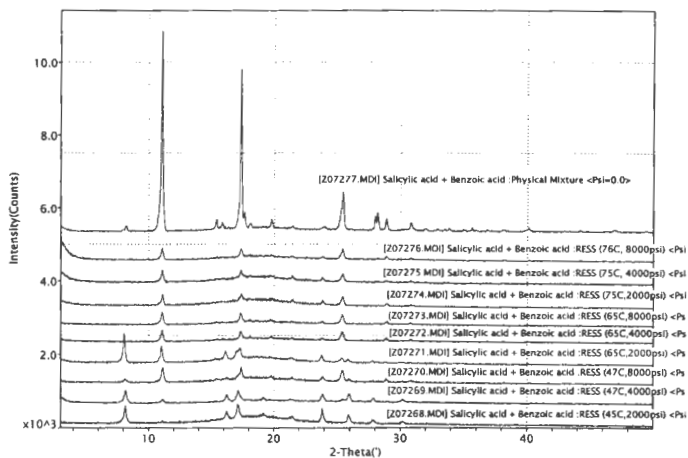
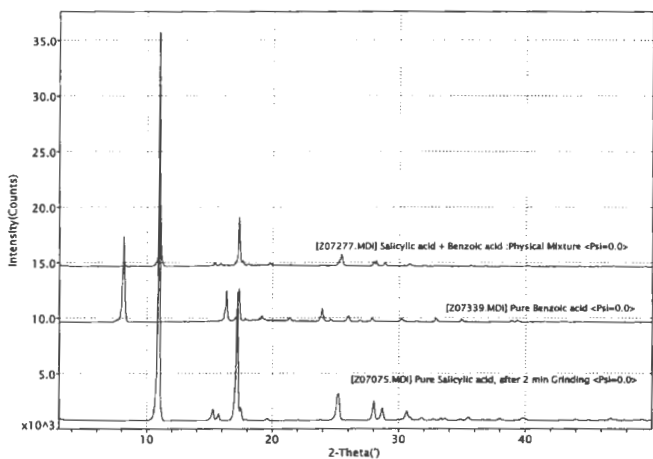
CONTENTS OF REACTION VESSEL : 4.8g Salicylic acid + 1.2g Benzoic acid (6g of blend)

Experiment	[P,T conditions]	Weight collected,mg	Collection time, min
1	[45C, 2000psi]	168	20
2	[47C, 4000psi]	235	5
3	[47C, 8000psi]	409	5
4	[65C, 2000psi]	40	10
5	[65C, 4000psi]	128	3
6	[65C, 8000psi]	185	1
7	[75C, 2000psi]	98	20
8	[75C, 4000psi]	194	5
9	[76C, 8000psi]	183	1

3C. DSC ANALYSIS:



3D.1. XRPD ANALYSIS:



3D.2. XRPD ANALYSIS:

Peak Search Report (21 Peaks, Max P/N = 93.6)

[Z07075.MDI] Pure Salicylic acid, after 2 min Grinding <Psi=0.0>

PEAK: 19-pts/Parabolic Filter, Threshold=3.0, Cutoff=0.1%, BG=3/1.0, Peak-Top=Summit

2-Theta	d(A)	BG	Height	I%	Area	I%	FWHM
10.98	8.051	41	35122	100	296650	100	0.14
15.28	5.793	41	1085	3.1	13023	4.4	0.21
15.74	5.625	46	667	1.9	6681	2.3	0.18
17.22	5.145	44	11620	33.1	142907	48.2	0.21
17.5	5.063	44	1237	3.5	30708	10.4	0.44
17.96	4.935	37	159	0.5	1286	0.4	0.18
19.62	4.52	36	259	0.7	2584	0.9	0.2
25.26	3.523	49	2452	7	39357	13.3	0.28
28.04	3.179	59	1790	5.1	21209	7.1	0.21
28.7	3.108	74	1172	3.3	14462	4.9	0.22
30.68	2.912	59	886	2.5	14469	4.9	0.3
31.82	2.81	53	294	0.8	2853	1	0.2
32.76	2.731	61	168	0.5	1013	0.3	0.16
33.34	2.685	48	244	0.7	3240	1.1	0.28
33.7	2.657	53	245	0.7	2968	1	0.26
34.86	2.571	52	161	0.5	1069	0.4	0.17
35.52	2.525	46	366	1	4493	1.5	0.24
38	2.366	48	226	0.6	2645	0.9	0.25
39.92	2.256	46	289	0.8	5969	2	0.42
44	2.056	46	149	0.4	1481	0.5	0.24
46.78	1.94	45	251	0.7	3900	1.3	0.32

Peak Search Report (20 Peaks, Max P/N = 43.8)

[Z07339.MDI] Pure Benzoic acid <Psi=0.0>

PEAK: 17-pts/Parabolic Filter, Threshold=3.0, Cutoff=0.1%, BG=3/1.0, Peak-Top=Summit

2-Theta	d(A)	BG	Height	I%	Area	I%	FWHM
6.88	12.838	55	95	1.2	236	0.3	0.1
8.16	10.825	73	7805	100	84984	100	0.19
16.34	5.421	162	2908	37.3	25687	30.2	0.16
17.34	5.11	189	3054	39.1	31514	37.1	0.19
17.84	4.967	205	318	4.1	943	1.1	0.14
19.18	4.625	200	644	8.3	5468	6.4	0.21
21.32	4.164	163	424	5.4	3169	3.7	0.21
23.94	3.714	125	1233	15.8	12036	14.2	0.18
24.58	3.618	129	329	4.2	1226	1.4	0.1
25.96	3.429	102	621	8	6324	7.4	0.21
26.94	3.307	94	214	2.7	1224	1.4	0.17
27.9	3.196	90	470	6	3836	4.5	0.17
30.2	2.957	79	378	4.8	3690	4.3	0.21
31.42	2.845	73	168	2.2	807	0.9	0.14
32.92	2.718	69	401	5.1	3623	4.3	0.19

34.92	2.567	66	320	4.1	2547	3	0.17
38.88	2.315	61	211	2.7	1525	1.8	0.17
39.32	2.289	60	235	3	2255	2.7	0.22
40.91	2.204	55	94	1.2	347	0.4	0.15
42.84	2.109	54	110	1.4	948	1.1	0.29

Peak Search Report (28 Peaks, Max P/N = 36.9)

[Z07277.MDI] Salicylic acid + Benzoic acid :Physical Mixture <Psi=0.0>

PEAK: 17-pts/Parabolic Filter, Threshold=3.0, Cutoff=0.1%, BG=3/1.0, Peak-Top=Summit

2-Theta	d(A)	BG	Height	I%	Area	I%	FWHM
3.14	28.142	69	178	3.2	2014	3.9	0.31
8.24	10.724	55	206	3.7	2119	4.1	0.24
11.06	7.993	66	5565	100	51782	100	0.16
15.43	5.736	116	382	6.9	2680	5.2	0.17
15.86	5.583	124	297	5.3	2169	4.2	0.21
17.34	5.11	157	4511	81.1	38998	75.3	0.15
17.64	5.024	164	578	10.4	6499	12.6	0.27
18.14	4.887	170	274	4.9	751	1.5	0.12
19.78	4.484	157	381	6.8	2079	4	0.16
21.48	4.134	129	210	3.8	779	1.5	0.16
24	3.705	103	185	3.3	1388	2.7	0.29
25.42	3.501	91	1113	20	15257	29.5	0.25
27.98	3.186	94	470	8.4	3651	7.1	0.17
28.18	3.164	84	562	10.1	6227	12	0.22
28.86	3.091	95	391	7	2516	4.9	0.14
30.82	2.899	74	288	5.2	3262	6.3	0.26
32.02	2.793	65	131	2.4	656	1.3	0.17
32.9	2.72	66	118	2.1	469	0.9	0.15
33.51	2.672	60	111	2	1139	2.2	0.38
33.82	2.648	62	135	2.4	968	1.9	0.23
35.07	2.556	57	94	1.7	423	0.8	0.19
35.62	2.518	53	161	2.9	1129	2.2	0.18
36.82	2.439	47	107	1.9	965	1.9	0.27
38.18	2.355	48	111	2	891	1.7	0.24
40.12	2.246	52	160	2.9	1556	3	0.24
44.23	2.046	44	76	1.4	494	1	0.26
46.9	1.936	43	106	1.9	893	1.7	0.24
49.4	1.844	41	72	1.3	356	0.7	0.2

Peak Search Report (15 Peaks, Max P/N = 9.8)

[Z07268.MDI] Salicylic acid + Benzoic acid :RESS (45C,2000psi) <Psi=0.0>

PEAK: 19-pts/Parabolic Filter, Threshold=3.0, Cutoff=0.1%, BG=3/1.0, Peak-Top=Summit

2-Theta	d(A)	BG	Height	I%	Area	I%	FWHM
8.18	10.803	111	586	93.2	6885	100	0.25
11.1	7.962	116	173	27.5	708	10.3	0.21
16.24	5.452	232	438	69.6	2355	34.2	0.19
17.12	5.174	265	629	100	4643	67.4	0.22

18.93	4.684	282	352	56	1700	24.7	0.41
19.18	4.624	283	383	60.9	1546	22.5	0.26
21.27	4.175	216	278	44.2	1071	15.6	0.29
21.46	4.136	208	297	47.2	1124	16.3	0.21
23.86	3.726	144	518	82.4	3893	56.5	0.18
25.92	3.434	120	339	53.9	2436	35.4	0.19
27.86	3.2	96	188	29.9	1535	22.3	0.28
30.16	2.961	87	154	24.5	946	13.7	0.24
32.15	2.782	73	106	16.9	143	2.1	0.07
32.15	2.782	73	106	16.9	143	2.1	0.07
39.12	2.301	53	85	13.5	420	6.1	0.22

Peak Search Report (17 Peaks, Max P/N = 8.6)

[Z07269.MDI] Salicylic acid + Benzoic acid :RESS (47C,4000psi) <Psi=0.0>

PEAK: 19-pts/Parabolic Filter, Threshold=3.0, Cutoff=0.1%, BG=3/1.0, Peak-Top=Summit

2-Theta	d(A)	BG	Height	I%	Area	I%	FWHM
3.26	27.119	71	182	44.8	1969	38.4	0.3
8.16	10.825	61	406	100	5131	100	0.25
11.16	7.923	61	164	40.4	1316	25.6	0.22
16.28	5.441	105	280	69	2211	43.1	0.21
17.18	5.158	118	401	98.8	4963	96.7	0.3
19.2	4.619	134	200	49.3	1015	19.8	0.26
21.3	4.168	115	173	42.6	919	17.9	0.27
21.56	4.119	113	156	38.4	957	18.7	0.38
22.24	3.995	104	142	35	396	7.7	0.18
23.93	3.715	98	303	74.6	3315	64.6	0.27
25.46	3.496	96	163	40.1	1605	31.3	0.41
25.96	3.429	95	309	76.1	3523	68.7	0.28
27.86	3.2	84	192	47.3	1510	29.4	0.24
28.9	3.087	81	120	29.6	188	3.7	0.08
30.18	2.959	75	162	39.9	1087	21.2	0.21
42.58	2.121	41	68	16.7	229	4.5	0.14
42.58	2.121	41	68	16.7	229	4.5	0.14

Peak Search Report (22 Peaks, Max P/N = 9.0)

[Z07270.MDI] Salicylic acid + Benzoic acid :RESS (47C,8000psi) <Psi=0.0>

PEAK: 17-pts/Parabolic Filter, Threshold=3.0, Cutoff=0.1%, BG=3/1.0, Peak-Top=Summit

2-Theta	d(A)	BG	Height	I%	Area	I%	FWHM
8.13	10.872	82	177	35.7	1365	25.2	0.24
10.63	8.314	85	129	26	530	9.8	0.2
11.1	7.963	88	483	97.4	5426	100	0.23
15.4	5.748	139	189	38.1	371	6.8	0.13
<i>16.02</i>	<i>5.528</i>	<i>147</i>	<i>190</i>	<i>38.3</i>	<i>1404</i>	<i>25.9</i>	<i>0.56</i>
16.26	5.445	157	215	43.3	851	15.7	0.25
17.18	5.157	179	295	59.5	2956	54.5	0.43
17.4	5.093	185	496	100	4699	86.6	0.26
19.41	4.569	196	248	50	607	11.2	0.2

19.8	4.481	195	277	55.8	608	11.2	0.13
21.43	4.144	160	227	45.8	577	10.6	0.15
23.88	3.723	118	236	47.6	1525	28.1	0.22
25.46	3.496	105	402	81	4976	91.7	0.28
25.95	3.431	124	182	36.7	168	3.1	0.05
27.84	3.202	90	127	25.6	243	4.5	0.11
28.88	3.089	83	181	36.5	1280	23.6	0.22
30.15	2.962	79	113	22.8	418	7.7	0.21
30.62	2.917	72	109	22	1778	32.8	0.82
30.77	2.904	78	118	23.8	1077	19.8	0.46
30.88	2.893	78	139	28	828	15.3	0.23
40.27	2.238	49	77	15.5	373	6.9	0.23
47.28	1.921	37	68	13.7	149	2.7	0.08

Peak Search Report (14 Peaks, Max P/N = 13.1)

[Z07271.MDI] Salicylic acid + Benzoic acid :RESS (65C,2000psi) <Psi=0.0>

PEAK: 17-pts/Parabolic Filter, Threshold=3.0, Cutoff=0.1%, BG=3/1.0, Peak-Top=Summit

2-Theta	d(A)	BG	Height	I%	Area	I%	FWHM	
8.06	10.959		103	883	100	9064	100	0.2
11.02	8.021		104	549	62.2	5440	60	0.21
16.14	5.487		190	427	48.4	2636	29.1	0.19
17.1	5.181		215	438	49.6	6115	67.5	0.47
17.3	5.121		221	493	55.8	6117	67.5	0.38
21.26	4.176		178	229	25.9	814	9	0.27
21.42	4.145		174	241	27.3	815	9	0.21
23.76	3.741		126	304	34.4	1934	21.3	0.18
25.34	3.512		109	225	25.5	1819	20.1	0.27
25.88	3.44		116	199	22.5	455	5	0.09
27.8	3.207		86	145	16.4	925	10.2	0.27
28.13	3.17		84	118	13.4	1083	11.9	0.54
34.5	2.598		56	85	9.6	500	5.5	0.29
40.07	2.248		48	81	9.2	196	2.2	0.1

Peak Search Report (14 Peaks, Max P/N = 7.9)

[Z07272.MDI] Salicylic acid + Benzoic acid :RESS (65C,4000psi) <Psi=0.0>

PEAK: 17-pts/Parabolic Filter, Threshold=3.0, Cutoff=0.1%, BG=3/1.0, Peak-Top=Summit

2-Theta	d(A)	BG	Height	I%	Area	I%	FWHM	
9.72	9.093		62	92	24.7	185	4.9	0.1
9.72	9.093		62	92	24.7	185	4.9	0.1
11.08	7.98		69	373	100	3762	100	0.21
17.4	5.094		139	347	93	3105	82.5	0.25
17.69	5.01		143	186	49.9	1551	41.2	0.61
18.06	4.908		157	204	54.7	370	9.8	0.13
19.8	4.481		150	200	53.6	698	18.6	0.24
23.83	3.731		119	165	44.2	245	6.5	0.09
25.38	3.506		98	333	89.3	3417	90.8	0.25
28.86	3.091		86	179	48	610	16.2	0.11

30.83	2.897	75	122	32.7	572	15.2	0.21
36.89	2.435	44	76	20.4	320	8.5	0.17
38.14	2.357	43	73	19.6	316	8.4	0.18
40.2	2.241	43	72	19.3	359	9.5	0.21

Peak Search Report (12 Peaks, Max P/N = 8.4)

[Z07273.MDI] Salicylic acid + Benzoic acid :RESS (65C,8000psi) <Psi=0.0>

PEAK: 17-pts/Parabolic Filter, Threshold=3.0, Cutoff=0.1%, BG=3/1.0, Peak-Top=Summit

2-Theta	d(A)	BG	Height	I%	Area	I%	FWHM
10.54	8.387	70	112	26.9	648	13.8	0.26
11.06	7.993	73	416	100	4681	100	0.23
15.4	5.749	107	160	38.5	656	14	0.21
17.32	5.115	152	382	91.8	2729	58.3	0.2
17.99	4.927	152	198	47.6	1178	25.2	0.44
18.04	4.914	152	209	50.2	1126	24.1	0.34
19.8	4.481	149	211	50.7	838	17.9	0.23
23.84	3.73	100	168	40.4	787	16.8	0.2
24.96	3.565	92	129	31	514	11	0.24
25.4	3.504	90	355	85.3	3725	79.6	0.24
28.92	3.085	79	163	39.2	832	17.8	0.17
30.76	2.904	70	118	28.4	498	10.6	0.18

Peak Search Report (11 Peaks, Max P/N = 7.1)

[Z07274.MDI] Salicylic acid + Benzoic acid :RESS (75C,2000psi) <Psi=0.0>

PEAK: 17-pts/Parabolic Filter, Threshold=3.0, Cutoff=0.1%, BG=3/1.0, Peak-Top=Summit

2-Theta	d(A)	BG	Height	I%	Area	I%	FWHM
11.1	7.963	120	407	96.7	3237	96.5	0.19
17.38	5.099	248	421	100	2059	61.4	0.2
19.62	4.52	252	309	73.4	810	24.1	0.24
19.88	4.463	244	304	72.2	672	20	0.19
21.5	4.13	189	278	66	510	15.2	0.1
23.84	3.73	134	248	58.9	1236	36.8	0.18
24.99	3.56	110	149	35.4	444	13.2	0.19
25.44	3.498	109	349	82.9	3355	100	0.24
28.86	3.091	88	163	38.7	823	24.5	0.19
30.82	2.899	79	120	28.5	774	23.1	0.32
37.83	2.376	52	80	19	280	8.3	0.17

Peak Search Report (15 Peaks, Max P/N = 8.0)

[Z07275.MDI] Salicylic acid + Benzoic acid :RESS (75C, 4000psi) <Psi=0.0>

PEAK: 17-pts/Parabolic Filter, Threshold=3.0, Cutoff=0.1%, BG=3/1.0, Peak-Top=Summit

2-Theta	d(A)	BG	Height	I%	Area	I%	FWHM
3.18	27.779	147	346	80.5	4205	92.8	0.36
10.7	8.262	101	139	32.3	585	12.9	0.26
11.1	7.966	97	430	100	4531	100	0.23
16.67	5.313	187	237	55.1	146	3.2	0.05
17.34	5.109	226	428	99.5	2399	52.9	0.2

19.69	4.506	232	289	67.2	498	11	0.15
21.44	4.141	175	280	65.1	687	15.2	0.11
23.84	3.73	121	228	53	1312	29	0.21
25.44	3.498	107	322	74.9	3084	68.1	0.24
28.86	3.091	81	139	32.3	1301	28.7	0.38
30.4	2.938	77	113	26.3	532	11.7	0.25
30.8	2.9	77	141	32.8	744	16.4	0.2
36.81	2.44	49	85	19.8	249	5.5	0.12
38.38	2.343	45	74	17.2	333	7.3	0.2
38.38	2.343	45	74	17.2	333	7.3	0.2

Peak Search Report (12 Peaks, Max P/N = 8.0)

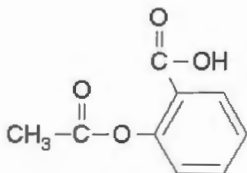
[Z07276.MDI] Salicylic acid + Benzoic acid :RESS (76C, 8000psi) <Psi=0.0>

PEAK: 17-pts/Parabolic Filter, Threshold=3.0, Cutoff=0.1%, BG=3/1.0, Peak-Top=Summit

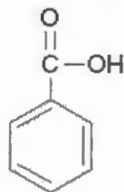
2-Theta	d(A)	BG	Height	%	Area	%	FWHM
3.23	27.335	168	537	100	5785	100	0.27
3.7	23.872	119	273	50.8	3109	53.7	0.34
8.67	10.193	74	106	19.7	322	5.6	0.17
11.08	7.981	77	394	73.4	3899	67.4	0.21
17.36	5.104	157	383	71.3	2736	47.3	0.21
21.42	4.145	135	176	32.8	354	6.1	0.15
23.82	3.732	109	170	31.7	686	11.9	0.19
25.42	3.501	95	371	69.1	3858	66.7	0.24
28.86	3.091	80	171	31.8	1045	18.1	0.2
30.83	2.898	75	128	23.8	427	7.4	0.14
38.26	2.35	44	75	14	293	5.1	0.16
40.14	2.244	41	72	13.4	344	5.9	0.19

4. ASPIRIN + BENZOIC ACID:

4A. CHEMICAL STRUCTURE:



Aspirin



Benzoic Acid

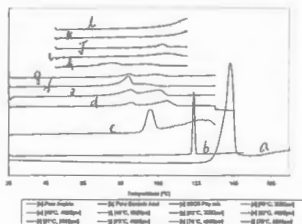
4B. SUMMARY OF RESS RECRYSTALLIATION:

COMPOSITION OF STARTING MIXTURE: 80% Aspirin + 20% Benzoic acid

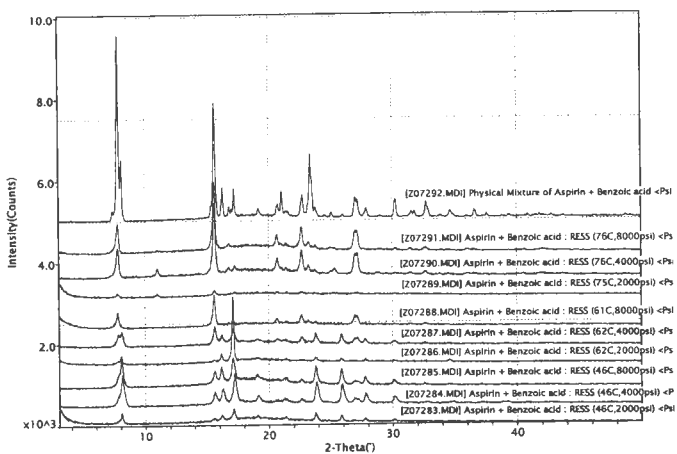
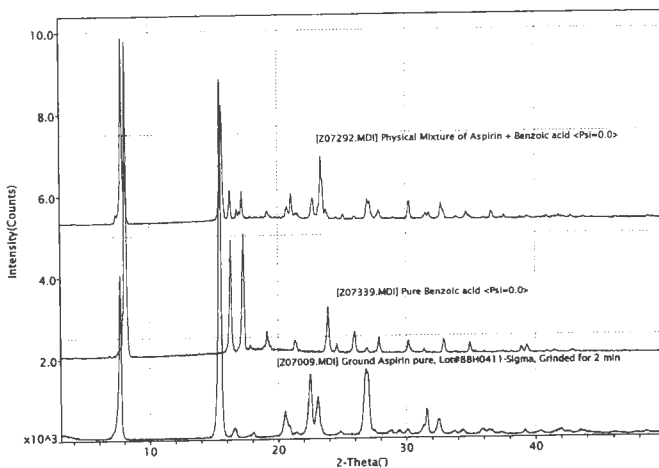
CONTENTS OF REACTION VESSEL : 4.8g Aspirin + 1.2g Benzoic acid (6g of blend)

Experiment	[P,T conditions]	Weight collected,mg	Collection time, min
1	[46C, 2000psi]	116	10
2	[46C, 4000psi]	253	5
3	[46C, 8000psi]	450	3
4	[62C, 2000psi]	73	20
5	[62C, 4000psi]	108	20
6	[61C, 8000psi]	160	5
7	[75C, 2000psi]	64	50
8	[76C, 4000psi]	302	20
9	[76C, 8000psi]	682	3

4C. DSC ANALYSIS:



4D.1. XRPD ANALYSIS:



4D.2. XRPD ANALYSIS:

Peak Search Report (21 Peaks, Max P/N = 46.7)

[Z07009.MDI] Ground Aspirin pure, Lot#88H0411-Sigma, Grinded for 2 min

PEAK: 23-pts/Parabolic Filter, Threshold=3.0, Cutoff=0.1%, BG=3/1.0, Peak-Top=Summit

2-Theta	d(A)	BG	Height	I%	Area	I%	FWHM
7.72	11.443	43	4049	45.8	49590	41.9	0.21
15.52	5.705	60	8845	100	118408	100	0.23
16.66	5.318	54	280	3.2	3442	2.9	0.26
18.08	4.903	41	169	1.9	2192	1.9	0.29
20.54	4.321	54	677	7.7	13761	11.6	0.38
21.42	4.145	102	153	1.7	480	0.4	0.16
22.56	3.938	98	1567	17.7	28701	24.2	0.33
23.14	3.841	64	1015	11.5	20475	17.3	0.37
24.84	3.581	69	160	1.8	1431	1.2	0.27
26.88	3.314	80	1655	18.7	40381	34.1	0.44
28.8	3.097	83	171	1.9	1423	1.2	0.27
29.46	3.029	74	176	2	1759	1.5	0.29
30.08	2.968	75	186	2.1	1416	1.2	0.22
31.6	2.829	75	685	7.7	8727	7.4	0.24
32.5	2.753	69	437	4.9	6309	5.3	0.29
33.76	2.653	61	140	1.6	1316	1.1	0.28
34.38	2.606	55	165	1.9	1999	1.7	0.31
35.86	2.502	60	184	2.1	3980	3.4	0.55
39.14	2.3	43	144	1.6	1287	1.1	0.22
40.44	2.229	48	122	1.4	1566	1.3	0.36
41.96	2.151	51	165	1.9	3679	3.1	0.55

Peak Search Report (20 Peaks, Max P/N = 43.8)

[Z07339.MDI] Pure Benzoic acid <Psi=0.0>

PEAK: 17-pts/Parabolic Filter, Threshold=3.0, Cutoff=0.1%, BG=3/1.0, Peak-Top=Summit

2-Theta	d(A)	BG	Height	I%	Area	I%	FWHM
6.88	12.838	55	95	1.2	236	0.3	0.1
8.16	10.825	73	7805	100	84984	100	0.19
16.34	5.421	162	2908	37.3	25687	30.2	0.16
17.34	5.11	189	3054	39.1	31514	37.1	0.19
17.84	4.967	205	318	4.1	943	1.1	0.14
19.18	4.625	200	644	8.3	5468	6.4	0.21
21.32	4.164	163	424	5.4	3169	3.7	0.21
23.94	3.714	125	1233	15.8	12036	14.2	0.18
24.58	3.618	129	329	4.2	1226	1.4	0.1
25.96	3.429	102	621	8	6324	7.4	0.21
26.94	3.307	94	214	2.7	1224	1.4	0.17
27.9	3.196	90	470	6	3836	4.5	0.17
30.2	2.957	79	378	4.8	3690	4.3	0.21
31.42	2.845	73	168	2.2	807	0.9	0.14
32.92	2.718	69	401	5.1	3623	4.3	0.19

34.92	2.567	66	320	4.1	2547	3	0.17
38.88	2.315	61	211	2.7	1525	1.8	0.17
39.32	2.289	60	235	3	2255	2.7	0.22
40.91	2.204	55	94	1.2	347	0.4	0.15
42.84	2.109	54	110	1.4	948	1.1	0.29

Peak Search Report (37 Peaks, Max P/N = 33.6)

[Z07292.MDI] Physical Mixture of Aspirin + Benzoic acid <Psi=0.0>

PEAK: 17-pts/Parabolic Filter, Threshold=3.0, Cutoff=0.1%, BG=3/1.0, Peak-Top=Summit

2-Theta	d(A)	BG	Height	%	Area	%	FWHM
7.4	11.932	45	265	5.8	4182	8.8	0.32
7.86	11.238	39	4586	100	47486	100	0.18
8.14	10.854	41	1536	33.5	18765	39.5	0.21
15.66	5.654	111	2915	63.6	31280	65.9	0.19
16.32	5.428	147	826	18	4751	10	0.12
16.84	5.262	143	364	7.9	1591	3.4	0.12
17.24	5.14	145	807	17.6	5693	12	0.15
19.2	4.618	142	309	6.7	2020	4.3	0.21
20.76	4.276	132	416	9.1	4257	9	0.25
21.06	4.215	124	722	15.7	9813	20.7	0.28
21.4	4.148	126	248	5.4	2877	6.1	0.4
22.76	3.904	175	633	13.8	4290	9	0.16
23.4	3.798	109	1633	35.6	20493	43.2	0.23
23.82	3.733	93	326	7.1	3561	7.5	0.26
24.56	3.622	92	134	2.9	305	0.6	0.12
25.12	3.542	88	201	4.4	738	1.6	0.11
25.98	3.426	84	143	3.1	519	1.1	0.15
27.04	3.295	94	557	12.1	8127	17.1	0.3
27.9	3.195	96	292	6.4	1849	3.9	0.16
30.3	2.948	71	501	10.9	4404	9.3	0.17
31.56	2.832	67	212	4.6	2238	4.7	0.26
31.8	2.811	68	213	4.6	1993	4.2	0.23
32.76	2.732	66	453	9.9	5085	10.7	0.22
32.92	2.719	65	288	6.3	4569	9.6	0.35
33.9	2.642	63	114	2.5	467	1	0.16
34.68	2.584	59	224	4.9	2506	5.3	0.26
34.92	2.567	58	140	3.1	1172	2.5	0.24
36.02	2.491	56	87	1.9	235	0.5	0.13
36.6	2.453	58	242	5.3	1980	4.2	0.18
37.58	2.391	58	150	3.3	851	1.8	0.16
39.34	2.288	59	115	2.5	557	1.2	0.17
40.89	2.205	55	126	2.7	945	2	0.23
41.85	2.157	59	131	2.9	1354	2.9	0.32
42.78	2.112	59	115	2.5	504	1.1	0.15
43.79	2.066	51	93	2	604	1.3	0.24
46.24	1.962	46	73	1.6	405	0.9	0.25
48.76	1.866	47	100	2.2	601	1.3	0.19

Peak Search Report (13 Peaks, Max P/N = 7.0)

[Z07283.MDI] Aspirin + Benzoic acid : RESS (46C,2000psi) <Psi=0.0>

PEAK: 17-pts/Parabolic Filter, Threshold=3.0, Cutoff=0.1%, BG=3/1.0, Peak-Top=Summit

2-Theta	d(A)	BG	Height	I%	Area	I%	FWHM
3.16	27.948	155	411	95.6	5672	100	0.38
7.88	11.21	90	178	41.4	2727	48.1	0.53
8.08	10.932	91	352	81.9	3724	65.7	0.24
15.6	5.676	154	205	47.7	243	4.3	0.08
16.22	5.461	158	272	63.3	2062	36.4	0.31
17.14	5.169	180	430	100	3112	54.9	0.21
19.12	4.639	194	271	63	1113	19.6	0.25
21.41	4.146	162	231	53.7	395	7	0.1
23.78	3.738	120	309	71.9	2294	40.4	0.21
25.86	3.443	100	239	55.6	1490	26.3	0.18
26.86	3.316	93	135	31.4	406	7.2	0.16
27.76	3.211	91	169	39.3	720	12.7	0.16
30.16	2.961	79	126	29.3	565	10	0.2

Peak Search Report (17 Peaks, Max P/N = 13.3)

[Z07284.MDI] Aspirin + Benzoic acid : RESS (46C,4000psi) <Psi=0.0>

PEAK: 21-pts/Parabolic Filter, Threshold=3.0, Cutoff=0.1%, BG=3/1.0, Peak-Top=Summit

2-Theta	d(A)	BG	Height	I%	Area	I%	FWHM
8.16	10.827	64	832	98.2	15835	100	0.35
15.62	5.668	92	406	47.9	5576	35.2	0.3
16.3	5.433	158	467	55.1	5154	32.5	0.28
17.22	5.145	166	847	100	11181	70.6	0.28
19.18	4.624	147	310	36.6	2886	18.2	0.3
20.74	4.28	144	200	23.6	826	5.2	0.25
21.3	4.168	133	237	28	2373	15	0.39
22.66	3.921	127	210	24.8	1167	7.4	0.24
23.88	3.723	123	616	72.7	8008	50.6	0.28
25.94	3.432	104	569	67.2	7395	46.7	0.27
26.9	3.311	119	215	25.4	1607	10.1	0.28
27.16	3.281	120	193	22.8	1599	10.1	0.37
27.82	3.204	113	329	38.8	3014	19	0.24
30.18	2.959	77	249	29.4	3090	19.5	0.31
32.76	2.732	66	108	12.8	652	4.1	0.26
34.98	2.563	58	104	12.3	870	5.5	0.32
38.83	2.317	54	94	11.1	1061	6.7	0.45

Peak Search Report (15 Peaks, Max P/N = 12.7)

[Z07285.MDI] Aspirin + Benzoic acid : RESS (46C,8000psi) <Psi=0.0>

PEAK: 21-pts/Parabolic Filter, Threshold=3.0, Cutoff=0.1%, BG=3/1.0, Peak-Top=Summit

2-Theta	d(A)	BG	Height	I%	Area	I%	FWHM
8.08	10.93	101	832	100	13471	100	0.31
15.64	5.662	195	482	57.9	4619	34.3	0.27

16.16	5.48	225	569	68.4	4729	35.1	0.23
17.12	5.175	257	782	94	8002	59.4	0.26
19.06	4.652	248	375	45.1	2658	19.7	0.36
20.71	4.285	217	278	33.4	1712	12.7	0.48
21.44	4.141	206	296	35.6	948	7	0.18
22.7	3.915	173	242	29.1	652	4.8	0.16
23.8	3.735	156	574	69	5179	38.4	0.21
25.88	3.44	116	493	59.3	5218	38.7	0.24
26.96	3.305	120	211	25.4	1544	11.5	0.29
27.18	3.278	123	187	22.5	1539	11.4	0.41
27.8	3.207	119	294	35.3	1894	14.1	0.18
30.16	2.961	87	210	25.2	2108	15.6	0.29
37.12	2.42	61	97	11.7	279	2.1	0.13

Peak Search Report (12 Peaks, Max P/N = 18.8)

[Z07286.MD1] Aspirin + Benzoic acid : RESS (62C,2000psi) <Psi=0.0>

PEAK: 17-pts/Parabolic Filter, Threshold=3.0, Cutoff=0.1%, BG=3/1.0, Peak-Top=Summit

2-Theta	d(A)	BG	Height	I%	Area	I%	FWHM
7.42	11.91	80	115	6.7	259	1.8	0.13
7.8	11.324	74	159	9.3	1961	13.5	0.39
8.08	10.934	76	272	15.9	3283	22.5	0.28
15.58	5.682	129	170	10	132	0.9	0.05
16.16	5.48	133	312	18.3	2108	14.5	0.2
17.1	5.181	152	1707	100	14575	100	0.16
19.03	4.659	166	212	12.4	745	5.1	0.28
22.83	3.892	117	162	9.5	384	2.6	0.15
23.76	3.741	110	197	11.5	1229	8.4	0.24
27.8	3.206	84	164	9.6	653	4.5	0.14
30.12	2.965	73	111	6.5	382	2.6	0.17
34.58	2.592	54	117	6.9	839	5.8	0.23

Peak Search Report (17 Peaks, Max P/N = 8.8)

[Z07287.MD1] Aspirin + Benzoic acid : RESS (62C,4000psi) <Psi=0.0>

PEAK: 21-pts/Parabolic Filter, Threshold=3.0, Cutoff=0.1%, BG=3/1.0, Peak-Top=Summit

2-Theta	d(A)	BG	Height	I%	Area	I%	FWHM
7.84	11.269	77	373	67.5	7955	87.4	0.46
8.1	10.904	81	429	77.6	9106	100	0.44
15.62	5.668	139	553	100	6721	73.8	0.28
16.22	5.46	164	346	62.6	2729	30	0.25
17.12	5.175	177	485	87.7	4641	51	0.26
19.06	4.653	174	243	43.9	1319	14.5	0.32
20.72	4.284	161	240	43.4	2067	22.7	0.44
21.16	4.196	157	204	36.9	1492	16.4	0.54
21.34	4.16	154	224	40.5	1511	16.6	0.37
22.7	3.915	160	274	49.5	1337	14.7	0.2
23.78	3.738	144	368	66.5	2326	25.5	0.18
25.88	3.44	106	337	60.9	2805	30.8	0.21

27.16	3.281	105	249	45	3414	37.5	0.4
27.74	3.213	115	216	39.1	926	10.2	0.16
30.2	2.957	83	156	28.2	1113	12.2	0.26
32.63	2.742	75	111	20.1	284	3.1	0.13

Peak Search Report (21 Peaks, Max P/N = 12.7)

[Z07288.MDI] Aspirin + Benzoic acid : RESS (61C,8000psi) <Psi=0.0>

PEAK: 19-pts/Parabolic Filter, Threshold=3.0, Cutoff=0.1%, BG=3/1.0, Peak-Top=Summit

2-Theta	d(A)	BG	Height	I%	Area	I%	FWHM
3.22	27.411	139	322	37.9	3689	36.2	0.34
3.36	26.285	128	283	33.3	3174	31.1	0.35
3.98	22.194	88	200	23.5	2116	20.8	0.32
3.98	22.194	88	200	23.5	2116	20.8	0.32
7.26	12.159	67	103	12.1	706	6.9	0.33
7.8	11.326	65	442	52	5835	57.2	0.26
8.63	10.241	58	89	10.5	90	0.9	0.05
8.63	10.241	58	89	10.5	90	0.9	0.05
15.62	5.669	110	850	100	10193	100	0.23
16.74	5.29	124	180	21.2	1040	10.2	0.32
17.18	5.157	127	178	20.9	1040	10.2	0.35
18.2	4.871	137	182	21.4	855	8.4	0.32
20.7	4.288	148	266	31.3	1844	18.1	0.27
21.46	4.138	152	200	23.5	284	2.8	0.1
22.66	3.921	143	347	40.8	3035	29.8	0.25
23.21	3.829	158	217	25.5	486	4.8	0.14
23.83	3.731	129	183	21.5	162	1.6	0.05
25.82	3.447	96	133	15.6	310	3	0.14
27.14	3.283	97	316	37.2	5077	49.8	0.39
32.56	2.748	71	104	12.2	425	4.2	0.22
32.76	2.731	70	105	12.4	447	4.4	0.22

Peak Search Report (12 Peaks, Max P/N = 6.2)

[Z07289.MDI] Aspirin + Benzoic acid : RESS (75C,2000psi) <Psi=0.0>

PEAK: 19-pts/Parabolic Filter, Threshold=3.0, Cutoff=0.1%, BG=3/1.0, Peak-Top=Summit

2-Theta	d(A)	BG	Height	I%	Area	I%	FWHM
3.21	27.525	128	367	100	3852	100	0.27
3.6	24.538	101	241	65.7	2425	63	0.29
7.78	11.355	66	152	41.4	1254	32.6	0.25
11	8.039	63	150	40.9	995	25.8	0.19
15.64	5.662	93	217	59.1	2026	52.6	0.28
17.28	5.128	131	173	47.1	449	11.7	0.18
20.64	4.299	124	171	46.6	269	7	0.1
21.46	4.138	114	158	43.1	972	25.2	0.38
22.72	3.911	109	162	44.1	955	24.8	0.31
25.23	3.527	92	138	37.6	1020	26.5	0.38
25.3	3.517	92	128	34.9	997	25.9	0.47
27.2	3.276	88	137	37.3	724	18.8	0.25

Peak Search Report (23 Peaks, Max P/N = 19.7)

[Z07290.MDI] Aspirin + Benzoic acid : RESS (76C,4000psi) <Psi=0.0>

PEAK: 21-pts/Parabolic Filter, Threshold=3.0, Cutoff=0.1%, BG=3/1.0, Peak-Top=Summit

2-Theta	d(A)	BG	Height	I%	Area	I%	FWHM
7.84	11.269	84	791	42.2	11399	48.2	0.27
9.31	9.495	89	131	7	358	1.5	0.14
11.04	8.01	111	287	15.3	2022	8.6	0.2
15.62	5.668	170	1873	100	23642	100	0.24
16.78	5.28	212	307	16.4	926	3.9	0.17
17.24	5.139	222	356	19	1583	6.7	0.2
19.2	4.619	229	283	15.1	477	2	0.15
20.68	4.291	229	533	28.5	4573	19.3	0.26
22.7	3.914	195	712	38	7742	32.7	0.25
23.26	3.821	179	348	18.6	3624	15.3	0.36
23.76	3.741	174	229	12.2	270	1.1	0.08
25	3.559	131	195	10.4	1510	6.4	0.4
25.34	3.512	129	265	14.1	2374	10	0.3
27.16	3.281	122	639	34.1	11384	48.2	0.37
28.76	3.102	102	149	8	694	2.9	0.25
30.25	2.952	95	136	7.3	704	3	0.29
31.49	2.838	91	148	7.9	592	2.5	0.18
32.68	2.738	83	165	8.8	1304	5.5	0.27
34.54	2.595	68	112	6	759	3.2	0.29
36.16	2.482	64	118	6.3	1753	7.4	0.55
36.57	2.455	69	118	6.3	1241	5.2	0.43
40.62	2.219	59	102	5.4	732	3.1	0.29
42.04	2.148	61	106	5.7	1223	5.2	0.46

Peak Search Report (19 Peaks, Max P/N = 19.2)

[Z07291.MDI] Aspirin + Benzoic acid : RESS (76C,8000psi) <Psi=0.0>

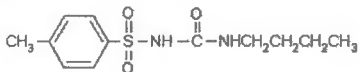
PEAK: 19-pts/Parabolic Filter, Threshold=3.0, Cutoff=0.1%, BG=3/1.0, Peak-Top=Summit

2-Theta	d(A)	BG	Height	I%	Area	I%	FWHM
7.82	11.297	89	780	43.2	10500	49.7	0.26
15.62	5.668	176	1807	100	21142	100	0.22
16.78	5.278	206	299	16.5	1236	5.8	0.23
18.33	4.837	231	287	15.9	596	2.8	0.18
20.7	4.288	220	511	28.3	4685	22.2	0.27
21	4.227	210	292	16.2	3337	15.8	0.69
21.41	4.148	220	297	16.4	608	2.9	0.13
22.7	3.914	194	678	37.5	7266	34.4	0.26
23.28	3.818	181	324	17.9	3449	16.3	0.41
23.79	3.738	170	239	13.2	483	2.3	0.12
25	3.559	126	191	10.6	1149	5.4	0.3
25.37	3.508	126	176	9.7	941	4.5	0.32
27.16	3.281	115	585	32.4	10521	49.8	0.38
30.26	2.951	97	147	8.1	427	2	0.15

31.44	2.843	85	140	7.7	840	4	0.26
32.72	2.734	81	174	9.6	1245	5.9	0.23
36.04	2.49	77	118	6.5	382	1.8	0.16
36.56	2.456	66	108	6	674	3.2	0.27
42.04	2.147	57	107	5.9	1385	6.6	0.47

5. TOLBUTAMIDE:

5A. CHEMICAL STRUCTURE:



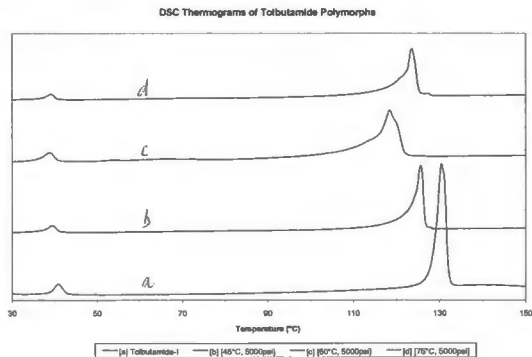
Tolbutamide

5B. SUMMARY OF RESS RECRYSTALLIATION:

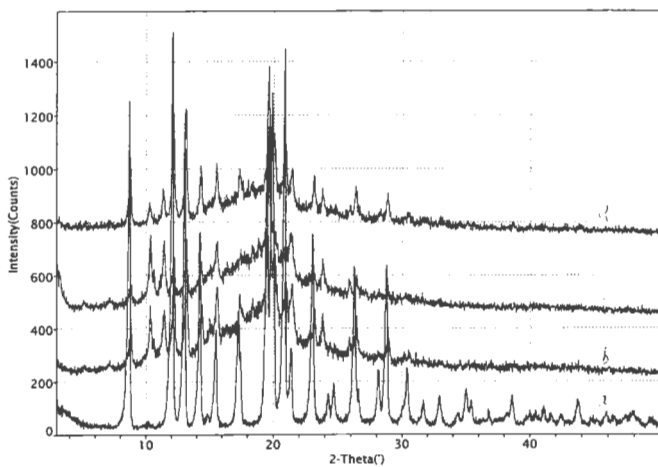
CONTENTS OF REACTION VESSEL : 3g of Tolbutamide

Experiment	[P,T conditions]	Weight collected mg	Collection time min
1	[45°C, 900psi]	136	30
2	[60°C, 5000psi]	76	20
3	[75°C, 4000psi]	361	10

5C. DSC ANALYSIS:



5D.1 XRPD ANALYSIS:



a-Commercial-Form I

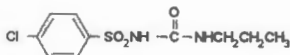
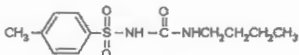
b-[45°C, 5000psi]

c-[60°C, 5000psi]

d-[75°C, 5000psi]

6. TOLBUTAMIDE + CHLORPROPAMIDE:

6A. CHEMICAL STRUCTURE:



Tolbutamide

Chlorpropamide

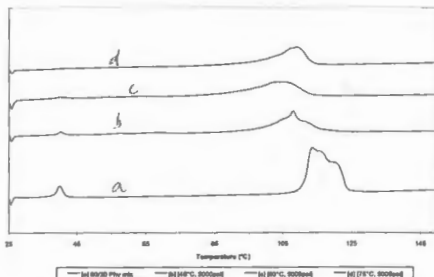
6B. SUMMARY OF RESS RECRYSTALLATION:

CONTENTS OF REACTION VESSEL: 80% Tolbutamide + 20% Chlorpropamide

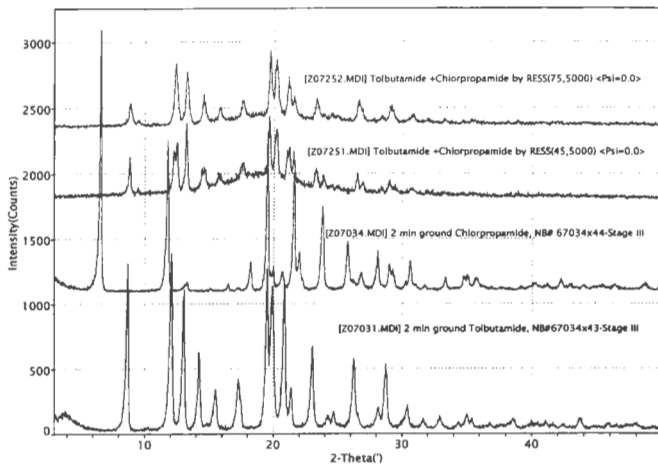
CONTENTS OF REACTION VESSEL : 2g Tolbutamide + 0.5g Chlorpropamide (2.5g of blend)

Experiment	[P,T conditions]	Weight collected,mg	Collection time, min
1	[45C, 5000psi]	165	5
2	[60C, 5000psi]	125	20
3	[75C, 8000psi]	261	20

6C. DSC ANALYSIS:



6D.1 XRPD ANALYSIS:



6D.2 XRPD ANALYSIS:

Peak Search Report (32 Peaks, Max P/N = 22.2)

[Z07034.MDI] 2 min ground Chlorpropamide, NB# 67034x44-Stage III

PEAK: 19-pts/Parabolic Filter, Threshold=3.0, Cutoff=0.1%, BG=3/1.0, Peak-Top=Summit

2-Theta	d(A)	BG	Height	1%	Area	1%	FWHM
6.64	13.307	19	2016	100	21465	100	0.18
11.76	7.518	23	1177	58.4	12954	60.3	0.19
13.26	6.671	18	90	4.5	1205	5.6	0.28
16.45	5.386	19	72	3.6	435	2	0.14
18.22	4.866	23	243	12.1	2451	11.4	0.19
19.52	4.544	23	1234	61.2	14406	67.1	0.2
19.98	4.441	49	200	9.9	2770	12.9	0.31
20.7	4.288	52	167	8.3	1416	6.6	0.21
21.6	4.111	45	929	46.1	12135	56.5	0.23
22	4.037	25	316	15.7	6325	29.5	0.37
23.78	3.738	29	665	33	8958	41.7	0.24
25.76	3.456	27	395	19.6	6342	29.5	0.29
26.22	3.396	40	103	5.1	2070	9.6	0.56
26.82	3.322	51	154	7.6	1347	6.3	0.22

28.08	3.175	40	326	16.2	3691	17.2	0.22
28.96	3.08	40	221	11	3673	17.1	0.34
29.26	3.05	37	181	9	2510	11.7	0.3
30.28	2.95	31	91	4.5	727	3.4	0.21
30.6	2.919	28	246	12.2	3606	16.8	0.28
31.77	2.814	25	54	2.7	369	1.7	0.22
33.36	2.684	27	122	6.1	1092	5.1	0.2
34.78	2.577	44	127	6.3	1814	8.5	0.37
35.06	2.558	48	125	6.2	1811	8.4	0.4
35.76	2.509	46	118	5.9	1256	5.9	0.3
40.32	2.235	34	72	3.6	957	4.5	0.43
41.18	2.19	33	76	3.8	387	1.8	0.15
42.24	2.138	37	106	5.3	774	3.6	0.19
42.96	2.104	39	69	3.4	231	1.1	0.13
44.02	2.055	34	60	3	185	0.9	0.12
45.43	1.995	31	60	3	707	3.3	0.41
46.28	1.96	28	64	3.2	685	3.2	0.32
48.68	1.869	24	78	3.9	913	4.3	0.29

Peak Search Report (35 Peaks, Max P/N = 18.1)

[Z07031.MDI] 2 min ground Tolbutamide, NB#67034x43-Stage III

PEAK: 21-pts/Parabolic Filter, Threshold=3.0, Cutoff=0.1%, BG=3/1.0, Peak-Top=Summit

2-Theta	d(A)	BG	Height	I%	Area	I%	FWHM
3.88	22.777	97	179	12.9	2241	8.7	0.46
3.96	22.301	95	165	11.9	2252	8.7	0.55
8.7	10.156	27	1311	94.4	15805	61.4	0.21
10.29	8.591	29	54	3.9	283	1.1	0.19
12.06	7.332	38	1389	100	20133	78.2	0.25
13.06	6.775	58	1108	79.8	12668	49.2	0.21
14.22	6.222	51	628	45.2	7493	29.1	0.22
15.48	5.719	49	342	24.6	4670	18.1	0.27
17.3	5.122	42	419	30.2	7080	27.5	0.32
19.5	4.548	46	1274	91.7	19399	75.4	0.27
19.88	4.462	55	1135	81.7	25742	100	0.41
20.84	4.259	50	1153	83	17062	66.3	0.26
21.4	4.149	51	351	25.3	4682	18.2	0.27
23.04	3.857	51	675	48.6	9151	35.5	0.25
24.24	3.669	57	141	10.2	1315	5.1	0.27
24.7	3.601	53	169	12.2	1918	7.5	0.28
26.26	3.391	49	580	41.8	9355	36.3	0.3
28.18	3.164	57	198	14.3	3020	11.7	0.36
28.74	3.104	58	534	38.4	7437	28.9	0.27
30.44	2.934	45	212	15.3	3101	12	0.32
31.7	2.821	41	111	8	1004	3.9	0.24
32.96	2.715	35	136	9.8	1639	6.4	0.28
34.36	2.608	49	84	6	235	0.9	0.11
35.06	2.557	39	146	10.5	2950	11.5	0.47

35.44	2.531	47	113	8.1	956	3.7	0.25
36.79	2.441	45	82	5.9	323	1.3	0.15
38.66	2.327	44	111	8	1228	4.8	0.31
39.98	2.253	45	93	6.7	919	3.6	0.33
40.47	2.227	47	84	6	845	3.3	0.39
41.08	2.196	48	89	6.4	596	2.3	0.25
41.65	2.167	42	81	5.8	320	1.2	0.14
42.42	2.129	38	68	4.9	326	1.3	0.18
43.7	2.07	40	113	8.1	1190	4.6	0.28
45.84	1.978	39	74	5.3	653	2.5	0.32
46.5	1.951	41	67	4.8	257	1	0.17

Peak Search Report (20 Peaks, Max P/N = 10.2)

[Z07251.MD1] Tolbutamide +Chlorpropamide by RESS(45,5000) <Psi=0.0>

PEAK: 19-pts/Parabolic Filter, Threshold=3.0, Cutoff=0.1%, BG=3/1.0, Peak-Top=Summit

2-Theta	d(A)	BG	Height	I%	Area	I%	FWHM
8.86	9.973	75	355	53.5	2909	42.2	0.18
12.22	7.236	105	402	60.6	3960	57.5	0.23
12.48	7.086	108	469	70.7	6886	100	0.32
13.2	6.701	110	613	92.5	5254	76.3	0.18
14.6	6.061	129	280	42.2	2716	39.4	0.31
15.78	5.612	154	225	33.9	732	10.6	0.18
17.67	5.015	208	314	47.4	1599	23.2	0.26
19.62	4.52	214	663	100	5733	83.3	0.22
20.22	4.388	212	566	85.4	5746	83.4	0.28
21.2	4.188	187	429	64.7	4330	62.9	0.3
21.52	4.125	175	396	59.7	2718	39.5	0.21
23.28	3.818	129	267	40.3	1841	26.7	0.23
23.86	3.726	131	211	31.8	845	12.3	0.18
26.48	3.363	89	222	33.5	1982	28.8	0.25
26.9	3.312	89	163	24.6	949	13.8	0.22
28.98	3.079	81	177	26.7	1668	24.2	0.3
29.42	3.033	78	138	20.8	1182	17.2	0.33
30.62	2.917	70	114	17.2	1064	15.5	0.41
31.93	2.801	63	98	14.8	439	6.4	0.21
38.37	2.344	46	81	12.2	305	4.4	0.15

Peak Search Report (27 Peaks, Max P/N = 10.4)

[Z07252.MD1] Tolbutamide +Chlorpropamide by RESS(75,5000) <Psi=0.0>

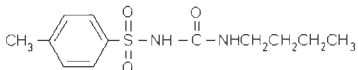
PEAK: 19-pts/Parabolic Filter, Threshold=3.0, Cutoff=0.1%, BG=3/1.0, Peak-Top=Summit

2-Theta	d(A)	BG	Height	I%	Area	I%	FWHM
8.9	9.931	38	201	33.6	3129	38.4	0.33
9.47	9.327	47	76	12.7	264	3.2	0.15
12.4	7.133	39	504	84.1	8158	100	0.3
13.22	6.69	68	442	73.8	5476	67.1	0.25
14.54	6.087	61	271	45.2	2911	35.7	0.24
15.86	5.584	76	172	28.7	1329	16.3	0.24

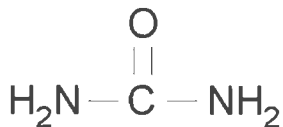
17.54	5.052	97	224	37.4	2055	25.2	0.28
19.7	4.503	121	599	100	7060	86.5	0.25
20.2	4.392	124	531	88.6	7634	93.6	0.32
21.12	4.203	123	402	67.1	5343	65.5	0.33
21.58	4.115	109	258	43.1	2663	32.6	0.3
23.3	3.815	89	236	39.4	2375	29.1	0.27
24.46	3.636	87	125	20.9	608	7.5	0.27
26.62	3.346	70	227	37.9	2956	36.2	0.32
26.7	3.336	70	180	30.1	2950	36.2	0.46
26.78	3.327	70	162	27	2945	36.1	0.54
28.43	3.137	65	102	17	453	5.6	0.21
29.26	3.05	62	148	24.7	2148	26.3	0.42
30.47	2.932	56	87	14.5	811	9.9	0.44
30.86	2.895	56	115	19.2	1148	14.1	0.33
31.94	2.8	53	88	14.7	389	4.8	0.19
33.21	2.696	48	86	14.4	353	4.3	0.16
35.32	2.539	46	80	13.4	658	8.1	0.33
38.86	2.315	40	71	11.9	335	4.1	0.18
42.27	2.136	37	63	10.5	545	6.7	0.36
47.6	1.909	36	62	10.4	112	1.4	0.07
47.6	1.909	36	62	10.4	112	1.4	0.07

7. TOLBUTAMIDE + UREA:

7A. CHEMICAL STRUCTURE:



Tolbutamide



Urea

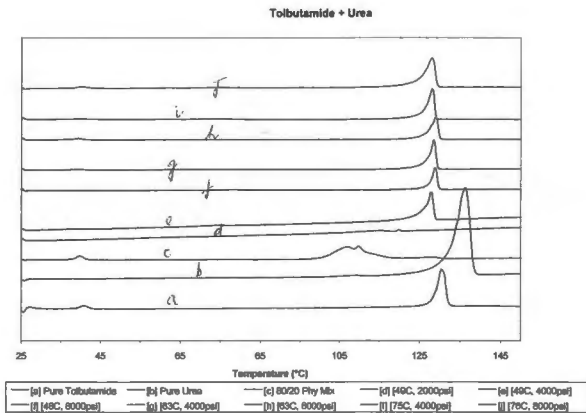
7B. SUMMARY OF RESS RECRYSTALLIATION:

COMPOSITION OF STARTING MIXTURE: 80% Tolbutamide + 20% Urea

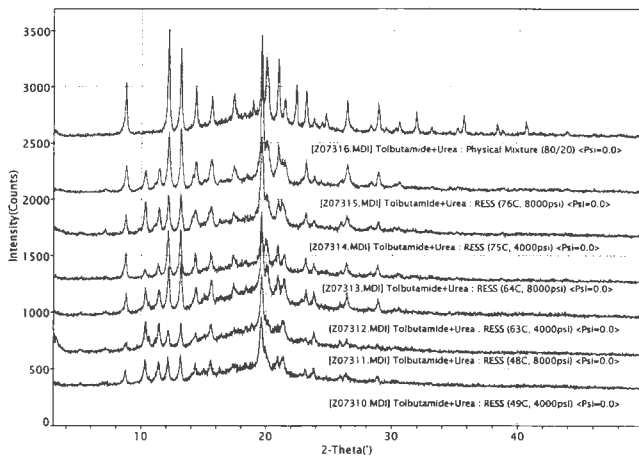
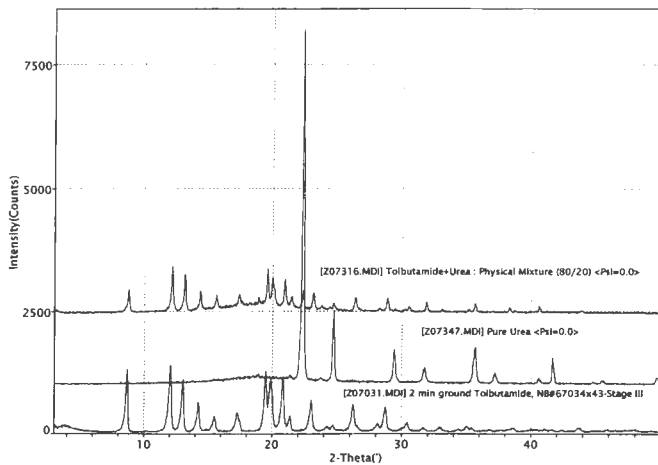
CONTENTS OF REACTION VESSEL : 3.2g Tolbutamide + 0.8g Urea (4g of blend)

Experiment	[P,T conditions]	Weight collected,mg	Collection time, min
1	[48C, 2000psi]	34	30
2	[48.5C, 4000psi]	118	20
3	[48C, 8000psi]	135	5
4	[64C, 2000psi]	28	30
5	[62C, 4000psi]	230	22
6	[62C, 8000psi]	117	5
7	[76C, 2000psi]	37	30
8	[75C, 4000psi]	325	20
9	[75C, 8000psi]	344	6
10	[90C, 2000psi]	34	30
11	[90C, 4000psi]	430	22
12	[91C, 8000psi]	326	5

7C. DSC ANALYSIS:



7D.1. XRPD ANALYSIS:



7D.2. XRPD ANALYSIS:

Peak Search Report (29 Peaks, Max P/N = 18.7)

[Z07030.MDI] 1 min ground Tolbutamide, NB#67034x43-Stage II

PEAK: 19-pts/Parabolic Filter, Threshold=3.0, Cutoff=0.1%, BG=3/1.0, Peak-Top=Summit

2-Theta	d(A)	BG	Height	I%	Area	I%	FWHM
8.68	10.176	27	1256	83.1	14684	69.4	0.2
12.08	7.322	56	1511	100	18153	85.8	0.21
13.06	6.775	42	1211	80.1	13171	62.3	0.19
14.24	6.214	45	762	50.4	8386	39.6	0.2
14.85	5.962	49	77	5.1	295	1.4	0.18
15.54	5.699	40	393	26	4511	21.3	0.22
17.28	5.128	35	463	30.6	7537	35.6	0.3
19.52	4.544	44	1234	81.7	17157	81.1	0.25
19.88	4.462	88	1284	85	21157	100	0.3
20.84	4.259	83	1449	95.9	16857	79.7	0.21
21.38	4.152	49	322	21.3	4558	21.5	0.28
23.04	3.857	48	754	49.9	9649	45.6	0.23
24.26	3.665	49	152	10.1	1226	5.8	0.2
24.68	3.604	45	192	12.7	2189	10.3	0.25
26.26	3.391	46	632	41.8	9567	45.2	0.28
28.12	3.17	50	241	15.9	2845	13.4	0.25
28.78	3.1	52	637	42.2	8169	38.6	0.24
30.4	2.938	41	249	16.5	3697	17.5	0.3
31.68	2.822	36	128	8.5	1303	6.2	0.24
32.92	2.718	31	144	9.5	1951	9.2	0.29
34.38	2.607	45	78	5.2	403	1.9	0.21
35.04	2.559	40	170	11.3	3492	16.5	0.46
35.42	2.532	48	129	8.5	1156	5.5	0.24
36.84	2.438	42	85	5.6	438	2.1	0.17
38.64	2.328	41	145	9.6	1703	8	0.28
39.96	2.254	51	84	5.6	349	1.6	0.18
41.06	2.196	47	105	6.9	951	4.5	0.28
43.66	2.071	38	129	8.5	1525	7.2	0.28
45.9	1.976	36	82	5.4	930	4.4	0.34

Peak Search Report (14 Peaks, Max P/N = 41.8)

[Z07347.MDI] Pure Urea <Psi=0.0>

PEAK: 19-pts/Parabolic Filter, Threshold=3.0, Cutoff=0.1%, BG=3/1.0, Peak-Top=Summit

2-Theta	d(A)	BG	Height	I%	Area	I%	FWHM
18.51	4.79	164	217	3	1568	2.2	0.5
18.92	4.687	169	247	3.4	1485	2.1	0.32
21.38	4.153	146	221	3.1	959	1.3	0.22
22.34	3.976	133	7237	100	71195	100	0.17
23.76	3.741	114	176	2.4	676	0.9	0.19
24.76	3.593	101	1549	21.4	14259	20	0.17
29.4	3.035	77	740	10.2	7773	10.9	0.2

31.76	2.815	71	368	5.1	4553	6.4	0.26
35.66	2.516	64	787	10.9	10303	14.5	0.24
37.2	2.415	59	266	3.7	2765	3.9	0.23
40.62	2.219	56	160	2.2	1039	1.5	0.17
41.64	2.167	56	570	7.9	4340	6.1	0.14
44.78	2.022	51	83	1.1	181	0.3	0.1
45.56	1.99	48	106	1.5	721	1	0.21

Peak Search Report (29 Peaks, Max P/N = 14.3)

[Z07316.MDI] Tolbutamide+Urea : Physical Mixture (80/20) <Psi=0.0>

PEAK: 17-pts/Parabolic Filter, Threshold=3.0, Cutoff=0.1%, BG=3/1.0, Peak-Top=Summit

2-Theta	d(A)	BG	Height	I%	Area	I%	FWHM
8.8	10.043	60	519	52	5195	55.6	0.19
12.18	7.261	94	999	100	9342	100	0.18
13.16	6.722	97	828	82.9	7306	78.2	0.17
14.36	6.162	115	491	49.1	3915	41.9	0.18
15.62	5.668	142	398	39.8	2624	28.1	0.17
17.42	5.087	193	419	41.9	2998	32.1	0.23
19.6	4.525	210	943	94.4	9179	98.3	0.21
19.98	4.44	224	752	75.3	8132	87	0.26
20.94	4.238	184	731	73.2	5890	63	0.18
21.5	4.13	179	380	38	1864	20	0.16
22.38	3.97	144	500	50.1	2901	31.1	0.14
23.18	3.834	130	446	44.6	3414	36.5	0.18
23.8	3.736	126	202	20.2	557	6	0.12
24.42	3.643	112	166	16.6	518	5.5	0.16
24.72	3.599	106	242	24.2	1832	19.6	0.23
26.4	3.373	86	358	35.8	3334	35.7	0.21
28.26	3.155	79	141	14.1	937	10	0.26
28.86	3.091	76	339	33.9	3370	36.1	0.22
29.45	3.03	76	120	12	340	3.6	0.13
30.24	2.953	69	118	11.8	554	5.9	0.19
30.5	2.928	68	166	16.6	1454	15.6	0.25
31.86	2.806	64	257	25.7	1996	21.4	0.18
33.09	2.705	63	122	12.2	506	5.4	0.15
35.16	2.55	63	115	11.5	657	7	0.21
35.6	2.519	61	233	23.3	1606	17.2	0.16
38.27	2.35	57	154	15.4	832	8.9	0.15
38.67	2.326	56	98	9.8	406	4.3	0.16
40.57	2.222	56	171	17.1	1431	15.3	0.21
43.88	2.062	49	93	9.3	554	5.9	0.21

Peak Search Report (23 Peaks, Max P/N = 8.6)

[Z07310.MDI] Tolbutamide+Urea : RESS (49C, 4000psi) <Psi=0.0>

PEAK: 19-pts/Parabolic Filter, Threshold=3.0, Cutoff=0.1%, BG=3/1.0, Peak-Top=Summit

2-Theta	d(A)	BG	Height	I%	Area	I%	FWHM
8.78	10.065	71	196	29.6	1505	16.2	0.2

10.3	8.578	89	288	43.4	2775	29.8	0.24
10.65	8.3	95	143	21.6	508	5.5	0.18
11.38	7.769	106	269	40.6	2110	22.7	0.22
12.16	7.774	109	315	47.5	2067	22.2	0.17
13.14	6.732	106	334	50.4	2426	26.1	0.18
14.12	6.268	130	173	26.1	363	3.9	0.14
14.35	6.165	138	258	38.9	1735	18.6	0.25
15.02	5.895	146	210	31.7	1931	20.8	0.51
15.6	5.677	165	284	42.8	1162	12.5	0.17
16.27	5.444	162	227	34.2	263	2.8	0.07
17.33	5.113	204	253	38.2	332	3.6	0.12
19.64	4.516	222	663	100	9303	100	0.36
20	4.437	220	356	53.7	5968	64.2	0.75
20.96	4.235	197	316	47.7	2559	27.5	0.37
21.38	4.152	180	322	48.6	2619	28.2	0.31
23.12	3.844	132	198	29.9	1223	13.1	0.32
23.84	3.73	126	216	32.6	809	8.7	0.15
25.93	3.434	107	155	23.4	314	3.4	0.11
26.36	3.378	110	170	25.6	574	6.2	0.16
28.24	3.157	85	124	18.7	466	5	0.2
28.9	3.087	83	145	21.9	884	9.5	0.24
36.9	2.434	50	82	12.4	282	3	0.15

Peak Search Report (25 Peaks, Max P/N = 9.0)

[Z07311.MDI] Tolbutamide+Urea : RESS (48C, 8000psi) <Psi=0.0>

PEAK: 21-pts/Parabolic Filter, Threshold=3.0, Cutoff=0.1%, BG=3/1.0, Peak-Top=Summit

2-Theta	d(A)	BG	Height	I%	Area	I%	FWHM
3.28	26.93	61	178	24	2179	23.7	0.32
7.12	12.409	65	97	13.1	394	4.3	0.21
8.82	10.018	77	141	19	795	8.6	0.21
10.36	8.535	110	331	44.7	2944	32	0.23
10.61	8.328	120	203	27.4	888	9.6	0.18
11.42	7.742	125	310	41.8	2183	23.7	0.2
12.16	7.272	119	249	33.6	1404	15.3	0.18
13.2	6.704	116	315	42.5	2089	22.7	0.18
14.37	6.157	152	231	31.2	841	9.1	0.18
15.62	5.67	166	307	41.4	2676	29.1	0.32
16.42	5.394	181	231	31.2	306	3.3	0.1
17.45	5.077	215	277	37.4	985	10.7	0.27
18.85	4.704	259	318	42.9	572	6.2	0.16
19.66	4.512	253	741	100	9206	100	0.32
20.22	4.389	270	334	45.1	967	10.5	0.26
20.9	4.247	225	290	39.1	1554	16.9	0.41
20.97	4.234	221	307	41.4	1637	17.8	0.32
21.4	4.148	197	338	45.6	3331	36.2	0.4
23.2	3.831	138	186	25.1	1238	13.4	0.44
23.82	3.732	130	239	32.3	1236	13.4	0.19

25.92	3.435	109	155	20.9	567	6.2	0.21
26.48	3.363	99	175	23.6	1857	20.2	0.42
28.19	3.163	91	126	17	533	5.8	0.26
28.88	3.089	93	140	18.9	175	1.9	0.06
31.6	2.829	73	111	15	383	4.2	0.17

Peak Search Report (24 Peaks, Max P/N = 11.0)

[Z07312.MDI] Tolbutamide+Urea : RESS (63C, 4000psi) <Psi=0.0>

PEAK: 19-pts/Parabolic Filter, Threshold=3.0, Cutoff=0.1%, BG=3/1.0, Peak-Top=Summit

2-Theta	d(A)	BG	Height	I%	Area	I%	FWHM
7.18	12.299	59	90	9.6	369	2.8	0.2
8.82	10.021	70	252	26.8	2409	18.5	0.23
10.34	8.548	97	298	31.7	2739	21.1	0.23
10.62	8.322	104	172	18.3	903	6.9	0.23
11.42	7.741	122	280	29.8	2083	16	0.22
12.18	7.259	126	480	51.1	3929	30.2	0.19
13.18	6.711	123	527	56.1	4456	34.3	0.19
14.42	6.139	155	301	32.1	1700	13.1	0.2
15.05	5.881	160	241	25.7	1818	14	0.38
15.62	5.669	169	368	39.2	3526	27.1	0.3
17.4	5.093	226	338	36	1237	9.5	0.19
19.66	4.512	264	939	100	13008	100	0.33
20.04	4.427	265	505	53.8	5972	45.9	0.42
20.94	4.239	226	408	43.5	3133	24.1	0.29
21.44	4.141	201	377	40.1	2806	21.6	0.27
22.84	3.89	154	201	21.4	733	5.6	0.27
23.2	3.831	143	282	30	2305	17.7	0.28
23.84	3.73	143	265	28.2	1188	9.1	0.17
26	3.424	108	152	16.2	843	6.5	0.33
26.46	3.366	106	255	27.2	2471	19	0.28
28.9	3.087	85	198	21.1	1648	12.7	0.25
30.18	2.958	78	118	12.6	920	7.1	0.39
30.52	2.926	78	126	13.4	1001	7.7	0.35
31.1	2.873	76	115	12.2	334	2.6	0.15

Peak Search Report (26 Peaks, Max P/N = 9.1)

[Z07313.MDI] Tolbutamide+Urea : RESS (64C, 8000psi) <Psi=0.0>

PEAK: 17-pts/Parabolic Filter, Threshold=3.0, Cutoff=0.1%, BG=3/1.0, Peak-Top=Summit

2-Theta	d(A)	BG	Height	I%	Area	I%	FWHM
8.78	10.064	64	287	43.8	2828	40.2	0.22
10.28	8.596	73	150	22.9	975	13.8	0.22
11.34	7.794	96	201	30.6	953	13.5	0.15
12.14	7.283	100	489	74.5	4599	65.3	0.2
13.14	6.732	100	500	76.2	4403	62.5	0.19
14.32	6.178	113	287	43.8	1714	24.3	0.17
15.56	5.69	131	296	45.1	2230	31.7	0.23
17.38	5.098	177	274	41.8	933	13.2	0.16

17.64	5.024	177	232	35.4	753	10.7	0.23
18.06	4.909	178	234	35.7	741	10.5	0.22
19.62	4.521	188	656	100	7043	100	0.26
19.96	4.444	194	416	63.4	4895	69.5	0.37
20.75	4.278	182	247	37.7	810	11.5	0.21
20.94	4.239	171	365	55.6	2850	40.5	0.25
21.46	4.137	155	277	42.2	1688	24	0.24
23.16	3.837	121	249	38	1541	21.9	0.2
23.8	3.735	121	202	30.8	591	8.4	0.12
24.8	3.587	104	142	21.6	338	4.8	0.15
25.94	3.432	96	136	20.7	361	5.1	0.15
26.38	3.376	93	207	31.6	1722	24.4	0.26
28.3	3.151	81	122	18.6	561	8	0.23
28.86	3.091	78	182	27.7	1652	23.5	0.27
30.54	2.925	73	106	16.2	495	7	0.25
33.03	2.71	62	97	14.8	292	4.1	0.14
33.03	2.71	62	97	14.8	292	4.1	0.14
33.14	2.701	61	92	14	306	4.3	0.17

Peak Search Report (27 Peaks, Max P/N = 12.0)

[Z07314.MD1] Tolbutamide+Urea : RESS (75C, 4000psi) <Psi=0.0>

PEAK: 23-pts/Parabolic Filter, Threshold=3.0, Cutoff=0.1%, BG=3/1.0, Peak-Top=Summit

2-Theta	d(A)	BG	Height	%	Area	%	FWHM
7.16	12.339	49	100	10.9	664	4.4	0.22
8.78	10.063	56	227	24.7	1956	13.1	0.19
9.75	9.066	65	100	10.9	603	4	0.29
10.34	8.55	76	342	37.3	3619	24.2	0.23
11.08	7.977	90	133	14.5	940	6.3	0.37
11.42	7.742	96	289	31.5	2510	16.8	0.22
12.14	7.282	96	402	43.8	3538	23.6	0.2
13.14	6.731	91	410	44.7	3709	24.8	0.2
14.34	6.172	121	272	29.6	2676	17.9	0.3
15.38	5.755	130	244	26.6	3145	21	0.47
15.62	5.669	129	298	32.5	3156	21.1	0.32
16.26	5.447	138	190	20.7	518	3.5	0.17
17.38	5.098	166	251	27.3	919	6.1	0.18
19.64	4.517	192	918	100	14970	100	0.35
20.06	4.423	198	404	44	7458	49.8	0.62
20.98	4.231	177	364	39.7	3610	24.1	0.33
21.3	4.168	163	324	35.3	4130	27.6	0.44
22.74	3.907	112	151	16.4	748	5	0.33
23.16	3.837	114	243	26.5	2059	13.8	0.27
23.78	3.739	115	176	19.2	871	5.8	0.24
26	3.425	98	164	17.9	1184	7.9	0.3
26.4	3.374	94	210	22.9	2809	18.8	0.41
28.34	3.147	86	125	13.6	755	5	0.33
28.88	3.089	87	164	17.9	1167	7.8	0.26

30.23	2.954	80	113	12.3	697	4.7	0.36
30.52	2.927	78	115	12.5	647	4.3	0.3
31.62	2.827	72	105	11.4	360	2.4	0.19

Peak Search Report (23 Peaks, Max P/N = 13.9)

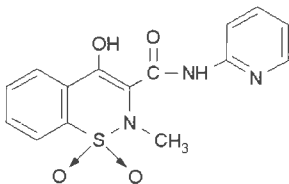
[Z07315.MDI] Tolbutamide+Urea : RESS (76C, 8000psi) <Psi=0.0>

PEAK: 23-pts/Parabolic Filter, Threshold=3.0, Cutoff=0.1%, BG=3/1.0, Peak-Top=Summit

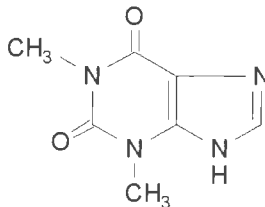
2-Theta	d(A)	BG	Height	I%	Area	I%	FWHM
8.8	10.038	42	271	25.1	3062	15.9	0.23
10.36	8.534	53	225	20.8	2581	13.4	0.26
11.46	7.716	86	245	22.7	2136	11.1	0.23
12.2	7.25	91	567	52.5	5864	30.5	0.21
13.16	6.721	80	602	55.7	6193	32.2	0.2
14.34	6.171	97	305	28.2	2975	15.5	0.24
15.04	5.885	106	146	13.5	720	3.7	0.31
15.64	5.662	101	323	29.9	4219	21.9	0.32
16.34	5.42	114	152	14.1	245	1.3	0.11
17.4	5.092	130	272	25.2	2252	11.7	0.27
18.42	4.812	143	201	18.6	495	2.6	0.15
19.62	4.521	165	1080	100	19253	100	0.36
20.04	4.427	182	487	45.1	10838	56.3	0.6
20.94	4.238	163	448	41.5	7116	37	0.42
21.52	4.126	143	288	26.7	3728	19.4	0.44
23.16	3.837	104	324	30	3320	17.2	0.26
23.84	3.73	111	177	16.4	674	3.5	0.17
25.94	3.432	97	140	13	836	4.3	0.33
26.44	3.368	90	284	26.3	3723	19.3	0.33
28.32	3.149	74	130	12	1238	6.4	0.38
28.88	3.089	76	212	19.6	2258	11.7	0.28
30.6	2.919	69	125	11.6	1122	5.8	0.34
35.18	2.549	50	82	7.6	1134	5.9	0.6

8. PIROXICAM + THEOPHYLLINE:

8A. CHEMICAL STRUCTURE:



Piroxicam



Theophylline

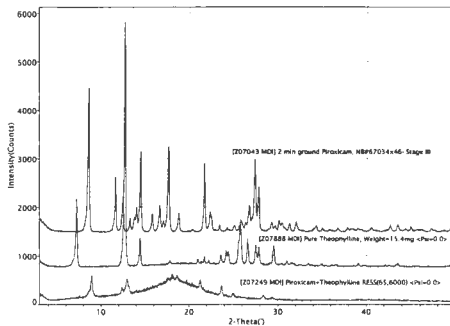
8B. SUMMARY OF RESS RECRYSTALLIATION:

COMPOSITION OF STARTING MIXTURE: 80% Piroxicam + 20% Theophylline

CONTENTS OF REACTION VESSEL : 2g Piroxicam + 0.5g Theophylline (2.5g of blend)

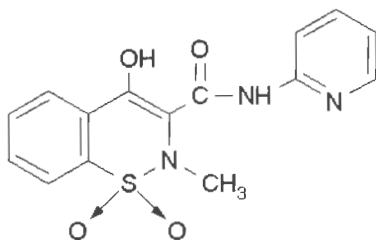
Experiment	[P,T conditions]	Weight collected,mg	Collection time, min
1	[65C, 6000psi]	91	10

8D.1. XRPD ANALYSIS:

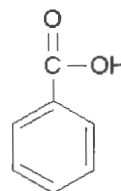


9. PIROXICAM + BENZOIC ACID:

9A. CHEMICAL STRUCTURE:



Piroxicam



Benzoic Acid

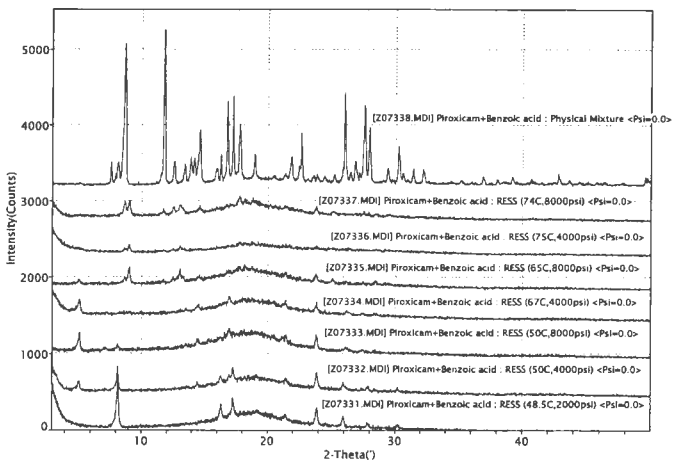
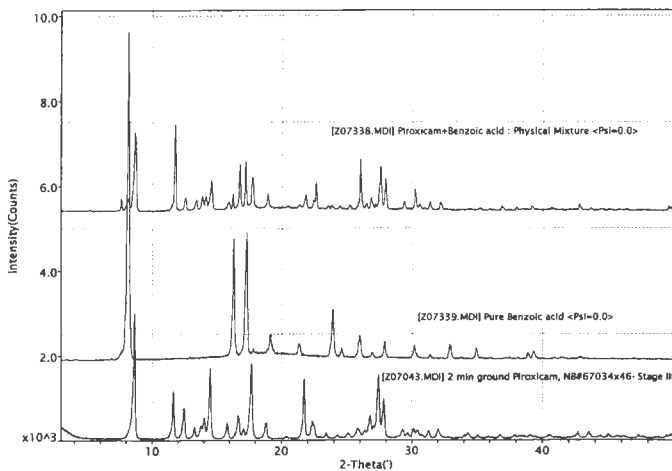
9B. SUMMARY OF RESS RECRYSTALLIATION:

COMPOSITION OF STARTING MIXTURE: 80% Piroxicam + 20% Benzoic acid

CONTENTS OF REACTION VESSEL : 1.6g Piroxicam + 0.4g Benzoic acid (2g of blend)

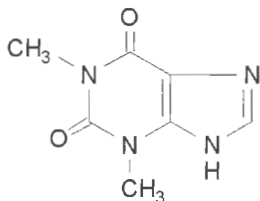
Experiment	[P,T conditions]	Weight collected,mg	Collection time, min
1	[48.5C, 2000psi]	85	30
2	[50C, 4000psi]	70	10
3	[50C, 8000psi]	85	5
4	[66C, 2000psi]	41	30
5	[67C, 4000psi]	59	10
6	[65C, 8000psi]	34	5
7	[78C, 2000psi]	31	30
8	[75C, 4000psi]	38	10
9	[74C, 8000psi]	46	5

9D.1. XRPD ANALYSIS:

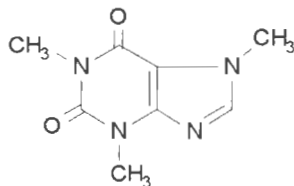


10. THEOPHYLLINE + CAFFEINE:

10A. CHEMICAL STRUCTURE:



Theophylline



Caffeine

10B. SUMMARY OF RESS RECRYSTALLIATION:

COMPOSITION OF STARTING MIXTURE: 80% Theophylline + 20% Caffeine

CONTENTS OF REACTION VESSEL : 4.8g Theophylline+ 1.2g Caffeine (6g of blend)

TEMPERATURE OF MICROMETERING VALVE: 150°C

RECRYSTALLIZING SOLVENT: Pure SCCO₂

Experiment	[P,T conditions]	Weight collected,mg	Collection time, min
1	[47.5C, 2000psi]	31	30
2	[46.5C, 4000psi]	195	35
3	[48C, 8000psi]	131	15
4	[63C, 2000psi]	35	30
5	[62.5C, 4000psi]	86	30
6	[64C, 8000psi]	127	30
7	[76.5C, 2000psi]	30	30
8	[76C, 4000psi]	32	30
9	[75.1C, 8000psi]	62	20
10	[100.1C, 2000psi]	21	30
11	[100C, 4000psi]	34	30
12	[100C, 8000psi]	127	30

COMPOSITION OF STARTING MIXTURE: 20% Theophylline + 80% Caffeine

CONTENTS OF REACTION VESSEL : 2g Theophylline+ 8g Caffeine (10g of blend)

TEMPERATURE OF MICROMETERING VALVE: 150°C

RECRYSTALLIZING SOLVENT: Pure SCCO₂

Experiment	[P,T conditions]	Weight collected,mg	Collection time, min	Ref
1	[47.7°C, 2000psi]	68	60	NB 72656x137
2	[48.2°C, 4000psi]	357	20	NB 72656x138
3	[47°C, 8000psi]	263	10	NB 72656x138
4	[63°C, 2000psi]	50	30	NB 72656x137
5	[63.2°C, 4000psi]	279	20	NB 72656x138
6	[62.2C, 8000psi]	203	30	NB 72656x139
7	[75.8°C, 2000psi]	61	30	NB 72656x139
8	[74.5°C, 4000psi]	160	25	NB 72656x140
9	[76.4°C, 8000psi]	296	15	NB 72656x140
10	[100.4°C, 2000psi]	58	20	NB 72656x140
11	[100.9°C, 4000psi]	136	30	NB 72656x140
12	[98.7°C, 8000psi]	282	30	NB 72656x141

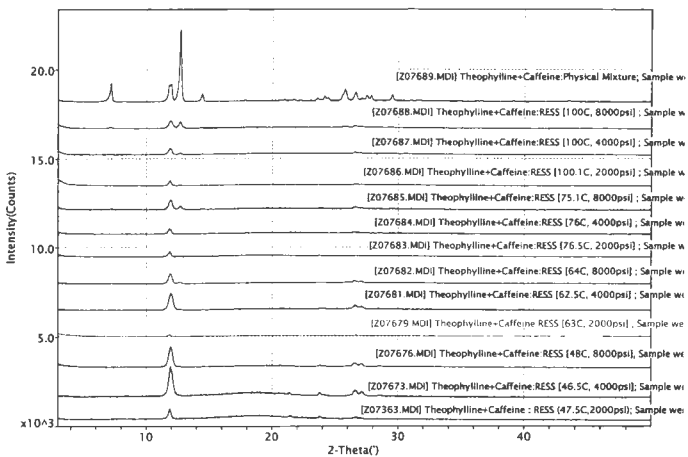
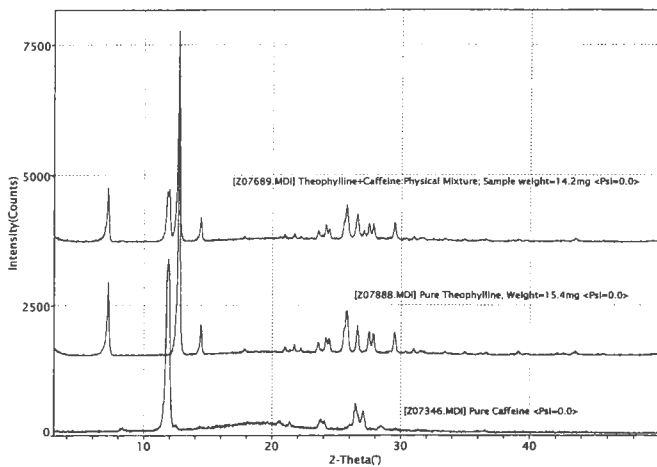
COMPOSITION OF STARTING MIXTURE: 80% Theophylline + 20% Caffeine
 CONTENTS OF REACTION VESSEL : 4.8g Theophylline+ 1.2g Caffeine (6g of blend)
 TEMPERATURE OF MICROMETERING VALVE: 100°C
 RECRYSTALLIZING SOLVENT: SCCO₂ + MeOH

Experiment	[P,T conditions]	Weight collected,mg	Collection time, min
1	[53C, 2000psi]	79	30
2	[53.6C, 4000psi]	123	30
3	[52.6C, 8000psi]	43	30

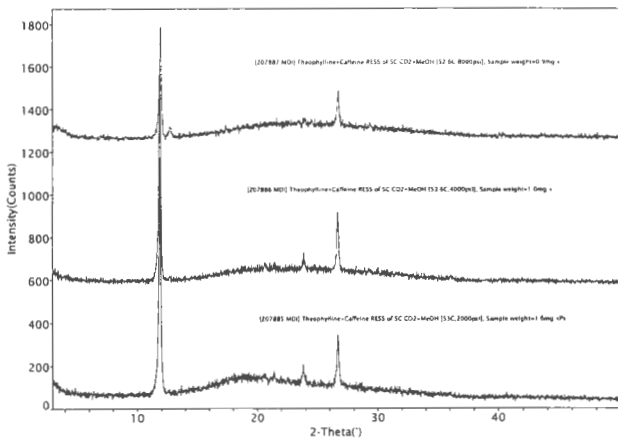
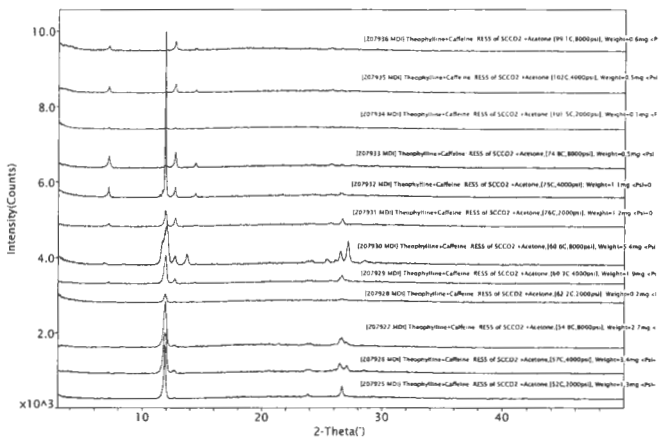
COMPOSITION OF STARTING MIXTURE: 80% Theophylline + 20% Caffeine
 CONTENTS OF REACTION VESSEL : 8g Theophylline+ 2g Caffeine (10g of blend)
 TEMPERATURE OF MICROMETERING VALVE: 100°C
 RECRYSTALLIZING SOLVENT: SCCO₂ + Acetone

Experiment	[P,T conditions]	Weight collected,mg	Collection time, min
1	[52C, 2000psi]	90	30
2	[57C, 4000psi]	381	10
3	[54.8C, 8000psi]	157	10
4	[62.2C, 2000psi]	22	32
5	[60.3C, 4000psi]	44	60
6	[60.6C, 8000psi]	108	30
7	[76.2C, 2000psi]	25	60
8	[75C, 4000psi]	27	60
9	[74.8C, 8000psi]	28	15
10	[101.5C, 2000psi]	24	60
11	[102C, 4000psi]	27	30
12	[99.1C, 8000psi]	18	10

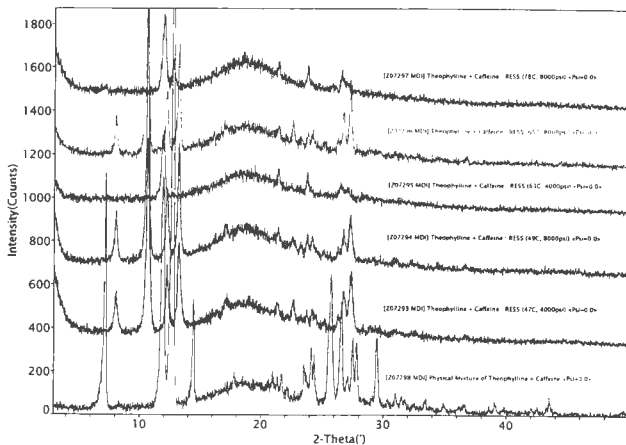
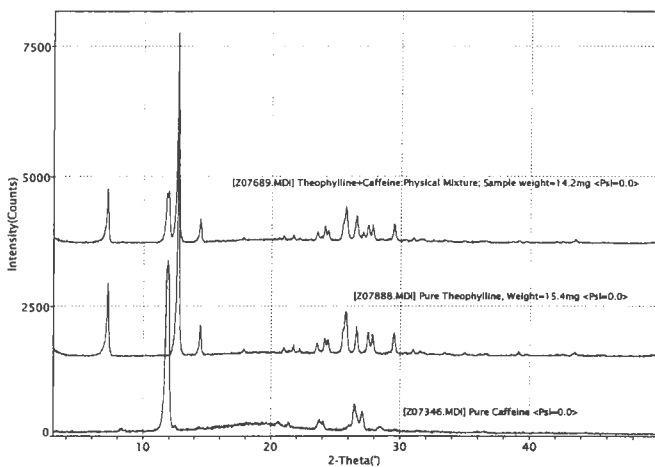
10.D.1 XRPD ANALYSIS:



10.D.1. XRPD ANALYSIS (Cont'd):



10.D.1 XRPD ANALYSIS (Cont'd):



10.D.2 XRPD ANALYSIS:

Peak Search Report (25 Peaks, Max P/N = 46.4)

[Z07020.MDI] Ground Theophylline, 2 min grinding time, NB#67034x39, Stage II

PEAK: 23-pts/Parabolic Filter, Threshold=3.0, Cutoff=0.1%, BG=3/1.0, Peak-Top=Summit

2-Theta	d(A)	BG	Height	I%	Area	I%	FWHM
7.16	12.342	31	2135	24.6	30012	25.5	0.24
12.6	7.019	47	8695	100	117914	100	0.23
14.34	6.171	36	1119	12.9	14900	12.6	0.23
17.78	4.986	28	150	1.7	1555	1.3	0.22
20.86	4.255	43	234	2.7	2051	1.7	0.18
21.6	4.11	47	294	3.4	3363	2.9	0.23
22.08	4.022	48	146	1.7	1231	1	0.21
23.44	3.792	43	476	5.5	6331	5.4	0.25
24.04	3.699	76	846	9.7	15583	13.2	0.34
25.58	3.479	82	1969	22.6	41091	34.8	0.37
26.48	3.363	153	1135	13.1	13875	11.8	0.24
27.36	3.257	112	1024	11.8	24518	20.8	0.46
27.68	3.22	103	924	10.6	14304	12.1	0.3
29.36	3.04	70	1029	11.8	15361	13	0.27
30.24	2.953	67	143	1.6	794	0.7	0.18
30.92	2.89	60	256	2.9	3121	2.6	0.27
31.4	2.847	60	190	2.2	2663	2.3	0.35
33.32	2.687	49	169	1.9	1976	1.7	0.28
34.84	2.573	45	146	1.7	1259	1.1	0.21
36.04	2.49	42	144	1.7	1642	1.4	0.27
36.44	2.464	41	150	1.7	2003	1.7	0.31
38.96	2.31	50	200	2.3	3260	2.8	0.37
42.4	2.13	44	108	1.2	2077	1.8	0.55
43.36	2.085	45	230	2.6	3895	3.3	0.36
45.5	1.992	35	94	1.1	1105	0.9	0.32

Peak Search Report (12 Peaks, Max P/N = 28.1)

[Z07346.MDI] Pure Caffeine <Psi=0.0>

PEAK: 21-pts/Parabolic Filter, Threshold=3.0, Cutoff=0.1%, BG=3/1.0, Peak-Top=Summit

2-Theta	d(A)	BG	Height	I%	Area	I%	FWHM
8.36	10.57	83	155	4.6	1041	1.6	0.25
11.88	7.443	118	3399	100	64100	100	0.33
14.39	6.148	133	179	5.3	141	0.2	0.05
18.07	4.904	212	263	7.7	1276	2	0.43
20.58	4.312	201	278	8.2	1170	1.8	0.26
21.36	4.156	176	263	7.7	714	1.1	0.14
23.82	3.733	126	319	9.4	4125	6.4	0.36
24.08	3.692	123	288	8.5	3221	5	0.33
26.46	3.365	114	611	18	11256	17.6	0.39
27.1	3.288	147	468	13.8	4362	6.8	0.23
28.48	3.132	99	186	5.5	1635	2.6	0.32

29.67 3.009 87 129 3.8 516 0.8 0.21

Peak Search Report (28 Peaks, Max P/N = 31.6)

[Z07689.MDI] Theophylline+Caffeine:Physical Mixture; Sample weight=14.2mg <Psi=0.0>

PEAK: 19-pts/Parabolic Filter, Threshold=3.0, Cutoff=0.1%, BG=3/1.0, Peak-Top=Summit

2-Theta	d(A)	BG	Height	I%	Area	I%	FWHM
7.2	12.266	54	1076	26.3	11616	27	0.19
11.96	7.394	49	1044	25.5	21497	50	0.37
12.7	6.964	53	4091	100	43027	100	0.18
14.44	6.129	56	506	12.4	4658	10.8	0.18
17.84	4.968	90	142	3.5	339	0.8	0.11
20.6	4.308	99	140	3.4	429	1	0.18
20.96	4.235	102	179	4.4	782	1.8	0.17
21.72	4.088	98	188	4.6	757	1.8	0.14
22.2	4.001	93	139	3.4	250	0.6	0.09
23.58	3.77	91	246	6	2436	5.7	0.27
24.14	3.684	88	361	8.8	5653	13.1	0.35
24.4	3.645	94	276	6.7	2988	6.9	0.28
25.76	3.456	114	738	18	9692	22.5	0.26
26.58	3.351	141	565	13.8	4995	11.6	0.2
27.1	3.288	112	245	6	2073	4.8	0.26
27.48	3.243	126	375	9.2	3682	8.6	0.25
27.84	3.202	109	386	9.4	2902	6.7	0.18
29.46	3.029	80	397	9.7	3793	8.8	0.2
30.4	2.938	72	105	2.6	241	0.6	0.12
31.01	2.881	71	133	3.3	1148	2.7	0.31
31.74	2.817	70	110	2.7	622	1.4	0.26
32.51	2.752	65	104	2.5	99	0.2	0.04
33.44	2.678	59	94	2.3	537	1.2	0.26
34.9	2.568	51	85	2.1	313	0.7	0.16
36.54	2.457	44	85	2.1	841	2	0.35
39.12	2.301	42	78	1.9	913	2.1	0.43
42.06	2.147	41	68	1.7	489	1.1	0.31
43.5	2.079	42	109	2.7	791	1.8	0.2

Peak Search Report (6 Peaks, Max P/N = 10.7)

[Z07363.MDI] Theophylline+Caffeine : RESS (47.5C,2000psi); Sample weight=0.7mg <Psi=0.0>

PEAK: 19-pts/Parabolic Filter, Threshold=3.0, Cutoff=0.1%, BG=3/1.0, Peak-Top=Summit

2-Theta	d(A)	BG	Height	I%	Area	I%	FWHM
11.88	7.443	133	701	100	8032	100	0.24
21.47	4.135	215	317	45.2	608	7.6	0.1
23.82	3.732	150	264	37.7	1378	17.2	0.21
26.68	3.338	109	216	30.8	2811	35	0.45
27.08	3.29	111	157	22.4	1250	15.6	0.46

Peak Search Report (11 Peaks, Max P/N = 19.3)

[Z07673.MDI] Theophylline+Caffeine:RESS [46.5C, 4000psi]; Sample weight =5.1mg <Psi=0.0>

PEAK: 21-pts/Parabolic Filter, Threshold=3.0, Cutoff=0.1%, BG=3/1.0, Peak-Top=Summit

2-Theta	d(A)	BG	Height	I%	Area	I%	FWHM
3.77	23.387	121	163	9.2	889	2.6	0.36
11.94	7.407	153	1779	100	33998	100	0.36
20.56	4.317	259	317	17.8	810	2.4	0.24
21.39	4.151	238	323	18.2	422	1.2	0.08
23.84	3.73	138	325	18.3	3631	10.7	0.33
24.16	3.681	143	223	12.5	1157	3.4	0.25
24.16	3.681	143	223	12.5	1157	3.4	0.25
26.6	3.348	122	476	26.8	8586	25.3	0.41
27.16	3.281	140	372	20.9	4200	12.4	0.31
28.44	3.136	106	164	9.2	1034	3	0.3
28.62	3.116	104	173	9.7	1050	3.1	0.26

Peak Search Report (9 Peaks, Max P/N = 16.1)

[Z07676.MDI] Theophylline+Caffeine:RESS [48C, 8000psi], Sample weight=3.3mg <Psi=0.0>

PEAK: 23-pts/Parabolic Filter, Threshold=3.0, Cutoff=0.1%, BG=3/1.0, Peak-Top=Summit

2-Theta	d(A)	BG	Height	I%	Area	I%	FWHM
11.94	7.406	79	1196	100	23257	100	0.35
20.63	4.302	139	185	15.5	115	0.5	0.04
21.48	4.134	127	167	14	134	0.6	0.06
23.78	3.739	103	160	13.4	1216	5.2	0.36
24.2	3.675	99	151	12.6	1503	6.5	0.49
26.6	3.349	97	305	25.5	5331	22.9	0.44
27.12	3.285	110	257	21.5	2690	11.6	0.31
28.58	3.121	85	126	10.5	610	2.6	0.25
29.7	3.005	74	106	8.9	750	3.2	0.4

Peak Search Report (3 Peaks, Max P/N = 4.2)

[Z07679.MDI] Theophylline+Caffeine:RESS [63C, 2000psi]; Sample weight=0.2mg <Psi=0.0>

PEAK: 19-pts/Parabolic Filter, Threshold=3.0, Cutoff=0.1%, BG=3/1.0, Peak-Top=Summit

2-Theta	d(A)	BG	Height	I%	Area	I%	FWHM
11.94	7.431	45	145	100	1519	100	0.26
26.69	3.337	80	116	80	726	47.8	0.34
26.69	3.337	80	116	80	726	47.8	0.34

Peak Search Report (8 Peaks, Max P/N = 14.8)

[Z07681.MDI] Theophylline+Caffeine:RESS [62.5C, 4000psi]; Sample weight=3.2mg <Psi=0.0>

PEAK: 25-pts/Parabolic Filter, Threshold=3.0, Cutoff=0.1%, BG=3/1.0, Peak-Top=Summit

2-Theta	d(A)	BG	Height	I%	Area	I%	FWHM
11.94	7.406	62	1000	100	20489	100	0.37
20.73	4.282	113	152	15.2	395	1.9	0.17
23.86	3.726	101	154	15.4	1397	6.8	0.45
24.15	3.683	103	150	15	1110	5.4	0.4
26.58	3.351	97	337	33.7	7001	34.2	0.5
27.1	3.287	112	252	25.2	2582	12.6	0.31
28.44	3.136	89	133	13.3	643	3.1	0.25

28.68 3.11 86 121 12.1 667 3.3 0.32

Peak Search Report (8 Peaks, Max P/N = 11.4)

[Z07682.MDI] Theophylline+Caffeine:RESS [64C, 8000psi] ; Sample weight=1.8mg <Psi=0.0>

PEAK: 25-pts/Parabolic Filter, Threshold=3.0, Cutoff=0.1%, BG=3/1.0, Peak-Top=Summit

2-Theta	d(A)	BG	Height	I%	Area	I%	FWHM
7.24	12.196	38	72	11.7	502	4.7	0.25
11.94	7.406	49	615	100	10694	100	0.32
12.66	6.985	64	150	24.4	887	8.3	0.18
23.94	3.714	90	130	21.1	954	8.9	0.41
26.58	3.351	91	210	34.1	3630	33.9	0.52
27.11	3.286	96	180	29.3	1596	14.9	0.32
31.18	2.866	66	99	16.1	79	0.7	0.04
47.89	1.898	26	48	7.8	261	2.4	0.2

Peak Search Report (4 Peaks, Max P/N = 7.9)

[Z07683.MDI] Theophylline+Caffeine:RESS [76.5C, 2000psi] ; Sample weight=0.6mg <Psi=0.0>

PEAK: 19-pts/Parabolic Filter, Threshold=3.0, Cutoff=0.1%, BG=3/1.0, Peak-Top=Summit

2-Theta	d(A)	BG	Height	I%	Area	I%	FWHM
11.86	7.455	63	364	100	4433	100	0.25
23.8	3.735	101	141	38.7	264	6	0.11
26.7	3.336	86	137	37.6	679	15.3	0.23
26.94	3.307	84	123	33.8	729	16.4	0.32

Peak Search Report (3 Peaks, Max P/N = 8.0)

[Z07684.MDI] Theophylline+Caffeine:RESS [76C, 4000psi] ; Sample weight=0.5mg <Psi=0.0>

PEAK: 23-pts/Parabolic Filter, Threshold=3.0, Cutoff=0.1%, BG=3/1.0, Peak-Top=Summit

2-Theta	d(A)	BG	Height	I%	Area	I%	FWHM
11.84	7.469	54	357	100	4589	100	0.26
26.46	3.366	94	153	42.9	1200	26.1	0.35
26.93	3.308	88	123	34.5	1450	31.6	0.7

Peak Search Report (8 Peaks, Max P/N = 10.7)

[Z07685.MDI] Theophylline+Caffeine:RESS [75.1C, 8000psi] ; Sample weight=2.0mg <Psi=0.0>

PEAK: 23-pts/Parabolic Filter, Threshold=3.0, Cutoff=0.1%, BG=3/1.0, Peak-Top=Summit

2-Theta	d(A)	BG	Height	I%	Area	I%	FWHM
7.27	12.146	61	116	19	662	6.6	0.2
11.96	7.394	81	609	100	10057	100	0.32
12.76	6.934	90	255	41.9	2184	21.7	0.23
23.89	3.721	107	158	25.9	1076	10.7	0.36
26.58	3.351	108	214	35.1	2574	25.6	0.41
27.1	3.287	105	166	27.3	1196	11.9	0.33
31.03	2.88	70	104	17.1	290	2.9	0.14

Peak Search Report (7 Peaks, Max P/N = 7.9)

[Z07686.MDI] Theophylline+Caffeine:RESS [100.1C, 2000psi] ; Sample weight=0.3mg <Psi=0.0>

PEAK: 17-pts/Parabolic Filter, Threshold=3.0, Cutoff=0.1%, BG=3/1.0, Peak-Top=Summit

2-Theta	d(A)	BG	Height	%	Area	%	FWHM
3.13	28.216	131	369	100	3874	100	0.28
3.27	27.015	112	322	87.3	3159	81.5	0.26
3.55	24.872	93	204	55.3	1924	49.7	0.29
11.88	7.444	51	343	93	3870	99.9	0.23
23.23	3.825	90	127	34.4	537	13.9	0.25
26.66	3.341	89	136	36.9	578	14.9	0.21
42.08	2.145	34	62	16.8	163	4.2	0.1

Peak Search Report (11 Peaks, Max P/N = 8.6)

[Z07687.MD1] Theophylline+Caffeine:RESS [100C, 4000psi] ; Sample weight=0.7mg <Psi=0.0>

PEAK: 19-pts/Parabolic Filter, Threshold=3.0, Cutoff=0.1%, BG=3/1.0, Peak-Top=Summit

2-Theta	d(A)	BG	Height	%	Area	%	FWHM
3.12	28.319	75	202	49.3	2700	48.6	0.36
3.22	27.427	63	187	45.6	2086	37.6	0.29
3.54	24.945	54	129	31.5	1184	21.3	0.27
7.2	12.268	44	79	19.3	333	6	0.16
11.88	7.443	63	410	100	5554	100	0.27
12.68	6.975	69	158	38.5	408	7.3	0.08
19.2	4.618	102	141	34.4	501	9	0.22
25.73	3.459	97	135	32.9	351	6.3	0.16
26.56	3.353	95	181	44.1	1603	28.9	0.32
27.01	3.298	90	136	33.2	1330	23.9	0.49
36.34	2.47	42	69	16.8	252	4.5	0.16

Peak Search Report (14 Peaks, Max P/N = 10.0)

[Z07688.MD1] Theophylline+Caffeine:RESS [100C, 8000psi] ; Sample weight=2.2mg <Psi=0.0>

PEAK: 23-pts/Parabolic Filter, Threshold=3.0, Cutoff=0.1%, BG=3/1.0, Peak-Top=Summit

2-Theta	d(A)	BG	Height	%	Area	%	FWHM
3.32	26.602	75	206	41	2156	24.1	0.28
3.4	25.974	75	186	37	1703	19	0.26
7.18	12.305	54	132	26.2	1227	13.7	0.27
11.92	7.418	56	503	100	8945	100	0.34
12.68	6.976	61	447	88.9	5985	66.9	0.26
14.34	6.172	66	109	21.7	622	7	0.25
16.47	5.377	84	121	24.1	221	2.5	0.1
17.97	4.933	106	148	29.4	341	3.8	0.14
23.67	3.756	98	138	27.4	1250	14	0.53
23.82	3.732	97	143	28.4	1238	13.8	0.46
25.76	3.456	101	176	35	1147	12.8	0.26
26.6	3.349	104	215	42.7	2084	23.3	0.32
27.1	3.288	98	158	31.4	1663	18.6	0.47
29.5	3.025	78	115	22.9	540	6	0.25

10.F. HPLC ANALYSIS:

RUN-1

Condition	% Theophylline	%Caffeine	%Extracted
[46.5C, 4000psi]	1.76	98.24	96.74
[48C, 8000psi]	4.45	95.55	96.95
[63C, 2000psi]	2.22	97.78	101.23
[62.5C, 4000psi]	6.87	93.13	96.83
[64C, 8000psi]	17.44	82.56	97.73
[76.5C, 2000psi]	4.82	95.18	96.87
[76C, 4000psi]	12.18	87.82	95.61
[75.1C, 8000psi]	33.43	66.57	98.11
[100.1C, 2000psi]	12.91	87.09	97.02
[100C, 4000psi]	25.19	74.81	96.35
[100C, 8000psi]	46.04	53.96	98.97
Physical Mixture	81.96	18.04	102.83

Run-2

Condition	% Theophylline	%Caffeine	%Extracted
[46.5C, 4000psi]	1.84	98.16	95.98
[48C, 8000psi]	4.71	95.29	98.83
[63C, 2000psi]	0.80	99.20	95.88
[62.5C, 4000psi]	6.98	93.02	95.67
[64C, 8000psi]	17.79	82.21	97.16
[76.5C, 2000psi]	4.10	95.90	95.11
[76C, 4000psi]	11.92	88.08	95.47
[75.1C, 8000psi]	32.54	67.46	98.39
[100.1C, 2000psi]	11.89	88.11	92.90
[100C, 4000psi]	25.03	74.97	95.95
[100C, 8000psi]	45.91	54.09	99.43
Physical Mixture	81.02	18.98	102.43

RUN-3

Condition	% Theophylline	%Caffeine	%Extracted
[47.7C, 2000psi]	1.69	98.31	97.97
[48.2C, 4000psi]	1.04	98.96	102.82
[47C, 8000psi]	1.54	98.46	104.42
[63C, 2000psi]	1.37	98.63	102.74
[63.2C, 4000psi]	1.57	98.43	101.99
[62.2C, 8000psi]	2.78	97.22	102.94
[75.8C, 2000psi]	3.17	96.83	103.93
[74.5C, 4000psi]	2.96	97.04	100.22
[76.4C, 8000psi]	4.80	95.20	102.79

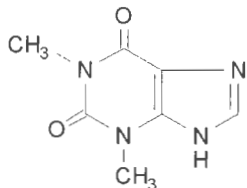
[100.9C, 4000psi]	4.47	95.53	103.14
[98.7C, 8000psi]	6.99	93.01	102.68
Physical Mixture	20.42	79.58	103.17

RUN-4

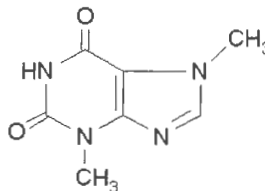
Condition	% Theophylline	%Caffeine	%Extracted
[47.7C, 2000psi]	1.80	98.20	97.91
[48.2C, 4000psi]	1.02	98.98	104.31
[47C, 8000psi]	1.70	98.30	96.14
[63C, 2000psi]	1.49	98.51	102.51
[63.2C, 4000psi]	1.57	98.43	99.74
[62.2C, 8000psi]	2.73	97.27	103.26
[75.8C, 2000psi]	3.25	96.75	102.48
[74.5C, 4000psi]	2.91	97.09	103.75
[76.4C, 8000psi]	4.79	95.21	101.73
[100.9C, 4000psi]	4.37	95.63	103.22
[98.7C, 8000psi]	7.06	92.94	102.57
Physical Mixture	20.28	79.72	103.75

11. THEOPHYLLINE + THEOBROMINE:

11A. CHEMICAL STRUCTURE:



Theophylline



Theobromine

11B. SUMMARY OF RESS RECRYSTALLIATION:

COMPOSITION OF STARTING MIXTURE: 80% Theophylline + 20% Theobromine

CONTENTS OF REACTION VESSEL : 8g Theophylline+ 2g Theobromine (10g of blend)

TEMPERATURE OF MICROMETERING VALVE: 150°C

RECRYSTALLIZING SOLVENT: Pure SCCO₂

Experiment	[P,T conditions]	Weight collected.mg	Collection time, min	Ref
1	[44°C, 2000psi]	43	45	NB 72917x 17
2	[48°C, 4000psi]	26	55	NB 72917x 18
3	[49.2°C, 8000psi]	28	30	NB 72917x 18
4	[62.8°C, 2000psi]	21	90	NB 72917x 18
5	[62°C, 4000psi]	25	60	NB 72917x 18
6	[62.5°C, 8000psi]	43	60	NB 72917x 19
7	[76°C, 2000psi]	15	60	NB 72917x 19
8	[76°C, 4000psi]	26	60	NB 72917x 19
9	[75.2°C, 8000psi]	92	45	NB 72917x 19
10	[101.4°C, 2000psi]	19	60	NB 72917x 20
11	[101.5°C, 4000psi]	36	60	NB 72917x 20
12	[101.5°C, 8000psi]	116	40	NB 72917x 20

COMPOSITION OF STARTING MIXTURE: 80% Theophylline + 20% Theobromine

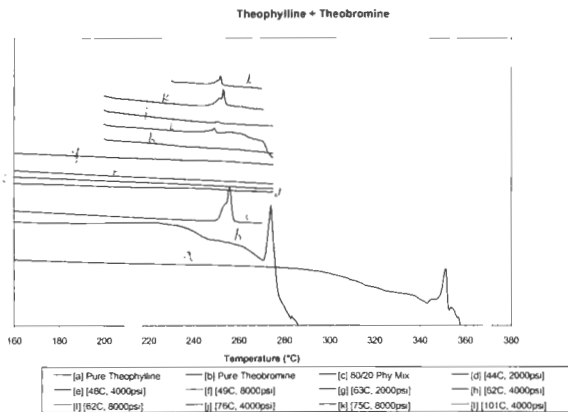
CONTENTS OF REACTION VESSEL : 8g Theophylline+ 2g Theobromine (10g of blend)

TEMPERATURE OF MICROMETERING VALVE: 150°C

RECRYSTALLIZING SOLVENT: SCCO₂ + MeOH

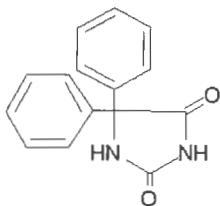
Experiment	[P,T conditions]	Weight collected,mg	Collection time, min	Ref
1	[99.7C, 2000psi]	25	60	NB 72917x 27
2	[101.5C, 4000psi]	52	30	NB 72917x 27
3	[101.1C, 8000psi]	166	3	NB 72917x 27

11C. DSC ANALYSIS:

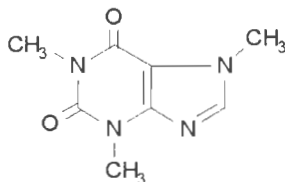


12. PHENYTOIN + CAFFEINE:

12A. CHEMICAL STRUCTURE:



Phenytoin



Caffeine

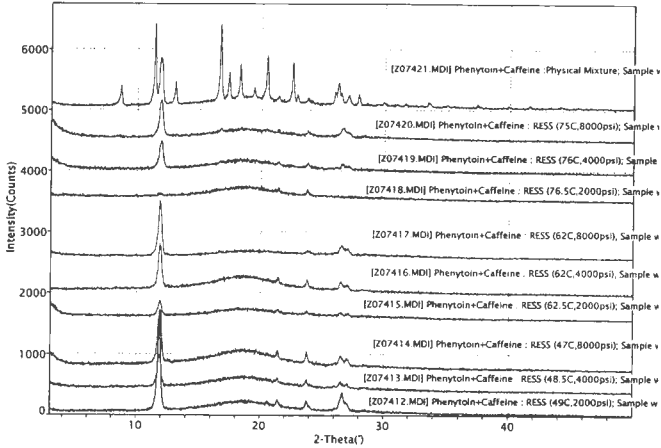
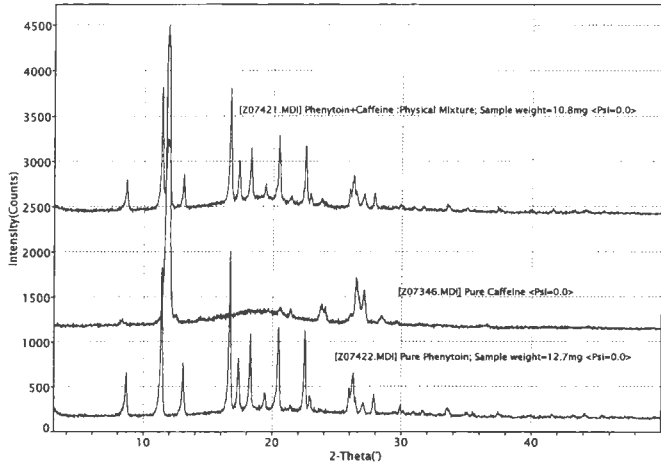
12B. SUMMARY OF RESS RECRYSTALLIATION:

COMPOSITION OF STARTING MIXTURE: 80% Phenytoin + 20% Caffeine

CONTENTS OF REACTION VESSEL : 4.8g Phenytoin+ 1.2g Caffeine (6g of blend)

Experiment	[P,T conditions]	Weight collected,mg	Collection time, min
1	[49C, 2000psi]	75	60
2	[48.5C, 4000psi]	78	20
3	[47C, 8000psi]	157	10
4	[62.5C, 2000psi]	35	60
5	[62C, 4000psi]	46	10
6	[62C, 8000psi]	48	5
7	[76.5C, 2000psi]	28	64
8	[76C, 4000psi]	43	30
9	[75C, 8000psi]	43	10

12.D.1. XRPD ANALYSIS:



12.D.2. XRPD ANALYSIS:

Peak Search Report (27 Peaks, Max P/N = 20.3)

[Z07422.MDI] Pure Phenytoin; Sample weight=12.7mg <Psi=0.0>

PEAK: 19-pts/Parabolic Filter, Threshold=3.0, Cutoff=0.1%, BG=3/1.0, Peak-Top=Summit

2-Theta	d(A)	BG	Height	I%	Area	I%	FWHM
8.68	10.18	65	550	29.1	5480	31.2	0.19
11.42	7.742	69	1719	91	17180	98	0.18
13.06	6.772	73	655	34.7	5545	31.6	0.16
16.7	5.304	122	1889	100	17539	100	0.17
17.36	5.103	148	698	37	5080	29	0.16
18.3	4.844	143	974	51.6	7602	43.3	0.16
19.44	4.563	147	322	17	1632	9.3	0.16
20.46	4.337	131	1051	55.6	9801	55.9	0.18
21.49	4.131	123	169	8.9	635	3.6	0.23
22.52	3.945	117	1015	53.7	8935	50.9	0.17
22.92	3.877	114	287	15.2	2161	12.3	0.21
23.29	3.816	116	156	8.3	164	0.9	0.07
25.98	3.427	98	373	19.7	4980	28.4	0.31
26.28	3.389	96	543	28.7	7761	44.2	0.3
27.06	3.292	95	210	11.1	1227	7	0.18
27.9	3.195	87	302	16	1979	11.3	0.16
29.94	2.982	81	178	9.4	1090	6.2	0.19
30.17	2.96	84	122	6.5	290	1.7	0.13
30.96	2.886	77	112	5.9	275	1.6	0.13
31.7	2.821	73	125	6.6	613	3.5	0.2
33.54	2.67	70	157	8.3	1143	6.5	0.22
35.04	2.559	55	105	5.6	1106	6.3	0.38
35.47	2.529	59	111	5.9	251	1.4	0.08
37.44	2.4	47	111	5.9	1128	6.4	0.3
41.58	2.17	42	84	4.4	803	4.6	0.33
43.21	2.092	45	76	4	327	1.9	0.18
44.09	2.052	44	92	4.9	509	2.9	0.18

Peak Search Report (12 Peaks, Max P/N = 28.1)

[Z07346.MDI] Pure Caffeine <Psi=0.0>

PEAK: 21-pts/Parabolic Filter, Threshold=3.0, Cutoff=0.1%, BG=3/1.0, Peak-Top=Summit

2-Theta	d(A)	BG	Height	I%	Area	I%	FWHM
8.36	10.57	83	155	4.6	1041	1.6	0.25
11.88	7.443	118	3399	100	64100	100	0.33
14.39	6.148	133	179	5.3	141	0.2	0.05
18.07	4.904	212	263	7.7	1276	2	0.43
20.58	4.312	201	278	8.2	1170	1.8	0.26
21.36	4.156	176	263	7.7	714	1.1	0.14
23.82	3.733	126	319	9.4	4125	6.4	0.36
24.08	3.692	123	288	8.5	3221	5	0.33
26.46	3.365	114	611	18	11256	17.6	0.39

27.1	3.288	147	468	13.8	4362	6.8	0.23
28.48	3.132	99	186	5.5	1635	2.6	0.32
29.67	3.009	87	129	3.8	516	0.8	0.21

Peak Search Report (27 Peaks, Max P/N = 17.6)

[Z07421.MDI] Phenytoin+Caffeine :Physical Mixture; Sample weight=10.8mg <Psi=0.0>

PEAK: 17-pts/Parabolic Filter, Threshold=3.0, Cutoff=0.1%, BG=3/1.0, Peak-Top=Summit

2-Theta	d(A)	BG	Height	I%	Area	I%	FWHM
8.68	10.18	79	412	28.7	3987	27.1	0.2
11.42	7.742	102	1438	100	14721	100	0.19
11.88	7.444	109	863	60	14381	97.7	0.32
13.06	6.773	106	474	33	3564	24.2	0.16
16.7	5.304	187	1430	99.4	11892	80.8	0.16
17.38	5.098	202	630	43.8	3612	24.5	0.14
18.3	4.844	212	767	53.3	5145	35	0.16
19.44	4.563	207	373	25.9	1564	10.6	0.16
20.46	4.337	182	907	63.1	7751	52.7	0.18
21.4	4.148	155	241	16.8	914	6.2	0.18
22.54	3.941	138	786	54.7	6920	47	0.18
22.92	3.877	136	264	18.4	1227	8.3	0.16
23.78	3.739	125	208	14.5	1333	9.1	0.27
24.13	3.686	121	165	11.5	467	3.2	0.18
25.96	3.429	118	309	21.5	2258	15.3	0.2
26.28	3.389	116	460	32	7265	49.4	0.36
26.46	3.366	102	286	19.9	6157	41.8	0.57
27.12	3.286	124	256	17.8	1147	7.8	0.15
27.88	3.197	101	262	18.2	1376	9.3	0.15
29.9	2.985	91	141	9.8	661	4.5	0.22
31.64	2.826	78	116	8.1	518	3.5	0.23
33.52	2.672	70	136	9.5	765	5.2	0.2
35.05	2.558	65	103	7.2	521	3.5	0.23
37.38	2.404	55	113	7.9	780	5.3	0.23
41.62	2.168	47	97	6.7	677	4.6	0.23
43.28	2.089	51	79	5.5	305	2.1	0.19
44.12	2.051	48	83	5.8	505	3.4	0.25

Peak Search Report (8 Peaks, Max P/N = 18.9)

[Z07412.MDI] Phenytoin+Caffeine : RESS (49C,2000psi); Sample weight=5.2mg <Psi=0.0>

PEAK: 23-pts/Parabolic Filter, Threshold=3.0, Cutoff=0.1%, BG=3/1.0, Peak-Top=Summit

2-Theta	d(A)	BG	Height	I%	Area	I%	FWHM
11.88	7.443	118	1656	100	25452	100	0.28
21.44	4.141	189	298	18	1189	4.7	0.19
23.82	3.733	131	271	16.4	2262	8.9	0.27
26.72	3.334	117	414	25	7430	29.2	0.43
27.04	3.295	117	241	14.6	3588	14.1	0.49
28.52	3.127	97	135	8.2	520	2	0.23
39.55	2.277	52	81	4.9	314	1.2	0.18

43.62 2.073 46 75 4.5 354 1.4 0.21

Peak Search Report (5 Peaks, Max P/N = 10.0)

[Z07413.MDI] Phenytoin+Caffeine : RESS (48.5C,4000psi); Sample weight=1.9mg <Psi=0.0>

PEAK: 23-pts/Parabolic Filter, Threshold=3.0, Cutoff=0.1%, BG=3/1.0, Peak-Top=Summit

2-Theta	d(A)	BG	Height	I%	Area	I%	FWHM
11.96	7.395	137	642	100	9551	100	0.32
21.46	4.137	195	270	42.1	628	6.6	0.14
23.8	3.735	133	246	38.3	1274	13.3	0.19
26.56	3.354	113	212	33	2269	23.8	0.39
27.12	3.285	105	180	28	1847	19.3	0.42

Peak Search Report (6 Peaks, Max P/N = 13.6)

[Z07414.MDI] Phenytoin+Caffeine : RESS (47C,8000psi); Sample weight=2.7mg <Psi=0.0>

PEAK: 25-pts/Parabolic Filter, Threshold=3.0, Cutoff=0.1%, BG=3/1.0, Peak-Top=Summit

2-Theta	d(A)	BG	Height	I%	Area	I%	FWHM
11.92	7.418	153	1019	100	17916	100	0.35
21.44	4.142	237	363	35.6	1014	5.7	0.14
23.78	3.738	155	351	34.4	2058	11.5	0.18
26.54	3.356	118	274	26.9	4080	22.8	0.44
27.08	3.29	124	228	22.4	2010	11.2	0.33
28.38	3.142	103	145	14.2	412	2.3	0.17

Peak Search Report (6 Peaks, Max P/N = 6.7)

[Z07415.MDI] Phenytoin+Caffeine : RESS (62.5C,2000psi); Sample weight=0.9mg <Psi=0.0>

PEAK: 21-pts/Parabolic Filter, Threshold=3.0, Cutoff=0.1%, BG=3/1.0, Peak-Top=Summit

2-Theta	d(A)	BG	Height	I%	Area	I%	FWHM
3.29	26.835	114	272	78.8	2185	48.7	0.24
11.9	7.43	97	345	100	4490	100	0.31
21.42	4.145	150	208	60.3	552	12.3	0.16
23.8	3.735	111	181	52.5	1378	30.7	0.33
26.56	3.354	96	160	46.4	1387	30.9	0.37
27.12	3.286	94	149	43.2	793	17.7	0.25

Peak Search Report (5 Peaks, Max P/N = 12.2)

[Z07416.MDI] Phenytoin+Caffeine : RESS (62C,4000psi); Sample weight=1.4mg <Psi=0.0>

PEAK: 23-pts/Parabolic Filter, Threshold=3.0, Cutoff=0.1%, BG=3/1.0, Peak-Top=Summit

2-Theta	d(A)	BG	Height	I%	Area	I%	FWHM
11.88	7.443	152	872	100	13068	100	0.31
21.41	4.147	237	324	37.2	498	3.8	0.1
23.78	3.738	147	278	31.9	1730	13.2	0.22
26.54	3.356	119	247	28.3	3322	25.4	0.44
27.12	3.286	108	193	22.1	2673	20.5	0.53

Peak Search Report (6 Peaks, Max P/N = 14.5)

[Z07417.MDI] Phenytoin+Caffeine : RESS (62C,8000psi); Sample weight=2.8mg <Psi=0.0>

PEAK: 27-pts/Parabolic Filter, Threshold=3.0, Cutoff=0.1%, BG=3/1.0, Peak-Top=Summit

2-Theta	d(A)	BG	Height	I%	Area	I%	FWHM
8.33	10.606		57	87	8.9	706	4.2 0.4
11.86	7.455		72	975	100	16802	100 0.32
21.42	4.146		118	157	16.1	266	1.6 0.12
23.86	3.727		101	161	16.5	945	5.6 0.27
26.6	3.348		96	246	25.2	4836	28.8 0.55
27.08	3.29		103	195	20	2042	12.2 0.38

Peak Search Report (7 Peaks, Max P/N = 3.4)

[Z07418.MDI] Phenytoin+Caffeine : RESS (76.5C,2000psi); Sample weight=0.3mg <Psi=0.0>

PEAK: 17-pts/Parabolic Filter, Threshold=3.0, Cutoff=0.1%, BG=3/1.0, Peak-Top=Summit

2-Theta	d(A)	BG	Height	I%	Area	I%	FWHM
4.2	21.027	107	146	57.3	539	57	0.23
11.67	7.574	113	154	60.4	410	43.4	0.17
11.82	7.479	114	157	61.6	470	49.7	0.19
11.82	7.479	114	157	61.6	470	49.7	0.19
21.42	4.144	179	255	100	613	64.9	0.14
23.74	3.744	129	232	91	945	100	0.16
27.26	3.269	86	124	48.6	137	14.5	0.06

Peak Search Report (4 Peaks, Max P/N = 9.5)

[Z07419.MDI] Phenytoin+Caffeine : RESS (76C,4000psi); Sample weight=1.4mg <Psi=0.0>

PEAK: 23-pts/Parabolic Filter, Threshold=3.0, Cutoff=0.1%, BG=3/1.0, Peak-Top=Summit

2-Theta	d(A)	BG	Height	I%	Area	I%	FWHM
11.94	7.405	110	560	100	9578	100	0.36
21.44	4.142	172	220	39.3	394	4.1	0.14
23.82	3.733	133	210	37.5	799	8.3	0.18
26.62	3.346	104	189	33.8	2226	23.2	0.45

Peak Search Report (11 Peaks, Max P/N = 11.2)

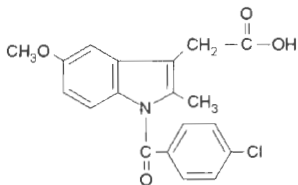
[Z07420.MDI] Phenytoin+Caffeine : RESS (75C,8000psi); Sample weight=2.2mg <Psi=0.0>

PEAK: 21-pts/Parabolic Filter, Threshold=3.0, Cutoff=0.1%, BG=3/1.0, Peak-Top=Summit

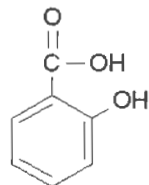
2-Theta	d(A)	BG	Height	I%	Area	I%	FWHM
3.23	27.34	160	340	48.9	3353	28.6	0.32
5.53	15.96	101	138	19.9	113	1	0.05
8.65	10.212	82	116	16.7	517	4.4	0.26
8.65	10.212	82	116	16.7	517	4.4	0.26
11.94	7.406	106	695	100	11713	100	0.34
16.79	5.275	176	233	33.5	734	6.3	0.22
20.58	4.311	176	223	32.1	1196	10.2	0.43
21.39	4.151	160	212	30.5	414	3.5	0.14
23.82	3.733	117	185	26.6	1340	11.4	0.34
26.64	3.343	99	236	34	4495	38.4	0.56
27.16	3.28	112	175	25.2	1027	8.8	0.28

13. INDOMETHACIN + SALICYLIC ACID:

13A. CHEMICAL STRUCTURE:



Indomethacin



Salicylic Acid

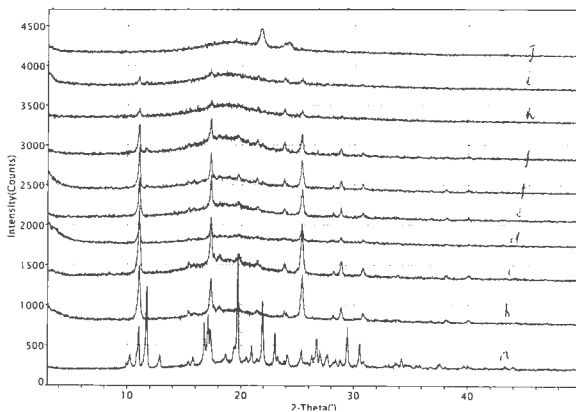
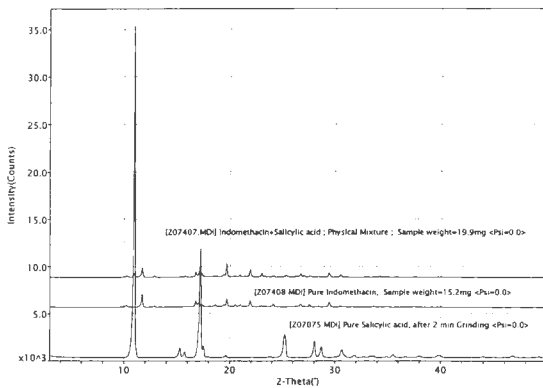
13B. SUMMARY OF RESS RECRYSTALLIATION:

COMPOSITION OF STARTING MIXTURE: 80% Indomethacin + 20% Salicylic acid

CONTENTS OF REACTION VESSEL : 4.8g Indomethacin+ 1.2g Salicylic acid (6g of blend)

Experiment	[P,T conditions]	Weight collected,mg	Collection time, min
1	[47C, 2000psi]	175	56
2	[47C, 4000psi]	103	10
3	[47.5C, 8000psi]	46	5
4	[63C, 2000psi]	67	30
5	[62.5C, 4000psi]	107	10
6	[64C, 8000psi]	63	3
7	[77C, 2000psi]	35	30
8	[76C, 4000psi]	33	10
9	[77C, 8000psi]	29	3

13.D.1. XRPD ANALYSIS:



a-Physical Mixture; b-[47°C, 2000psi]; c-[47°C, 4000psi]; d-[47.5°C, 8000psi]; e-[63°C, 2000psi]
 f-[62.5°C, 4000psi]; g-[64°C, 8000psi]; h-[77°C, 2000psi]; i-[76°C, 4000psi]; j-[77°C, 8000psi]

13.D.2. XRPD ANALYSIS:

Peak Search Report (41 Peaks, Max P/N = 18.4)

[Z07408.MDI] Pure Indomethacin, Sample weight=15.2mg <Psi=0.0>

PEAK: 19-pts/Parabolic Filter, Threshold=3.0, Cutoff=0.1%, BG=3/1.0, Peak-Top=Summit

2-Theta	d(A)	BG	Height	I%	Area	I%	FWHM
9.8	9.014	44	117	8.1	764	6.3	0.18
10.26	8.616	46	241	16.6	2697	22.3	0.24
11.7	7.557	48	1450	100	12078	100	0.15
12.88	6.868	56	185	12.8	1238	10.3	0.16
15.85	5.587	86	126	8.7	373	3.1	0.16
16.76	5.285	101	725	50	7870	65.2	0.21
17.08	5.187	105	588	40.6	6942	57.5	0.24
17.4	5.093	115	316	21.8	2141	17.7	0.18
18.64	4.757	130	287	19.8	1473	12.2	0.16
19.42	4.567	129	323	22.3	3508	29	0.31
19.68	4.507	130	900	62.1	7497	62.1	0.17
20.5	4.329	123	345	23.8	1561	12.9	0.12
20.96	4.235	119	303	20.9	1575	13	0.15
21.47	4.136	113	152	10.5	899	7.4	0.39
21.9	4.055	101	775	53.4	6425	53.2	0.16
22.94	3.873	88	199	13.7	1195	9.9	0.18
23.3	3.815	91	183	12.6	1177	9.7	0.22
24.16	3.681	82	380	26.2	3208	26.6	0.18
25.79	3.452	75	120	8.3	674	5.6	0.25
26.29	3.388	75	181	12.5	1959	16.2	0.31
26.7	3.336	91	372	25.7	4603	38.1	0.28
27	3.3	73	206	14.2	1727	14.3	0.22
27.54	3.236	78	325	22.4	1951	16.2	0.13
28.37	3.144	71	149	10.3	675	5.6	0.15
29.42	3.033	70	553	38.1	4847	40.1	0.17
30.52	2.927	64	152	10.5	1164	9.6	0.22
30.86	2.895	62	125	8.6	742	6.1	0.2
31.68	2.822	59	89	6.1	198	1.6	0.11
32.76	2.732	57	93	6.4	231	1.9	0.11
33.66	2.661	55	158	10.9	822	6.8	0.14
34.28	2.613	53	106	7.3	994	8.2	0.32
35	2.562	49	128	8.8	1339	11.1	0.29
35.52	2.525	46	77	5.3	340	2.8	0.19
35.8	2.506	47	115	7.9	720	6	0.18
37.56	2.393	42	122	8.4	974	8.1	0.21
39.72	2.267	42	70	4.8	556	4.6	0.34
41.66	2.166	42	72	5	321	2.7	0.18
43.41	2.083	41	81	5.6	861	7.1	0.37
43.9	2.061	41	72	5	253	2.1	0.14
47.56	1.91	40	74	5.1	364	3	0.18
48.78	1.865	33	63	4.3	330	2.7	0.19

Peak Search Report (21 Peaks, Max P/N = 93.6)

[Z07075.MDI] Pure Salicylic acid, after 2 min Grinding <Psi=0.0>

PEAK: 19-pts/Parabolic Filter, Threshold=3.0, Cutoff=0.1%, BG=3/1.0, Peak-Top=Summit

2-Theta	d(A)	BG	Height	I%	Area	I%	FWHM
10.98	8.051	41	35122	100	296650	100	0.14
15.28	5.793	41	1085	3.1	13023	4.4	0.21
15.74	5.625	46	667	1.9	6681	2.3	0.18
17.22	5.145	44	11620	33.1	142907	48.2	0.21
17.5	5.063	44	1237	3.5	30708	10.4	0.44
17.96	4.935	37	159	0.5	1286	0.4	0.18
19.62	4.52	36	259	0.7	2584	0.9	0.2
25.26	3.523	49	2452	7	39357	13.3	0.28
28.04	3.179	59	1790	5.1	21209	7.1	0.21
28.7	3.108	74	1172	3.3	14462	4.9	0.22
30.68	2.912	59	886	2.5	14469	4.9	0.3
31.82	2.81	53	294	0.8	2853	1	0.2
32.76	2.731	61	168	0.5	1013	0.3	0.16
33.34	2.685	48	244	0.7	3240	1.1	0.28
33.7	2.657	53	245	0.7	2968	1	0.26
34.86	2.571	52	161	0.5	1069	0.4	0.17
35.52	2.525	46	366	1	4493	1.5	0.24
38	2.366	48	226	0.6	2645	0.9	0.25
39.92	2.256	46	289	0.8	5969	2	0.42
44	2.056	46	149	0.4	1481	0.5	0.24
46.78	1.94	45	251	0.7	3900	1.3	0.32

Peak Search Report (46 Peaks, Max P/N = 17.6)

[Z07407.MDI] Indomethacin+ Salicylic acid ; Physical Mixture ; Sample weight=19.9mg
<Psi=0.0>

PEAK: 19-pts/Parabolic Filter, Threshold=3.0, Cutoff=0.1%, BG=3/1.0, Peak-Top=Summit

2-Theta	d(A)	BG	Height	I%	Area	I%	FWHM
9.93	8.9	54	117	7.9	295	2.6	0.08
10.26	8.615	61	217	14.7	1936	16.8	0.21
11.03	8.012	61	565	38.3	4748	41.3	0.16
11.72	7.546	78	1071	72.5	8283	72	0.14
12.88	6.867	52	215	14.6	1633	14.2	0.17
15.41	5.743	76	138	9.3	694	6	0.19
15.76	5.617	81	194	13.1	940	8.2	0.14
16.76	5.284	101	612	41.4	5729	49.8	0.19
17.1	5.181	103	710	48.1	9343	81.2	0.26
17.3	5.121	112	528	35.7	8605	74.8	0.35
18.64	4.755	125	232	15.7	1256	10.9	0.2
19.34	4.585	128	312	21.1	5804	50.4	0.54
19.68	4.507	126	1477	100	11509	100	0.14
20.46	4.337	120	197	13.3	785	6.8	0.17
20.92	4.242	114	323	21.9	1554	13.5	0.13

21.44	4.14	108	180	12.2	1056	9.2	0.25
21.9	4.055	101	881	59.6	7863	68.3	0.17
23.03	3.858	94	492	33.3	3446	29.9	0.15
23.3	3.815	95	198	13.4	1227	10.7	0.2
23.8	3.736	86	136	9.2	1102	9.6	0.37
24.09	3.692	86	219	14.8	1510	13.1	0.19
25.38	3.507	78	274	18.6	2920	25.4	0.25
25.88	3.439	83	127	8.6	861	7.5	0.33
26.32	3.384	83	218	14.8	1125	9.8	0.14
26.7	3.336	82	416	28.2	4486	39	0.23
27	3.299	79	275	18.6	1960	17	0.17
27.68	3.22	76	231	15.6	1638	14.2	0.18
28.18	3.164	77	123	8.3	705	6.1	0.26
28.42	3.138	75	163	11	1027	8.9	0.2
28.8	3.097	73	157	10.6	1253	10.9	0.25
29.42	3.033	69	554	37.5	4828	41.9	0.17
30.52	2.926	65	359	24.3	3490	30.3	0.2
30.9	2.892	64	136	9.2	1382	12	0.33
32.81	2.727	62	96	6.5	83	0.7	0.04
33.11	2.704	64	99	6.7	132	1.1	0.06
33.66	2.66	68	127	8.6	499	4.3	0.14
34.22	2.618	61	177	12	1785	15.5	0.26
34.57	2.593	68	101	6.8	690	6	0.36
35.51	2.526	47	89	6	738	6.4	0.3
35.86	2.502	46	95	6.4	843	7.3	0.29
36.78	2.442	45	72	4.9	229	2	0.14
37.58	2.391	44	114	7.7	1367	11.9	0.33
38.16	2.357	47	75	5.1	201	1.7	0.12
39.72	2.268	48	81	5.5	459	4	0.24
43.28	2.089	49	86	5.8	218	1.9	0.1
44.12	2.051	40	68	4.6	375	3.3	0.23

Peak Search Report (16 Peaks, Max P/N = 12.3)

[Z07398.MDI] Indomethacin+ Salicylic acid: RESS ; Sample weight=4.3mg

<Psi=0.0>

PEAK: 17-pts/Parabolic Filter, Threshold=3.0, Cutoff=0.1%, BG=3/1.0, Peak-Top=Summit

2-Theta	d(A)	BG	Height	I%	Area	I%	FWHM
11.04	8.008	76	754	100	9348	100	0.23
15.36	5.764	130	184	24.4	449	4.8	0.14
17.32	5.115	182	598	79.3	5046	54	0.21
17.62	5.029	171	255	33.8	3360	35.9	0.68
18.05	4.911	193	251	33.3	600	6.4	0.18
19.44	4.562	176	232	30.8	1667	17.8	0.51
19.78	4.485	185	283	37.5	892	9.5	0.15
21.41	4.146	153	209	27.7	440	4.7	0.13
23.84	3.73	118	194	25.7	540	5.8	0.12
25.42	3.501	110	645	85.5	7173	76.7	0.23

28.12	3.17	90	140	18.6	406	4.3	0.14
28.88	3.089	85	238	31.6	1767	18.9	0.2
30.78	2.903	76	160	21.2	1579	16.9	0.32
36.84	2.437	51	80	10.6	246	2.6	0.14
38.1	2.36	49	88	11.7	481	5.1	0.21
40.1	2.247	46	85	11.3	672	7.2	0.29

Peak Search Report (20 Peaks, Max P/N = 13.7)

[Z07399.MD1] Indomethacin+ Salicylic acid: RESS ; Sample weight=5.3mg
<Psi=0.0>

PEAK: 19-pts/Parabolic Filter, Threshold=3.0, Cutoff=0.1%, BG=3/1.0, Peak-Top=Summit

2-Theta	d(A)	BG	Height	I%	Area	I%	FWHM
8.44	10.472	89	129	13.4	294	2.8	0.12
11.04	8.007	112	965	100	10430	100	0.21
15.36	5.764	178	263	27.3	1327	12.7	0.27
15.86	5.584	191	253	26.2	961	9.2	0.26
17.32	5.116	253	818	84.8	6585	63.1	0.2
17.64	5.025	245	356	36.9	3851	36.9	0.59
18.06	4.907	276	356	36.9	822	7.9	0.17
19.74	4.494	249	360	37.3	1486	14.2	0.23
21.39	4.151	196	278	28.8	1036	9.9	0.21
23.84	3.73	136	253	26.2	1269	12.2	0.18
24.97	3.564	124	186	19.3	792	7.6	0.22
25.38	3.506	119	741	76.8	8584	82.3	0.23
28.16	3.166	90	150	15.5	817	7.8	0.23
28.88	3.089	94	267	27.7	2078	19.9	0.2
30.76	2.904	81	186	19.3	1752	16.8	0.28
33.87	2.644	66	102	10.6	528	5.1	0.25
35.91	2.498	58	88	9.1	206	2	0.12
36.89	2.434	55	88	9.1	370	3.5	0.19
38.16	2.356	54	103	10.7	538	5.2	0.19
40.09	2.247	57	99	10.3	586	5.6	0.24

Peak Search Report (7 Peaks, Max P/N = 8.6)

[Z07400.MD1] Indomethacin+ Salicylic acid: RESS(47.5C,8000psi) ; Sample weight=1mg
<Psi=0.0>

PEAK: 17-pts/Parabolic Filter, Threshold=3.0, Cutoff=0.1%, BG=3/1.0, Peak-Top=Summit

2-Theta	d(A)	BG	Height	I%	Area	I%	FWHM
11.02	8.022	65	418	100	3567	100	0.17
12.52	7.067	63	95	22.7	239	6.7	0.13
17.3	5.122	133	328	78.5	1870	52.4	0.16
19.75	4.492	139	183	43.8	718	20.1	0.28
25.34	3.511	93	293	70.1	2501	70.1	0.21
28.8	3.097	80	148	35.4	600	16.8	0.15
30.76	2.904	71	111	26.6	484	13.6	0.21

Peak Search Report (15 Peaks, Max P/N = 9.9)

[Z07401.MDI] Indomethacin+ Salicylic acid: RESS(63C,2000psi) ; Sample weight=4.1mg
<Psi=0.0>

PEAK: 19-pts/Parabolic Filter, Threshold=3.0, Cutoff=0.1%, BG=3/1.0, Peak-Top=Summit

2-Theta	d(A)	BG	Height	I%	Area	I%	FWHM
11.04	8.008	96	569	93.7	5689	100	0.2
15.43	5.739	151	204	33.6	211	3.7	0.07
17.34	5.111	212	607	100	4288	75.4	0.18
19.76	4.489	202	274	45.1	1750	30.8	0.41
21.4	4.149	166	216	35.6	596	10.5	0.2
23.8	3.735	124	191	31.5	737	13	0.19
25.4	3.504	99	426	70.2	5040	88.6	0.26
28.14	3.168	87	146	24.1	495	8.7	0.14
28.84	3.094	82	200	32.9	1453	25.5	0.21
30.8	2.901	69	142	23.4	1487	26.1	0.35
36.76	2.443	48	76	12.5	276	4.9	0.17
38.19	2.354	45	78	12.9	537	9.4	0.28
40.07	2.249	50	90	14.8	187	3.3	0.08
40.07	2.249	50	90	14.8	187	3.3	0.08
43.27	2.089	42	70	11.5	344	6	0.21

Peak Search Report (14 Peaks, Max P/N = 10.5)

[Z07402.MDI] Indomethacin+ Salicylic acid: RESS(62.5C,4000psi) ; Sample weight=2.9mg
<Psi=0.0>

PEAK: 17-pts/Parabolic Filter, Threshold=3.0, Cutoff=0.1%, BG=3/1.0, Peak-Top=Summit

2-Theta	d(A)	BG	Height	I%	Area	I%	FWHM
11.04	8.009	95	620	100	5987	100	0.19
11.63	7.603	96	134	21.6	286	4.8	0.13
15.84	5.591	158	207	33.4	595	9.9	0.21
17.32	5.116	194	540	87.1	4445	74.2	0.22
17.58	5.041	203	267	43.1	1563	26.1	0.42
19.74	4.494	207	273	44	515	8.6	0.13
21.38	4.152	159	236	38.1	793	13.2	0.18
23.8	3.736	126	222	35.8	696	11.6	0.12
25.34	3.512	101	449	72.4	5017	83.8	0.25
28.12	3.17	87	132	21.3	514	8.6	0.19
28.85	3.092	83	190	30.6	1336	22.3	0.21
30.78	2.903	73	155	25	1080	18	0.22
38.12	2.359	45	84	13.5	507	8.5	0.22
40.11	2.246	44	75	12.1	521	8.7	0.29

Peak Search Report (13 Peaks, Max P/N = 8.1)

[Z07403.MDI] Indomethacin+ Salicylic acid: RESS(64C,8000psi) ; Sample weight=2.7mg
<Psi=0.0>

PEAK: 19-pts/Parabolic Filter, Threshold=3.0, Cutoff=0.1%, BG=3/1.0, Peak-Top=Summit

2-Theta	d(A)	BG	Height	I%	Area	I%	FWHM
11.02	8.024	129	485	86.8	4004	100	0.19
11.63	7.603	133	190	34	577	14.4	0.17
13.02	6.793	135	178	31.8	229	5.7	0.09

17.31	5.117	283	559	100	3146	78.6	0.19
19.72	4.498	276	342	61.2	1764	44.1	0.45
21.39	4.151	224	300	53.7	895	22.4	0.2
21.86	4.063	201	252	45.1	244	6.1	0.08
23.82	3.733	138	263	47	1763	44	0.24
25.36	3.509	123	366	65.5	2961	74	0.21
28.8	3.097	95	179	32	914	22.8	0.18
30.73	2.907	86	130	23.3	371	9.3	0.14
35.73	2.511	57	86	15.4	457	11.4	0.27
38.24	2.352	54	83	14.8	537	13.4	0.31

Peak Search Report (10 Peaks, Max P/N = 3.6)

[Z07404.MDI] Indomethacin+ Salicylic acid: RESS(77C,2000psi) ; Sample weight=0.2mg
<Psi=0.0>

PEAK: 15-pts/Parabolic Filter, Threshold=3.0, Cutoff=0.1%, BG=3/1.0, Peak-Top=Summit

2-Theta	d(A)	BG	Height	I%	Area	I%	FWHM
11.06	7.996	107	212	67.1	1288	100	0.21
15.1	5.861	152	204	64.6	203	15.8	0.07
16.1	5.5	186	238	75.3	253	19.6	0.08
16.1	5.5	186	238	75.3	253	19.6	0.08
17.32	5.115	227	316	100	647	50.2	0.12
21.41	4.146	177	232	73.4	342	26.6	0.11
23.84	3.73	122	211	66.8	1137	88.3	0.22
25.36	3.509	109	192	60.8	726	56.4	0.15
28.9	3.087	88	125	39.6	247	19.2	0.11
35.5	2.526	52	80	25.3	250	19.4	0.15

Peak Search Report (10 Peaks, Max P/N = 3.5)

[Z07405.MDI] Indomethacin+ Salicylic acid: RESS(76C,4000psi) ; Sample weight=0.3mg
<Psi=0.0>

PEAK: 17-pts/Parabolic Filter, Threshold=3.0, Cutoff=0.1%, BG=3/1.0, Peak-Top=Summit

2-Theta	d(A)	BG	Height	I%	Area	I%	FWHM
11	8.035	100	198	66.4	955	100	0.17
17.11	5.178	192	241	80.9	596	62.4	0.21
17.28	5.128	198	298	100	853	89.3	0.15
18.68	4.746	212	273	91.6	703	73.6	0.2
18.68	4.746	212	273	91.6	703	73.6	0.2
21.49	4.132	160	205	68.8	501	52.5	0.19
23.78	3.738	121	188	63.1	845	88.5	0.21
24.05	3.697	119	160	53.7	819	85.8	0.34
25.38	3.507	104	187	62.8	885	92.7	0.18
28.12	3.171	82	119	39.9	809	84.7	0.37

Peak Search Report (7 Peaks, Max P/N = 5.7)

[Z07406.MDI] Indomethacin+Salicylic acid: RESS(77C,8000psi) ; Sample weight=1.7mg
<Psi=0.0>

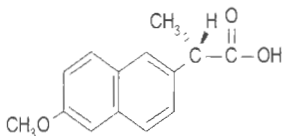
PEAK: 23-pts/Parabolic Filter, Threshold=3.0, Cutoff=0.1%, BG=3/1.0, Peak-Top=Summit

2-Theta	d(A)	BG	Height	I%	Area	I%	FWHM
---------	------	----	--------	----	------	----	------

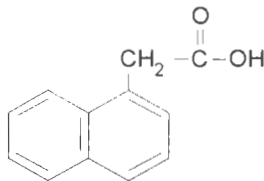
7.68	11.496	79	114	29.8	366	6.6	0.18
18.34	4.833	185	232	60.6	792	14.3	0.29
19.47	4.556	191	256	66.8	1145	20.7	0.3
19.47	4.556	191	256	66.8	1145	20.7	0.3
21.8	4.074	160	383	100	5536	100	0.42
23.84	3.73	130	202	52.7	2618	47.3	0.62
24.2	3.675	121	208	54.3	2970	53.6	0.58

14. NAPROXEN + α -NAPHTHALENE ACETIC ACID:

14A. CHEMICAL STRUCTURE:



Naproxen



α -Naphthalene acetic acid

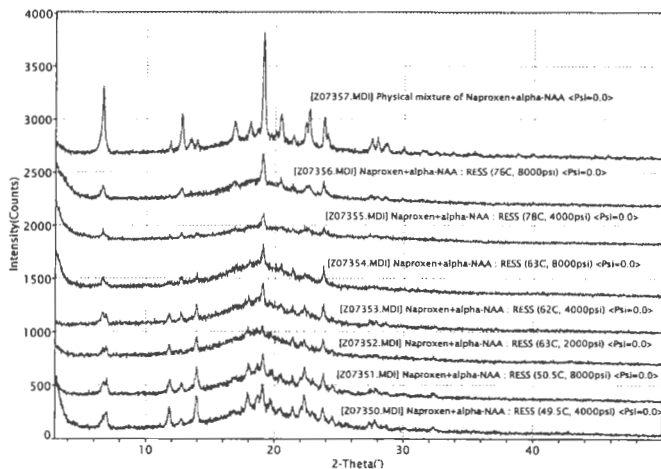
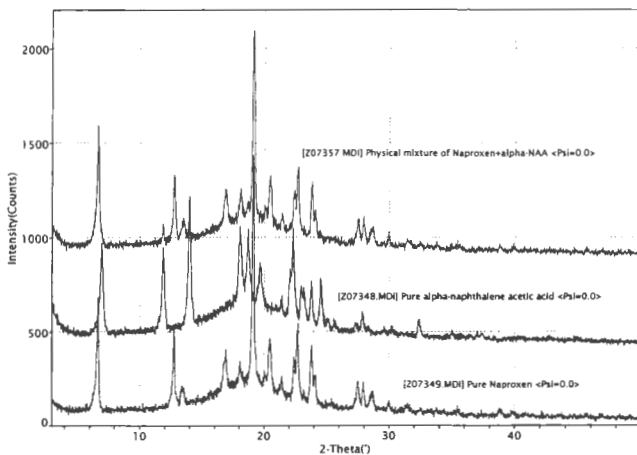
14B. SUMMARY OF RESS RECRYSTALLIATION:

COMPOSITION OF STARTING MIXTURE: 80% Naproxen + 20% α -Naphthalene acetic acid

CONTENTS OF REACTION VESSEL : 4.8g Naproxen+ 1.2g α -Naphthalene acetic acid (6g of blend)

Experiment	[P,T conditions]	Weight collected,mg	Collection time, min
1	[50C, 2000psi]	28	45
2	[49.5C, 4000psi]	69	45
3	[50.5C, 8000psi]	56	10
4	[63C, 2000psi]	31	45
5	[62C, 4000psi]	60	30
6	[63C, 8000psi]	57	10
7	[82C, 2000psi]	37	30
8	[78C, 4000psi]	102	30
9	[76C, 8000psi]	280	20

14.D.1. XRPD ANALYSIS:



14.D.2. XRPD ANALYSIS:

Peak Search Report (21 Peaks, Max P/N = 15.9)

[Z07349.MD1] Pure Naproxen <Psi=0.0>

PEAK: 19-pts/Parabolic Filter, Threshold=3.0, Cutoff=0.1%, BG=3/1.0, Peak-Top=Summit

2-Theta	d(A)	BG	Height	I%	Area	I%	FWHM
6.68	13.221	92	688	47.6	7047	52.1	0.2
12.72	6.953	126	521	36.1	4079	30.2	0.18
13.42	6.593	132	217	15	1107	8.2	0.22
16.94	5.231	203	413	28.6	3416	25.3	0.28
18.08	4.902	236	348	24.1	1038	7.7	0.16
19.08	4.647	239	1444	100	13519	100	0.19
20.06	4.422	223	289	20	1197	8.9	0.31
20.46	4.337	211	470	32.5	3810	28.2	0.25
21.43	4.143	185	269	18.6	298	2.2	0.06
22.38	3.969	168	373	25.8	2762	20.4	0.23
22.7	3.914	162	551	38.2	5718	42.3	0.25
23.84	3.73	136	436	30.2	4477	33.1	0.25
24.06	3.696	133	273	18.9	1798	13.3	0.22
27.5	3.241	101	243	16.8	2113	15.6	0.25
27.94	3.191	100	238	16.5	1972	14.6	0.24
28.7	3.108	98	188	13	1296	9.6	0.24
30	2.976	83	138	9.6	563	4.2	0.17
31.49	2.838	73	123	8.5	1061	7.8	0.36
33.79	2.65	70	102	7.1	315	2.3	0.17
37.36	2.405	56	86	6	123	0.9	0.07
38.81	2.319	56	96	6.6	427	3.2	0.18

Peak Search Report (22 Peaks, Max P/N = 11.7)

[Z07348.MD1] Pure alpha-naphthalene acetic acid <Psi=0.0>

PEAK: 19-pts/Parabolic Filter, Threshold=3.0, Cutoff=0.1%, BG=3/1.0, Peak-Top=Summit

2-Theta	d(A)	BG	Height	I%	Area	I%	FWHM
6.96	12.686	92	570	69.4	8370	86.5	0.3
11.84	7.468	117	549	66.9	6034	62.3	0.24
13.96	6.339	148	821	100	9680	100	0.24
18.04	4.914	280	659	80.3	6233	64.4	0.28
18.68	4.747	268	649	79	6278	64.9	0.28
19.68	4.508	250	468	57	3628	37.5	0.28
21.42	4.146	195	292	35.6	1048	10.8	0.18
22.06	4.026	188	435	53	5730	59.2	0.39
22.3	3.984	188	651	79.3	7355	76	0.27
22.98	3.867	184	345	42	2695	27.8	0.28
23.22	3.827	175	309	37.6	2879	29.7	0.37
23.78	3.739	162	368	44.8	1907	19.7	0.16
24.5	3.63	139	383	46.7	3327	34.4	0.23
25.72	3.461	113	156	19	331	3.4	0.13
27.34	3.26	105	150	18.3	561	5.8	0.21

27.84	3.202	102	207	25.2	1826	18.9	0.3
29.59	3.016	91	128	15.6	293	3	0.13
30.22	2.955	88	130	15.8	368	3.8	0.15
32.42	2.759	73	167	20.3	1275	13.2	0.23
35.01	2.561	69	108	13.2	368	3.8	0.16
37.02	2.426	64	96	11.7	725	7.5	0.39
37.44	2.4	58	91	11.1	896	9.3	0.46

Peak Search Report (24 Peaks, Max P/N = 14.0)

[Z07357.MD1] Physical mixture of Naproxen+alpha-NAA <Psi=0.0>

PEAK: 19-pts/Parabolic Filter, Threshold=3.0, Cutoff=0.1%, BG=3/1.0, Peak-Top=Summit

2-Theta	d(A)	BG	Height	I%	Area	I%	FWHM
6.68	13.219	88	721	58.9	9416	79.9	0.25
11.84	7.467	108	199	16.2	470	4	0.09
12.74	6.943	119	459	37.5	3960	33.6	0.2
13.48	6.563	128	232	18.9	1498	12.7	0.24
13.94	6.347	132	211	17.2	696	5.9	0.15
16.86	5.253	199	388	31.7	3044	25.8	0.27
18.1	4.898	239	388	31.7	1615	13.7	0.18
18.66	4.751	237	320	26.1	2361	20	0.48
19.1	4.643	245	1225	100	11788	100	0.2
20.05	4.425	228	292	23.8	804	6.8	0.21
20.48	4.333	218	457	37.3	2833	24	0.2
21.44	4.142	184	255	20.8	440	3.7	0.11
22.4	3.966	159	377	30.8	4747	40.3	0.37
22.7	3.914	154	503	41.1	6039	51.2	0.29
23.84	3.73	133	423	34.5	4589	38.9	0.27
24.08	3.693	128	272	22.2	2847	24.2	0.34
27.53	3.237	103	225	18.4	1936	16.4	0.27
27.94	3.191	95	238	19.4	1944	16.5	0.23
28.66	3.112	100	181	14.8	1186	10.1	0.25
29.96	2.98	80	154	12.6	531	4.5	0.12
31.4	2.846	78	120	9.8	552	4.7	0.22
33.78	2.652	68	103	8.4	235	2	0.11
38.78	2.32	56	89	7.3	343	2.9	0.18
45.68	1.985	40	75	6.1	369	3.1	0.18

Peak Search Report (24 Peaks, Max P/N = 8.9)

[Z07350.MD1] Naproxen+alpha-NAA : RESS (49.5C, 4000psi) <Psi=0.0>

PEAK: 19-pts/Parabolic Filter, Threshold=3.0, Cutoff=0.1%, BG=3/1.0, Peak-Top=Summit

2-Theta	d(A)	BG	Height	I%	Area	I%	FWHM
3.12	28.31	157	590	100	10133	100	0.4
3.65	24.201	142	316	53.6	1897	18.7	0.19
6.69	13.21	101	217	36.8	3873	38.2	0.57
6.86	12.867	102	234	39.7	3603	35.6	0.46
7	12.616	101	257	43.6	3604	35.6	0.39
11.82	7.48	125	304	51.5	2302	22.7	0.22

12.74	6.94	140	201	34.1	476	4.7	0.13
13.96	6.339	157	405	68.6	3446	34	0.24
<i>17.92</i>	<i>4.945</i>	<i>280</i>	<i>444</i>	<i>75.3</i>	<i>1913</i>	<i>18.9</i>	<i>0.2</i>
18.74	4.731	308	419	71	1788	17.6	0.27
19.06	4.652	296	521	88.3	4159	41	0.31
19.67	4.51	280	388	65.8	1439	14.2	0.23
20.51	4.326	237	303	51.4	574	5.7	0.15
21.42	4.144	218	311	52.7	638	6.3	0.12
22.1	4.019	224	312	52.9	1565	15.4	0.3
22.3	3.983	208	421	71.4	4637	45.8	0.37
22.98	3.867	216	269	45.6	470	4.6	0.15
23.8	3.736	168	298	50.5	1736	17.1	0.23
24.5	3.63	154	221	37.5	619	6.1	0.16
27.35	3.258	124	167	28.3	141	1.4	0.06
27.86	3.2	102	167	28.3	2319	22.9	0.61
28.69	3.109	100	142	24.1	111	1.1	0.04
30.99	2.883	79	114	19.3	480	4.7	0.23
32.31	2.769	78	119	20.2	550	5.4	0.23

Peak Search Report (22 Peaks, Max P/N = 5.6)

[Z07351.MDI] Naproxen+alpha-NAA : RESS (50.5C, 8000psi) <Psi=0.0>

PEAK: 21-pts/Parabolic Filter, Threshold=3.0, Cutoff=0.1%, BG=3/1.0, Peak-Top=Summit

2-Theta	d(A)	BG	Height	I%	Area	I%	FWHM
6.76	13.066	101	216	44.9	3007	64.9	0.44
7	12.622	99	251	52.2	3079	66.5	0.34
11.86	7.455	119	242	50.3	1672	36.1	0.23
12.76	6.933	128	209	43.5	891	19.2	0.19
13.57	6.519	139	186	38.7	719	15.5	0.26
13.94	6.347	147	359	74.6	2806	60.6	0.23
<i>17.98</i>	<i>4.928</i>	<i>286</i>	<i>394</i>	<i>81.9</i>	<i>999</i>	<i>21.6</i>	<i>0.16</i>
18.68	4.747	276	395	82.1	4244	91.6	0.61
19.12	4.638	274	481	100	4438	95.8	0.36
20.53	4.323	229	293	60.9	321	6.9	0.09
21.41	4.147	194	264	54.9	440	9.5	0.11
22	4.036	187	258	53.6	1505	32.5	0.36
22.36	3.973	175	355	73.8	4631	100	0.44
22.64	3.924	168	247	51.4	3761	81.2	0.81
23	3.864	188	252	52.4	472	10.2	0.13
23.8	3.735	150	299	62.2	1499	32.4	0.17
24.52	3.628	135	192	39.9	520	11.2	0.16
27.34	3.26	99	145	30.1	1600	34.5	0.59
27.6	3.23	101	141	29.3	1313	28.4	0.56
27.9	3.195	100	153	31.8	1368	29.5	0.44
32.32	2.768	74	120	24.9	510	11	0.19
32.47	2.755	73	108	22.5	489	10.6	0.24

Peak Search Report (12 Peaks, Max P/N = 3.8)

[Z07352.MDI] Naproxen+alpha-NAA : RESS (63C, 2000psi) <Psi=0.0>

PEAK: 21-pts/Parabolic Filter, Threshold=3.0, Cutoff=0.1%, BG=3/1.0, Peak-Top=Summit

2-Theta	d(A)	BG	Height	I%	Area	I%	FWHM
6.7	13.176	106	189	48.3	2070	56.1	0.42
6.94	12.722	109	201	51.4	1560	42.3	0.29
11.78	7.503	136	218	55.8	663	18	0.14
13.96	6.339	162	290	74.2	1722	46.7	0.23
<i>17.94</i>	<i>4.94</i>	<i>306</i>	<i>384</i>	<i>98.2</i>	<i>603</i>	<i>16.3</i>	<i>0.13</i>
<i>18.36</i>	<i>4.828</i>	<i>288</i>	<i>359</i>	<i>91.8</i>	<i>3691</i>	<i>100</i>	<i>0.88</i>
18.64	4.755	291	378	96.7	3658	99.1	0.71
19.08	4.649	305	391	100	1538	41.7	0.3
21.47	4.135	221	289	73.9	353	9.6	0.09
22.06	4.026	191	250	63.9	1188	32.2	0.34
22.35	3.974	182	258	66	1465	39.7	0.33
23.76	3.741	152	272	69.6	1411	38.2	0.2

Peak Search Report (21 Peaks, Max P/N = 4.6)

[Z07353.MDI] Naproxen+alpha-NAA : RESS (62C, 4000psi) <Psi=0.0>

PEAK: 21-pts/Parabolic Filter, Threshold=3.0, Cutoff=0.1%, BG=3/1.0, Peak-Top=Summit

2-Theta	d(A)	BG	Height	I%	Area	I%	FWHM
6.7	13.181	115	220	44.3	2320	61.9	0.38
6.94	12.719	111	206	41.4	2679	71.5	0.48
<i>10.67</i>	<i>8.287</i>	<i>121</i>	<i>165</i>	<i>33.2</i>	<i>302</i>	<i>8.1</i>	<i>0.12</i>
11.81	7.49	130	218	43.9	897	23.9	0.17
12.7	6.962	138	230	46.3	913	24.4	0.17
13.55	6.532	149	195	39.2	648	17.3	0.24
13.92	6.356	157	302	60.8	1776	47.4	0.21
<i>17.98</i>	<i>4.93</i>	<i>303</i>	<i>375</i>	<i>75.5</i>	<i>567</i>	<i>15.1</i>	<i>0.13</i>
18.75	4.728	307	372	74.8	1393	37.2	0.36
19.1	4.643	293	497	100	3748	100	0.31
20.02	4.431	269	324	65.2	759	20.3	0.23
20.49	4.33	252	307	61.8	406	10.8	0.13
21.43	4.144	214	292	58.8	442	11.8	0.1
22.34	3.977	190	293	59	1812	48.3	0.3
23.84	3.73	151	305	61.4	2047	54.6	0.23
24.43	3.64	142	185	37.2	276	7.4	0.11
27.42	3.25	99	147	29.6	1082	28.9	0.38
27.86	3.199	98	149	30	974	26	0.32
28.62	3.116	93	142	28.6	447	11.9	0.16

Peak Search Report (13 Peaks, Max P/N = 6.5)

[Z07354.MDI] Naproxen+alpha-NAA : RESS (63C, 8000psi) <Psi=0.0>

PEAK: 17-pts/Parabolic Filter, Threshold=3.0, Cutoff=0.1%, BG=3/1.0, Peak-Top=Summit

2-Theta	d(A)	BG	Height	I%	Area	I%	FWHM
3.1	28.493	162	431	82.6	6305	100	0.4
3.27	27.003	155	370	70.9	3712	58.9	0.29
6.73	13.114	123	212	40.6	1484	23.5	0.28

7.04	12.552	121	162	31	679	10.8	0.28
12.76	6.935	159	216	41.4	405	6.4	0.12
13.96	6.337	171	251	48.1	535	8.5	0.11
18.69	4.744	308	375	71.8	2637	41.8	0.67
19.08	4.647	311	522	100	2761	43.8	0.22
20.11	4.411	276	338	64.8	656	10.4	0.18
21.38	4.152	236	297	56.9	216	3.4	0.06
22.38	3.969	189	247	47.3	1183	18.8	0.35
23.78	3.738	154	316	60.5	1536	24.4	0.16
47.67	1.906	38	63	12.1	167	2.6	0.11

Peak Search Report (11 Peaks, Max P/N = 5.8)

[Z07355.MDI] Naproxen+alpha-NAA : RESS (78C, 4000psi) <Psi=0.0>

PEAK: 23-pts/Parabolic Filter, Threshold=3.0, Cutoff=0.1%, BG=3/1.0, Peak-Top=Summit

2-Theta	d(A)	BG	Height	I%	Area	I%	FWHM
3.28	26.934	149	373	100	4020	100	0.31
6.68	13.212	87	175	46.9	955	23.8	0.18
11.8	7.497	84	124	33.2	104	2.6	0.04
12.69	6.968	94	141	37.8	233	5.8	0.08
19.1	4.643	181	317	85	1832	45.6	0.23
22.3	3.983	135	201	53.9	923	23	0.24
22.44	3.959	136	192	51.5	908	22.6	0.28
22.64	3.924	128	184	49.3	1302	32.4	0.4
23.8	3.736	117	190	50.9	898	22.3	0.21
24.17	3.679	110	156	41.8	556	13.8	0.21
27.36	3.257	86	131	35.1	700	17.4	0.26

Peak Search Report (13 Peaks, Max P/N = 6.0)

[Z07356.MDI] Naproxen+alpha-NAA : RESS (76C, 8000psi) <Psi=0.0>

PEAK: 21-pts/Parabolic Filter, Threshold=3.0, Cutoff=0.1%, BG=3/1.0, Peak-Top=Summit

2-Theta	d(A)	BG	Height	I%	Area	I%	FWHM
3.4	25.983	162	348	66.5	4831	100	0.44
3.54	24.948	153	332	63.5	4217	87.3	0.4
3.64	24.25	141	318	60.8	3628	75.1	0.35
3.83	23.067	124	303	57.9	3045	63	0.29
6.64	13.298	101	226	43.2	2256	46.7	0.31
12.76	6.932	125	203	38.8	1081	22.4	0.24
16.8	5.273	208	263	50.3	983	20.3	0.3
19.04	4.657	247	523	100	4127	85.4	0.25
21.35	4.159	181	242	46.3	374	7.7	0.1
22.66	3.921	145	229	43.8	1925	39.8	0.39
23.76	3.742	128	271	51.8	1851	38.3	0.22
24.04	3.699	125	170	32.5	556	11.5	0.21
27.47	3.245	89	137	26.2	1236	25.6	0.44

BIBLIOGRAPHY

Aal-Saeq SS, Riley GS. Polymorphism in sulfonylurea hypoglycemic agents: II. Chlorpropamide. *Pharmaceutica Acta Helvetica* 1982, 57(1):p8-11.

Addadi L. Resolution of conglomerates with the assistance of tailor-made impurities : Generality and mechanistic aspects of the "Rule of reversal". A new method for assignment of absolute configuration. *Journal of American Chemical Society* 1982, 104:p4610-4617.

Aki H, Niiya T, Iwase Y, Yamamoto M. Multimodal inclusion complexes between barbiturates and 2-hydroxypropyl-beta-cyclodextrin in aqueous solution: Isothermal titration microcalorimetry, (13)C NMR spectrometry, and molecular dynamics simulation. *Journal of Pharmaceutical Sciences* 2001, 90(8):p1186-97.

Alessi P et al. Determination and correlation of solubility of pharmaceutical products in supercritical carbon dioxide. *Chemical and Biochemical Engineering Quarterly* 1997, 11(1) :p19-23.

Alessi P et al. Particle production of steroid drugs using supercritical fluid processing. *Industrial and Engineering Chemistry Research* 1996, 35 : p4718-4726.

Al-Saeq SS, Riley GS. Polymorphism in sulfonylurea hypoglycemic agents. I. Tolbutamide. *Pharmaceutica Acta Helvetica* 1981, 56(4-5):p125-129.

Aravazhi S et al. Growth and characterization of L-Alanine and L-Valine doped Triglycine sulfate crystals. *Materials Research Bulletin* 1997, 32(11):p1503-1513.

Atencio R et al. Synthesis and single crystal structure of the 1:1 binary complex between pyrene and ferrocene. *Crystal Engineering* 2000, 3:p63-69.

Badawi AA. High energy forms of Lorazepam. *Bulletin of the Faculty of Science of Cairo University* 1997, 35(3) : p207-211.

Bauer J et al. Ritonavir: an extraordinary example of conformational polymorphism, *Pharmaceutical Research* 2001, 18(6):p 859-866.

Beach S et al. Control of the physical form of Salmeterol Xinafoate. *Organic Process Research and Development* 1999, 3:p370-376.

Behme RJ, Brooke D. Heat of fusion measurement of a low melting polymorph of carbamazepine that undergoes multiple phase changes during DSC. *Journal of Pharmaceutical Sciences* 1991, 80(10):p986-990.

Benedetti L et al. Production of micronic particles of biocompatible polymer using supercritical carbon dioxide. *Biotechnology and Bioengineering* 1997, 53(2) : p232-237.

Berens AR et al. Process for incorporating an additive into a polymer and product produced thereby. *United States Patent* 1989, Number:4820752.

Bertucco A et al. Formation of biocompatible polymer microspheres for controlled drug delivery by a supercritical antisolvent technique. *Process Technology Proceedings: High Pressure Chemical Engineering* 1996, 12: p:217-222.

Bettinetti G et al. Structure and solid state chemistry of anhydrous and hydrated crystal forms of the Trimethoprim-Sulfamethoxypyridazine 1:1 molecular complex. *Journal of Pharmaceutical Sciences* 2000, 89(4):p478-489.

Biradha K et al. Interpenetrating covalent and non-covalent nets in the crystal structures of $[M(4,4'-Bipyridine)_2(NO_3)_2] \cdot 3C_{10}H_8$. *Crystal Engineering* 1999, 2(1):p37-45.

Bisrat M, Moshashace S. Composition comprising finely divided, crystalline particles of budesonide. *International Patent Publication* 1998, Number : WO 98/52544.

Bleich J et al. Aerosol solvent extraction system- a new microparticle production technique. *International Journal of Pharmaceutics* 1993, 97 : p111-117.

Bleich J, Muller BW. Production of drug loaded microspheres by the use of supercritical gases with the aerosol solvent extraction system (ASES) process. *Journal of Microencapsulation* 1996, 13(2) : p131-139.

Bodmeier R et al. Polymeric microspheres prepared by spraying into compressed carbon dioxide. *Pharmaceutical Research* 1995, 12980 : p 1211-1217.

Bondar V. Photostimulated transformation of defects in cadmium iodide with copper and coactivators. *Materials Science and Engineering B* 2000, 71:p 258-262

Bonner J. A particularly fine way of making drugs. *Chemistry & Industry*, June 2000

Bosela AA. Improvement of dissolution and bioavailability of khellin by crystal modification technique. *Bulletin of the Faculty of Science of Cairo University* 1997, 35(2): p163-169.

Bristow S et al. Analysis of the supersaturation and precipitation process with supercritical CO₂. *Journal of Supercritical Fluids* 2001, 21:p257-271.

Burger A. In German. *Sci. Pharm* 1975, 43:p152-161.

Burt HM, Mitchell AG. Crystal defects and dissolution. *International Journal of Pharmaceutics* 1981, 9 : p137-152.

Carli F et al. Pharmaceutical compositions having the shape of powders of cross-linked polymers loaded with drugs and related preparation process by supercritical fluids. *International Patent Publication* 1999, Number: WO 99/25322.

Castor TP, Chu L. Methods and apparatus for making liposomes containing hydrophobic drugs. *United States Patent* 1998, Number: 5776486.

Chan HK, Grant DJW. Influence of compaction on the intrinsic dissolution rate of modified acetaminophen and adipic acid crystals. *International Journal of Pharmaceutics* 1989, 57 ; p117-124.

Chang CJ, Randolph AD. Precipitation of microsize organic particles from supercritical fluids. *AIChE Journal* 1989, 35(11) : p1876-1882.

Chattopadhyay P, Gupta RB. Production of griseofulvin nanoparticles using supercritical CO₂ antisolvent with enhanced mass transfer. *International Journal of Pharmaceutics* 2001, 228(1-2):19-31.

Chow AHL et al. Assessment of wettability and its relationship to the intrinsic dissolution rate of doped phenytoin crystals. *International Journal of Pharmaceutics* 1995, 126:p21-28.

Chow AHL et al. Modification of phenytoin crystals : influence of growth in aqueous solutions containing p-acetoxyacetanilide on crystal properties. *International Journal of Pharmaceutics* 1985, 24 ; p239-258.

Chow AHL et al. Modification of phenytoin crystals. III Influence of 3-butanoyloxymethyl-5,5-diphenyl hydantoin on solution-phase crystallization and related crystal properties. *International Journal of Pharmaceutics* 1995a, 126:p11-19.

Chow AHL et al. Modification of phenytoin crystals. Modification of phenytoin crystals : Influence of 3-acetoxymethyl-5,5-diphenyl hydantoin on solution-phase crystallization and related crystal properties. *International Journal of Pharmaceutics* 1991, 75:p219-230.

Chow AHL, Grant DJW. Influence of crystallization conditions on the physical properties of acetaminophen crystals : Evaluation by multiple linear regression. *International Journal of Pharmaceutics* 1989a, 51 ; p115-127.

Chow AHL, Grant DJW. Physical factors influencing the aqueous dissolution rate of acetaminophen crystals doped with p-acetoxyacetanilide : evaluation by multiple linear regression. *International Journal of Pharmaceutics* 1989b, 51 ; p129-135.

Coffey MP and Krukoni VJ. Supercritical fluid nucleation: An improved ultrafine particle formation process. Phasex Corporation Final report to National Science Foundation, Contract ISI 8660823, 1989. Cited in *Supercritical Fluid Extraction*.

Condo PD et al. Glass transition behavior including retrograde vitification of polymers with compressed fluid diluents. *Macromolecules* 1992, 25 :p6119-6127.

Daly, AT et al. Continuous processing of powder coating compositions. *United States Patent* 2001, Number: 6228897.

Dandge DK et al. Structure solubility correlations : Organic compounds and dense carbon dioxide binary systems. *Industrial and Engineering Chemistry Product Research and Development* 1985, 24 : p162-166.

De Villiers MM, Wurster DE. Isothermal interconversion of chlorpropamide polymorphs kinetically quantified by XRPD, diffuse reflectance FTIR and isoperibol solution calorimetry. *Acta Pharmaceutica* 1999, 49:p79-88.

Debenedetti PG et al. Application of supercritical fluids for the production of sustained release delivery devices. *Journal of Controlled Release* 1993b, 24 : p27-44.

Debenedetti PG et al. Rapid expansion of supercritical solutions (RESS): Fundamentals and applications. *Fluid Phase Equilibria* 1993a, 82 : p311-321.

Diefenbacher A, Turk M. Phase equilibria of organic solid solutes and supercritical fluids with respect to the RESS process. *Journal of Supercritical Fluids* 2002, 22:p175-184.

Dixon DJ et al. Polymeric materials formed by precipitation with a compressed fluid antisolvent. *AIChE Journal* 1993, 39(1) : p127-139.

Dixon DJ, Johnston KP. On Supercritical fluids in *Kirk-Othmer Encyclopedia of Chemical Technolog* 1997, Vol.23, Ed.4; p 453-477.

Dobbs JM et al. Modification of supercritical fluid phase behavior using polar cosolvents. *Industrial and Engineering Chemistry Research* 1987, 26 : p56-65.

Dobbs JM et al. Nonpolar co-solvents for solubility enhancement in supercritical fluid carbon dioxide. *Journal of Chemical and Engineering Data* 1986, 31 : p303-308.

Donsi G, Reverchon E. Micronization by means of supercritical fluids: possibility of application to pharmaceutical field. *Pharmaceutica Acta Helvetica* 1991;66(5-6):p170-3.

Duddu SP, Grant DJW. The use of thermal analysis in the assessment of crystal disruption. *Thermochimica Acta* 1995, 248:p131-145.

Duncan-Hewitt WC, Grant DJW. True density and thermal expansivity of pharmaceutical solids : comparison of methods and assessment of crystallinity. *International Journal of Pharmaceutics* 1986, 28 ; p75-84.

Ekart MP et al. Cosolvent interactions in supercritical fluid solutions. *AIChE Journal* 1993, 39(2) : p235-248.

Engwicht A et al. Critical properties of lactide-co-glycolide polymers for the use in microparticle preparation by the aerosol solvent extraction system. *International Journal of Pharmaceutics* 1999 185 p:61-72.

Fischer et al. Method and apparatus for the manufacture of a product having a substance embedded in a carrier. *United States Patent* 1991, Number: 5043280.

Ford JL et al. The assay and stability of chlorpropamide in solid dispersion with urea. *Journal of Pharmacy and Pharmacology* 1979, 31:p726-729.

Ford JL, Rubinstein MH. Phase equilibria and stability characteristics of chlorpropamide-urea solid dispersions. *Journal of Pharmacy and Pharmacology* 1977, 29:p209-211.

Foxman BM et al. Environmentally benign synthesis using crystal engineering:steric accommodation in non-covalent derivatives of hydroquinones. *Crystal Engineering* 1998, 1(1):p109-118.

Frederiksen L et al. Preparation of liposomes encapsulating water-soluble compounds using supercritical carbon dioxide. *Journal of Pharmaceutical Sciences* 1997, 86(8) : p921-928.

Gallagher PM et al. Gas antisolvent recrystallization : New process to recrystallize compounds insoluble in supercritical fluids. *Supercritical fluid science and technology*, ACS Symposium Series-406; Johnston KP, Penninger JML Eds., American Chemical Society, Washington DC, 1989, Chapter 22 : p334-354.

Ghaderi R et al. Preparation of biodegradable microparticles using solution enhanced dispersion by supercritical fluids. *Pharmaceutical Research* 1999; 16(5) p:676

Ghenciu EG, Beckman EJ. Affinity extraction into carbondioxide I. Extraction of Avidin into CO₂ using a Biotin-Functional fluoroether surfactant. *Industrial and Engineering Chemistry* 1997, 36:p5366.

Ghenciu EG, Beckman EJ. Extraction of subtilisin into carbon dioxide via fluoroaether surfactants. *Biotechnology and Bioengineering* 1998, 58:p572.

Gordon JD, Chow AHL. Modification of phenytoin crystals. II. Influence of 3-propanoyloxymethyl-5,5-diphenylhydantoin on solution-phase crystallization and related crystal properties. *International Journal of Pharmaceutics* 1992, 79 : p171-181.

Gosselin PM et al. Comparison of microparticles prepared from the rapid expansion of supercritical solutions and by spray drying. Paper Presentation #3599, *AAPS Annual meeting*, Indianapolis 2000.

Grant DJW, York P. A disruption index for quantifying the solid state disorder induced by additives or impurities. II. Evaluation from heat of solution. *International Journal of Pharmaceutics* 1986, 28 : p103-112.

Greiner RW. Treating skin lesions. *United States Patent* 1993, Number:5183663.

Gu CH, Grant DJ. Effects of crystallization in the presence of the diastereomer on the crystal properties of (SS)-(+)-pseudoephedrine hydrochloride. *Enantiomer* 2000, 5:p271-80.

Gustafsson C et al. Comparison of solid-state NMR and isothermal microcalorimetry in the assessment of the amorphous component of lactose. *International Journal of Pharmaceutics* 1998, 174: p243-252.

Hanna M et al. Control of the polymorphic forms of a drug substance by SEDS. Poster presentation-*5th Meeting of Supercritical Fluids*, Nice, France; March 1998.

Hanna M et al. Method of particle formation. *International Patent Publication* 1999, Number: WO99/44733.

Helfgen B et al. Theoretical and experimental investigations of the micronization of organic solids by rapid expansion of supercritical solutions. *Powder Technology* 2000, 110:p22-28.

Henriksen IB et al. Insoluble drug delivery. *International Patent Publication* 1997, Number :WO 97/14407.

Herman J et al. Instability of drug release from anhydrous theophylline-microcrystalline cellulose formulations. *International Journal of Pharmaceutics* 1989, 55:p143-146.

Hirose Y et al. Dilution of polyethylene by sorption of carbon dioxide. *Journal of Polymer Science: Part B : Polymer physics* 1986, 24 : p2107-2115.

Hoke SH et al. Comparison of packed-column supercritical fluid chromatography-tandem mass spectrometry with liquid chromatography--tandem mass spectrometry for bioanalytical determination of (R)- and (S)-ketoprofen in human plasma following automated 96-well solid-phase extraction. *Analytical Chemistry* 2000, 1;72(17):4235-4241.

Howdle S. Biofunctional polymers prepared in supercritical fluid. *International Patent Publication* 1998, Number: WO 98/51347.

Hyatt, JA. Liquid and supercritical carbon dioxide as organic solvents. *Journal of Organic Chemistry* 1984, 49 : p5097-5101.

Jaarmo S et al. Particle tailoring with supercritical fluids:Production of amorphous pharmaceutical particles. *Proceedings: 4th International Symposium on Supercritical Fluids*, May 11-14, 1997, Sendai p:263-266.

Juvekar A. Study of a novel polymer loading process using near-critical carbon dioxide and a model drug. *M.S. Thesis, University of Rhode Island*, 1994.

Kazarian SG et al. In situ spectroscopy of polymers subjected to supercritical CO₂: Plasticization and dye impregnation. *Applied Spectroscopy* 1997, 51(4) : p491-494.

Kazarian SG et al. Specific intermolecular interaction of carbon dioxide with polymers. *Journal of American Chemical Society* 1996, 118 : p1729-1736.

- Kerc J et al. Micronization of drugs using supercritical carbon dioxide. *Farm Vestn (Ljubljana)* 48(Post Stev) 1997 p:282-283.
- Kerc J et al. Micronization of drugs using supercritical carbon dioxide. *International Journal of Pharmaceutics* 1999, 182 : p33-39.
- Kim JH et al. Microencapsulation of naproxen using rapid expansion of supercritical solutions. *Biotechnology Progress* 1996, 12(5) : p650-661.
- Kimura K. Characterization of Tolbutamide polymorphs (Burger's forms II and IV) and polymorphic transition behavior. *Journal of Pharmaceutical Sciences* 1999, 88(4):p385-391.
- Koo et al. The crystal and molecular structure of chlorpropamide. *Archives of Pharmaceutical Research* 1980, 3(1):p37-49.
- Kopp S et al. Methodology for a better evaluation of the relation between mechanical strength of solids and polymorphic form. *Journal of Pharmacy and Pharmacology* 1989, 41 : p79-82.
- Kordikowski et al. Resolution of ephedrine in supercritical CO₂ : A novel technique for separation of chiral drugs. *Journal of Pharmaceutical Sciences* 1999, 88(8):p786-791.
- Kordikowski A et al. Phase equilibria for the CO₂ + methanol + sulfathiazole system at high pressure. *Fluid Phase Equilibria* 2002, 194-197:p905-917.
- Krukoniš VJ. Supercritical fluid nucleation of difficult-to-comminute solids. Paper presented at the *AIChE Annual Meeting*, San Francisco, CA, November 1984.
- Kulshreshtha AK et al. Process for sizing prednisolone acetate using a supercritical fluid anti-solvent. *United States Patent* 1998, Number: 5803966.
- Kumar SK. Modelling the solubility of solids in supercritical fluids with density as the independent variable. *Journal of Supercritical Fluids* 1988, 1 : p15-22.
- Kurnik RT, Reid RC. Solubility of solid mixtures in supercritical fluids. *Fluid Phase Equilibria* 1982, 8:p93
- Laihanen et al. Solubility and intrinsic dissolution rate of Alprazolam crystal modifications. *Pharmaceutical Development and Technology* 1996, 1(4) : p373-380.

Larson KA, King ML. Evaluation of supercritical fluid extraction in the pharmaceutical industry. *Biotechnology Progress* 1986, 2(2) : p73-82.

Leary JR et al. On the characterization of the polymorphs of tolbutamide. *Pharmaceutisch Weekblad Scientific Edition* 1981, 3:p62-66.

Lee M et al. Extrusion of PE/PS blends with supercritical carbon dioxide. *Polymer Engineering and Science* 1998, 38(7):p1112-1120.

Lele AK, Shine AD. Morphology of polymers precipitated from a supercritical solvent. *AIChE Journal* 1992, 38(5) : p742-752.

Li T et al. Influence of solvent and crystalline supramolecular structure on the formation of etching patterns on acetaminophen single crystals: A study with atomic force microscopy and computer simulation. *Journal of Physical Chemistry B* 2000, 104:p2019-2032.

Lindsay AD, Omilinsky BA. Method of preparing mixtures of active ingredients and excipients using liquid carbon dioxide. *United States Patent* 1992, Number:5169433.

Loth H, Hemgesberg. Properties and dissolution of drugs micronized by crystallization from supercritical gases. *International Journal of Pharmaceutics* 1986, 32 : p265-267.

Lucien FP, Foster NR. Solubilities of solid mixtures in supercritical carbon dioxide : a review. *Journal of Supercritical Fluids* 2000, 17:p111-134.

Lynch DE et al. Molecular cocrystals of 2-amino-5-chlorobenzooxazole. *Crystal Engineering* 2000, 3:p71-79.

Magnan C et al. Impregnation of porous supports with active substances by means of supercritical fluids. *High Pressure Chemical Engineering*, Rudolph von Rohr, Trepp C Eds., Elsevier Science 1996, p509-514.

Mandel FS. Mixing system for processes using supercritical fluids. *United States Patent* 1999, Number: 5993747.

Martin A, Swarbrick J, Cammarata A, Chun AH (Eds). *Physical Pharmacy* 1993, 4th Edition; Lea & Febiger, Philadelphia.

Matson DW et al. Rapid expansion of supercritical fluid solutions : Solute formation of powders, thin films and fibres. *Industrial and Engineering Chemistry Research* 1987, 26 : p2298-2306.

Matsumoto T et al. Effects of compression temperature on the consolidation mechanism of chlorpropamide polymorphs. *Journal of Pharmaceutical Sciences* 1995, 84(5):p614-618.

McClain JB et al. Design of nonionic surfactants for supercritical carbon dioxide. *Science* 1996, 274:p2049-2052.

McHugh MA, Krukonis VJ. *Supercritical Fluid Extraction*. 2nd Edition; Butterworth-Heinemann:Newton, MA, 1994.

Mohamed RS et al. Effects of process conditions on crystals obtained from supercritical mixtures. *AIChE Journal*, 1989a, 35(2), p:325-328.

Mohamed RS et al. Solids formation after the expansion of supercritical mixtures. Supercritical fluid science and technology, *ACS Symposium Series-406*; Johnston KP, Penninger JML Eds., American Chemical Society, Washington DC, 1989b, Chapter 23 : p355-378.

Mooney DJ et al. Novel approach to fabricate porous sponges of poly(D,L-lactic-co-glycolic acid) without the use of organic solvents. *Biomaterials* 1996, 17(14):p1417-1422.

Moshashae S et al. Supercritical fluid processing of proteins. I: lysozyme precipitation from organic solution. *European Journal of Pharmaceutical Sciences* 2000 Sep;11(3):239-45.

Mroso PV et al. Solid-state stability of aspirin in the presence of excipients: Kinetic interpretation, modeling and prediction. *Journal of Pharmaceutical Sciences* 1982, 71(10): p1096-1101.

Mulcahey LJ, Taylor LT. Supercritical fluid extraction of active components in a drug formulation. *Analytical Chemistry* 1992, 64(9):p981-984.

Muller BW, Steckel H. Budesonide microparticles for pulmonary delivery produced by supercritical carbon dioxide. *Proceedings-International symposium on Controlled Release of Bioactive Materials* 1997, 24 : p69-70.

Mura G, Pozzoli S. Process for the production of powders with controlled particle sizes and powdery product so obtained. *European Patent Application* 1995, Publication Number 0661091.

Muth O et al. Polymer modification by supercritical impregnation. *Journal of Supercritical Fluids* 2000, 17 :p65-72.

Ohgaki K et al. Whisker formation from jet of supercritical fluid solution. *Journal of Supercritical Fluids*, 1990, 3, p:103-107.

Palakodaty S et al. Particle formation using supercritical fluids- A novel approach.. In Proc. 1997 *ICHEME Event*, UK 1997, p501-504.

Palakodaty S et al. Supercritical fluid processing of materials from aqueous solutions: The application of SEDS to lactose as a model substance. *Pharmaceutical Research* 1998, 15(12) : p1835 -1843.

Palakodaty S, York P. Phase behavioral effects on particle formation processes using supercritical fluids. *Pharmaceutical Research* 1999, 16(7):p976-985.

Pennisi KJ, Chimowitz EH. Solubilities of solid 1,10-Decanediol and a solid mixture of 1,10-Decanediol and benzoic acid in supercritical carbon dioxide. *Journal of Chemical and Engineering Data* 1986, 31:p285.

Perry's Chemical Engineers' Handbook, Mc Graw-Hill, New York, 7th Ed. 1997.

Pikal MJ, Grant DJW. A theoretical treatment of changes in entropy of solids caused by additives or impurities in solid solution. *International Journal of Pharmaceutics* 1987, 39: p243-253.

Prasad KVR et al. Crystallization of paracetamol from solution in the presence and absence of impurity. *International Journal of Pharmaceutics* 2001, 215:p29-44.

Rajagopalan P, McCarthy TJ. Two-Step Surface Modification of Chemically Resistant Polymers: Blend Formation and Subsequent Chemistry. *Macromolecules*. 1998, 31(15):p4791.

Rauls M et al. The influence of impurities on crystallization kinetics-a case study on ammonium sulfate. *Journal of Crystal Growth* 2000, 213(1-2):p 116-128.

Reverchon E et al. Solubility and micronization of griseofulvin supercritical CHF₃. *Industrial and Engineering Chemistry Research* 1995, 34(11) : p4087-4091.

Reverchon E, Donsi G. Salicylic acid solubilization in supercritical CO₂ and its micronization by RESS. *Journal of Supercritical Fluids* 1993, 6(4) : p241-248.

Robertson J et al. Novel techniques for particle production from supercritical solutions. *ICChemE Research. Event. Conf. Young Res. Che. Eng.*, Publisher: Institute of Chemical Engineers, Rugby UK. 1996, 2:p988-990.

Rodriguez-Hornedo N, Wu HJ. Crystal growth kinetics of theophylline monohydrate. *Pharmaceutical Research* 1991, 8(5):p643-648.

Rogers TL, Johnston KP, Williams RO 3rd. Solution-based particle formation of pharmaceutical powders by supercritical or compressed fluid CO₂ and cryogenic spray-freezing technologies. *Drug Development and Industrial Pharmacy* 2001.27(10):p1003.

Rowe EL, Anderson BD. Thermodynamic studies of Tolbutamide polymorphs. *Journal of Pharmaceutical Sciences* 1984, 73(11):p1673-1675.

Ruchatz F et al. Residual solvents in biodegradable microparticles. Influence of process parameters on the residual solvent in microparticles produced by the aerosol solvent extraction system (ASES) process. *Journal of Pharmaceutical Sciences* 1997, 86(1) : p 101-105.

Sand ML. Method of impregnating a thermoplastic polymer. *United States Patent* 1986, Number : 4,598,006.

Sand ML. Method of impregnating a thermoplastic polymer. *United States Patent* 1987, Number : 4,678,684.

Sano C et al. Effects of additives on the growth of L-glutamic acid crystals (β -form). *Journal of Crystal Growth* 1997, 178(4):p568-574.

Schmitt WJ. Finely divided solid crystalline powders via precipitation into an anti-solvent. *International Patent Publication* 1990, Number: WO 90/03782.

Sefcik MD. Dilution and plasticization of polystyrene by carbon dioxide. *Journal of Polymer Science: Part B : Polymer Physics* 1986a, 24 : p957-971.

Sefcik MD. Dilution of polycarbonate by carbon dioxide. *Journal of Polymer Science: Part B : Polymer Physics* 1986b, 24 : p935-956.

Sencar-Bozic P et al. Improvement of nifedipine dissolution characteristics using supercritical CO₂. *International Journal of Pharmaceutics* 1997, 148 : p123-130.

Shekunov BY et al. Crystallization in turbulent supercritical flows. *Journal of Crystal Growth* 1999, 198/199 p:1345-1351.

Shieh YT et al. Interaction of supercritical carbon dioxide with polymers. I. Crystalline polymers. *Journal of Applied Polymer Science* 1996a, 59 : p695-705.

Shieh YT et al. Interaction of supercritical carbon dioxide with polymers. II. Amorphous polymers. *Journal of Applied Polymer Science* 1996b, 59 : p707-717.

Simmons DL et al. Polymorphism in pharmaceuticals III. *Canadian Journal of Pharmaceutical Sciences* 1973, 8(4): p125-127.

Simonelli AP, Mehta SC, Higuchi WI. Dissolution rates of high energy sulfathiazole-povidone coprecipitates II: characterization of form of drug controlling its dissolution rate via solubility studies. *Journal of Pharmaceutical Sciences* 1976, 65(3): p355-61.

Staab E et al. *Advanced Materials* 1990, 2:p40

Steckel H et al. Micronizing of steroids for pulmonary delivery by supercritical carbon dioxide. *International Journal of Pharmaceutics* 1997, 152 : p99-110.

Subramaniam B et al. Methods for a particle precipitation and coating using near-critical and supercritical antisolvents. *United States Patent* 1998, Number: 5833891.

Subramaniam B et al. Pharmaceutical processing with supercritical carbon dioxide. *Journal of Pharmaceutical Sciences* 1997, 86(8) : p885-890.

Suga H. A facet of perspectives in materials science, 1999. <http://www.rist.kindai.ac.jp/no.12/suga.pdf>, Last accessed 4/3/02.

Suga H. A facet of recent ice sciences. *Thermochimica Acta* 1997, 300:p117-126.

Super, Beckman EJ. Copolymerizations employing CO₂ as comonomer. *Trends in Polymer science* 1997, 5:p236.

Tavana A et al. Scanning cosolvents for supercritical fluids solubilization of organics. *AIChE Journal* 1989, 35 : p645-648.

Tavana A, Randolph AD. Isobaric-isothermal fractional crystallization of organic solids from supercritical fluid mixtures : Particle design via crystallization, *AIChE Symposium Series* 1990, 87(284):p5-15.

Ting SST et al. Solubility of Naproxen in supercritical carbon dioxide with and without cosolvents. *Industrial and Engineering Chemistry Research* 1993, 32 : p1471-1481.

Tom JW et al. Applications of supercritical fluids in the controlled release of drugs. Supercritical fluid engineering science, *ACS Symposium Series-514*; Brennecke JF, Kiran E Eds., American Chemical Society, Washington DC, 1993, Chapter 19 : p238-257.

Tom JW, Debenedetti PG. Formation of bioerodible polymeric microspheres and microparticles by rapid expansion of supercritical solutions. *Biotechnology Progress* 1991a, 7(5) : p403-411.

Tom JW, Debenedetti PG. Particle formation with supercritical fluids-A review. *Journal of Aerosol Science* 1991b, 22(5) : p555-584.

Tom JW, Debenedetti PG. Precipitation of Poly (L-Lactic acid) and composite Poly(L-Lactic acid)-Pyrene particles by rapid expansion of supercritical solutions. *Journal of Supercritical Fluids* 1994, 7 : 9-29.

Tudor AM. The qualitative and quantitative analysis of chlorpropamide polymorphic mixtures by near-infrared FTIR spectroscopy. *Pharmaceutical Research* 1993, 10(12):p1772-1776.

Turk M et al. Micronization of pharmaceutical substances by the Rapid Expansion of Supercritical Solutions: A promising method to improve bioavailability of poorly soluble pharmaceutical agents. *Journal of Supercritical Fluids* 2002, 22:p75-84.

Turk M Formation of small organic particles by RESS: Experimental and theoretical investigations. *Journal of Supercritical Fluids* 1999, 15:p79-89.

Ueda H et al. Dissolution behavior of Chlorpropamide polymorphs. *Chemical and Pharmaceutical Bulletin* 1984, 32(1):p244-250.

Van Hees T et al. Application of supercritical carbon dioxide for the preparation of a Piroxicam- β -Cyclodextrin inclusion compound. *Pharmaceutical Research* 1999; 16(12) :p1864-1870.

Walas SM. *Phase Equilibria in Chemical Engineering* 1985, Butterworth Publishers, Stoneham, MA.

Weber A et al. Compressed fluid antisolvent crystallization for controlled particle design. In *4th International Workshop on Crystal Growth Organic Matter* 1997. Editors: Ulrich, Joachim. Publisher: Shaker Verlag, Aachen. Issue:4: p214-221.

Weidner E et al. Powder generation from polyethyleneglycols with compressible fluids. *Process Technology Proceedings-12, High Pressure Chemical Engineering*; Rudolf von Rohr P, Trepp C Eds., Elsevier Science B. V, 1996, p223-228.

Weidner E et al. Process for preparing particles or powders. *International Patent Publication* 1995, Number: WO 95/21688.

Weisinger-Lewin Y et al. Reduction in crystal symmetry of a solid solution: A neutron diffraction study at 15K of the host/guest system asparagine/aspartic acid. *Journal of American Chemical Society* 1989, 111:p1035-1040.

Weissbuch I et al. Molecular recognition at crystal interfaces. *Science* 1991, 253:p637-645.

Weissbuch I et al.. Tailor made additives and impurities In : Mersmann A (Ed), *Crystallization Technology Handbook* 2001 , Second Edition, Marcel Dekker, New York.

Werling JO, Debenedetti PG Numerical modeling of mass transfer in the supercritical antisolvent process. *Journal of Supercritical Fluids* 1999, 16:p167-181.

Williams-Seton et al. Disorder and twinning in molecular crystals: Impurity-induced effects in adipic acid. *Journal of Pharmaceutical Sciences* 2000, 89(3): p346-354.

Wissinger RG, Paulaitis ME. Glass transitions in polymer/CO₂ mixtures at elevated pressures. *Journal of Polymer Science: Part B : Polymer Physics* 1991, 29 : p631-633.

Wissinger RG, Paulaitis ME. Swelling and sorption in polymer-CO₂ mixtures at elevated pressures. *Journal of Polymer Science: Part B : Polymer Physics* 1987, 25 : 2497-2510.

Wong JM, Johnston KP. Solubilization of biomolecules in carbon dioxide based supercritical fluids. *Biotechnology Progress* 1986, 2(1) : p29-39.

Wong SH. Advances in chromatography for clinical drug analysis: supercritical fluid chromatography, capillary electrophoresis, and selected high-performance liquid chromatography techniques. *Therapeutic Drug Monitoring* 1993, 15(6):p576-580.

Yang C, Xu YR, Yao WX. Extraction of pharmaceutical components from Ginkgo biloba leaves using supercritical carbon dioxide. *Journal of Agricultural and Food Chemistry* 2002, 50(4):p846.

Yatsenko AV et al. NMR study of intrinsic defects in congruent LiNbO₃. 1. "Unoverlapping" defects. *Physica B. Condensed matter* 1997, 240(3):p254-262.

Yazdi AV, Beckman EJ. Design of highly CO₂-soluble chelating agents II. Effect of chelate structure and process parameters on extraction efficiency. *Industrial and Engineering Chemistry* 1997, 36:p2368

Yeo SD et al. Formation of microparticulate protein powders using a supercritical fluid antisolvent. *Biotechnology and Bioengineering* 1993, 41(3) : p341-346.

York P et al. Controlled particle formation using the solution enhanced dispersion by supercritical fluids (SEDS) process. Presented at *16th Pharmaceutical Technology Conference*, Athens, Greece, April 1997.

York P et al. *Proceedings, Respiratory Drug Delivery*, South Carolina May 1998.

York P, Grant DJW. A disruption index for quantifying the solid state disorder induced by additives or impurities. I. Definition and evaluation from heat of fusion. *International Journal of Pharmaceutics* 1985, 25 : p57-72.

York P, Hanna M. Salmeterol Xinafoate with controlled particle size. *International Patent Publication* 1995, Number: WO 95/01324.

York P, Hanna M. Particle engineering by supercritical fluid technologies for powder inhalation drug delivery. *Respiratory Drug Delivery V* 1996, p231-239.

York P. Strategies for particle design using supercritical fluid technologies. *Pharmaceutical Science & Technology Today* 1999, 2(11).

Yoshihashi Y et al. Quantitative correlation between initial dissolution rate and heat of fusion of drug substances. *International journal of Pharmaceutics* 2000, 204:p1-6.

Young TJ et al. Encapsulation of lysozyme in a biodegradable polymer by precipitation with a vapor-over-liquid antisolvent. *Journal of Pharmaceutical Sciences* 1999, 88(6) p:640-650.

Yu L. Inferring thermodynamic stability relationship of polymorphs from melting data. *Journal of Pharmaceutical Sciences* 1995, 84(8):p966-974.

Yu, L Amorphous pharmaceutical solids: preparation, characterization and stabilization. *Advanced Drug Delivery Reviews* 2001, 48(1):p 27-42.

Zhang GGZ, Grant DJW. Incorporation mechanism of guest molecules in crystals: solid solution or inclusion? *International Journal of Pharmaceutics* 1999, 181:p61-70.

Zhen FR et al. Phase behavior and reaction of polyethylene terephthalate-water systems at pressures upto 173 MPa and temperatures up to 490°C. *Journal of Supercritical Fluids* 1999, 15:p229-243.

Zia H et al. Comparison of nasal insulin powders prepared by supercritical fluid and freeze-drying techniques. *Particulate Science and Technology* 1997, 15:p273-301.